GEOCHEMICAL AND MINERALOGICAL STUDY OF OVERBURDEN PROFILES IN GLACIATED TERRAIN, FINLAND
– IMPLICATION FOR THE ASSESSMENT OF RADON EMISSION –

by

Dániel Breitner
M.Sc., Earth Sciences, Eötvös Loránd University, Budapest, 2006

Lithosphere Fluid Research Lab, Institute of Geography and Earth Sciences,
Eötvös University, Hungary

Dissertation submitted to the Ph.D. program for Environmental Earth Sciences
at the Ph.D. School of Environmental Sciences,
Eötvös Loránd University, Budapest

Chair of the doctoral school:	Prof. Ádám Kiss *(Department of Atomic Physics, Budapest)*
Chair of the Environmental Earth Sciences Doctoral Program:	Prof. András Galácz *(Department of Palaeontology)*
Advisor:	Csaba Szabó, Ph.D. associate professor *(Department of Petrology and Geochemistry, Budapest)*
Tutors:	Hannu Arvela, Ph.D. research professor *(Radiation and Nuclear Safety Authority of Finland)*
	Marja Siitari-Kauppi, Ph.D. university lecturer *(Laboratory of Radiochemistry, Helsinki University)*
	Karl-Heinz Hellmuth, Ph.D. senior scientist *(Radiation and Nuclear Safety Authority of Finland)*

2011. ELTE, Budapest

ACKNOWLEDGEMENTS

This work was financially supported by

- *the Ph.D. fellowship of Hungary to D. Breitner 2006-2009;*
- *the CIMO fellowship of Finland to D. Breitner 2006-2007;*
- *the Laboratory of Radiochemistry at University of Helsinki to D. Breitner 2007;*
- *the Radiation and Nuclear Safety Authority of Finland to D. Breitner 2006-2007.*

I am greatful to my supervisor Csaba Szabó (Lithosphere Fluid Research Lab, Eötvös University, Budapest) and my tutors Hannu Arvela (Radiation and Nuclear Safety Authority of Finland (STUK), Marja Siitari-Kauppi (Laboratory of Radiochemistry, University of Helsinki, Finland (HYRL)) and Karl-Heinz Hellmuth (STUK) for their pations and help during this complex study.

I am thankful to Marja Lehtonen (Geological Survey of Finland (GTK)) for her help in scanning electron microscopy and Bo Johanson (GTK) for the electron microprobe analyses.

Special thank to Jussi Ikonen (HYRL) for his help in sequential extraction and ICP-MS analyses, Laina Salonen (STUK) for her advice in liquid scintillation counting, Tuukka Turtiainen (STUK) and Pirkka Koskela (HYRL) for their help in ^{226}Ra-measurements and Juhanni Suksi for the fruitful discussions.

I owe thanks to the members of the Lithosphere Fluid Research Lab, HYRL and STUK for the long, sometimes neverending discussions and for the great athomsphere.

I would like to thank to Peter Zagyvai for his help in correction of the thesis, and to my colleges in Atomic Energy Research Institute for their pations and understanding.

dedicated to the memory of my uncle dr. István Pálfalvi

TABLE OF CONTENTS

1. INTRODUCTION 13

2. LITERATURE OVERVIEW 15

2.1. GENERAL DESCRIPTION OF GEOLOGY OF FINLAND 15

2.1.1. Precambrian geology 15

2.1.2. Quaternary geology 16

2.2. PHYSICAL AND GEOCHEMICAL CHARACTERISATION OF TH, U, RA AND RN 19

2.2.1. Uranium, thorium and radium 19

2.2.2. Radon 30

3. ANALYTICAL METHODS 36

3.1. ^{238}U, ^{232}TH, AND ^{226}RA DETERMINATION BY GAMMA-SPECTROSCOPY 36

3.2. DETERMINATION OF EMANATION RATE AND EMANATION FACTOR 36

3.3. SEQUENTIAL CHEMICAL EXTRACTION AND MAJOR AND TRACE ELEMENTS ANALYSES 38

3.4. RADIUM-226 MEASUREMENT BY LIQUID SCINTILLATION COUNTING 41

3.6. SCANNING ELECTRON MICROSCOPY AND ELECTRON PROBE MICROANALYSES 42

4. ASKOLA SAMPLING SITE 43

4.1. LOCATION OF ASKOLA SAMPLING SITE 43

4.2. GEOLOGICAL BACKGROUND OF ASKOLA SAMPLING SITE 44

4.2.1. Bedrock at Askola sampling site 44

4.2.2. Uranium mineralisation at Lakeakallio 45

4.2.3. Quaternary geology 46

4.3. RESULTS OF ANALYSES ON ASKOLA SAMPLES 47

4.3.1. Description of Askola samples 47

4.3.2. U-, Th- and Ra-content of bulk samples from Askola 51

4.3.3. Radon production and emanation rate of bulk samples from Askola 52

4.3.4. Major and trace elements of bulk samples from Askola 53

4.3.5. Major and trace elements of soil portions extracted from Askola samples 54

4.3.6. Mineralogical study of Askola samples 59

5. PALMOTTU SAMPLING SITE 70

5.1. LOCATION OF PALMOTTU SAMPLING SITE 70

5.2. GEOLOGICAL BACKGROUND OF PALMOTTU SAMPLING SITE 71

5.2.1. Bedrock at Palmottu sampling site 71

5.2.2. Uranium mineralisation at Palmottu 73

5.2.3. Quaternary geology 74

5.2.4. Hydrogeology of the area 76
5.3. RESULTS OF ANALYSES MADE ON PALMOTTU SAMPLES 78
5.3.1. Description of Palmottu samples 78
5.3.2. U-, Th- and Ra-content of bulk samples from Palmottu 81
5.3.3. Radon production and emanation rate of bulk samples from Palmottu 82
5.3.4. Major and trace elements of bulk samples from Palmottu 82
5.3.5. Major and trace elements of soil portions extracted from Palmottu samples .. 83
5.3.6. Mineralogical study of Palmottu samples 89
6. OLKILUOTO SAMPLING SITE 100
6.1. LOCATION OF OLKILUOTO SAMPLING SITE 100
6.2. GEOLOGICAL BACKGROUND OF OLKILUOTO SAMPLING SITE 101
6.3. RESULTS OF ANALYSES MADE ON OLKILUOTO SAMPLES 105
6.3.1. Description of Olkiluoto samples 105
6.3.2. U-, Th- and Ra-content of bulk samples from Olkiluoto 108
6.3.3. Radon production and emanation rate of bulk samples from Olkiluoto 109
6.3.4. Major and trace elements of bulk samples from Olkiluoto 109
6.3.5. Major and trace elements of soil portions extracted from Olkiluoto samples 110
6.3.6. Mineralogical study of Olkiluoto samples 116
7. DISCUSSION 121
7.1. COMPARISON OF THE MINERALOGICAL AND GEOCHEMICAL FEATURES OF ASKOLA, OLKILUOTO AND PALMOTTU SAMPLING SITES 121
7.2. COMPARISON OF THE RADIATION PROPERTIES OF ASKOLA, PALMOTTU AND OLKILUOTO SAMPLING SITES 126
7.3. WEATHERING EFFECT ON CHEMICAL COMPOSITION OF U-, TH-BEARING MINERALS 131
8. SUMMARY 132
ENGLISH ABSTRACT 134
MAGYAR NYELVŰ ÖSSZEFOGLALÓ 135
REFERENCES 136
APPENDICES 146

LIST OF FIGURES

Figure 1-1: Annual average radiation dose of Finns (Muikku et al., 2005) 13

Figure 1-2: The three sampling sites in Finland 15

Figure 2-1: Simplified geological map of the Fennoscandian Shield after Koistinen et al. (2001). TIB denotes the Transscandinavian igneous belt. The subdivisions of the Svecofennian are: (A) The Primitive arc complex of central Finland; (B) The Accretionary arc complex of central and western Finland; (C) The Accretionary arc complex of southern Finland; (D) The Skellefte district; (E) The Bothnian basin; and (F) The Bergslagen district. Sampling sites for this study are marked by small filled black squares in domain C. 16

Figure 2-2: Geological map of quaternary sediments of Finland (GTK, 2010) 18

Figure 2-3: Decay chains of ^{238}U, ^{232}Th and ^{235}U 20

Figure 2-4: Distribution of uranyl complexes vs. pH for some typical ligand concentrations in ground waters of the Wind River Formation at 25 °C, $P_{CO2} = 10^{-2.5}$ atm, ΣF = 0.3 ppm, ΣCl = 10 ppm, ΣSO_4 = 100 ppm, ΣSiO_2 = 30 ppm (Langmuir, 1978) 23

Figure 2-5: Distribution of thorium complexes vs pH for some typical ligand concentrations in ground water at 25 °C withΣTh = 0 .01 ppb (Langmuir and Herman, 1980) 24

Figure 2-6: Eh-pH diagram for part of the system Ra-O-H-C-S (Eh = oxidation potential). Assumed activities for dissolved species are: Ra = 10^{-8}, S = 10^{-3}, C = 10^{-3} (Takeno, 2005) ... 25

Figure 2-7: Schematic representation of radon production and migration in soil its entry into building (Nazaroff and Nero, 1988) 33

Figure 2-8: Recoil effects in soil grains, showing differences when water vs. air is present (Tanner, 1980). (A = recoiling Rn does not escape host grain: B = recoil directly into adjacent grain; C = recoil into water, leaving Rn in pore space /direct-recoil/: D = recoil into air, leaving Rn embedded in adjacent grain /indirect-recoil/) 34

Figure 3-1: Schematic diagram of the apparatus used in radon emanation measurements (Turtiainen, 2009) 37

Figure 3-2: Methods used for sequential extraction at HYRL (modified after Tessier (1979) and Quejido (2005)) 40

Figure 4-1: Topographical map of the sampling area in Askola and the location of Askola in Finland. The sampling site has marked by X on the topographical map. The arrow shows glacial transport direction. Degrees represent the average trend of glacial striate (modified after Hirvas and Nenonen (1980)) 43

Figure 4-2: Sampling place (a) in former sand quarry, Askola, Finland and position of the samples in the approximately 3 m deep soil profile (b). A = Ask-A, B = Ask-B, C = Ask-C, 1 = Ask-1, 2 = Ask-2 and 3 = Ask-3 44

Figure 4-3: Pre Quaternary geological map of Askola study site and location of the sampling site marked by X (modified after Laitakari and Simonen (1962)) 45

Figure 4-4: Map of Quaternary sediments at Askola sampling site, Finland (Tynni and Kukkonen, 1968). Sampling site is marked by filled black dot 47

Figure 4-5: Soil sample from the uppermost 10 cm (Ask-A) from Askola, Finland 47

Figure 4-6: Soil sample from 10 to 30 cm in depth (Ask-B) from Askola, Finland 48

Figure 4-7: Sediment sample from 30 to 130 cm in depth (Ask-C) from Askola, Finland 48

Figure 4-8: Sediment sample from 130 to 180 cm in depth (Ask-1) from Askola, Finland 49

Figure 4-9: Sediment sample from 180 to 245 cm in depth (Ask-2) from Askola, Finland. (a) and reddish silty layer between argillic layers in the sample of Ask-2 (b)..... 49

Figure 4-10: Sediment sample from 245 to 260 cm in depth (Ask-3) from Askola, Finland 50

Figure 4-11: Grain size distribution of the six soil and sediment samples collected at Askola sampling site, Finland 50

Figure 4-12: Summarised chart of lithology of the soil and sediment samples collected at Askola sampling site, Finland 51

Figure 4-13: Activity concentrations of ^{238}U (a), ^{226}Ra (b) and ^{228}Ra (^{228}Ac), ^{228}Th (^{208}Tl) as representing ^{232}Th-decay chain (c) in function of depth in soil and sediment samples from Askola, Finland. The reported uncertainties are expanded uncertainties using a coverage factor k=1 52

Figure 4-14: Elements of < 250 mm grain size fraction of Askola samples normalized to upper continental crust (UCC) (Taylor and McLennan, 1995). Activity concentration of ^{226}Ra normalized to average soil and sediment concentration of Eastern USA (Greeman and Rose, 1996) (a). Chondrite-normalized REE concentrations (McDonough and Sun, 1995) (b) 53

Figure 4-15: Proportion (%) of elements extracted at the first extraction step (Figure 3-2.) from the total amount of these elements in samples from Askola 54

Figure 4-16: Chondrite-normalised REE concentrations in leachates extracted at the first extraction step (Figure 3-2) from samples from Askola (McDonough and Sun, 1995) 55

Figure 4-17: Proportion (%) of elements extracted at the third extraction step (Figure 3-2) from the total composition of samples from Askola 56

Figure 4-18: Chondrite-normalised REE concentrations in leachates extracted at the third extraction step (Figure 3-2) from samples from Askola (McDonough and Sun, 1995) 56

Figure 4-19: Proportion (%) of elements extracted at the fourth extraction step (Figure 3-2) from the total composition of samples from Askola..... 57

Figure 4-20: Proportion (%) of elements extracted at the last extraction step (Figure 3-2) from the total composition of samples from Askola 57

Figure 4-21: Chondrite-normalised REE concentrations in leachates extracted at the last extraction step (Figure 3-2) from samples from Askola (McDonough and Sun, 1995) 58

Figure 4-22: Sum (%) of extracted concentrations during the first three and four (in the case of Ask-A) extraction step 59

Figure 4-23: Heavy mineral (ρ > 2.8 g/cm^3) distribution of 0.125-0.250 mm sized grain fraction of Askola samples 60

Figure 4-24: Heavy mineral (ρ > 3.3 g/cm^3) distribution of < 0.063 mm sized grain fraction of Askola samples 60

Figure 4-25: Back scattered electron images of weathered heavy minerals from grain size fraction of 0.125-0.250 mm (a) and < 0.063 mm (b) of soil sample Ask-B, and fresh

(unweathered) from grain size fraction of 0.125-0.250 mm (c) and < 0.063 mm (d) of soil sample Ask-1. gr = garnet; am = amphibole; py = pyroxene; mg = magnetite/hematite/goethite; il = ilmenite; ti = titanite; zr = zircon 61

Figure 4-26: Back scattered electron images (BSE) of major U- and Th bearing minerals from grain size fraction of < 0.063 mm. a: U- and Th-bearing monazite (mn) grain in sample Ask-B; b: Th-bearing monazite (mn) with zircon (zr) inclusion in sample Ask-B; c: U-bearing, zoned, weathered xenotime (xen) in sample Ask-1; d: lenticular structured thorite (tho) in sample Ask-2; e: small (ca 20μm) uraninite (ur) grain with dark grey goethite in sample Ask-3; f: isometric uranothorite (utho) grain in sample Ask-B 62

Figure 4-27: Onion structured, zoned xenotime grain with iron rich layers < 0.063 mm of sample Ask-1. a: BSE image of the grain and the analysing points; b: X-ray map of P Kα analysed by energy dispersive spectrometer (EDS); c: X-ray map of Fe Kα analysed by wavelength dispersive spectrometer (WDS); d: X-ray map of Dy Mα analysed by WDS; e: X-ray map of Y Kα analysed by EDS; f: X-ray map of U Mα analysed by WDS. BSE image has a different orientation than X-ray maps. 64

Figure 4-28: Weathered uranothorite grain from grain size fraction < 0.063 mm of sample Ask-1. a: BSE image of the grain and the analysing points; b: X-ray map of P Kα analysed by energy dispersive spectrometer (EDS); c: X-ray map of Fe Kα analysed by wavelength dispersive spectrometer (WDS); d: X-ray map of Si Kα analysed by EDS; e: X-ray map of Th Mα analysed by WDS; f: X-ray map of U Mα analysed by WDS. BSE image has a different orientation than X-ray maps. 65

Figure 4-29: Uraninite grain with goethite filling in the middle from grain size fraction < 0.063 mm of sample Ask-3. a: BSE image of the grain and the analysing points; b: X-ray map of Ce Lα analysed by energy dispersive spectrometer (EDS); c: X-ray map of Fe Kα analysed by wavelength dispersive spectrometer (WDS); d: X-ray map of Si Kα analysed by WDS; e: X-ray map of U Mα analysed by WDS; f: X-ray map of Th Mα analysed by WDS. BSE image has a different orientation than X-ray maps. 66

Figure 4-30: Th-bearing orthobrannerite grain from grain size fraction < 0.063 mm of sample Ask-3. a: BSE image of the grain and the analysing points; b: X-ray map of Fe Kα analysed by wavelength dispersive spectrometer (WDS); c: X-ray map of U Mα analysed by WDS; d: X-ray map of Th Kα analysed by WDS. BSE image has a different orientation than X-ray maps. 67

Figure 5-1: Topographical map of the sampling area in Palmottu and the location of Palmottu in Finland. The sampling points are marked by red dots on the topographical map (modified after Kaija et al. (2003)). Elevation contour data © National Land Survey of Finland 70

Figure 5-2: Sampling points of samples Palm-C, Palm-384 (a) and Palm-362 (b) 71

Figure 5-3: Pre Quaternary geological map of the Nummi-Pusula area, southern Finland (Räisänen, 1986; Kuivamäki, 1997) 72

Figure 5-4: Detailed pre Quaternary geological map of the Palmottu study site (EGR: Eastern Granite, WGR: Western Granite) (modified after Kuivamäki (1997)) 72

Figure 5-5: A vertical section showing the general geological setting at Palmottu. WMG = Western Mica Gneiss, WG = Western Granite, PB = Palmottu Brook Valley, EG = Eastern Granite. Yellow lines show the six subvertical fracture zones (Blomqvist et al., 1998) 73

Figure 5-6: Quaternary deposits around Palmottu. Retreating ice sheet is depicted in the upper left corner. Flow lines show the main routes of melt water discharge. The insert at the lower right corner visualizes the position of the Palmottu site during retreat of the ice sheet, at the upper left corner the Palmottu site in Finland (denoted by red dot) and the four ice-marginal formations (I-III = Salpausselkä I-III and IV = Central Finland Ice Marginal Formation) (Ahonen et al., 2004) 75

Figure 5-7: Quaternary geological map of Palmottu area (Niemelä, 1985). The arrows show the sampling points 76

Figure 5-8: Soil sample from the top 40 cm (Palm-C) from Palmottu, Finland 78

Figure 5-9: Soil sample from depth 50-60 cm (Palm-384) from Palmottu, Finland..... 79

Figure 5-10: Sediment sample from depth 120 to 180 cm (Palm-362) from Palmottu, Finland..... 79

Figure 5-11: Grain size distribution of the three samples (Palm-C, Palm-384 and Palm-362) collected from Pamottu, Finland..... 80

Figure 5-12: Summarised chart of lithology of the samples (Palm-C, Palm-384 and Palm-362) collected from Palmottu sampling site, Finland 80

Figure 5-13: Activity concentrations of ^{226}Ra, ^{238}U and ^{228}Ra (^{228}Ac), ^{228}Th (^{208}Tl) as representing ^{232}Th-decay chain in samples from Palmottu. The reported uncertainties are expanded uncertainties using a coverage factor k=1..... 81

Figure 5-14: Elements of < 250 μm grain size fraction of Palmottu samples normalized to upper continental crust (UCC) (Taylor and McLennan, 1995). Activity concentration of ^{226}Ra normalized to average soil and sediment concentration of Eastern USA (Greeman and Rose, 1996) (a). Chondrite-normalised REE concentrations (McDonough and Sun, 1995) (b)..... 83

Figure 5-15: Portion (%) of elements extracted at the 1st extraction step (Figure 3-2) from the total composition of Palmottu samples 83

Figure 5-16: Chondrite-normalised REE concentrations (McDonough and Sun, 1995) in leachates extracted at the 1st extraction step (Figure 3-2) from Palmottu samples 84

Figure 5-17: Portion (%) of elements extracted at the 3rd extraction step (Figure 3-2) from the total composition of Palmottu samples 85

Figure 5-18: Chondrite-normalised REE concentrations (McDonough and Sun, 1995) in leachates extracted at the 3rd extraction step (Figure 3-2) from Palmottu samples..... 86

Figure 5-19: Portion (%) of elements extracted at the 4th extraction step (Figure 3-2) from the total composition of Palmottu samples 86

Figure 5-20: Portion (%) of elements extracted at the 6th extraction step (Figure 3-2) from the total composition of Palmottu samples 87

Figure 5-21: Chondrite-normalised REE concentrations (McDonough and Sun, 1995) in leachates extracted at the 6th extraction step (Figure 3-2) from Palmottu samples..... 88

Figure 5-22: Sum of extracted concentrations (%) during the four extraction steps from Palmottu samples..... 88

Figure 5-23: Heavy mineral ($\rho \geq 3.3$ g/cm^3) composition of < 0.063 mm grain size fractions of the three Palmottu samples 89

Figure 5-24: Back scattered electron images of heavy minerals ($\rho \geq 3.3$ g/cm^3) separated from the grain size fraction < 0.063 mm of the samples Palm-C (a), Palm-384 (b) and Palm-362 (c) (gr = garnet, il = ilmenite, ky = kyianite, mg = magnetite/hematite/goethite, mon = monazite, py = pyroxene, rut = rutile, ti = titanite, zr = zircon)..... 90

Figure 5-25: Back scattered electron images (BSE) of major U- and Th bearing minerals from grain size fraction of < 0.063 mm. a: Th containing monazite (mon) grain with U-thorite (U-tho) inclusion from sample Palm-C; b: Th-containing monazite (mon) with zircon (zr) from sample Palm-384; c: xenotime grain with Th-bearing zircon and zirkelite from the sample Palm-362; d: Th-bearing xenotime coexisting with zircelite from the sample Palm-362; e: thorite (tho) grain from the sample Palm-C; f: lenticular structured thorite (tho) from the sample Palm-C 91

Figure 5-26: Partly weathered Th-bearing monazite grain from grain size fraction < 0.063 mm of sample Palm-C. a: BSE image of the monazite and the analysing points; b: X-ray map of Ce Lα analysed by energy dispersive spectrometer (EDS); c: X-ray map of Fe Kα analysed by wavelength dispersive spectrometer (WDS); d: X-ray map of Si Kα analysed by WDS; e: X-ray map of Th Mα analysed by WDS; g: X-ray map of U Mα analysed by WDS 94

Figure 5-27: Partly weathered Th-bearing monazite grain from grain size fraction < 0.063 mm of sample Palm-C. a: BSE image of the monazite and the analysing points; b: X-ray map of Ce Lα analysed by energy dispersive spectrometer (EDS); c: X-ray map of Fe Kα analysed by wavelength dispersive spectrometer (WDS); d: X-ray map of Nd Lα analysed by EDS; e: X-ray map of Th Mα analysed by WDS; g: X-ray map of U Mα analysed by WDS 95

Figure 5-28: Highly weathered monazite grain from grain size fraction 0.125-0.250 mm of sample Palm-384. a: BSE image of the monazite and the analysing points; b: X-ray map of Ce Lα analysed by energy dispersive spectrometer (EDS); c: X-ray map of P Kα analysed by wavelength dispersive spectrometer (WDS); d: X-ray map of Fe Kα analysed by WDS; e: X-ray map of Th Mα analysed by WDS; f: X-ray map of U Mα analysed by WDS. BSE image has a different orientation than X-ray maps 96

Figure 5-29: Goethite with Th-rich rim from grain size fraction <0.063 mm of sample Palm-362. a: BSE image of the goethite and the analysing points; b: X-ray map of P Kα analysed by energy dispersive spectrometer (EDS); c: X-ray map of Fe Kα analysed by wavelength dispersive spectrometer (WDS); d: X-ray map of Si Kα analysed by WDS; e: X-ray map of Th Mα analysed by WDS; g: X-ray map of U Mα analysed by WDS..... 97

Figure 6-1: Location of the sampling area in Olkiluoto (Huhta, 2008) and Olkiluoto in Finland (a), and the position of the samples on profile 1 (b) 100

Figure 6-2: Pre-quaternary geological map of the Olkiluoto Island (W-Finland) (POSIVA, 2009)..... 102

Figure 6-3: Quaternary geological map of Olkiluoto Island (W-Finland). The investigation trench OL-TK14 where from the samples were collected is marked by an arrow 103

Figure 6-4: Geological section of trench OL-TK 14 (Huhta, 2008). The red frame shows section sampled 104

Figure 6-5: Photo of sample Olk-1 collected at 70 cm depth in profile 1 of trench OL-TK14, Olkiluoto, Finland 105

Figure 6-6: Photo of sample Olk-2 collected at 250 cm depth in profile 1 of trench OL-TK14, Olkiluoto, Finland 105

Figure 6-7: Photo of sample Olk-3 collected at 400 cm depth in profile 1 of trench OL-TK14, Olkiluoto, Finland 106

Figure 6-8: Grain size distribution of the three samples collected from the OL-TK14 trench at Olkiluoto sampling site (Huhta, 2008) 107

Figure 6-9: Summarised chart of lithology of the samples collected from OL-TK14 trench at Olkiluoto sampling site, Finland 107

Figure 6-10: Activity concentrations of ^{226}Ra, ^{238}U and ^{228}Ra (^{228}Ac), ^{228}Th (^{208}Tl) as representing ^{232}Th-decay chain in function of depth in samples from Olkiluoto. The reported uncertainties are expanded uncertainties using a coverage factor k=1 108

Figure 6-11: Upper continental crust- (UCC) (Taylor and McLennan, 1995) normalised trace elements of bulk samples from Olkiluoto. Activity concentration of ^{226}Ra was normalised to average soil and sediment concentration of Eastern USA (Greeman and Rose, 1996) (A). Chondrite-normalised (McDonough and Sun, 1995) REE concentrations (B) 110

Figure 6-12: Proportion (%) of elements extracted at the 1st extraction step (Figure 3-2) from the total composition of samples from Olkiluoto 111

Figure 6-13: Proportion (%) of elements extracted at the 2nd extraction step (Figure 3-2) from the total composition of samples from Olkiluoto 111

Figure 6-14: Chondrite-normalised REE concentrations (McDonough and Sun, 1995) in leachates extracted at the 2nd extraction step (Figure 3-2) from samples from Olkiluoto 112

Figure 6-15: Proportion (%) of elements extracted at the 5th extraction step (Figure 3-2) from the total composition of samples from Olkiluoto 113

Figure 6-16: Chondrite-normalised REE concentrations in leachates extracted at the 5th extraction step (Figure 3-2) from samples from Olkiluoto (McDonough and Sun, 1995) 113

Figure 6-17: Proportion (%) of elements extracted at the 6th extraction step (Figure 3-2) from the total composition of samples collected from Olkiluoto, Finland 114

Figure 6-18: Chondrite-normalised REE concentrations (McDonough and Sun, 1995) in leachates extracted at the last extraction step (Figure 3-2) from samples collected from Olkiluoto, Finland 115

Figure 6-19: Sum of extracted concentrations (%) during the four extraction steps from samples collected from Olkiluoto 115

Figure 6-20: Heavy mineral ($\rho \geq 2.8$ g/cm^3) composition of < 0.063 mm grain size fractions of the three Olkiluoto samples. 116

Figure 6-21: Back scattered electron images of heavy minerals ($\rho \geq 2.8$ g/cm^3) separated from the grain size fraction < 0.063 mm of the samples Olk-1 (a), Olk-2 (b) and Olk-3 (c) (am = amphibole, ap = apatite, bi = biotite, gr = garnet, il = ilmenite, ky = kyanite, mg = magnetite/hematite/goethite, mon = monazite, py = pyroxene, pyr = pyrite, rut = rutile, ti = titanite, zr = zircon) 117

Figure 6-22: Back scattered electron images of sulphide minerals identified in the samples from Olkiluoto, Finland. a: weathered pyrite from the grain size fraction 0.063-0.125 mm of the uppermost sample Olk-1; b: moderately weathered pyrite from the grain size fraction < 0.063 mm of the sample Olk-2; c: fresh, idiomorphic sphalerite from the grain size fraction < 0.063 mm of sample Olk-2; d: fresh arsenopyrite grain from the grain size fraction < 0.063 mm of sample Olk-2 118

Figure 6-23: Back scattered electron images of major U- and Th-bearing minerals in Olkiluoto samples and the points of analyses marked by arrows. a: altered apatite grain with monazite intercalation from grain size fraction 0.063-0.125 mm of the sample Olk-1; b: idiomorphic monazite grain with uranothorianite inclusion from grain size fraction 0.063-0.125 mm of the sample Olk-1; c: idiomorphic monazite grain neighbouring by pyrite and ilmenite minerals from grain size fraction < 0.063 mm of the sample Olk-2; d: idiomorphic, partly weathered xenotime grain with fractures from grain size fraction < 0.063 mm of the sample Olk-3; e: idiomorphic, fresh xenotime grain from grain size fraction 0.063-0.125 mm of the sample Olk-1; f: U-ThPO_4 –SiO_4 mineral coexisting with iron oxide from grain size fraction 0.063-0.125 mm of the sample Olk-2 119

LIST OF TABLES

Table 3-1: Lowest limit of detection (LLD) (ppm) for major and trace elements of bulk samples analysed by ICP-MS and ICP-AES at SGS, Toronto..... 41

Table 4-1: Activity concentrations (Bq/kg) of ^{238}U, ^{226}Ra and ^{228}Ra (^{228}Ac), ^{228}Th (^{208}Tl) as representing ^{232}Th-decay chain in vertical profile in bulk samples, from Askola, Finland. Activity concentration of ^{232}Th was calculated from Th concentration (ppm) measured by ICP-MS in SGS Lab, Toronto. The reported uncertainties are expanded uncertainties using a coverage factor k=1. 52

Table 4-2: Activity concentrations (Bq/kg) of ^{226}Ra, Rn production (Bq/(kg h)) and emanation factor in bulk and < 0.250 mm sized grain fraction of Askola (Ask) samples. The reported uncertainties are expanded uncertainties using a coverage factor k=1. 52

Table 4-3: Chemical composition of different areas of the weathered, zoned xenotime grain presented in Figure 4-27 from grain size fraction of < 0.063 mm of sample Ask-1. Concentrations are presented in wt.%. 68

Table 4-4: Chemical composition of different areas of the weathered uranothorite grain presented in Figure 4-28 from grain size fraction of < 0.063 mm of sample Ask-1. Concentrations are presented in wt.%. 68

Table 4-5: Chemical compositions of different areas of the Nb-bearing uraninite grain with goethite filling presented in Figure 4-29 from grain size fraction of < 0.063 mm of sample Ask-3. Concentrations are presented in wt.%. 69

Table 4-6: Chemical compositions of different area of the weathered Th-bearing orthobrannerite grain presented in Figure 4-30 from grain size fraction of < 0.063 mm of sample Ask-3. Concentrations are presented in wt.%. 69

Table 5-1: Activity concentrations (Bq/kg) of ^{238}U, ^{226}Ra and ^{228}Ra (^{228}Ac), ^{228}Th (^{208}Tl) as representing ^{232}Th-decay chain in Palmottu (Palm) samples..... 81

Table 5-2: Activity concentrations (Bq/kg) of ^{226}Ra, Rn production (Bq/(kg h)) and emanation factor in Palmottu (Palm) samples..... 82

Table 5-3: Chemical composition of partly weathered Th-bearing monazite grain from grain size fraction < 0.063 mm of sample Palm-C (Figure 5-26). POI = Point of interest. 98

Table 5-4: Chemical composition of partly weathered Th-bearing monazite grain from grain size fraction < 0.063 mm of sample Palm-C (Figure 5-27). POI = Point of interest. 98

Table 5-5: Chemical composition of highly weathered Th- and U-bearing monazite grain from grain size fraction 0.063-0.125 mm of sample Palm-384 (Figure 5-28). POI = Point of interest. 98

Table 5-6: Chemical composition of goethite grain with Th-rich rim from grain size fraction < 0.063 mm of sample Palm-362 (Figure 5-28). POI = Point of interest. 99

Table 6-1: Activity concentrations (Bq/kg) of ^{238}U (^{234m}Pa), ^{226}Ra and ^{228}Ra (^{228}Ac), ^{228}Th (^{208}Tl) as representing ^{232}Th-decay chain in vertical profile of trench OL-TK14, Olkiluoto, Finland..... 108

Table 6-2: Activity concentrations (Bq/kg) of ^{226}Ra, ^{222}Rn production (Bq/(kg h)) and emanation factor of Olkiluoto (Olk) samples..... 109

Table 6-3: Chemical composition of major uranium and thorium bearing minerals presented on Figure 6-23, The codes of analysing points are in parentheses (mn = monazite, utho = uranothorite, xen = xenotime, POI = point of interest)..... 120

Table 7-1: Correlation (Pearson product moment) factors between total and extracted concentration of the elements (extr-total) and portion of the finest fraction and the extracted proportion of the elements analysed. Ex = “exchangeable” step, Ox = “oxide” step, Res = “residual” step. 123

Table 7-2: Summarised table of ^{226}Ra-content and emanation coefficients of bulk and < 0.250 mm grain size fraction, the proportion of the < 0.250 mm grain size fraction and proportion of ^{226}Ra in the extractants compared to the sum of Ra leached out from < 0.250 mm grain size fractions of the six studied samples from Askola, Finland..... 128

Table 7-3: Summarised table of ^{226}Ra-content and emanation coefficients of bulk and < 0.250 mm grain size fraction, the proportion of the < 0.250 mm grain size fraction and proportion of ^{226}Ra in the extractants compared to the sum of Ra leached out from < 0.250 mm grain size fractions of the three samples from Palmottu, Finland..... 129

Table 7-4: Summarised table of ^{226}Ra-content and emanation coefficients of bulk sample, the proportion of the < 0.250 mm grain size fraction and proportion of ^{226}Ra in the extractants compared to the sum of Ra leached out from < 0.250 mm grain size fractions of the three samples from Olkiluoto, Finland..... 131

APPENDICES

Annex 1 Major and trace element content of bulk samples.

Annex 2 Major and trace element content of leachates extracted by sequential chemical extraction.

Annex 3 Raw chemical composition of minerals analysed by EPMA using WDS and the correlation coefficients between the selected elements.

1. INTRODUCTION

In Finland, indoor radon concentrations are among the highest in the world. The reasons of the high concentrations are the cold climate, the foundation construction and air tightness of buildings, elevated uranium concentration in the soil and bedrock and permeable sand and gravel areas especially at esker areas. In some cases, radon-rich water from drilled wells is a notable source of radon. From the annual average radiation dose of the population more than 50 percent is due to indoor radon (Figure 1-1.) (Arvela, 2002).

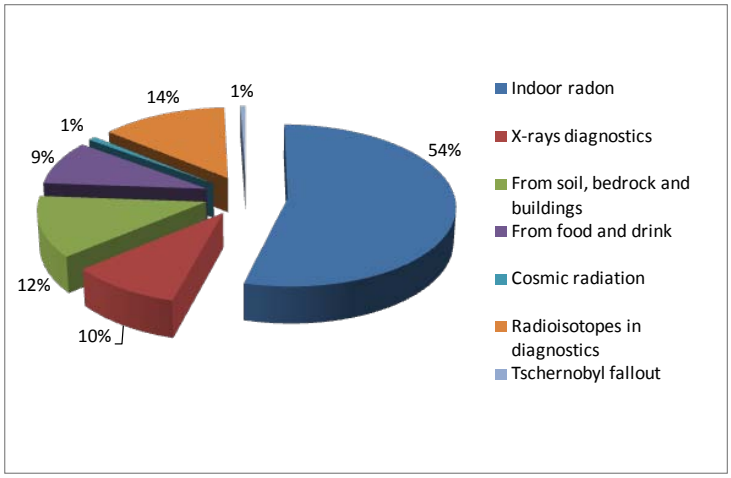

Figure 1-1: Annual average radiation dose of Finns (Muikku et al., 2005)

When the major contribution from radon in indoor air to radiation dose was first understood during the 1970s, a study of its geographical distribution in Finland started. The new Finnish Radiation Act came into force on January 1st, 1992. According to the Act, the Radiation and Nuclear Safety Authority (referred as STUK hereafter) is the competent authority. The Act also requires natural radiation to be monitored. Safety guides concerning radon in mining, underground excavation and other workplaces, as well as radioactivity in building materials have already been issued. In 1992 the Ministry of Social Affairs and Health issued a new resolution on limits for radon concentration in residences. According to the resolution, the indoor radon concentration should not exceed 400 Bq/m^3 in already existing houses. Future buildings should be planned and constructed in such a way that the radon concentration does not exceed 200 Bq/m^3. In this connection radon concentration means the annual average ^{222}Rn activity concentration. The resolution also states that the concentration must be measured using a method approved by the STUK, the measuring period being at least two months (Arvela, 1995a). Data on radon concentration, the type of construction of the building and the geology of the building site were recorded in the STUK's indoor radon database, which

includes today data on around 80,000 dwellings (Valmari et al., 2010). The variations in the uranium concentration and the permeability of the soil and bedrock affect the geographical distribution of indoor radon concentrations. The mean radon concentration is usually the highest in areas where houses are built on permeable soil types. On the basis of indoor radon measurements, the most radon-critical landforms in Finland are the eskers. These long and narrow, steep-sided ridges formed by glacial rivers are composed of stratified sand and gravel, making them permeable to water and air (Voutilainen and Mäkeläinen, 1993; Mäkeläinen et al., 2001). Less than 20 % of the houses are built on eskers and other permeable soil types in Finland. However, about 40 % of the cases exceeding the limit are found in areas consisting of sand and gravel. In the most radon-prone area, the percentages of houses exceeding the limit are about 30 % and 50 %, respectively. Therefore more detailed measurements in the area are necessary (Weltner et al., 2002).

In this thesis the behaviour of natural radionuclides (mainly U-series) and chemical fronts in the geo-environment as a basis for assessment of radon emission were studied. Understanding the behaviour of natural U-series radionuclides in the geo-environment is indispensible for the evaluation and quantification of safety risks caused by radon emission. Natural weathering processes in rock and overburden cause mobilisation, migration and, eventually, subsequent immobilisation of uranium and its decay products. Different geochemical behaviour of the U-series radionuclides leads to separation and selective enrichment of nuclides. Observations on primary and secondary U-bearing minerals and in overburden in natural geological settings are necessary to understand and quantify the process mechanisms and the spatial and time scales involved. The phenomenological and mechanistic description of natural geochemical cycles builds the basis for deeper understanding of groundwater evolution, chemical buffering and migration mechanisms.

For these purposes three sampling sites were selected in southern Finland (Figure 1-2). Askola and Palmottu sites represent glacial sediments with enhanced uranium content. In Olkiluoto site a till with well developed redox profile and normal background U content was studied. In two areas (Askola and Olkiluoto) the vertical migration and in one (Palmottu) the horizontal migration was studied. All together 12 samples were collected from the three areas, and multidisciplinary analysis were carried out in order to find the answer for the abovementioned questions.

Figure 1-2: The three sampling sites in Finland

In the thesis first I present the literature overview on geological description of the studied areas of Finland as well as the relevant information on uranium, thorium, radium an radon dispersion in hydrogeological media. In the following the description of the different analytical methods I used is given. The selected three sampling sites and the results of the analyses carried out on the samples are introduced followed by discussion of the results. Finally, I will sum up the most important conclusions of the study.

2. LITERATURE OVERVIEW

2.1. General description of geology of Finland

2.1.1. Precambrian geology

The bedrock of Finland belongs to the Precambrian East European craton of northern and eastern Europe and north-western Russia. Precambrian crystalline rocks are cropped out only in the northern and south-western parts of the craton, in the Fennoscandian and Ukrainian shields, respectively. The most important events during the evolution of the Finnish bedrock occurred at 2800-2700 Ma and 1900-1800 Ma. In those times, continental crust segregated from Earth's mantle in two major orogenies resulted the in the Achaean and Paleoproterozoic crust of Finland. Finland forms about one third of the Fennoscandian Shield which are exposed with younger sedimentary rocks and the Caledonian mountain chain. Four areas can be distinguished from one another at the Fennoscandian Shield: the Achaean, the Svecofennian, and the Sveconorwegian domains, and the Transscandinavian igneous belt lying between the latter two (Figure 2-1) (Vaasjoki et al., 2005, and references therein).

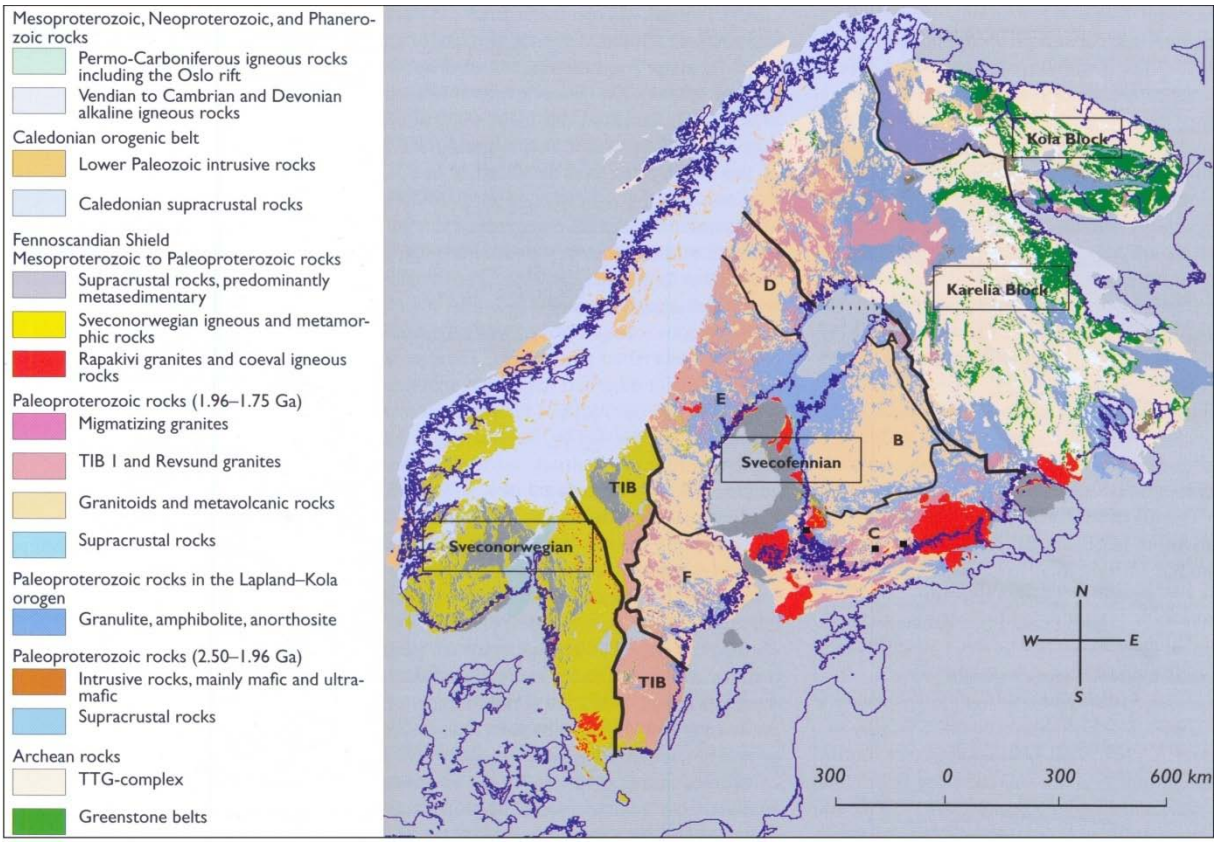

Figure 2-1: Simplified geological map of the Fennoscandian Shield after Koistinen et al. (2001). TIB denotes the Transscandinavian igneous belt. The subdivisions of the Svecofennian are: (A) The Primitive arc complex of central Finland; (B) The Accretionary arc complex of central and western Finland; (C) The Accretionary arc complex of southern Finland; (D) The Skellefte district; (E) The Bothnian basin; and (F) The Bergslagen district. Sampling sites for this study are marked by small filled black squares in domain C.

The northern and eastern parts of Finland belong to the >2.5 Ga Achaean domain, divided usually into the Kola and Karelia blocks, whereas the central and southern parts comprise the Svecofennian Paleoproterozoic rocks, 1.93-1.80 Ga in age. The orogenic movement waned in southern Finland about 1.8 Ga ago. As the bedrock cooled, fissures opened and yielded way for deep-seated magmas, which crystallised in the upper crust as the so-called postorogenic (1.81-1.77 Ga) granites (Vaasjoki et al., 2005). Only a small part of the Finnish bedrock is younger than 1.8 Ga; the most significant formations are the 1.65-1.54 Ga rapakivi granites. After the intrusion and solidification of the rapakivi granite magmas in batholiths no major magmatism has occurred in Finland, but considerable graben formation took place during the Mesoproterozoic and at least southern Finland was covered by Palaeozoic-Mesozoic sediments (Vaasjoki et al., 2005, and references therein).

2.1.2. Quaternary geology

In Finland, as in glaciated areas in general, the bedrock and overlying sediments usually show sharp contact. A geological discontinuity, or hiatus, prevails between the bedrocks, which are at least 1,000 million years old, and the young sediments, which are no more than

150,000 years old. Nearly all sediments and rocks formed during this time interval have been eroded and removed away. Sediments and soils in Finland have formed during the Quaternary, during the interglacial events. The last ice age ended ca. 9,000 years ago. A sedimentary cover of about seven meters average thickness overlay the bedrocks. The outcrops of bedrock, which nearly always are composed of unaltered rocks, account for 3 % of the surface, and areas where the sediment cover is less than 1 m thick account for 12 % of the surface (Koljonen, 1992) (Figure 2-2). The clastic deposits are predominately quaternary formations and till, which is found nearly everywhere, is the most common component. The till was formed from bedrock when the slowly flowing glacial ice dislodged, crushed, and ground the rock material. Unsorted or somewhat sorted sediment, it is composed of angular or slightly rounded mineral and rock fragments ranging in size from boulders to clay. Gravely till accounts for ca. 10 %, sandy till for 75 %, and fine-grained till for 15 % of all tills. The melting ice water from glaciers have abraded, rounded, and sorted the sediments during transport, and accumulated them in glaciofluvial deposits composed of rounded cobbles and boulders, gravel, sand, or fine sand. The flat alluvial plans and deltas also have glaciofluvial origin. The most important glaciofluvial formations in Finland are the eskers, which are elongate, narrow, sinuous ridges of glacial till which commonly show a measure of sorting, or rude stratification. Their crests are rounded, their side slopes are moderately steep, and their longitudinal slope is gentle. Their crests seldom stand much higher than 30 meters above their surrounding areas. Some eskers may be as long as 500 kilometres, although most are shorter. Small eskers have been seen forming in the marginal zone of the glaciers. There is consensus today that eskers are deposits, which are made by streams flowing in ice tunnels at the bottom of the glacier (Putnam, 1971). Like conventional streams they may meander, occasionally they are joined by tributaries, but unlike ordinary streams they may climb up hill slopes, especially where they cross low ridges through passes. The Salpausselkä ice marginal formations in southern Finland (Figure 2-2) are typical of the gravel and sand deposits that form during deglaciation at the margin of a stagnant continental ice sheet. The First Salpausselkä was formed 11,200-10,950 years ago, the Second Salpausselkä 10,450-10,250 years ago, and the Third Salpausselkä, in south-western Finland, 10,050-9,950 years ago. The finest material is carried in suspension and, as the rate of flow decreases, is deposited at the bottom of water basins. An example of this is the extensive clay deposit covering the bottom of the ancient Baltic Sea. Today these deposits lie above sea level and form Finland’s most important agricultural areas. The organic-rich sediments, which include gyttja, peat, and mull humus, are also considerable in Finland (Koljonen, 1992).

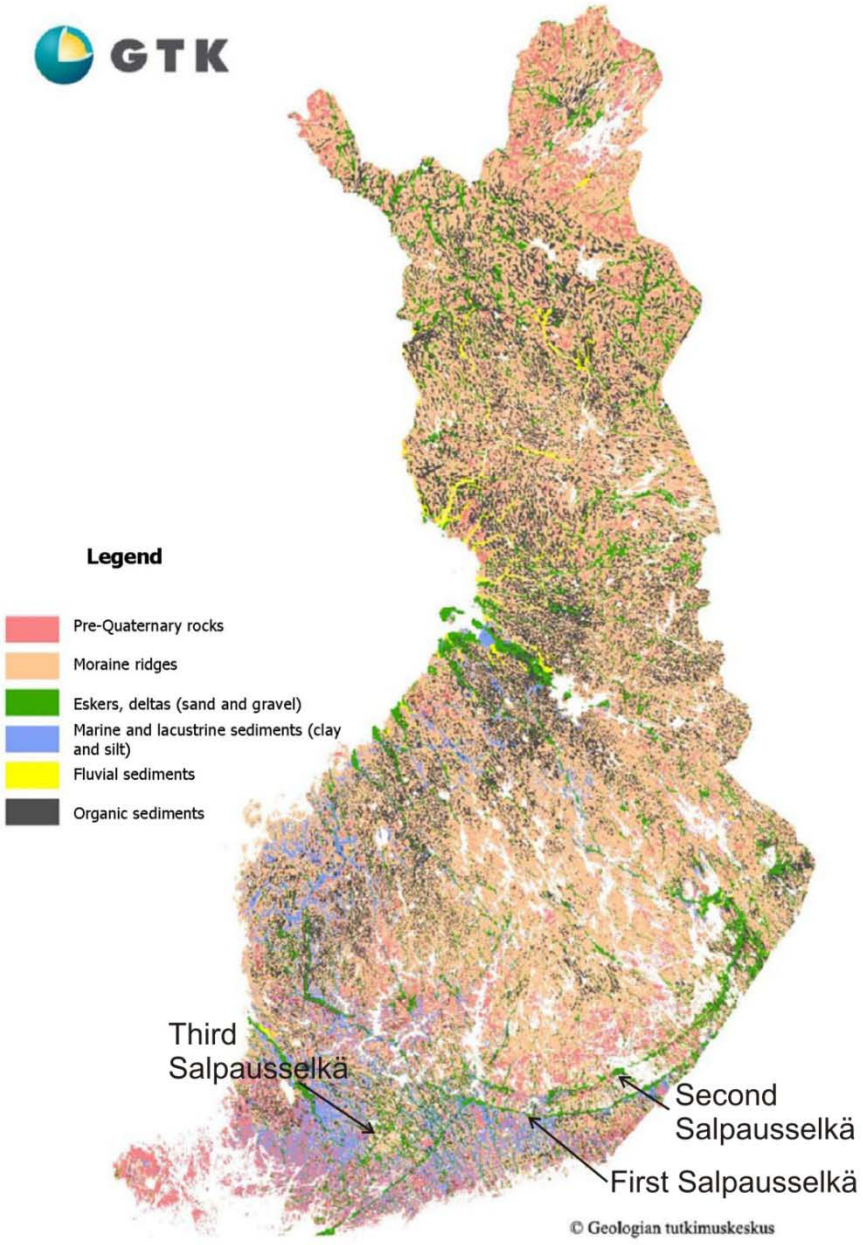

Figure 2-2: Geological map of quaternary sediments of Finland (GTK, 2010)

In Finland the ice age began about 2.4 Ma ago; during the last 1 Ma about ten glaciations occurred, which were interrupted by warm interglaciation of only short duration (about 10,000 years). The first glaciations removed most of the weathered layers and exposed the fresh bedrock surface. During the too short periods of the interglacials most probably no significant weathering layers could be formed. The thickness of the total layer eroded by the glaciations has been often overestimated. The total thickness probably did not exceed about 10 m, except in basins and along weakness zones now forming lakes and river valleys (Hellmuth et al., 2003).

The most common soil type in Finland is podzol soil which form on glaciofluvial deposits. The typical horizon sequence of podzol consists of a dark organic surface layer (O) on top, followed by a gray depleted eluvial horizon (E) and enriched illuvial[1] B horizons that are coloured by organic matter (Bh) and iron oxides (Bs). The pedogenic process leading to this horizon pattern is called podzolisation and has been subject to numerous studies. However, the podzolisation mechanisms are still debated intensively in literature (Anderson et al., 1982; Buurman and Jongmans, 2005; Jansen et al., 2005; Wiederhold et al., 2007). General prerequisite for podzolisation is well-drained substrate that is poorly-buffered against acidification (typically quartz-rich sands or granite), a cool humid climate, and a vegetation producing litter that is only slowly biodegradable (typically coniferous forests or heath). Organic acids that are released from the organic surface layer (O horizon) under very acidic conditions (pH < 4) form complexes with iron and aluminum thereby leaching the upper soil and creating the iron-depleted, gray E horizon. The iron–aluminum–organic complexes are then transported vertically downward until they re-precipitate in the B horizon. Often, an organic-rich black Bh horizon is overlying a reddish oxide-rich Bs horizon. The podzolisation process has important consequences on many physical and chemical soil properties and influences ecosystem functions and land use. Podzolisation also changes the element distribution of elements other than iron and aluminum (Tyler, 2004; Donisa et al., 2005).

2.2. Physical and geochemical characterisation of Th, U, Ra and Rn

2.2.1. Uranium, thorium and radium

2.2.1.1. Uranium, thorium and radium in rocks

The series of nuclides resulting from the decay of ^{238}U, consists of isotopes of U, Th, Pa, Ra, Rn, Po, Pb and Bi with mass number $4n+2$, where n is an integer. Also known as uranium decay series or uranium-radium series (Figure 2-3).

[1] Illuviation is a process by which material is washed down from one layer of soil to a lower layer.

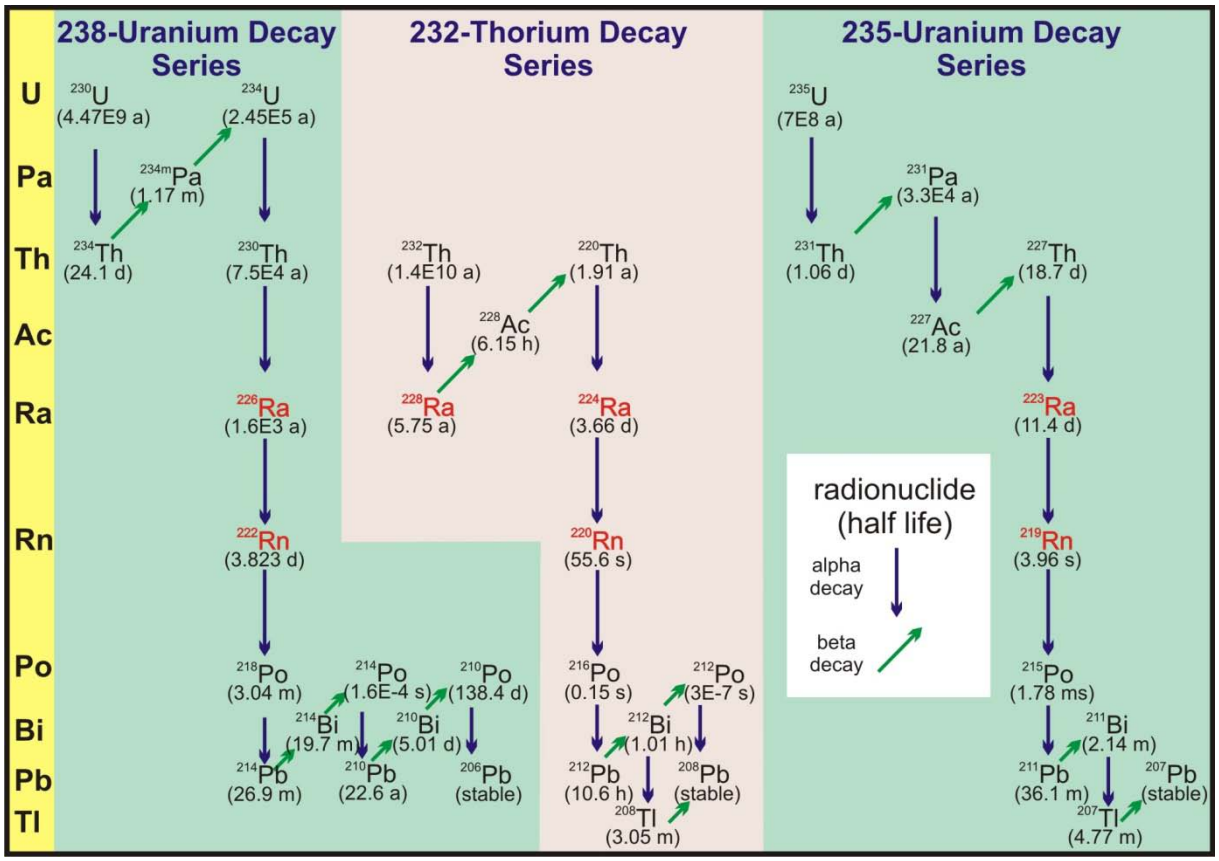

Figure 2-3: Decay chains of ^{238}U, ^{232}Th and ^{235}U

Uranium has more than 20 isotopes but from these only ^{238}U, ^{235}U and ^{234}U with half life of 4.46 Ga, 0.7 Ga and 245 ka, respectively, are relevant in the environment. From these ^{238}U and ^{235}U have their own decay series, ^{234}U is a member of ^{238}U decay series (Figure 2-3). Uranium exists in four valence states: U^{3+}, U^{4+}, U^{5+} and U^{6+}, although only the tetra- and hexavalent states are commonly found in naturally occurring groundwater. Hexavalent uranium is invariably found associated with oxygen as the very stable divalent uranyl ion (UO_2^{2+}) and occurs whenever the electrochemical potential is oxidizing such as in weathered rock and surficial material. Tetravalent uranium is found in reducing environments such as in unweathered and unaltered rock where a reducing electrochemical potential is maintained. The uranium most commonly occurs as oxides, hydroxides, phosphates, but is also present as carbonates, sulphates, arsenates, vanadates, molybdenates and silicates form and tends to have affinities with hydrocarbon complexes (Durrance, 1986). It is often associated with Th, Zr, Hf, Rare Earth Elements, Nb and Ta enrichment. The uranium is one of the LIL (Large Ion Lithophile) elements (Cortini, 1984). Numerous researchers (Tanner, 1980; Greeman and Rose, 1996; von Gunten et al., 1999; Payne et al., 2001; Jerden et al., 2003) suggests that uranium and thorium are not compatible with the crystalline structure of major minerals and, hence, are commonly found in accessory minerals such as allanite, monazite, apatite, zircon,

xenotime, etc., are adsorbed on the surface of clay particles, or are present in other coatings. In many granites and volcanic rocks, however, there is also appreciable concentration on grain borders or disseminated through the major minerals (Szalay and Sámsoni, 1969; Hamilton, 1975; Rich et al., 1977). In comagmatic suites of igneous rocks, U appears to follow closely the usual differentiation sequence, the highest concentrations normally occurring in the most potassic and most silica-rich members. Gabbros and other basic igneous rocks have their alpha activity distributed fairly evenly among the various major constituents. However, probably, in basic rocks the most important uranium carrier is apatite, which may incorporate small quantities of uranium by isomorphic substitution of U^{4+} for Ca^{2+} ions (Dongarra, 1984). Volcanic rocks have a uniform distribution of radioactivity among their constituent phases, and rapid cooling of magma leaves a large part of the uranium scattered through the non- or cryptocrystalline matrix (Dongarra, 1984). Adams et al. (1959) estimated that 60-85 % of the uranium in igneous rocks is present in mineral phases that are resistant to chemical alteration; approximately 15-40 % is transported in the dissolved form by liquid water.

Thorium has generally been considered to be a lithophile element of low geochemical mobility, because it cannot be oxidised under geologic conditions to a hexavalent state to form an analogue of the uranyl ion, and occurs naturally only as the comparatively insoluble tetravalent ion (Langmuir and Herman, 1980). Thorium is the largest of the tetravalent cations with an ionic radius comparable to that of U^{4+} and Ce^{4+}. The similarities in ionic size, outer electron configuration and bond character are the main reasons for the close relationship between the crystal chemistry of thorium, cerium, uranium and zirconium. Only two long-lived isotopes of thorium occur in nature. The major one is ^{232}Th, which is the parent nuclide of a long decay series terminating with ^{208}Pb. The other important natural isotope of thorium, ^{230}Th, is generally present in minerals, which contain uranium. Thorium-230 is the decay product of ^{234}U, an intermediate in the decay chain of ^{238}U (Figure 2-3). Thorium concentration of igneous rocks generally increases toward the silicic, more differentiated members of a series. Thorium is a major cation in a variety of minerals, none of which are at all common. Pure thorium minerals, like thorianite (ThO_2) or thorite ($ThSiO_4$), are rather rare. The rarity of thorium, its ability to substitute for other elements in crystal lattices, and the absence of a geochemical mechanism of concentration of the element all combine to render thorium a highly dispersed material. Dispersal contrasts markedly with the tendency of uranium to become concentrated by precipitation from waters carrying the soluble, oxidised uranium (Sheppard, 1980b).

The radium isotopes are members of the uranium and thorium decay schemes. Radium, along with uranium and thorium is a naturally occurring radioactive element found in the Earth's crust. All of the isotopes of radium are radioactive; those most commonly found in nature are ^{226}Ra, ^{228}Ra, ^{224}Ra and ^{223}Ra (Figure 2-3). The half-lives of ^{226}Ra, ^{228}Ra, ^{224}Ra and ^{223}Ra are 1620 years, 6.7 years 3.64 days and 11.4 days, respectively. Radium is an alkaline earth element with chemical properties similar to those of barium. It has only one oxidation state (+2) in solution, is highly basic and it does not form complexes easily (Kirby and Salutsky, 1964). Radium hydroxide, $Ra(OH)_2$, is the most soluble one of the alkaline earth hydroxides. It is more soluble than the actinium and thorium hydroxides. Radium forms water-so1uble bicarbonate and chloride compounds. It co-precipitates with Ba^{2+} as chromate or sulphate (Koczy, 1961). Consequently, it is found in lower concentrations in nature than is uranium. The content of radium (like uranium and thorium) is higher in granites and other acidic rocks than in basic rocks (Vinogradov, 1959). Megumi and Mamuro (1977), gives ^{226}Ra/^{228}U activity ratios for various natura1 materials and these show that there is more radium than uranium in some of the solid materials due to the solubility differences of the two elements. The ^{226}Ra, as well as uranium and thorium concentration increases with particle size below 100 μm (Megumi and Mamuro, 1977; Landa, 1984; Breitner et al., 2008). In addition to its different chemical nature, radium has different ionic radius compared to its parent uranium, it can leach out from the crystal lattice more readily than uranium (Titaeva, 1967). Therefore, water circulating in an ore body may contain more radium than is in equilibrium with uranium and, consequently, sediments containing organic matter may become enriched in radium. Titaeva (1967) reported a radium/uranium ratio of 10 in a stratum of peat buried in a sedimentary uranium deposit.

2.2.1.2. Behaviour of uranium, radium and thorium during low temperature secondary processes

Mobilisation

Mobilisation of U from primary mineralisation by weathering and subsequent immobilisation leads to secondary U mineralisation. A characteristic feature of uranium is its ability to be oxidised to the highly soluble uranyl ion (UO_2^{2+}). This ion is easily mobilised in surface and near-surface waters. Data reported by Richardson (1964) and Rogers (1964) indicate a near-surface depletion of uranium, except in a few zones where the mobilised uranium is redeposited by circulating ground water. Uranium in carbonate solution could form negatively charged or neutral carbonate and hydroxide complexes, which would be highly

mobile in the soil-rock system (Grabovnikov and Samsonova, 1968; Yamamoto et al., 1973). The fact that uranium forms complexes will greatly increase its solubility in an oxidizing environment. In carbonate-free water oxide and hydroxide complexes predominate at all geologically realistic pH's (4-9) (Bird, 1979). Langmuir (1978) and Tripathi (1979) showed that fluoride complexes increase the solubility of uraninite by two orders of magnitude relative to its solubility in fluoride-free waters. The phosphate ion also increases the solubility of uraninite. More specifically, phosphate complexes are expected to predominate over other inorganic complexes of uranyl in waters in the pH range from 4 to 7.5 with $P_{CO_2} = 10^{-2.5}$ atm, $\Sigma mU^{6+} = 10^{-8}$ and $\Sigma\, mPO_4 = 10^{-6}$ (Langmuir, 1978). The comparative importance of the various uranyl complexes is evident from Figure 2-4. The diagram shows concentrations of chloride, fluoride, sulphate, phosphate and silica, typical of ground waters in the uraniferous Wind River Formation in the Shirley Basin of Wyoming as a function of of pH at 25°C and $10^{-2.5}$ atm CO_2 partial pressure (Langmuir, 1978). The plot shows that fluoride complexation would predominate below pH 4. Within the pH range (4-9) of general ground waters in Palmottu and Olkiluoto areas studied (Kaija et al., 2003; Itävaara et al., 2008) both phosphate and carbonate complexes can predominate.

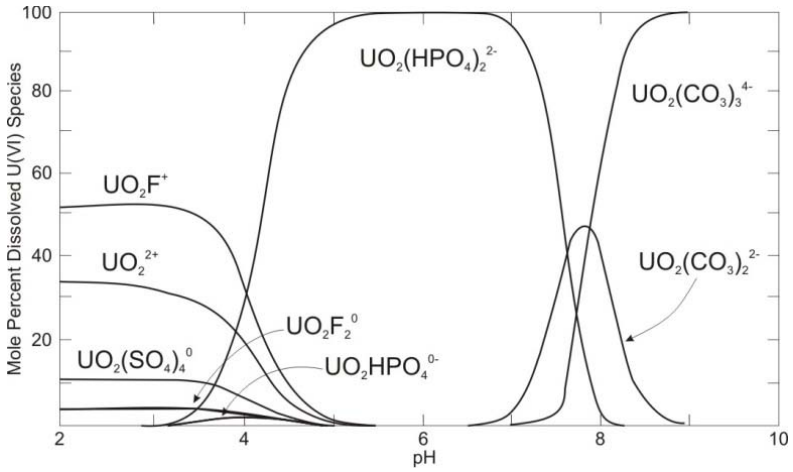

Figure 2-4: Distribution of uranyl complexes vs. pH for some typical ligand concentrations in ground waters of the Wind River Formation at 25 °C, $P_{CO_2} = 10^{-2.5}$ atm, ΣF = 0.3 ppm, ΣCl = 10 ppm, ΣSO_4 = 100 ppm, ΣSiO_2 = 30 ppm (Langmuir, 1978)

Uranium is mobile in waters with low concentrations of calcium salts, and it can be concentrated from water if the geochemical setting is suitable (Titaeva, 1967). As weathering and soil profile development continue and the system sustains plant growth, the naturally occurring uranium is redistributed. Uranium in solution will move to the plant root system, or it may be leached into the groundwater (Sheppard, 1980b). Advective transport in solution is one mechanism by which soluble uranium may move vertically or horizontally in a profile. Downward movement could be in response to the gravitational potential; upward movement

could be facilitated either by capillary action in fine-textured materials or by forces exerted by plant roots extracting water from the surrounding medium. Horizontal migration, often referred to as through flow, is a possible mechanism for transport in a sloping landscape (Sheppard, 1980b). Another mode of transport which seems to have been neglected in radioactive solute modelling is transport by the particles themselves. Particles move in response to gravitational forces, helped along by turbulent water. The macroscale processes are usually considered to be runoff and erosion. The microscale processes which are connected to phenomena like matrix diffusion and sorption could contribute significantly to radionuclide movement where finely weathered minerals such as biotite and clay minerals are loaded with the nuclide because of adsorption (Sheppard, 1980b).

Most Th host minerals are highly refractory to weathering and thorium has long been considered a very insoluble and immobile element in natural waters. However, thorium complexation can increase the mobility of dissolved thorium by many orders of magnitude below pH 8 relative to the solubility of thorium bearing minerals in pure water. The predominant thorium species are $Th(SO_4)_2^0$, ThF_2^{2+} and $Th(HPO_4)_2^0$, below pH ca. 4.5; $Th(HPO_4)_3^{2-}$ from about pH 4.5 to 7.5; and $Th(OH)_4^0$ above pH 7.5 (Figure 2-5).

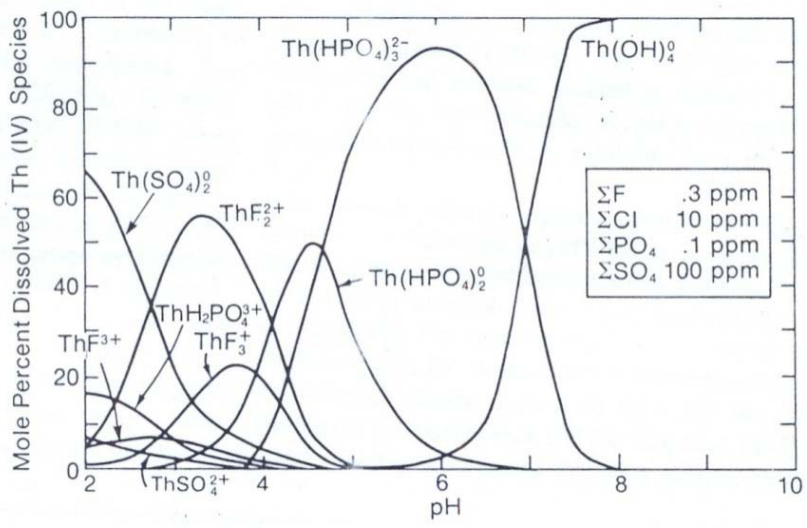

Figure 2-5: Distribution of thorium complexes vs pH for some typical ligand concentrations in ground water at 25 °C with ΣTh = 0.01 ppb (Langmuir and Herman, 1980)

Evidence indicates that the transport of thorium in solution is a very negligible process. Since a significant amount of the thorium in the environment is adsorbed onto clay-sized particles, or precipitated, the major means of transport are by wind and water erosion, and by mineral and/or organic particles moving through the soil system. Baranov et al. (1964) stated that, unlike uranium, thorium in the natural environment is transported primarily in the colloidal

form. Dementyev and Syromyatnikov (1965) concluded that thorium migrated in groundwater as colloidal particles and as anionic complexes, the latter probably with organic acids.

In fresh waters, the relationships between Ra isotopes and between Ra and Rn suggest that Ra found in aqueous samples is generated primarily by alpha recoil from the decay of its Th parents on the aquifer solids, rather than by weathering processes, and that transport of Ra along a flow path is retarded several orders of magnitude relative to conservative solutes (Krishnaswami et al., 1982). Of all the aqueous species and solids listed by Wagman et al. (1982), only Ra^{2+} ion and $RaSO_{4(c)}$ (if sulphide presents in the system) are likely to have any significance in the environment (Figure 2-6).

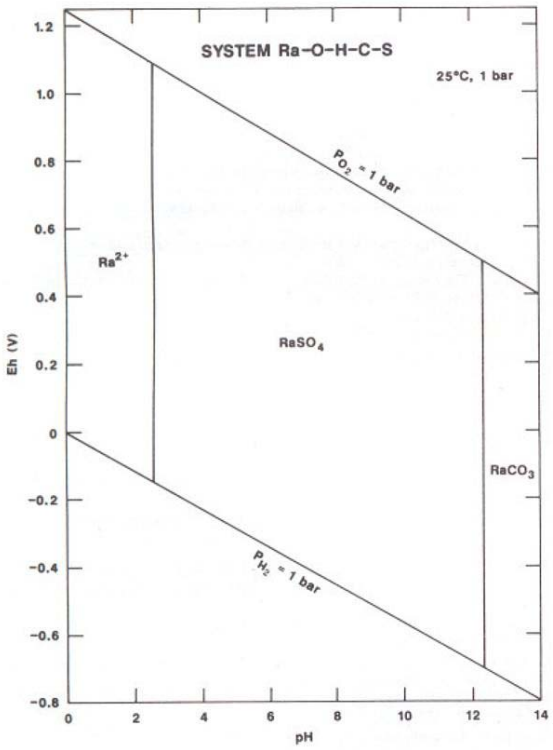

Figure 2-6: Eh-pH diagram for part of the system Ra-O-H-C-S (Eh = oxidation potential). Assumed activities for dissolved species are: Ra = 10^{-8}, S = 10^{-3}, C = 10^{-3} (Takeno, 2005)

On the other hand, $RaCO_{3(c)}$ as a solid solution component and the complexes $RaOH^+$, $RaCl^+$, $RaCO_3^0$ and $RaSO_4^0$ should influence radium mobility in some waters (Langmuir and Riese, 1985). Radium mobility or adsorption effectiveness is understood to vary with chemical parameters including pH, salinity, reduced conditions, supersaturation with respect to barite, microbial sulphate reduction affecting barite stability, and microbial Fe oxide reduction (Herczeg et al., 1988; Landa et al., 1991; Dickson and Herczeg, 1992; Martin et al., 2003; Wood et al., 2004; Grundl and Cape, 2006). Vinson et al. (2009) pointed out that the primary source of Ra in groundwater is recoil from parent radionuclides on fracture surfaces,

which is balanced by adsorption of Ra. While groundwater chemistry is mostly acquired during recharge through the soil and saprolite, radionuclides are generated by recoil in the saturated bedrock fracture network. Thus, the efficiency of adsorption of Ra is influenced by the redox-sensitive stability of adsorption sites and/or competition with other divalent cations.

Kovalevsky et al. (1966) extracting uranium-rich soils concluded that 2-19 % of the total uranium in the soil was mobile. Greeman et al. (1999) pointed out that on average 35 % of the total radium is easily extractable compared to only 16 % of the parent uranium. Sequential extraction of Finnish podzol samples showed that ca. 20 % of total uranium and 40 % of total radium is present in easily leachable pedogenic phases (Breitner et al., 2008). Aubert et al. (2004) concluded that more than 10% of total uranium and thorium could be leached from podzol soils in Vosges Mountains. To assess the behaviour of uranium under oxidizing conditions in soil or rock media accurately, the relative stability of the various complexes with the number of ligands present in the system must be known. The groundwater chemistry must be well defined. Very little thermodynamic data for temperature below 20 °C are available for the actinides and, in Finland at least, the groundwater and unconsolidated media near the surface are probably below this temperature for most of the year.

Immobilisation

Uranium can be removed from the ground water by many processes, one of which is reduction – notably by organic matter among a number of reducing agents. Reduction commonly results in the formation of UO_2 or one of its hydrates. Uranium may also undergo precipitation directly in its hexavalent state by variety of anions, mainly phosphate, vanadate and silicate (Dongarra, 1984). Among the geochemical factors possibly responsible for the reduction and precipitation of uranium from groundwater, Eh is most effective, but insoluble uraninite may be precipitated by redox reaction, therefore Fe^{2+} and sulphides, in addition to organic matter, deserve mention (Dongarra, 1984). Many other natural materials, including several metal hydroxides (Fe, Al, Mn), as well as clays, are capable of adsorbing uranium. Sorption proceeds to a variable extent. It usually depends on the pH of the solution and the pH range of mineral solubility of uranyl minerals (Dongarra, 1984). The decaying plant material or organic matter at the soil surface is another important factor determining the distribution of uranium in soil. Uranium in a reducing environment will be in the tetravalent form, which has a high affinity for organic material (Koczy, 1961). Retention of uranium by organic matter can cause enrichment lower in the profile such as in a B horizon, which contains illuviated organic material. Szalay (1964) pointed out that the sorption of uranium on peat or organic

material is by cation exchange, identical to the exchange of Ca^{2+} or K^{+} and other cations in soil. If uranium is held by cation exchange, the adsorption of uranium should be dependent on cation-exchange capacity. Sakaune (1960) and Kuznetsov et al. (1968) reported that phosphate precipitation quickly immobilizes uranium migration, and the correlation of uranium and phosphorus in sediments (Ames et al., 1983) may also implicate uranium phosphate in an immobilisation process. De Putter et al. (1999) note that uranium concentrates on the high specific surface area of weathering products by two main mechanisms: adsorption and subsequent crystallisation. The latter means that the adsorbed uranium is concentrated in newly formed (secondary) minerals (e.g., Y, REE-phosphates) (Koppi et al., 1996; Nicaise et al., 1996; De Putter et al., 1999). Murakami et al. (2005) also found nano-crystallisation. These authors pointed out that upon the crystallisation, U, P, and Cu or Mg adsorbed onto ferrihydrite are released from ferrihydrite, accumulated on the surface of hematite and goethite, and finally form nanocrystals of uranyl phosphates. It is conspicuous that the phosphates have been shown to immobilize uranium by sorption and/or by facilitating the precipitation of secondary uranium bearing phosphate minerals (Braun et al., 1998; Arey et al., 1999; Fuller et al., 2002; Jerden and Sinha, 2003; Jerden et al., 2003). Megumi and Mamuro (1977) reported that uranium content of soils and sediments increases with decreasing particle size below 100 μm, indicating that mineralogy and surface area are important factors in the retention of uranium by soil. This observation tends to imply that a surface reaction is an important retention mechanism (Sheppard, 1980b).

Thorium is concentrated in natural sediments largely either in detrital resistant minerals such as monazite, rutile and thorianite, or adsorbed onto natural colloidal-size materials. The tendency of thorium to be strongly adsorbed by clays and oxy-hydroxides explains both low thorium/uranium ratio observed in natural waters and its anomalously high mean concentrations in bauxites (49 ppm), bentonites (30 ppm) and pelagic clays (30 ppm), and its range in marine manganese nodules (24-124 ppm) (Adams and Weaver, 1958; Pliler and Adams, 1962; Langmuir and Herman, 1980). Because the comparatively insoluble thorium is concentrated in resistant minerals or is adsorbed on clays, whereas uranium is redistributed in surface and ground waters, thorium and uranium are commonly fractionated during superficial processes owing to oxidation of uranium to the soluble uranyl ion. Rancon (1973) identified four types of soil-thorium adsorption reactions:

(1) $Th(OH)_4$ precipitation caused by calcareous soil buffering,
(2) strong adsorption on clay soils from dilute solutions (< 1 g Th/dm^3 solution, pH > 2),

(3) strong adsorption on organic soils under neutral and acidic conditions, and

(4) reduced adsorption in basic solutions caused by humic acid dissolution

Thorium is enriched relative to uranium in the soil zone (Pliler and Adams, 1962; Harris and Adams, 1966). The thorium content of sandy podzol soils, which are common in Finland as well, is approximately twice that in rock. In the eluviated horizon of a podzol soi1, the thorium content is one-half of that in alluvial soi1, and in sandy ferruginous soils the thorium accumulates in the ferruginous-enriched humus horizon. There appears to be an association between the distribution of thorium in the soi1 profile and the podzolic and hydratogenous accumulation processes (Tyuryukanova and Kalugina, 1971).

During weathering ^{226}Ra is released from the primary minerals and adsorbed on the surface of the minerals particles in the soil. Ra adsorption is a rapid process in freshwater at near neutral pH (Krishnaswami et al., 1982), but the effects of redox processes and relatively low ion concentrations on adsorption and desorption are not well constrained in existing field investigations. In addition, many previous studies of Ra in freshwaters have not included detailed characterisation of redox conditions or analysis of short-lived Ra isotopes to apply the full range of Ra half-lives in order to determine geochemical conditions (Vinson et al., 2009). Since the specific surface area increases with decreasing particle size, the relative enrichment of ^{226}Ra increases with decreasing particle size. Titaeva (1967) reported that radium is associated with the insoluble residue, whereas uranium is bound to the humic and fulvic acids which are soluble in alkaline medium. Under oxidizing conditions these elements appear to be retained by ion exchange but in the presence of high concentrations of calcium in the water, the radium in peat and in the insoluble residue becomes near1y unexchangeable. In soil, the amount of exchangeable radium is inversely proportional to the amount of alkaline earth elements (Ca^{2+} and Mg^{2+}) present in mobile forms (Rusanova, 1962; Verkovskaja et al., 1966). Megumi (1979), Greeman et al. (1999), Edsfelt (2001) and Breitner et al. (2008) reported that about one-half of the radium in soil is adsorbed as exchangeable ions on the surface of soil particles. In mountain podzol soils, the high radium concentrations are correlated with the humus content and the higher is the content of organic substances and adsorbed bases in a soil horizon, the higher is the radium content (Verkovskaja et al., 1966). Hansen and Huntington (1969) also found an increased concentration of radium in the uppermost horizons, however, speculated that it might be the result of uranium retention and subsequent accumulation of ^{226}Ra by radioactive decay or by enrichment of the radium in plants via recycling to the organic matter on the soil surface. This indicates that vegetation

probably a significant influence on the distribution of radium in the soil profile (Sheppard, 1980a).

Radioactive disequilibrium in the ^{238}U decay chain

The existence of the radioactive disequilibrium is the one of the most important question in the radon research. Let us see briefly what it is exactly. The daughter nuclides of Th and U are present in concentrations determined by the concentration of parent U or Th isotope and the time since the system became closed to nuclide mobility. Because of the relatively short half-lives of these daughters, their chemical concentration is several orders of magnitude less than that of their parent. If a system has been closed for a time which is long relative to the half-life of the parent nuclide, (five times 245 thousand years, the half-life of ^{234}U, less than 10^7 y), the activities of all daughter nuclides should be equal to the activity of their respective parent; this state is known as radioactive secular equilibrium. However, most surface and near-surface geological environments are subject to mobility of nuclides due either to physical or chemical processes. Radioactive disequilibrium is, therefore, induced between the nuclides above and below in the decay series.

Rosholt (1957) established a six-fold classification of disequilibrium patterns: 1) *Daughter product deficiency*. This may be due to very recent introduction of the parent, or to chemical leaching of daughters; the latter process is considered more important, especially where U is fixed by vanadate or phosphate; ^{226}Ra is the most easily leachable daughter, while loss of ^{222}Rn does not appear to be a major cause of long-term disequilibrium. 2) *Time-related daughter product deficiency.* Here, the amount of each daughter present is such that they have all been generated over the same period of time; that is, they have all grown following the introduction of ^{238}U but have not had time to reach equilibrium. 3) *^{230}Th deficiency.* This usually arises through deposition of ^{238}U from a solution from which other U daughter were also deposited but which did not carry the relatively insoluble Th isotope. 4) *Daughter product excess.* This is usually found in oxidizing environments and is produced by leaching of the parent ^{238}U; daughter product addition does not normally occur but is sometimes indicated by a low ^{230}Th content; ^{231}Pa is particularly important in this type of disequilibrium because it is easily hydrolyzed and precipitated from solution once mobilized and is, thus, the least mobile of the U decay products. 5) *^{226}Ra excess.* In some very acidic environments associated with oxidizing sulphide deposits, leaching of U and other daughters take place but Ra is retained as an insoluble sulphate. 6) *The presence of Ra isotopes exclusively.* This type of disequilibrium, found in oil field brines and radioactive hot springs and their deposits,

results from the coprecipitation of Ra with Ba and Sr sulphates and Fe oxyhydroxides; the low ^{210}Pb content of these precipitates often indicates a very recent origin.

The fractionation of U and Ra in stream waters and sediments is another important aspect of disequilibrium. In the streams of the Bancroft area of Ontario, ^{226}Ra is enriched in clastic sediments relative to ^{238}U, as a result of either the leaching of U or the precipitation or adsorption of Ra (Tachi et al., 2001). In organic sediments, a ^{226}Ra deficiency has been produced by preferential precipitation of U.

2.2.2. Radon

2.2.2.1. Properties and effects of radon

Radon is a radioactive noble gas. It has three naturally occurring isotopes: ^{222}Rn, which formed in the ^{238}U decay chain from decay of ^{226}Ra, ^{220}Rn, member of the ^{232}Th decay chain and ^{219}Rn, which formed in the ^{235}U decay chain (Figure 2-3). The ^{222}Rn is the most important radon isotope because it has the longest half-life, 3.82 days. In contrast, although the production rate of ^{220}Rn (thoron) is approximately the same as of ^{222}Rn, substantially less reaches the atmosphere because its short half-life (56 s) limits the distance it can travel in condensed maater before decay. Finally, very little amount of radon isotope, ^{219}Rn (actinon), is present in air because the activity of ^{235}U is 21 times less than that of ^{238}U and because of ^{219}Rn's short half-life (4 s). The second important characteristic of radon is the occurrence of decay products, which are chemically active and relatively short-lived. As indicated in Figure 2-3, the four radionuclides following decay of ^{222}Rn have half-lives of less than 30 minutes, therefore, if collected in the lung when inhaled, they are likely to decay to ^{210}Pb before removal by lung clearance mechanism (Nazaroff and Nero, 1988). At birth from its ^{222}Rn parent, ^{218}Po is a free, positive ion and is usually not attached to an aerosol particle. However, subsequently, unattached ^{218}Po may participate in one or more of the following processes: 1) neutralisation, 2) reaction, including hydration followed by nucleation and 3) sometimes attachment to an aerosol particle. The process of attachment is a result of the random movements of the progeny and the aerosol particles and may be considered as a special case of aerosol coagulation. Following attachment, the behaviour of the radon progeny is a function of the aerosol particle mechanism. The unattached fraction has a diffusivity of the same order as that of the parent gas, ^{222}Rn, which is much higher than that of the attached fraction, whose diffusivity is governed by the aerosol size distribution (Nazaroff and Nero, 1988).

The radiation released on decay of the short-lived decay products imparts the lung dose to which increased risk of lung cancer is attributed. The alpha radiation from the polonium isotopes contributes the radiologically significant dose, primarily because alpha particles deposit their energy within such a small thickness of tissue. As a result, the alpha energy is deposited in the relatively sensitive lung lining and also has a dense deposition pattern, which has much greater biological impact (Nazaroff and Nero, 1988). It is expressed in the value of the radiation weight factor of alpha particles, which is $W_R = 20$. However, some other studies find negative correlation between the indoor radon concentration and the lung cancer in the interval of low and medium ^{222}Rn-activity concentration (Lazar et al., 2005). The most recent collaborative and representative risk study was issued in 2004 (Darby et al., 2004). According to this study the risk of lung cancer increased by 16 % (95 % confidence interval) per 100 Bq/m^3 increase in radon concentration. In the absence of other causes of death, the absolute risks of lung cancer by age 75 years at radon concentrations of 0, 100, and 400 Bq/m^3 would be about 0.4 %, 0.5 %, and 0.7 %, respectively, for lifelong non-smokers, and about 25 times greater (10 %, 12 %, and 16 %) for cigarette smokers. Collectively, though not separately, these studies show appreciable hazards from residential radon, particularly for smokers and recent ex-smokers, and indicate that radon is responsible for about 2 % of all deaths from cancer in Europe.

2.2.2.2. Radon in the environment

Radon arises from trace concentration of radium in the soils, sediments and near surface rocks, and indoor concentrations usually depend on access of this radon to building interiors. Radon can enter directly from surface layers of soils or rocks, via utilities such as water (and, in principle, natural gas) that carry radon, or from crustal rocks that are incorporated into the building structure in the form of concrete and brick. The relative importance of these pathways depends on the circumstances, but it has become clear that the first direct ingress from the soil ordinarily dominates the higher indoor concentrations that have been observed in homes (Nazaroff and Nero, 1988; Arvela, 1995b). The study of Peake and Schumann (1991) shows, that 2 ppm equilibrium concentration of ^{238}U can already cause radon problems. Considering the average concentration of uranium which is 2.8 ppm in the continental crust (Taylor and McLennan, 1995), radon problematic area could be everywhere. Those areas, where uranium mineralisation are near to the surface or where soils were formed from weathering of the uranium bearing rocks, are potential radon-prone areas (Henry et al., 1991).

To find the problematic area, attempts for radon potential estimation methods were made (Duval, 1991; Henry et al., 1991; Csige, 1998; Mäkeläinen et al., 2001).

The physical characteristics of the soil plays a key role in determining the radon concentration in nearby buildings. One of the most important physical characteristics of soil pertinent to indoor radon is its permeability. The importance of soil permeability in the study of indoor radon arises from the very broad range of values of the permeability of common soils spanning more than 10 orders of magnitude. At the upper end of this range, convective flow is the dominant radon transport mechanism. Since the convective flow rate increases with increasing permeability, and since the radon entry rate increases with convective flow of soil gas into the substructure, the potential for radon entry is expected to increase monotonically with permeability for coarse grained soils (Nazaroff and Nero, 1988). As stated above coarse grained soils generally have higher permeability, because their pores are larger, and consequently the frictional resistance to fluid flow at the surface of the grains is of less importance than it is in the fine-grained soils. The clay content of the soils widely influences the permeability. This is more effective in case of the swelling clays. Desiccation cracking that occurs during drier periods increases the gas permeability of the soil (Schumann and Gundersen, 1996). In case of houses, which were built on permeable eskers, the fluctuating wind blowing towards the eskers affects strongly the diurnal variation in indoor radon concentration. This factor, together with the convective subterranean air-flow in the esker, affect the pressure difference across the structure under the ground, the flow of soil gas and the radon concentration in soil pores (Arvela et al., 1994; Keskikuru et al., 2001). Considering the two types of transport mechanisms, the diffusive transport (Fick's law) and the convective flow (Darcy's law), the latter is the major mechanism, which affects the radon transport in the soil system. The convective flow of soil gas drawn into homes follows Darcy's law. The law states that the local bulk-average velocity of soil gas is proportional to the local gradient of pressure and to the permeability of the soil. The driving force for this convective entry is the difference between indoor and outdoor pressure arising from the stack effect and other causes (Arvela, 1995b).

Moisture content is a very important factor for radon emanation and migration in soil. For a well-drained soil the void volume contains water in the smaller pores and air in the larger pores. The capillary water increases the radon emanation (see section 2.2.2.2.) fraction by absorbing the recoil energy of the newly formed atom. However, this water does not increase the resistance of the soil to airflow to a great degree since it is the larger pores that make the

dominant contribution (Stranden et al., 1984). A schematic representation of the key elements of soil as a source of indoor radon is presented in Figure 2-7.

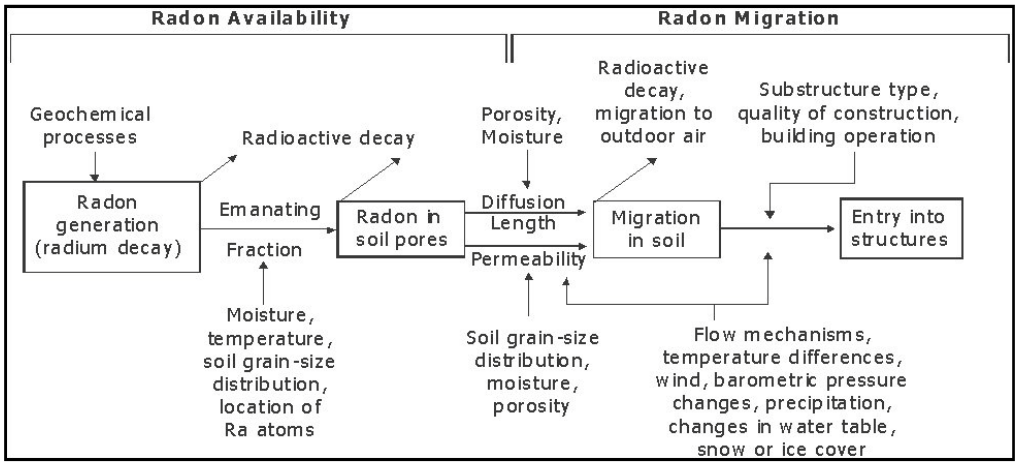

Figure 2-7: Schematic representation of radon production and migration in soil its entry into building (Nazaroff and Nero, 1988)

2.2.2.3. Emanation coefficient

Only a fraction of the radon generated in soil ever leaves the solid grains and enters to pore volume of the soils. This fraction is known as the emanation coefficient or emanating power. Experimental measurements of the emanation coefficient of rocks and soils have been made by many researchers (Megumi and Mamuro, 1977; Markkanen and Arvela, 1992; Greeman and Rose, 1996; Schumann and Gundersen, 1996). This is approximately in the range of 0.05-0.7 for soil.

Conservation of linear momentum dictates that, upon being created by the alpha decay of radium, ^{222}Rn and ^{220}Rn atoms possess kinetic energies of 86 and 103 keV, respectively. The newly formed atom travels from its site of generation until its energy is transferred to the surrounding medium. The decay of Ra to form Rn atom is accompanied by recoil of the Rn in a direction opposite to the emitted α-particle. The distance travelled depends on the density and composition of the material. The range of ^{222}Rn is 0.02-0.07 μm for common minerals, 0.1 μm for water, and 63 μm in air; the range of ^{220}Rn in air is 83 μm (Tanner, 1980). The emanation coefficient is considered to have three components: direct recoil, indirect recoil and diffusion. These components arise from the locations of the end points of the path of the recoiling radon atoms. The direct recoil fraction refers to radon atoms that terminate their recoil in the fluid-filled pore space. Atoms that leave the grain in which they were created, traverse a pore, and penetrate another grain from the basis for the indirect recoil fraction. Then they probably migrate out of the pocket created by their passage to enter a pore (Figure

2-8). The diffusion fraction refers to radon atoms that begin and end their recoil within a single grain then migrate to the pore through molecular diffusion.

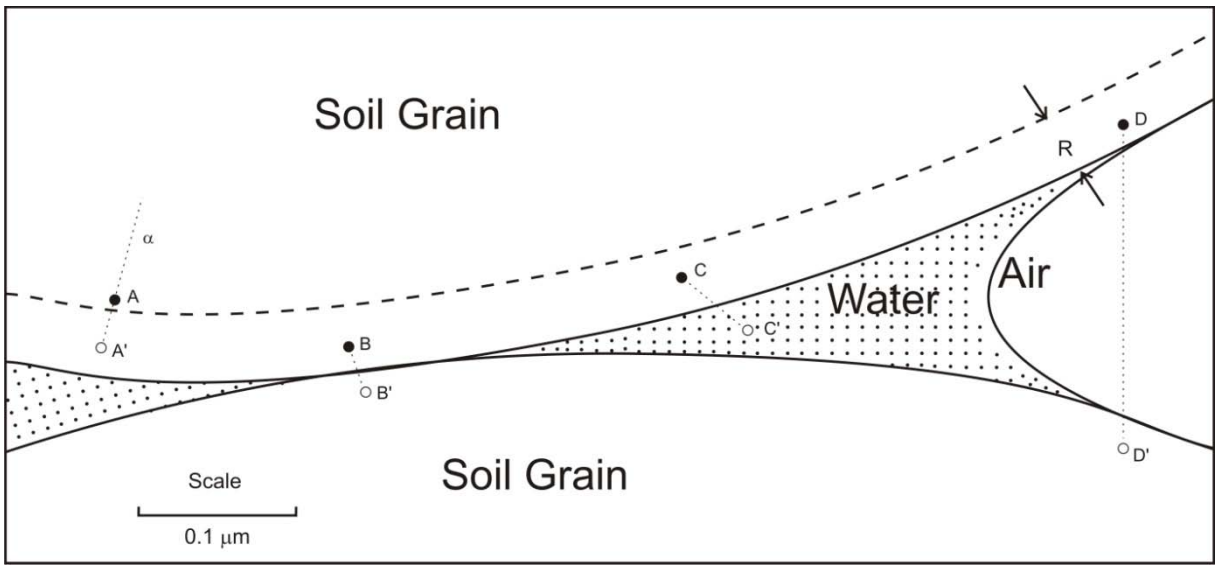

Figure 2-8: Recoil effects in soil grains, showing differences when water vs. air is present (Tanner, 1980). (A = recoiling Rn does not escape host grain: B = recoil directly into adjacent grain; C = recoil into water, leaving Rn in pore space /direct-recoil/: D = recoil into air, leaving Rn embedded in adjacent grain /indirect-recoil/)

The emanation coefficient is affected by numerous factors:

1. For a radon atom to escape from a soil or mineral grain into a pore space the decay must occur within the recoil distance of the grain surface and the radon atom must be ejected in a direction that carries it outward from the solid. Grain size and shape are the two important factors that control the soil emanation coefficient because they determine in part how much uranium and radium is close enough to the surface of the soil grain to allow the newly-formed radon to escape into pore space (Schumann and Gundersen, 1996). Bossus (1984) found that the emanation coefficient increases linearly with increasing specific surface area.

2. The presence of grain coatings in which radium is concentrated on the surfaces of soil or mineral grains increases the emanating power of soils relative to those in which radium is uniformly distributed throughout the grains. Sorption or co-precipitation of radionuclides with metal oxides in grain coatings is one of the most important geochemical processes that can enhance the radon emanation coefficient of rocks and soils (Schumann and Gundersen, 1996).

3. Microscopic fractures, fissures and pits or openings, caused by damage to soil or mineral grains from previous radioactive decays, provide additional pathways for radon release that can increase the radon emanation coefficient. If a soil or mineral grain is rich in micro fissures, the specific surface area of the grain is increased to such an extent that the

radon emanation coefficient can be as much as one to two orders of magnitude higher than can be accounted for by escape from the outer surface of the grain alone, particularly for sand-sized and larger grains (Rama and Moore, 1984).

4. Soil moisture is significant for several reasons. The radon release from soil, combining emanation and transport, is maximal when the soil is moist. Having the small pores filled with water results in a high radon emanation coefficient, but, as most transport takes place through the larger pores, radon transport is reduced only to a small degree. When dry, the soil has slightly enhanced transport, but greatly reduced emanation coefficient. When wet, the emanation coefficient is slightly higher, whereas the diffusivity and permeability are greatly reduced (Nazaroff and Nero, 1988). When the moisture content is high, the radon atom may be trapped within the soil pores (Washington and Rose, 1990), thus less radon is available in the gas phase. This has no effect on the emanation coefficient, however it would have a significant effect on radon concentrations in soil gas and on radon transport and entry into buildings (Schumann and Gundersen, 1996). Markkanen and Arvela (1992) measured the dependence of the emanation moisture content and they found that radon emanation reaches its maximum at about 1-2 % water content in gravel when the internal pores within the grains fill up. In clay, the specific surface areas are rather high hence fairly high water contents are needed to cover all the surfaces with water: the maximum emanation is found at higher water content. In routine measurements, if water content is to be standardized at a certain value for all types of soil the use of 5 % is recommended. Breitner et al. (2010) pointed out that no significant differences occurred in emanation coefficients between 5 % and 10 % of moisture content, which means, emanation coefficients reaches its maximum value already at 5 % of moisture content.

The measured emanation coefficients are considerably higher than predicted by simple physical models. Two hypotheses have been advanced to account for the large discrepancy between measured and theoretical emanation coefficients: the first is that radium is not distributed uniformly instead it is concentrated in secondary films on the surface of the grains. The second hypothesis suggests that chemical corrosion and particularly radiation damage due to the decay of its parents, damages the crystalline structure in the vicinity of the newly formed radon atom, thereby permitting it to migrate more readily than would otherwise be possible (Tanner, 1980; Sasaki et al., 2005).

3. ANALYTICAL METHODS

3.1. ^{238}U, ^{232}Th, and ^{226}Ra determination by gamma-spectroscopy

Gamma-spectroscopic measurements were carried out using high-resolution, low-background HPGe detectors. The spectra were analysed using GAMMA-99 computer code developed for environmental sample measurements (Sinkko, 1981). Corrections for sample thickness and density and the effect of true coincidence summing were taken into account in the calculation of the results (Sinkko and Aaltonen, 1985). Accreditation, based on the standard EN ISO/IEC 17025:2005, has been given to the laboratory (code T167) by the Finnish Accreditation Service. The method is modified from IEC 1452 standard (IEC, 1995; STUK, 2007).

The bulk samples were measured in Marinelli beakers (535 ml) and the ^{238}U, ^{232}Th and ^{226}Ra contents determined. ^{238}U was determined directly from the ^{234m}Pa photopeak and ^{226}Ra by subtracting the equivalent ^{235}U (4.66 % of ^{238}U activity) from the 186 keV doublet photopeak of ^{235}U and ^{226}Ra. The minimum detectable concentration (MDC) of ^{234m}Pa in a 900 g sample using 1000 min counting time was about 20 Bq/kg. The ^{232}Th content was determined by measuring ^{228}Ra and ^{228}Th and verifying secular equilibrium between these nuclides. ^{228}Ra was determined from the ^{228}Ac 338 keV and 911 keV photopeaks, while ^{228}Th was determined from the ^{208}Tl 583 keV and 2614 keV photopeaks. These measurements were carried out at STUK.

3.2. Determination of emanation rate and emanation factor

The method used for emanation rate and emanation factor determination was developed by STUK (Turtiainen, 2009).

Approximately 0.5 kg bulk samples dried in an oven at 105 ºC were put into a 2.34 l glass from Schott Company as a radon tight container for allowing radon emanation from samples and added 5 % of Milli-Q water. Based on previous studies at ca. 5 % of moisture content the emanation reaches its maximum (Markkanen and Arvela, 1992; Breitner et al., 2010). A stainless hook was attached to the bottom of the stopper and liquid scintillation vials were hung on the hooks using Tubinette surgical stockinet (Figure 3-1). Glass liquid scintillation vials (25 ml) from Packard and screw-on caps with an aluminium liner from Perkin Elmer were used.

The conditions under which radon emanation was measured were defined by the Radon Safety Laboratory (at STUK) as room temperature and a moisture content of 5 %. All

calibrations and measurements were carried out at a temperature of 24.5±1.0 °C. The bottle was gently shaken to accelerate water distribution through the sample.

All liquid scintillation measurements were carried out with a Guardian 1414 liquid scintillation counter by Wallac Company. The counter is equipped with a pulse-shape analysis (PSA) circuit, i.e., it is capable of separating alpha- and beta-pulses into their respective counting windows. The counting efficiency for the alpha window, including ^{222}Rn, ^{218}Po and ^{214}Po, is 292±7 %.

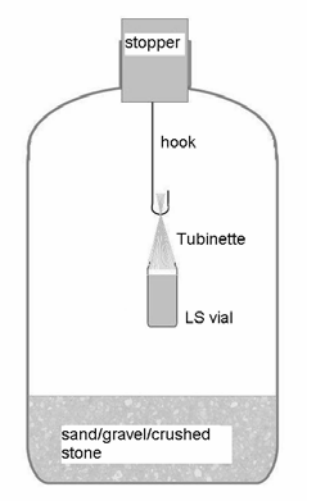

Figure 3-1: Schematic diagram of the apparatus used in radon emanation measurements (Turtiainen, 2009)

The reported uncertainties related to the measurement results are standard uncertainties and those related to equations are combined uncertainties, thus giving a level of confidence of approximately 68 %. Lowest limit of detection (LLD) was calculated according to:

$$LLD = 2.71 + 4.65\sqrt{C_{bg} \times t} \qquad (1.)$$

where LLD is defined as the fewest net counts for which there is 95 % confidence that radioactivity is present (Currie, 1968), C_{Bg} = background intensity (cps) and t = measuring time.

Other method performed to determine ^{226}Ra-concentration and emanation of less than 0.250 mm grain-sized samples is based on open-closed measurements. Samples were oven-dried and 5 % water was added. Each sample was vacuum sealed into a 150 ml plastic vial and stored for three weeks to allow the radon and radium to reach equilibrium. After the sealed measurements using gamma spectroscopy (closed measurements) the vials were opened and the analysis was repeated (open measurements) allowing 4 h for the radon progeny to decay before measurement. The emanation coefficient was calculated using the

weighted mean of the net count rate ratios (the gamma lines of radon daughters ^{214}Pb and ^{214}Bi) of sealed and open measurements. Any errors in the energy calibration were avoided by using direct counting rate ratios instead of measured concentrations. The same method was used to determine influence of moisture content and grain sizes on emanation. In this case the method was repeated after adding 5 % of water until we reached 10 % of moisture content. All uncertainties related to gamma spectroscopic measurements are expanded uncertainties using a coverage factor of 1, which gives a level of confidence of approximately 68 %. These measurements were carried out at STUK.

3.3. Sequential chemical extraction and major and trace elements analyses

Selective chemical extractions provide semi quantitative information on elemental partitioning within soil fractions. In order to determine the leachability of different physico-chemical forms of radium, uranium, thorium and other trace and major elements sequential extraction was performed on all bulk samples from study sites. Sequential extraction results for trace and major elements provide additional information on the mineralogical constituents of the sand, whereas results for radium can be used to study the exact radon source.

Sequential extraction of trace and major elements from the bulk samples was performed according to the combination of the methods of Tessier et al. (1979) and Quejido (2005) with fewer steps in order to reduce the possible overlapping between extraction steps. These chemical methods are based on three to five successive extraction steps. The steps used in our study varied for different groups (3) of samples according to the differences within the materials/soils. In the first step which was performed for all sample groups, easily removable elements were extracted. In the second step, which was done for samples from Olkiluoto, elements from carbonates should be leached out. Elements fixed with iron bearing minerals were released in the third extraction step which was performed again for all of the sample groups. In the fourth step which was performed on soils from Askola and Palmottu, elements fixed in organic material was leached out. In the final extraction step the strongly bound portion of the elements was leached out. The amounts of uranium, thorium, radium and other trace and major elements leached from the samples were determined for each extraction reagent. Finally, the proportions of trace and major elements leached in each step were calculated. The lists of the three sequential extraction schemes are presented on Figure 3-2. The additional treatment of leachetes for ICP-MS analysis is as follows:

- Step 1: Samples were diluted to 1:5 and nitric acid was added so that analysed solution was 0.2 M NH_4Cl and 5 % HNO_3.

- Step 2: Samples were analysed as undiluted, diluted to 1:10 and diluted to 1:100. By dilution extraction liquid analysed was modified as 1 M NH_4-acetate + 0.05 M EDTA.

- Step 3: Most of the samples were diluted 1:5 and nitric acid was added so that analysed solution was 0.02 M oxalic acid 0.035 M ammonium oxalate 5 % nitric acid. Samples Palm-C and ASK-B were diluted 1:100 so those analysed solution was 0.001 M oxalic acid 0.00175 M ammonium oxalate.

- Step 4: Samples were analysed as undiluted, diluted 1:10 and diluted 1:100. These dilutions were made so that extraction solution was not diluted. Samples were also analysed so that extraction solution was diluted to 1:100.

- Step 5: Samples were analysed as undiluted, diluted to 1:10 and diluted to 1:100. By dilution extraction liquid analysed was modified as 0.04 M $NH_2OH{\cdot}HCl$ in 25 % acetic acid.

- Step 6: Samples were diluted to 1:10 by deionised water. Then they were diluted to 1:100 in 0.9 % HNO_3 1.5 % HCl. Both 1:10 and 1:100 dilutions were analysed so that analysed solution was 0.9% HNO_3 1.5 % HCl.

The samples were sieved to less than 0.250 mm and dried in oven at 105 ºC. The mineral-to-extraction reagent ratio was 1:10. In each case 3 grams of sample with grain size fraction finer than 0.250 mm were used. To check the reproducibility of the method duplicate samples were used. The samples were put into a 35 ml centrifuge tube. After each steps the liquid phase was separated from solid one by centrifugation (30 minutes at 10,000 rpm). The liquids were removed either with pipette or just decanted and filtered (0.45 μm). Before the 6th, microwave digestion step, the residuals were put into teflon vials. Digestion was made by CEM MARS 5^{tm} microwave. Digestion took 20 minutes at 55 bar, 165 ºC and 1600 W. The extraction solutions analysed by ICP-MS were chemically different for each extraction step. The matrix effect within the analyses affected the results to some extent. The sequential extraction was carried out at the Radiochemical Laboratory of University of Helsinki as well as the ICP-MS analyses of extraction solutions. Major and trace elements of the liquids extracted were analysed by Agilent 7500ce ICP-MS with quadrupole as mass-analyser and octopole as reaction chamber. Reaction chamber was used with helium as reaction gas. Standard solutions used for calibration was made from commercial certified standard solutions. They were made from the solutions what were used for the different extraction. Germanium was used as internal standard for Na, Mg, K and Ca and for uranium thallium was used. Sequential

chemical extraction was performed at Laboratory of Radiochemistry at University of Helsinki (referred as HYRL hereafter).

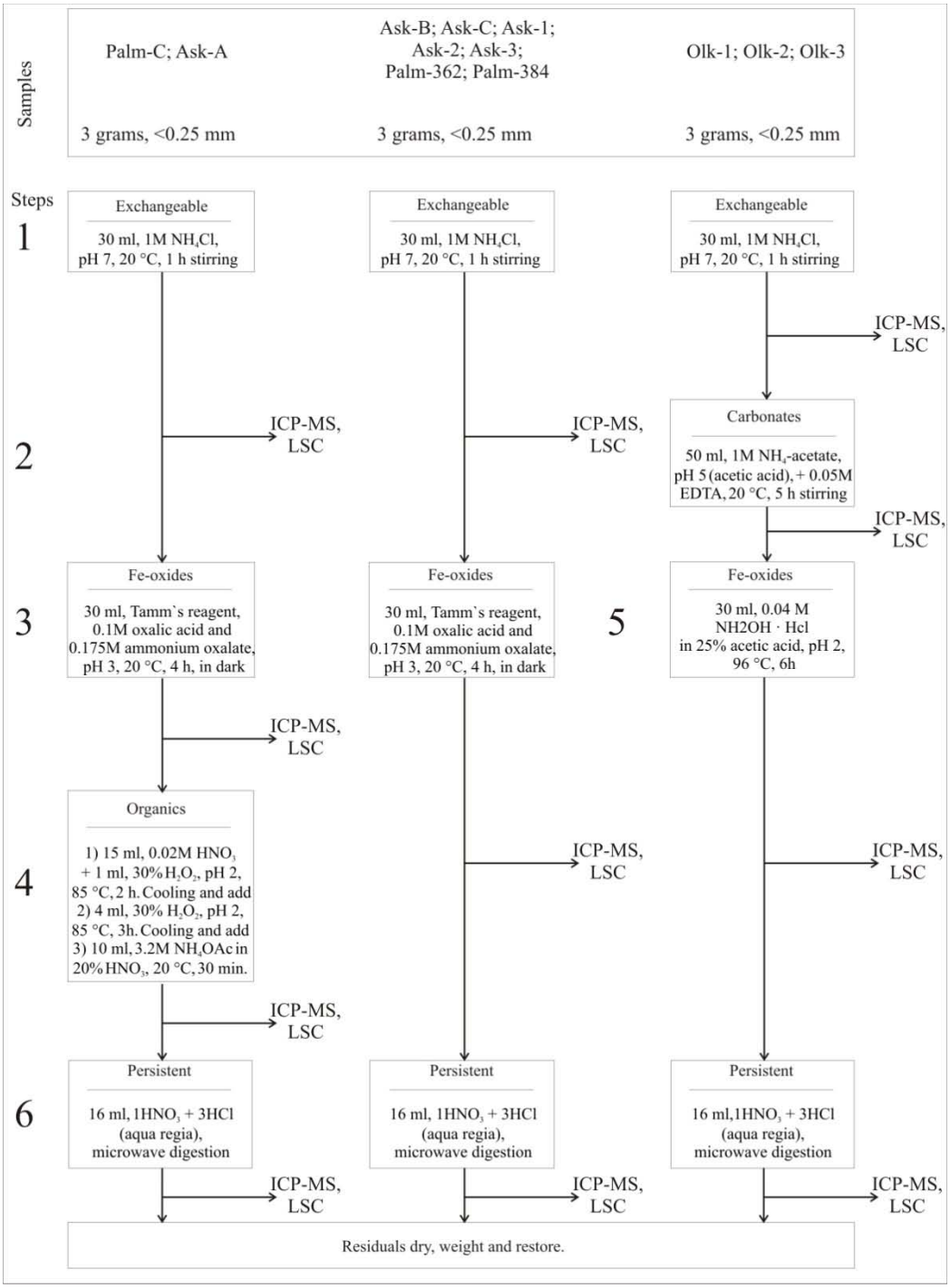

Figure 3-2: Methods used for sequential extraction at HYRL (modified after Tessier (1979) and Quejido (2005))

Since our laboratory facility at HYRL was not able for making very aggressive digestions, major and trace element content of 12 bulk samples (< 0.250 mm sized grain fraction) were sent and analysed in the laboratory of SGS Group Mineral Services, Toronto (referred as SGS hereafter). For analyses sodium peroxide fusion digestion was used. Fusion processes involve

the complete dissolution of the sample in molten flux. Fusions are generally more aggressive than acidic dissolution methods and are suitable for many refractory, difficult-to-dissolve minerals. They are presumed to be "total" by the industry. Analyses were made at SGS by ICP-MS and ICP-AES using ISO 17025 standard which is accredited for specific tests. The lowest limit of detection for elements analysed is presented in Table 3-1.

Table 3-1: Lowest limit of detection (LLD) (ppm) for major and trace elements of bulk samples analysed by ICP-MS and ICP-AES at SGS, Toronto

	LLD		LLD
P	100	Gd	0.05
K	100	Tb	0.05
Ti	100	Dy	0.05
Fe	100	Ho	0.05
Sr	0.1	Er	0.05
Y	0.5	Tm	0.05
Zr	0.5	Yb	0.1
Nb	1	Lu	0.05
Ba	0.5	Pb	5
La	0.1	Th	0.1
Ce	0.1	U	0.05
Pr	0.05		
Nd	0.1		
Sm	0.1		
Eu	0.05		

3.4. Radium-226 measurement by liquid scintillation counting

In the leachates ^{226}Ra was measured indirectly (Schonhofer, 1989). 10 ml of aliquot sample was put into glass LSC vials (22 ml) and 10 ml of water-immiscible scintillation cocktail was added. The vials were closed for 4 weeks to reach the secular equilibrium between ^{226}Ra and daughters of ^{222}Rn. After 4 weeks ^{222}Rn and its daughters were measured by Guardian 1414 liquid scintillation counter by Wallac Company.

The counting efficiency for the alpha window, including ^{222}Rn, ^{218}Po and ^{214}Po, is 122±6 %. The reported uncertainties related to the measurement results are standard uncertainties and those related to equations are combined uncertainties, thus giving a level of confidence of approximately 68 %. The lowest limit of detection (LLD) was 42 counts by using the definition by Currie (1968) that translated into 0.376 gross cpm (count per minute). Thus, the minimum detectable activity (MDA) in a sample was 0.001 Bq or expressed otherwise, the minimum detectable concentration (MDC) was 0.1 Bq/l.

The leachates from the 6th extraction step were highly acidic and the above mentioned method was not available because the liquid scintillation cocktail react with the acid. For these leachates the analysis were done using a membrane method (Durecova et al., 1999;

Purkl and Eisenhauer, 2003) was used. Empore^{TM} Radium Rad Disks enable complete separation of ^{226}Ra from leachates; radium retains the disk and other nuclides passes through the membrane. The commercial disks (diameter of 47mm) were cut into four smaller disks (diameter of 20 mm) and 15 ml of leachate was filtrated by suction. The recovery was defined using ^{226}Ra standard (activity 89±4 Bq/g, ref. day 24. 8. 2005) being 70 %. After the selective extraction the disks were left to stay 3-4 weeks to get the secular equilibrium. The content of ^{222}Ra was measured by liquid scintillation counting (Quantulus 1220, Wallac; Ultima Gold F as scintillation liquid) through ^{214}Po (Vesterbacka et al., 2005). The uncertainty sum was calculated through the combined errors using 3σ confidence level. The minimum detectable activity (MDA) in a sample was 0.00230 Bq (Ikonen, in prep). The analyses were carried out at HYRL.

3.6. Scanning electron microscopy and electron probe microanalyses

Heavy mineral assemblage of the finest fraction of soil and sediment samples and semi-quantitative elemental composition of heavy minerals are analysed by JEOL LSM 5900LV scanning electron microscope equipped with an energy dispersive x-ray (EDX) analytical system (Vareikiené and Lehtonen, 2004). Preparations were made from the heavy fraction of 0.125-0.250 mm and < 0.063 mm grain size fractions of bulk samples (> 2.8 g/cm^3 and > 3.3 g/cm^3, respectively) by mounted them onto a glass slide. With this technique the mineral identification is faster and better than it is by binocular microscope. On hundred randomly selected grains grain statistics were made (Geological Survey of Finland, Espoo (GTK)). Heavy mineral assemblage of Olkiluoto samples were studied by AMRAY-1860 IT-6 scanning electron microscope operated at 20 kV and 0.5 nA at Department of Petrology and Geochemistry of Eötvös University, Budapest, Hungary.

Quantitative chemical composition of selected, partly weathered U-Th-bearing minerals, and chemical composition of weathered and not weathered part of these minerals were measured by electron microprobe analyses. Analyses were performed by the wavelength dispersive technique using a Cameca SX100 instrument at GTK. Analyses were determined using an accelerating voltage of 15 kV. Probe current and beam diameter used were 10 nA and 1 micrometer respectively. Natural minerals and metals were employed as standards. Analytical results were corrected using the PAP on-line correction programme (Pouchou and Pichoir, 1986). These measurements were carried out at GTK.

4. ASKOLA SAMPLING SITE

4.1. Location of Askola sampling site

One of our three study site is in Askola municipality locates ca. 80 km NE to Helsinki (Figure 4-1). For sampling, an old, small sand quarry close to test uranium mine (Lakeakallio) was selected (Figures 4-1 and 4-2). North-northwest to the sampling site plenty of uranium indication identified by airborne gamma survey (Appelqvist, 1972), therefore, high uranium, thorium concentration has been assumed in the glacial sediment which has transported from the mineralisations.

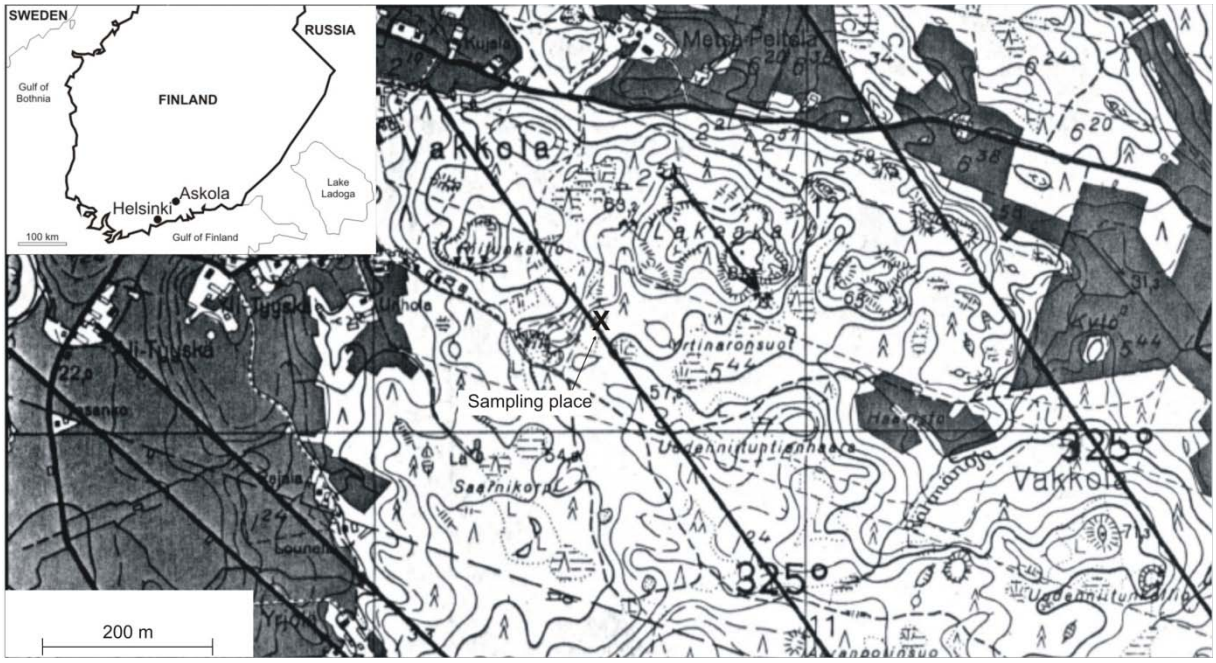

Figure 4-1: Topographical map of the sampling area in Askola and the location of Askola in Finland. The sampling site has marked by X on the topographical map. The arrow shows glacial transport direction. Degrees represent the average trend of glacial striate (modified after Hirvas and Nenonen (1980))

On the north-western slope of the quarry (Figure 4-2a) a ca. three meters deep pit was dug out. In the profile seven horizons were distinguished. Three samples were collected from the upper three soil horizons: from A, organic rich top horizon (Ask-A); from B, mainly B2 illuvial horizon as precipitation zone in podzol soils (B1 horizon, which is an eluvial horizon and was too thin for collecting reasonable amount of sample) (Ask-B); and from C horizon which has diffuse border with underlying pebbly sediments without graded bedding whereon podzol soil has been formed out (Ask-C) (Figure 4-2b). Three samples were collected from the underlying sediments: from the uppermost cross bedded sandy horizon (Ask-1); from a laminated clayey sand/silt one (Ask-2); and at the bottom from unsorted pebbly sand horizon without graded bedding (Ask-3) (Figure 4-2b).

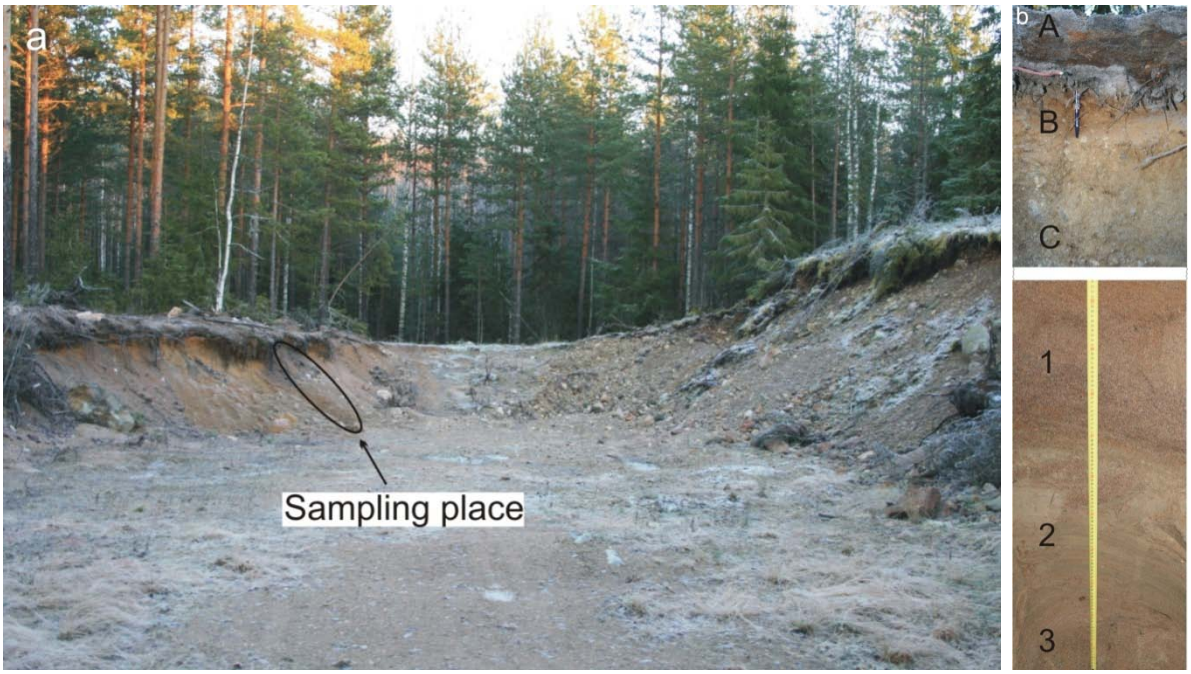

Figure 4-2: Sampling place (a) in former sand quarry, Askola, Finland and position of the samples in the approximately 3 m deep soil profile (b). A = Ask-A, B = Ask-B, C = Ask-C, 1 = Ask-1, 2 = Ask-2 and 3 = Ask-3

4.2. Geological background of Askola sampling site

4.2.1. Bedrock at Askola sampling site

The Svecofennian bedrock at Askola consists of synorogenic granodiorites, late orogenic granites and suppracrustal rocks as mica schist and mica gneiss, quartz-feldspar schist, amphibolite and basic tufites (Figure 4-3). Close to the study area, Lakeakallio (Figure 4-1), the bedrock consists of mica gneiss and microcline granite. At Askola area granodiorite is the main rock type (Figure 4-3). It occurs as vast massifs, which are sharply confined with other infracrustal rocks around and within it. Borders with mica schist and granite are less sharp. North from Askola granodiorite contains locally abundant granite veins, which seem to assimilate into granodiorite without sharp contacts. Granite in the study area is reddish, medium grained and fairly inhomogeneous. At near contact with mica schist it contains schist xenoliths and they intrude into the schist causing veined gneiss. Many of the granite veins in veined gneiss also contain garnets. Veined gneiss south from Askola is marked to the geological map as mica schist and mica gneiss. Biotite gneisses are usually medium grained, and some striped ones are also found. Stripes, which are orientated as schistosity, are probably caused by different layers (Kuivamäki et al., 1993). Fine grained grey quartz-feldspar schist occurs as small bodies in context with other rock types. According to the field observations and the geological map they are most probably metamorphosed acidic tuffs and sandy interlayers of clay sediments. Amphibolite and basic tufite areas are scattered around Askola.

Amphibolite is probably metamorphosed basic, volcanic rocks. Some of the amphibolites may also be metamorphosed gabbros (Kuivamäki et al., 1993).

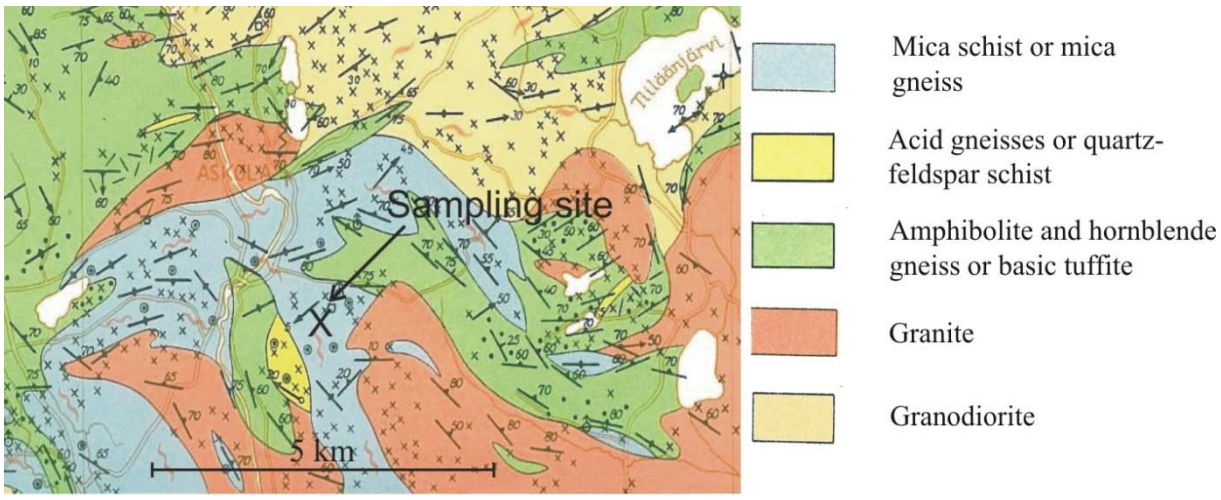

Figure 4-3: Pre Quaternary geological map of Askola study site and location of the sampling site marked by X (modified after Laitakari and Simonen (1962))

4.2.2. Uranium mineralisation at Lakeakallio

In Askola area syn-, epigenetic and supergenetic U enrichments have been found. Uranium mineralisation occurs in lenses. The syngenetic mineralisations are pegmatites and granites, their most general U minerals are allanite and zircon, often with uraninite inclusions. According to the fluid inclusions, they crystallized from ”gas-like” fluid enriched in CO_2 which is typical for pegmatites (Roedder, 1972). Epigenetic U enrichments are represented by boulders found SE to Lakeakallio and carbonate-chlorite-hematite-uraninite fracture fillings found in drill cores 301 and 302 drilled ca. 2 km SW to Lakeakallio. Supergenetic mineralisations are secondary U enrichments where uranophane and boltwoodite have been found. Vertical fractures in low radioactive granite indicate leaching by groundwater. Also the measured high U and Rn contents in groundwater do point to the leaching (Appelquist and Kinnunen, 1977). The Lakeakallio U-mineralisation is dominated by syngenetic features. In the granitic rocks U-minerals formed during granite crystallisation is crystallised more or less at the same time as quartz. Main minerals of U-bearing rock as it has been described by Appelquist (1982) are K-feldspar, plagioclase (albite-oligoclase), quartz, biotite and garnet. Garnet occurs as separate grains and grain accumulations grains are 2 mm – 2 cm in size with inclusions of other minerals. Around garnet grains biotite orientated around grain margins. Quartz in this rock is in relatively low amount, and typically has mosaic extinction. Accessory minerals in the rock are monazite, zircon, uraninite, molybdenite and pyrite. These minerals have a clear tendency to occur together at grain boundaries and in micro fissures. These grains, sometimes as aggregates are often connected by micro fissures. The fissures connected

to uraninite grains are partly filled with secondary uranium minerals. Zircon is zoned and fairly metamict, it appears often as inclusion in monazite. The U-containing granites are nearly exclusively beneath the hornblende gneiss, which is at the contact often chloritised and the feldspars are altered. The carbonate in micro fractures might originate from this alteration. The occurrence of garnet does not seem to be correlated with the U-content. It is found also in granite without uranium (Appelqvist, 1982). The radiogenic age of uraninite is about 600 Ma and of zircon 1750 Ma. The latter age is consistent with the ages of younger svecokarelidic pegmatites, and is consistent with those of South-Finnish hydrothermal uraninites (Appelqvist, 1982). Appelquist (1982) assumed that the annihilation of the clock time 600 Ma ago has happened at the same time as the microscopically observed partly mobilisation and these movements have created the majority of the mineralised micro fissures. The same reasons may have caused the features observed in quartz (mosaic extinction).

Uranium in the U-containing zone is distributed irregularly and it is not economically interesting. The numerous boulders of the same kind in the zone S and SE of the Lakeakallio indicate that there might be other similar enrichments (Appelqvist, 1982).

4.2.3. Quaternary geology

In the final stage of glaciations, the area was covered by the Baltic ice lake. The deglaciation producing varved clays have been deposited at 11,600 to 11,300 years ago (Sauramo, 1918). As it can be seen on Figure 4-4 clay is the predominant soil constituent in the area. The abundance of clay is due to the subaquatic evolution of the area during the late glacial and early postglacial periods, particularly because later, when the land uplift movement raised the area, the clays were not exposed to littoral erosion. Till is the second most common soil constituent and covers about 30 % of the surface area. Sandy till is the predominant type; the second commonest is silty till. The trends of esker trains are approximately SE to NW traverse the area (Figure 4-4). In places they contain small glaciofluvial marginal formations or deltaic accumulations. According to estimates, sand is the predominant sediment in the eskers, seconded by gravel. Peat bogs cover less than 5 % of the area. They are predominantly raised bogs. A characteristic feature is the higher level of the middle part of the bog compared to the marginal parts (Tynni et al., 1976).

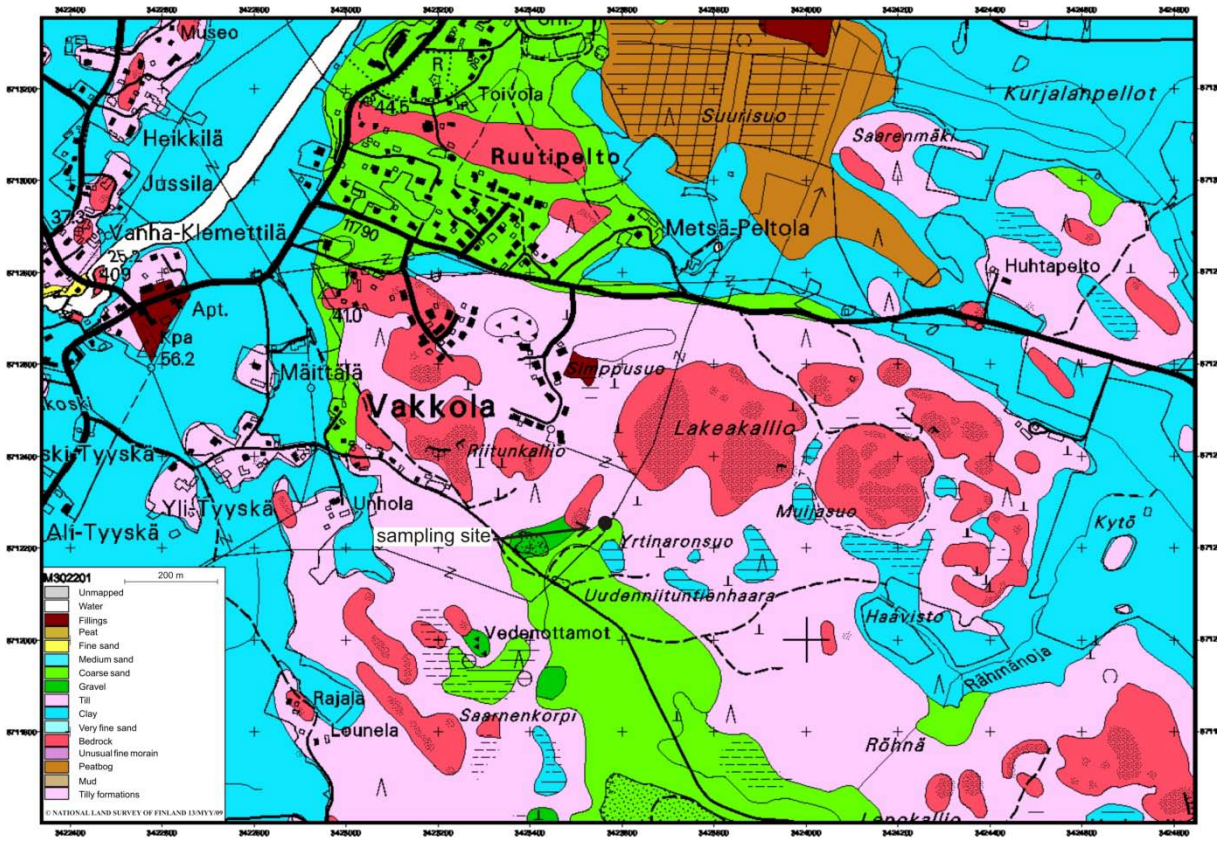

Figure 4-4: Map of Quaternary sediments at Askola sampling site, Finland (Tynni and Kukkonen, 1968). Sampling site is marked by filled black dot

4.3. Results of analyses on Askola samples

4.3.1. Description of Askola samples

Ask-A (Figure 4-5)

In wet the sample is black and not grainy disintegrated. In dry the sample is black with white particles, crumb structured, organic rich. The identified grains are quartz, feldspar, rock fragments and roots; feldspar grains are rounded. Post alteration on the feldspars is visible. Ca-carbonate content was not observed (tested by 12 % HCl).

Figure 4-5: Soil sample from the uppermost 10 cm (Ask-A) from Askola, Finland

Ask-B (Figure 4-6)

In wet the sample is reddish-brown and grainy disintegrated. In dry the sample is reddish/yellowish-brown, crumb structured, poorly sorted, some bigger (1-3 cm) pebbles are present, the larger grains are more rounded, the identified grains are quartz, feldspar, mica, rock fragments and roots. Ca-carbonate content was not observed (tested by 12 % HCl).

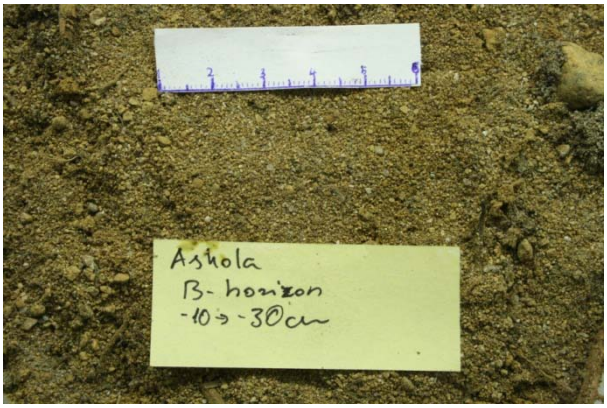

Figure 4-6: Soil sample from 10 to 30 cm in depth (Ask-B) from Askola, Finland

Ask-C (Figure 4-7)

In wet the sample is light-brown and grainy disintegrated. In dry the sample is crumb structured, not sorted, pebbles are sub-angular and polymictic (many different type of rock). Boulders (20 cm) are also present. Pebbles and boulders are rounded. The identified grains are quartz, (1-4 mm) feldspar (in the size of cm), mafic minerals, rock fragments and roots. The pebbles are granite, mica schist, granodiorite, mica gneiss and garnet containing leuco-granite. Post alteration is not visible. Ca-carbonate content was not observed (tested by 12 % HCl).

Figure 4-7: Sediment sample from 30 to 130 cm in depth (Ask-C) from Askola, Finland

Ask-1 (Figure 4-8)

In wet the sample is reddish-brown and grainy disintegrated. In dry the sample is crumb structured, well sorted, the grains are lightly rounded and vary in size between 0.5 mm and 5

mm. The identified grains are feldspar, quartz, mafic minerals, micas (biotite and muscovite) rock fragments and roots, Post alteration is not visible, Ca-carbonate content was not observed (tested by 12 % HCl).

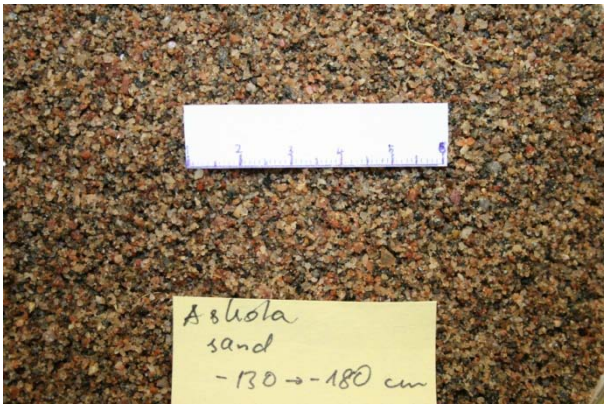

Figure 4-8: Sediment sample from 130 to 180 cm in depth (Ask-1) from Askola, Finland

Ask-2 (Figure 4-9)

In wet the sample is reddish-brown and two layers, an argillic (1-2 mm) and a silty/sandy (1-4 mm) alternate. The sample is easily disintegrates along the layers. The argillic layers are lubricatable. In dry the sandy/silty layers of the sample are crumb structured. The sample is quite well sorted and quartz, mica, feldspar and rock fragments grains were identified. Post alteration is not visible, and Ca-carbonate content was not observed (tested by 12 % HCl).

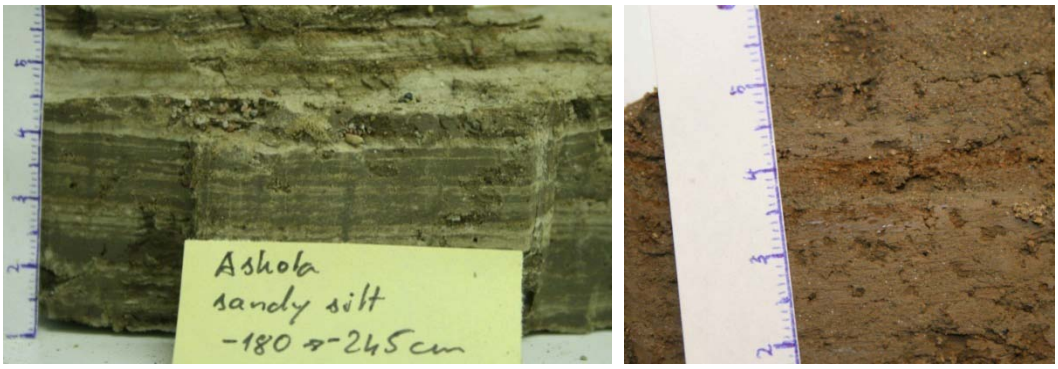

Figure 4-9: Sediment sample from 180 to 245 cm in depth (Ask-2) from Askola, Finland. (a) and reddish silty layer between argillic layers in the sample of Ask-2 (b)

Ask-3 (Figure 4-10)

In wet the sample is dark-brown, grainy disintegrated and slightly lubricatable. In dry the sample is crumb structured and badly sorted. The grains vary in size between 1 mm – >20 cm. The pebbles are rounded and sub-angular. Identified grains are mica, quartz, feldspar, mafic minerals and rock fragments. Granite, quartz pegmatite, mica schist, gneiss, migmatite and diorite pebbles were distinguished. Post alteration is not visible and Ca-carbonate content was not observed (tested by 12 % HCl).

Figure 4-10: Sediment sample from 245 to 260 cm in depth (Ask-3) from Askola, Finland

Grain size distributions of the samples are different, except the two uppermost samples Ask-A and -B, which have almost the same grain size pattern (Figure 4-11). These two samples consist mainly of medium and coarse sand and its fine fractions and gravels are negligible. Sample Ask-1 is well sorted coarse sand. Sample Ask-2 is consisted mainly by fine grain size fraction. There is a very high amount of clay-silt fraction in it (ca. 50 %). The coarsest samples are Ask-C and Ask-3; the amounts of gravels are ca. 50 % and 25 %, respectively. Sample Ask-3 contains more sandy fractions than Ask-C. Based on the grain size distributions, samples lithologically are the following: Ask-A and Ask-B are sandy soils, Ask-1 is coarse-very coarse sand, Ask-C and Ask-3 are sandy tills and Ask-2 is sandy silt/clay.

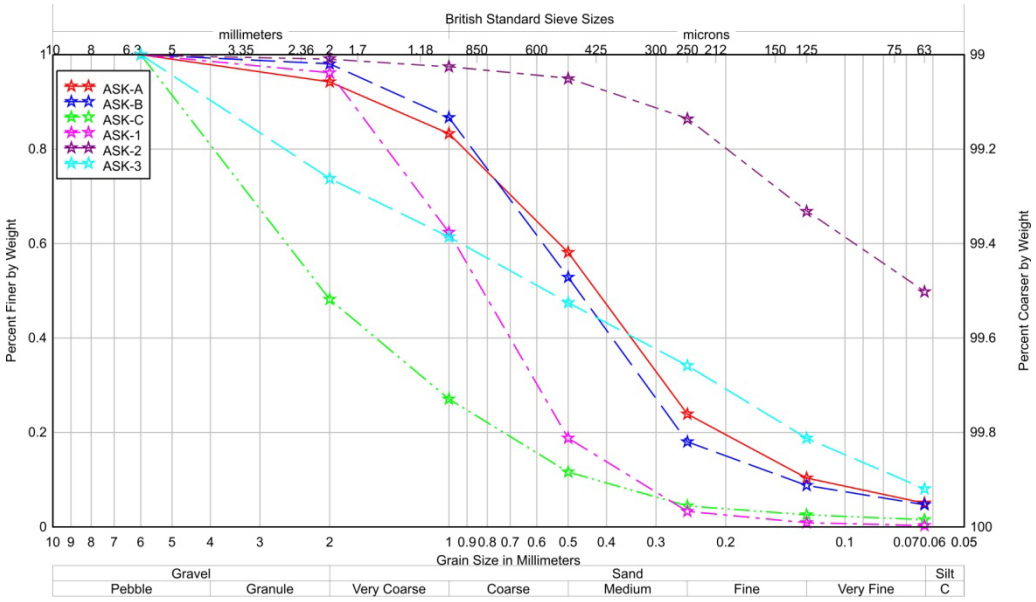

Figure 4-11: Grain size distribution of the six soil and sediment samples collected at Askola sampling site, Finland

The description of lithology of the samples is summarised in Figure 4-12.

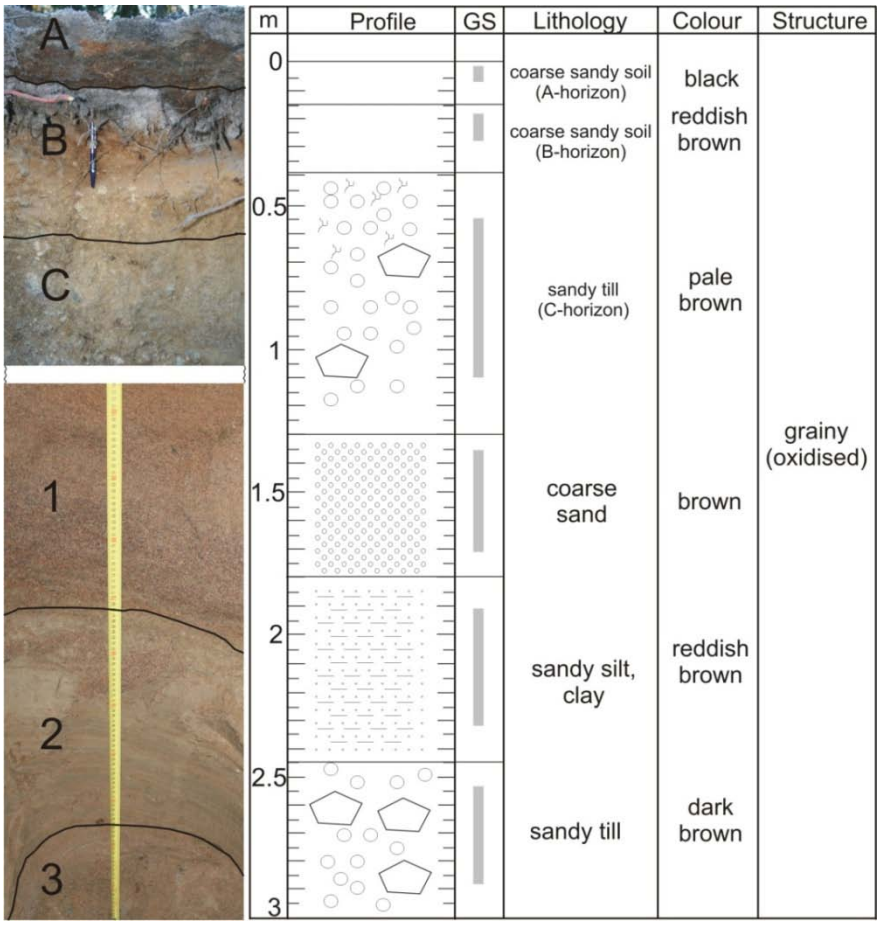

Figure 4-12: Summarised chart of lithology of the soil and sediment samples collected at Askola sampling site, Finland

4.3.2. U-, Th- and Ra-content of bulk samples from Askola

In Askola samples activity concentration of ^{238}U shows very weak increase (Pearson product-moment correlation coefficient[2] (r) = 54) versus depth (Figure 4-13a), whereas ^{226}Ra and ^{228}Ra increase in a function of depth significantly (r = 0.87 and 0.78, respectively) (Figure 4-13b, c). In Askola samples secular equilibrium between ^{238}U and ^{226}Ra has been occurred only in the deepest sample (Ask-3). Highest disequilibrium occurred in the samples of Ask-C and Ask-1, the ^{226}Ra/^{238}U ratio is 1.6 (Table 4-1). In the uppermost two soil horizons A and B (Ask-A, Ask-B) higher uranium than radium concentrations were measured. In the deeper horizons radium concentrations are higher than uranium. In ^{232}Th decay chain significant disequilibrium were measured between ^{232}Th and ^{228}Ra except in the deepest sample Ask-3. The highest disequilibrium has been found in sample Ask-1 (^{228}Ra/^{232}Th = 0.4) (Table 4-1).

[2] Pearson's correlation coefficient between two variables is defined as the covariance of the two variables divided by the product of their standard deviations:

$$\rho_{x,y} = \frac{cov(X,Y)}{\sigma_X \sigma_Y} \frac{E[(X-\mu_X)(Y-\mu_Y)]}{\sigma_X \sigma_Y}$$

Table 4-1: Activity concentrations (Bq/kg) of ^{238}U, ^{226}Ra and ^{228}Ra (^{228}Ac), ^{228}Th (^{208}Tl) as representing ^{232}Th-decay chain in vertical profile in bulk samples, from Askola, Finland. Activity concentration of ^{232}Th was calculated from Th concentration (ppm) measured by ICP-MS in SGS Lab, Toronto. The reported uncertainties are expanded uncertainties using a coverage factor k=1.

Samples	Depth (cm)	^{238}U	^{226}Ra	^{226}Ra/^{238}U	^{228}Ra (^{228}Ac)	^{228}Th (^{208}Tl)	^{232}Th	^{228}Ra/^{232}Th
Ask-A	5	65±7	42±10	0.6±0.2	14±1	14±1	20±1	0.7±0.1
Ask-B	20	73±11	45±8	0.6±0.2	22±3	21±2	37±1	0.6±0.1
Ask-C	80	62±9	96±13	1.6±0.2	41±7	40±3	52±1	0.8±0.2
Ask-1	150	41±9	66±8	1.6±0.3	28±3	27±27	66±1	0.4±0.1
Ask-2	210	82±8	116±11	1.4±0.1	59±7	58±4	51±1	1.2±0.1
Ask-3	250	118±5	117±7	1.0±0.1	43±3	42±3	40±1	1.1±0.1

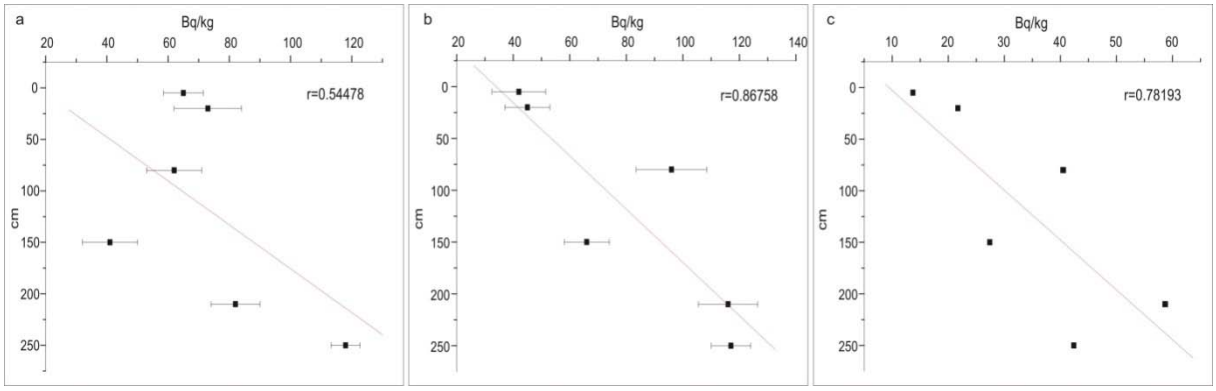

Figure 4-13: Activity concentrations of ^{238}U (a), ^{226}Ra (b) and ^{228}Ra (^{228}Ac), ^{228}Th (^{208}Tl) as representing ^{232}Th-decay chain (c) in function of depth in soil and sediment samples from Askola, Finland. The reported uncertainties are expanded uncertainties using a coverage factor k=1

4.3.3. Radon production and emanation rate of bulk samples from Askola

Radium contents of the grain size fraction < 0.250 mm is higher in the cases of samples Ask-B and Ask-C. Sample Ask-2 has significantly lower. Radon production and emanation factor of bulk samples varying between 0.11-0.36 Bq/(kg h) and 0.28-0.41, respectively (Table 4-2). Clayey sample Ask-2 has the highest radon production and emanation factor, 0.36 and 0.41, respectively of all the samples collected at Askola sampling site. This sample is one of the two samples which have the highest ^{226}Ra content (116 Bq/kg). The well sorted sand sample Ask-1 has the lowest emanation factor (0.28). The lowest radon production was measured in the uppermost soil sample Ask-A (Table 4-2).

Table 4-2: Activity concentrations (Bq/kg) of ^{226}Ra, Rn production (Bq/(kg h)) and emanation factor in bulk and < 0.250 mm sized grain fraction of Askola (Ask) samples. The reported uncertainties are expanded uncertainties using a coverage factor k=1.

Samples	^{226}Ra (bulk)	^{226}Ra (<0.250 mm)	^{222}Rn production (bulk)	Emanation factor (bulk)	Emanation factor (<0.250 mm)
Ask-A	42±10	30±4	0.11±0.01	0.35±0.08	0.34±0.13
Ask-B	45±8	62±4	0.12±0.01	0.36±0.07	0.26±0.04
Ask-C	96±13	138±4	0.21±0.01	0.30±0.04	0.31±0.02
Ask-1	66±8	82±4	0.14±0.01	0.28±0.04	0.17±0.02
Ask-2	116±11	79±4	0.36±0.02	0.41±0.04	0.20±0.02
Ask-3	117±7	107±4	0.32±0.02	0.36±0.03	0.32±0.02

Emanation factor in grain size fraction < 0.250 mm is significantly lower in the cases of samples Ask-1 and Ask-2 than of the other samples; others are similar within the errors.

4.3.4. Major and trace elements of bulk samples from Askola

Results of the ICP-MS analyses of major (K, Fe) and trace elements (Ra, Ba, U, Th, Nb, Pb, Sr, P, Zr, Ti, Y and REE) of the 6 bulk, < 0.250 mm sized grain fraction of soil and sediment samples from Askola are presented in Annex 1 and plotted on Figure 4-14.

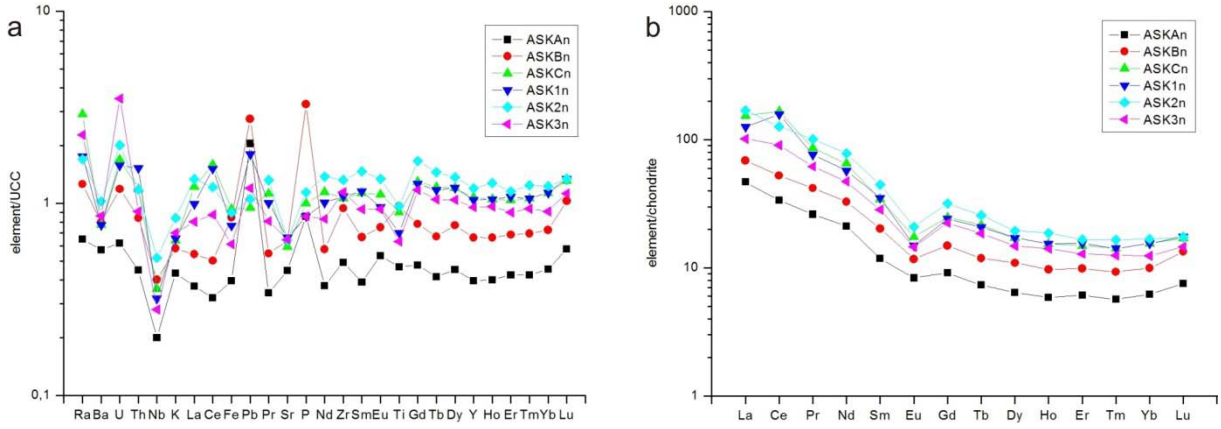

Figure 4-14: Elements of < 250 mm grain size fraction of Askola samples normalized to upper continental crust (UCC) (Taylor and McLennan, 1995). Activity concentration of ^{226}Ra normalized to average soil and sediment concentration of Eastern USA (Greeman and Rose, 1996) (a). Chondrite-normalized REE concentrations (McDonough and Sun, 1995) (b)

The amount of trace elements analysed in the samples from Askola are increased with depth in the case of the uppermost three samples (Ask-A, -B and -C). Trace element concentrations in samples Ask-A and B are significantly lower than in other samples. Trace element content of the deeper samples Ask-C, -1, -2 and -3 do not differ much to each other, and they are close to the average chemical content of the upper continental crust (UCC). Niobium has a negative anomaly in all of the samples. Positive Fe-anomaly occurred in the A and B-horizons (Ask-A and -B) and negative in the deeper ones. Lead has positive anomaly in all of the samples except Ask-C and Ask-2 (Figure 4-14a). Positive anomaly of phosphorus was detected in the uppermost two samples (Ask-A and Ask-B). The samples from the deeper horizons have negative Sr-anomaly (Ask-C, -1, -2 and -3). Titanium has positive anomaly in the B-horizon and negative in the deeper horizons. Positive uranium and radium anomaly occur in all of the samples (Figure 4-14a).

Chondrite-normalised rare earth elements (REE) in all of the samples have a granitoid-type pattern. The materials collected are highly enriched in light and medium rare earth elements (LMREE = La-Gd) compared to heavy rare earth elements (HREE = Gd-Lu). An intermediate negative Eu-anomaly in all of the samples and a small positive Ce-anomaly are

occurred in samples Ask-C and Ask-1 (Figure 4-14b). Clearly visible on Figure 4-14b that REE-content of the samples Ask-A and B are separated from the other samples.

4.3.5. Major and trace elements of soil portions extracted from Askola samples

4.3.5.1. Exchangeable fraction

By the first extraction step the exchangeable cations were extracted. Portion of major (K, Fe) and trace elements (Ra, Ba, U, Th, Nb, Pb, Sr, P, Zr, Ti, Y and REE) extracted at this step from the total concentrations are presented in Annex 2 and plotted on Figure 4-15.

As general quite low amount (< 10%) of trace elements were extracted in this step except radium. Iron and zirconium were extracted only from the upper three in the cases of phosphorus and niobium only from the uppermost and from the upper two soil horizons, respectively. Very low amount of niobium and zirconium (< 0.1 %) and quite high amount of radium (6-55 %) were extracted. Trace elements extracted in higher portion from the uppermost sample compared to the underlying B horizon. In general, the highest portions were extracted from the clayey sample Ask-2 following by the deepest sample Ask-3. However, more exchangeable Ra and Pb where extracted from the sandy samples Ask-1 and Ask-C than from Ask-2, furthermore, Nb, K, Fe, and Zr which were not extracted from the argillaceous sample. No thorium, uranium and titanium extracted in the exchangeable step. Exchangeable radium is present in the highest amount in the sample Ask-C (ca. 60 % of the total) and rather low in B horizon (ca. 6 %).

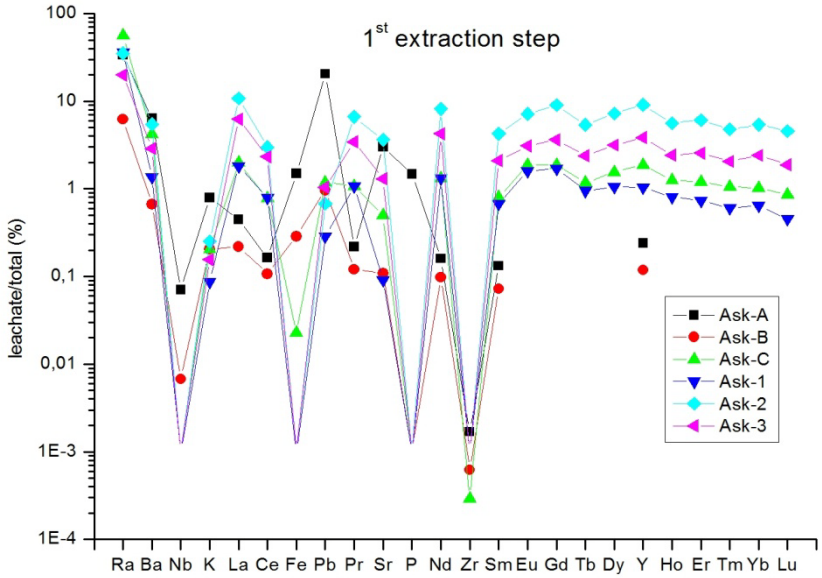

Figure 4-15: Proportion (%) of elements extracted at the first extraction step (Figure 3-2.) from the total amount of these elements in samples from Askola

The chondrite-normalised rare earth elements in extractants are decreasing from light to heavy ones. The highest concentrations were measured in the solvent extracted from the clayey sample Ask-2. Composition of Ask-1 and Ask-C is quite similar; differences occurred only in the contents of heavy rare earth elements. Cerium ratio in the argillaceous and in the underlying deepest samples do show slight negative anomaly. Except in the uppermost two samples Sm and Eu have negative, Gd positive anomaly.

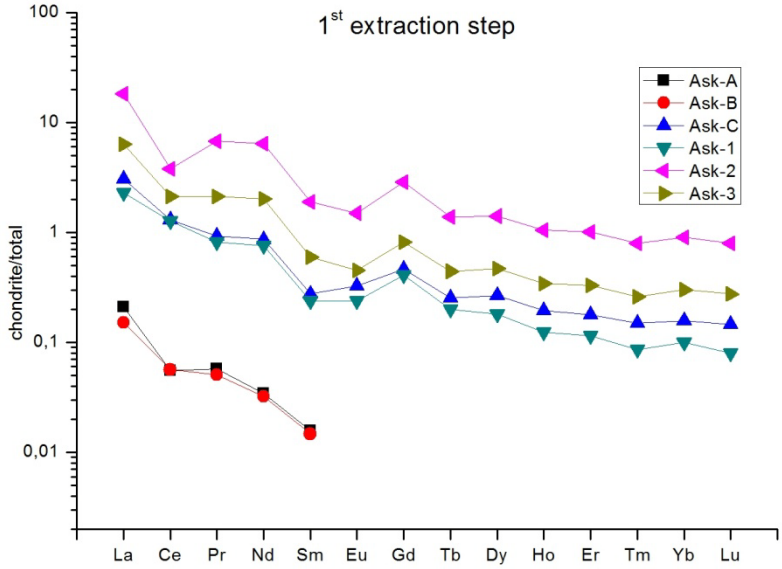

Figure 4-16: Chondrite-normalised REE concentrations in leachates extracted at the first extraction step (Figure 3-2) from samples from Askola (McDonough and Sun, 1995)

4.3.5.2. Oxide fraction

Portion of major (K, Fe) and trace elements (Ra, Ba, U, Th, Nb, Pb, Sr, P, Zr, Ti, Y and REE) extracted at this step from the total concentrations are presented in Annex 2, and plotted on Figure 4-17. In the third extraction step very low amount of Ba (< 0.7 %), K (< 0.1 %), Sr (< 0.2 %) and Zr (< 1.2 %) and large part of the phosphorus (30-80 %) and uranium were extracted (10-55 %). Quite low amount of titanium (few %), and significant portion of Ce were extracted (12-30 %) from mineral horizons (deeper than B horizon).The largest differences were measured in radium and uranium concentrations, portions varied between 0.8-10 % and 10-60 %, respectively.

Rare earth element concentrations measured in the extractants of the six samples do not differ significantly from each other. Cerium concentrations have high positive, europium has slight negative anomaly. Medium and heavy rare earth elements (Gd-Lu) in argillaceous sample Ask-2 do show moderate increase unlike in the other samples where ratios do decrease (Figure 4-18.).

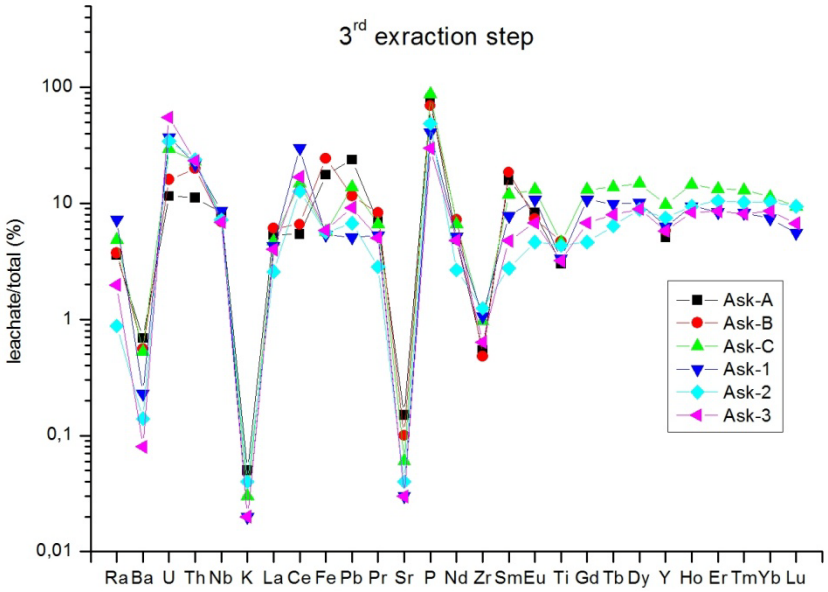

Figure 4-17: Proportion (%) of elements extracted at the third extraction step (Figure 3-2) from the total composition of samples from Askola

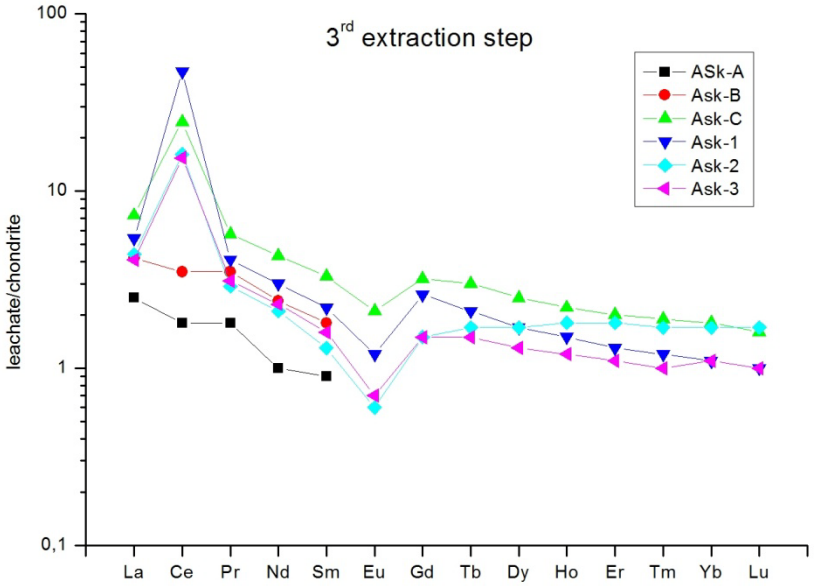

Figure 4-18: Chondrite-normalised REE concentrations in leachates extracted at the third extraction step (Figure 3-2) from samples from Askola (McDonough and Sun, 1995)

4.3.5.3. Organic fraction

Portion of major (K, Fe) and trace elements (Ra, Ba, U, Th, Nb, Pb, Sr, P, Zr, Ti, Y and REE) extracted at this step from the total concentrations are presented in Annex 2, and plotted on Figure 4-19. The "organic" extraction step was performed only on sample Ask-A because accountable amount of organic material was expected only in this sample. Proportions of most of the trace elements extracted at this step were less than 10 % whereas those of Ra (15 %), Ti (15 %), Pb (30 %) and P (40 %) were higher. Only 2 % of total uranium was digested in this step, and no Th, medium and heavy rare earth elements (Eu-Lu) were extracted at all (Figure 4-19).

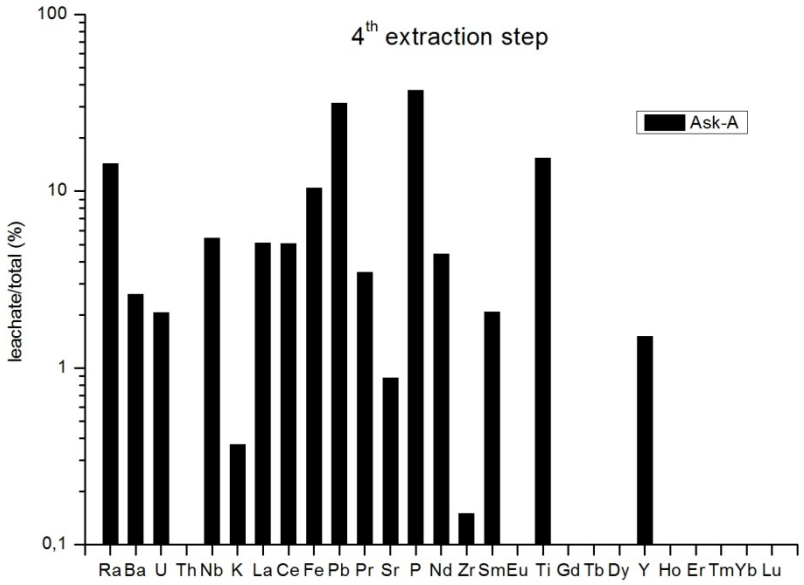

Figure 4-19: Proportion (%) of elements extracted at the fourth extraction step (Figure 3-2) from the total composition of samples from Askola

4.3.5.3. Residual fraction

Portion of major (K, Fe) and trace elements (Ra, Ba, U, Th, Nb, Pb, Sr, P, Zr, Ti, Y and REE) extracted by the sixth "residual" sequential extraction step presented in Annex 2 and the proportion of extracted major and trace elements in the leachates are plotted on Figure 4-20.

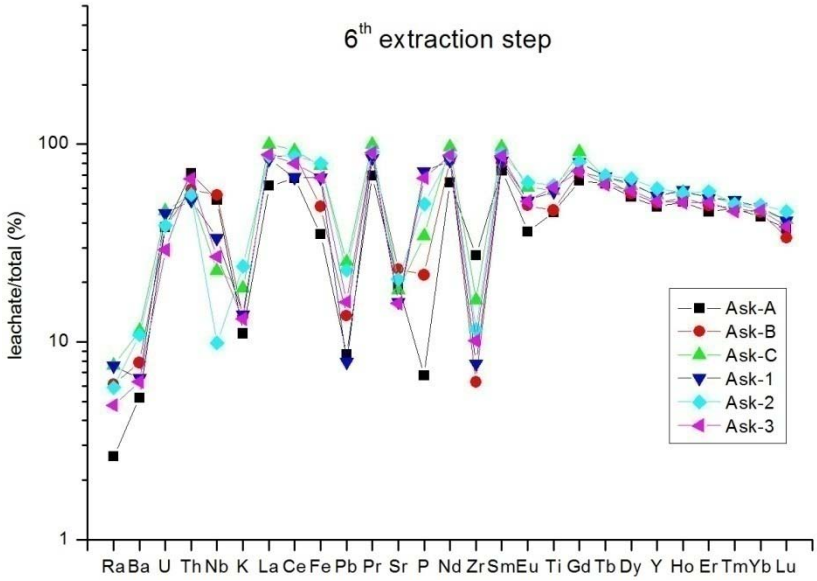

Figure 4-20: Proportion (%) of elements extracted at the last extraction step (Figure 3-2) from the total composition of samples from Askola

Major part of most trace elements were extracted in this sequential extraction step (> 40 %), except some elements, such as radium (< 10 %), barium (< 12 %), potassium (10-20 %), lead, strontium and zirconium (< 0 %). From Ra (2.5 %), Ba (12 %), K (12 %), La (60 %), Fe (35 %), P (6.8 %) and Eu (36 %) the lowest, from zirconium (27.5 %) the highest portion were extracted from the uppermost sample Ask-A.

Patterns of the chondrite-normalised rare earth elements in the extractants of the six samples are similar to each other and to granitoids (Figure 4-2). The increase in heavy rare earth elements measured in bulk samples has vanished. After the three extraction step the negative europium anomalies still exist (Figure 4-21).

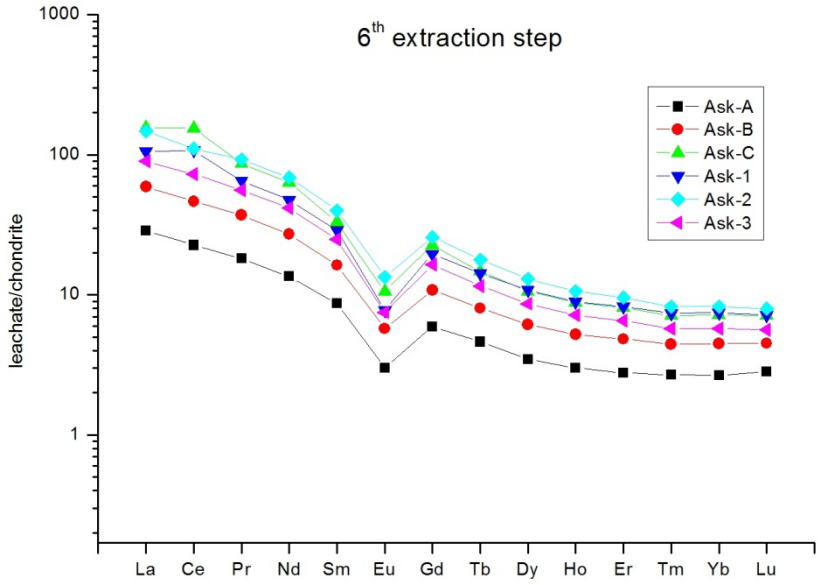

Figure 4-21: Chondrite-normalised REE concentrations in leachates extracted at the last extraction step (Figure 3-2) from samples from Askola (McDonough and Sun, 1995)

From the bulk concentrations low amount of Ba (< 20 %), K (< 25 %), Pb (< 50 %, except from Ask-A, where from ca 80 % were extracted), Sr (< 25 %) and Zr (< 30 %) were digested during the extraction (Figure 4-22). High variation occurred in total concentration of radium, niobium and lead extracted during these steps. Radium was in extracted the highest portion from the sample Ask-C (67 %), in the lowest from Ask-B (16 %), the most of the Nb was extracted from the uppermost two samples Ask-A and Ask-B. From lead the highest portion from Ask-A, the lowest from Ask-1 were leached out. Light and medium rare earth elements (La-Gd) were extracted in the highest amount (ca. 100 %) from Ask-C. Heavy rare earths were extracted in the highest amount from the argillaceous sample Ask-2 (Figure 4-22).

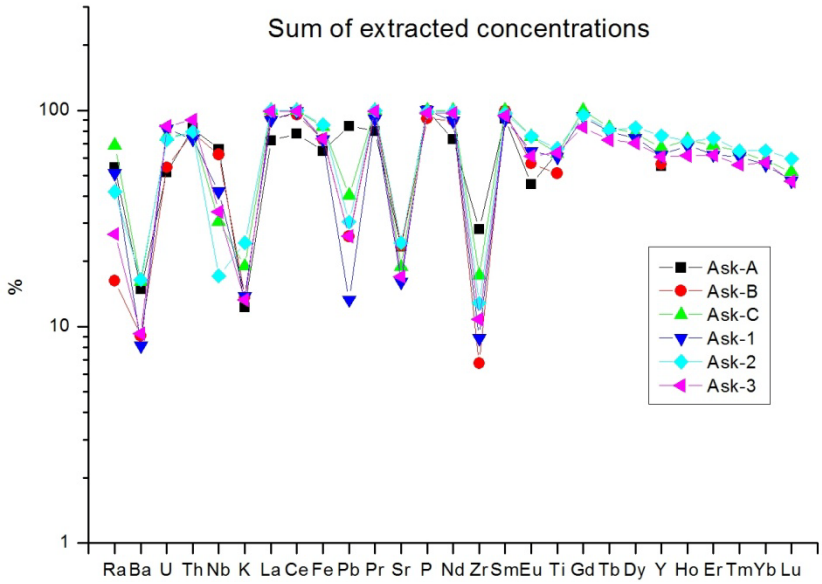

Figure 4-22: Sum (%) of extracted concentrations during the first three and four (in the case of Ask-A) extraction step

4.3.6. Mineralogical study of Askola samples

4.3.6.1. Heavy mineral composition of Askola samples

Heavy minerals separated by heavy liquid with density of $\rho > 2.8$ g/cm^3 from 0.125-0.250 mm and of $\rho > 3.3$ g/cm^3 from 0.063 mm sized grain fraction of Askola samples represents the source material of the eroded and deposited sediments and the possible primary source of uranium (radium) and thorium.

No significant variation occurred in heavy mineral distribution between soil horizons. The upper two horizons (B and C) are less variable than others. Heavy mineral assemblage of grain size fraction 0.125-0.250 mm consists mainly of around 50 %, amphiboles (actinolite and tremolite), except in Ask-1, wherein it is a bit lower (ca. 40 %). In the second and the third highest amount garnet and pyroxene present in the samples, respectively (Figure4-23). In < 0.063 mm sized grain fraction garnets are present in the highest abundant (> 40 %), in sample Ask-B has higher than 70 % garnet content. This fraction is the richest in heavy minerals whereas amount of amphiboles is less relevant (Figure 4-24). Heavy minerals in sample Ask-B are highly weathered and less variable than in sample at greater depth (Figures 4-23, 4-24). The heavy minerals at deeper horizons show slight alteration and grains are fresh though frequently fractured (Figure 4-25).

Garnets are mainly almandine and pyrop. Grossular is present in low amount. Amphiboles are tremolite and actinolite, pyroxenes are diopside, hypersthene and enstatite. Among iron oxides magnetite, Ti-magnetite, hematite and goethite were recognized. Furthermore, apatite, titanite, ilmenite, micas, rutile, zircon were identified.

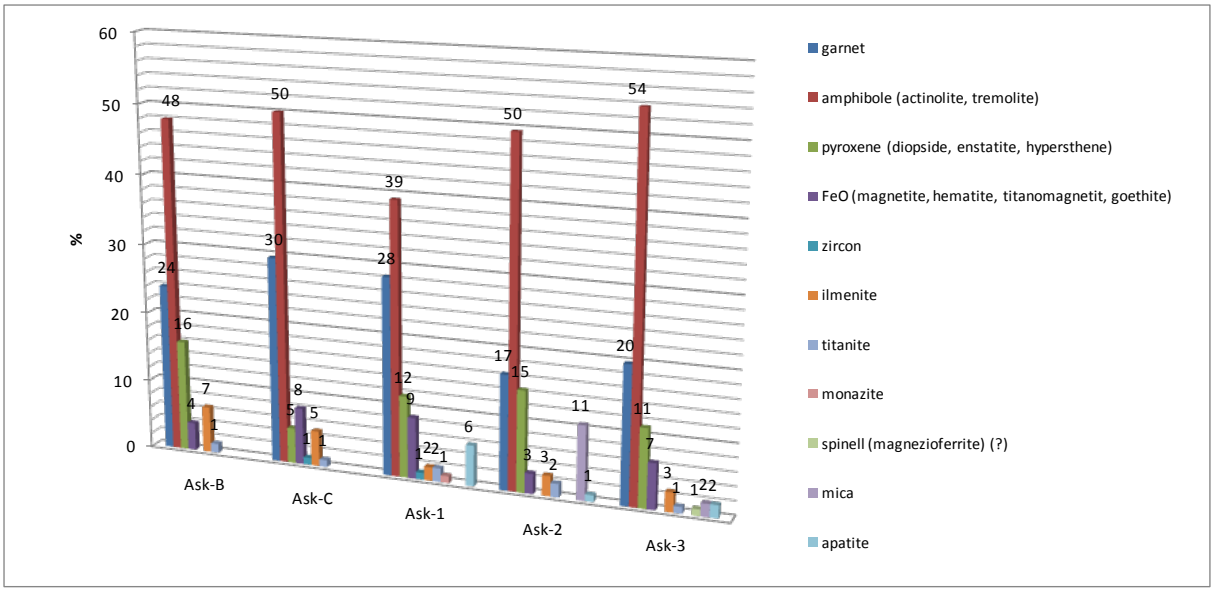

Figure 4-23: Heavy mineral ($\rho > 2.8$ g/cm^3) distribution of 0.125-0.250 mm sized grain fraction of Askola samples

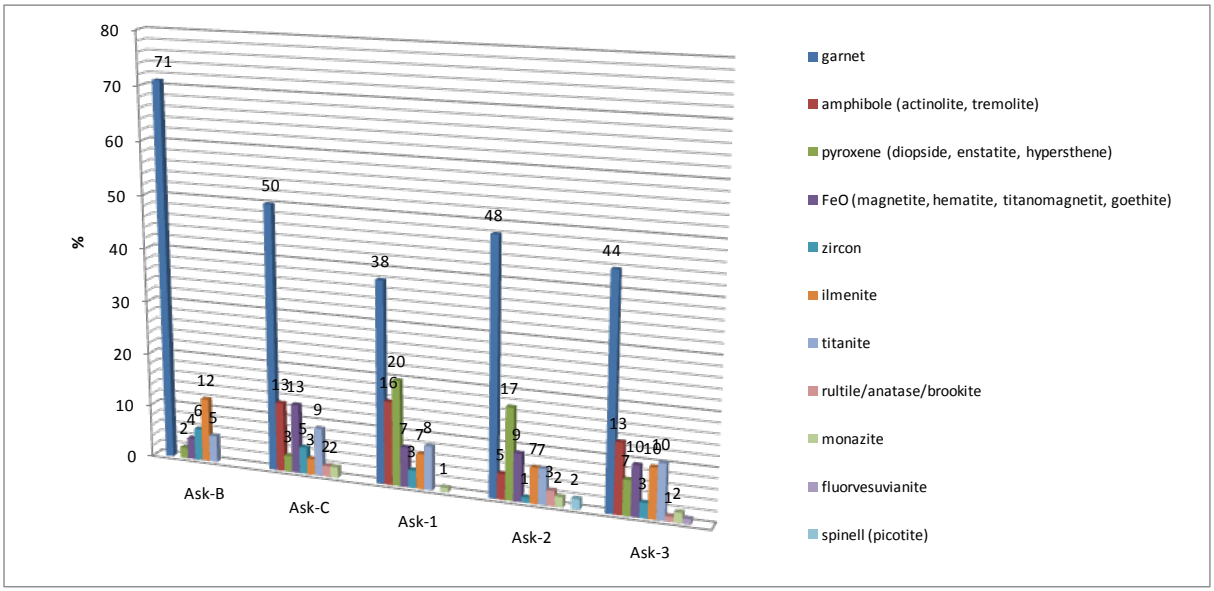

Figure 4-24: Heavy mineral ($\rho > 3.3$ g/cm^3) distribution of < 0.063 mm sized grain fraction of Askola samples

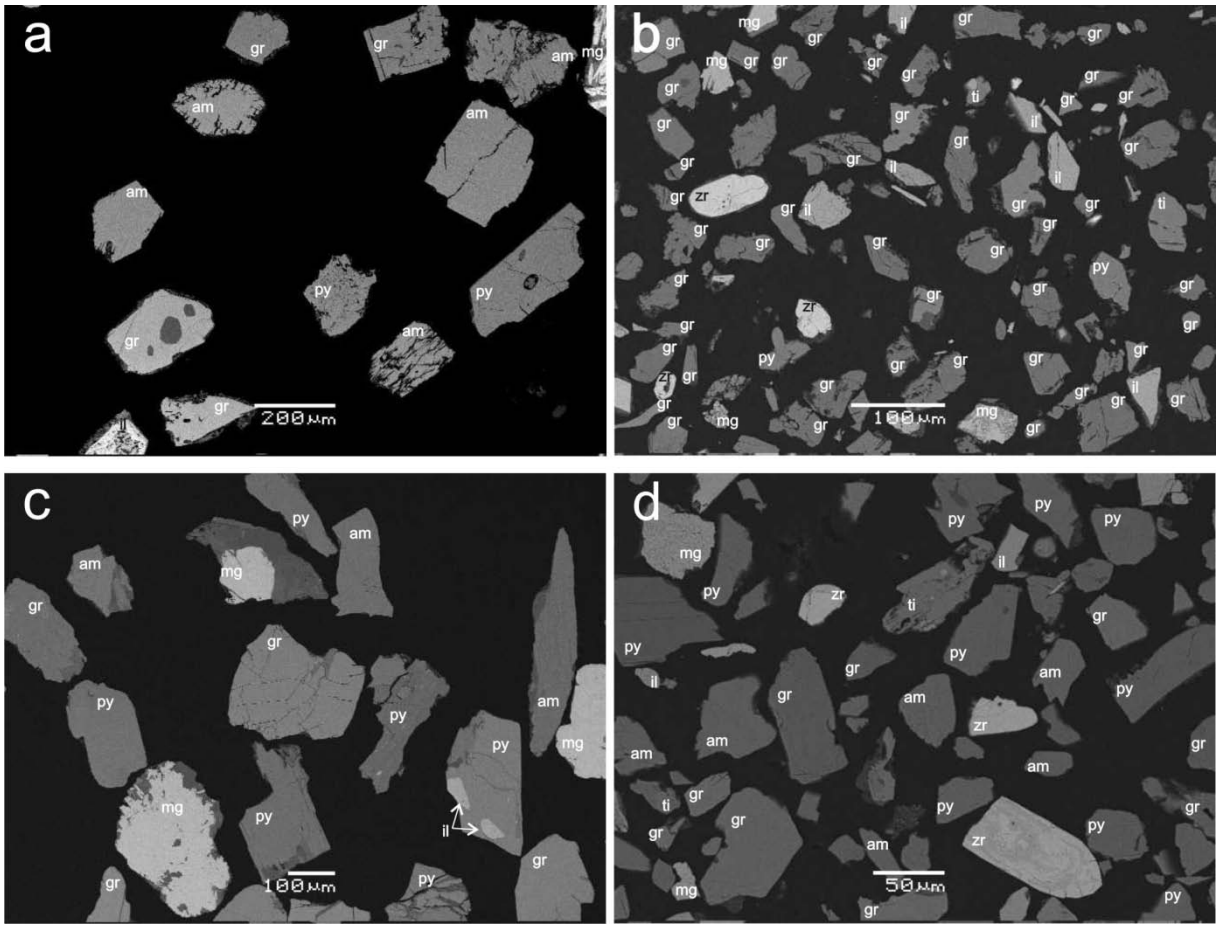

Figure 4-25: Back scattered electron images of weathered heavy minerals from grain size fraction of 0.125-0.250 mm (a) and < 0.063 mm (b) of soil sample Ask-B, and fresh (unweathered) from grain size fraction of 0.125-0.250 mm (c) and < 0.063 mm (d) of soil sample Ask-1. gr = garnet; am = amphibole; py = pyroxene; mg = magnetite/hematite/goethite; il = ilmenite; ti = titanite; zr = zircon

As major U- and Th-bearing minerals uraninite, uranothorite, thorianite, brannerite/orthobrannerite, monazite, xenotime and other Th-, U-silicates and oxides (Figure 4-26) were identified. In the samples more Th- than U-rich minerals were found. Uranium and Th-rich minerals are rather weathered and have various habits from isometric through fractured aggregate to lenticular shape. Uranium and Th concentrations do vary from few percent up to more than 50 %.

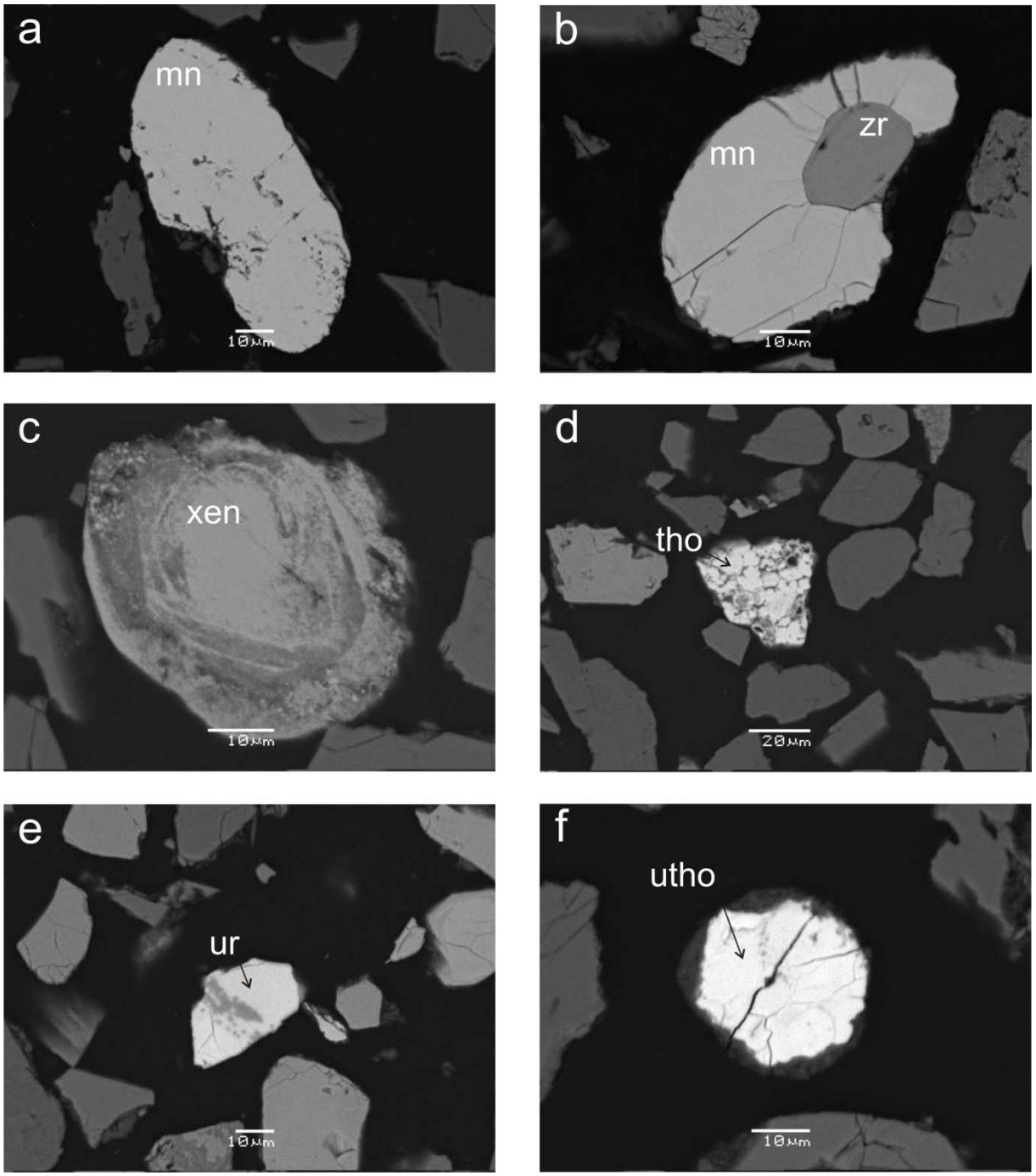

Figure 4-26: Back scattered electron images (BSE) of major U- and Th bearing minerals from grain size fraction of < 0.063 mm. a: U- and Th-bearing monazite (mn) grain in sample Ask-B; b: Th-bearing monazite (mn) with zircon (zr) inclusion in sample Ask-B; c: U-bearing, zoned, weathered xenotime (xen) in sample Ask-1; d: lenticular structured thorite (tho) in sample Ask-2; e: small (ca 20µm) uraninite (ur) grain with dark grey goethite in sample Ask-3; f: isometric uranothorite (utho) grain in sample Ask-B

4.3.6.2. Effect of weathering on chemical composition of U-, Th-bearing minerals in Askola samples

For studying weathering effects on chemical composition of U- and Th-bearing minerals, moderate and highly weathered monazite, xenotime, thorite, uranothorite, uraninite and brannerite/orthobrannerite were selected from Askola samples and studied by electron microprobe. From these, four representative grains were selected for X-ray mapping which

are presented on Figure 4-27 – 4-30 with the corresponding chemical compositions (Table 4-3 – 4-6 and Annex-3). Chemical composition was measured by wavelength dispersive spectrometer and normalized up to 100/total concentration measured. This method was used in order to the better comparison. Since we concentrated on the weathering effect, only weathered minerals were selected for this study. The weathering resulted in structural non-homogeneity in minerals which caused lower total concentrations. Considering all of the minerals are weathered, iron was calculated and presented as Fe_2O_3 (Table 4-3 – 4-6).

Weathering resulted in onion skin structured xenotime grain presented in Figure 4-26c and 4-27a has similar major constituent, Y_2O_3/P_2O_5 ratio (1.3-1.4) as it has been published by Hetherington et al. (2008) (ca. 1.2), therefore, the correction of the concentrations in order to get total of 100 is probably not cause large modification in chemical ratios of other elements. Correlation coefficient (Pierson product-moment coefficient) between Fe and U is negative and quite low (-0.48), between P and U is rather high (0.66) and between P and Fe is negative and high (-0.85) (Table 4-3, Annex 3). In two measuring points (#10 and #11), where the highest uranium contents were measured, the iron content (ca. 2.5 wt.%) is higher than in the fresh part at 1st and 2nd measuring points (lower than the detection limit), but not the highest as it was measured at points of 3-6 and 8-9 (10-18 wt.%) (Figure 4-27, Table 4-3 and Annex-3).

The uranothorite grain from grain size fraction < 0.063 mm of sample Ask-1 demonstrated in Figure 4-28 contains phosphorus, cerium, neodymium and yttrium, too. Thorium and uranium concentrations varies between 9-60 wt.% and 3-17 wt.%, respectively (Table 4-4). Very good positive correlations occurred between Fe and Th, Fe and U and Fe and Ce 99 %, 74 % and 91 %, respectively (Annex-3).

The uraninite/brannerite/orthobrannerite grain from grain size fraction < 0.063 mm of sample Ask-3 presented in Figure 4-29 contains significant amount of niobium (ca. 10 wt.%), titanium (ca. 10 wt.%) and some thorium (ca. 1 wt%) (Table 4-5). The uranium content varies between 40-60 wt.%. The lowest concentrations of U (ca. 2 wt.%) measured in Fe-rich parts (goethite) in the middle of the grain at 3rd and 4th measuring points (Figure 4-29a). The correlations between Fe and Th and Fe and U are almost -100 % (Annex-3).

A Nb-, Th-bearing brannerite/orthobrannerite with thorianite intercalation presented in Figure 4-30 has a uranium content of up to 65 wt.% (Table 4-6). Thorium content varies between 1 to 45 wt.%. The grain contains ca. 10 % (5-15 wt.%) of Nb. In the area (6th and 7th points) (Figure 4-30a), where the highest amount of Fe and Ti were measured (14 and 67 wt.%,

respectively), Th and U are the lowest < 1 and < 3 wt.%, respectively (Figure 4-30b-c, Table 4-6). The correlation between iron and uranium was rather high, 77 % in contrast of Fe and Th, where low correlation occurred (31 %) (Annex-3). Also, there is low correlation between uranium and thorium (36 %).

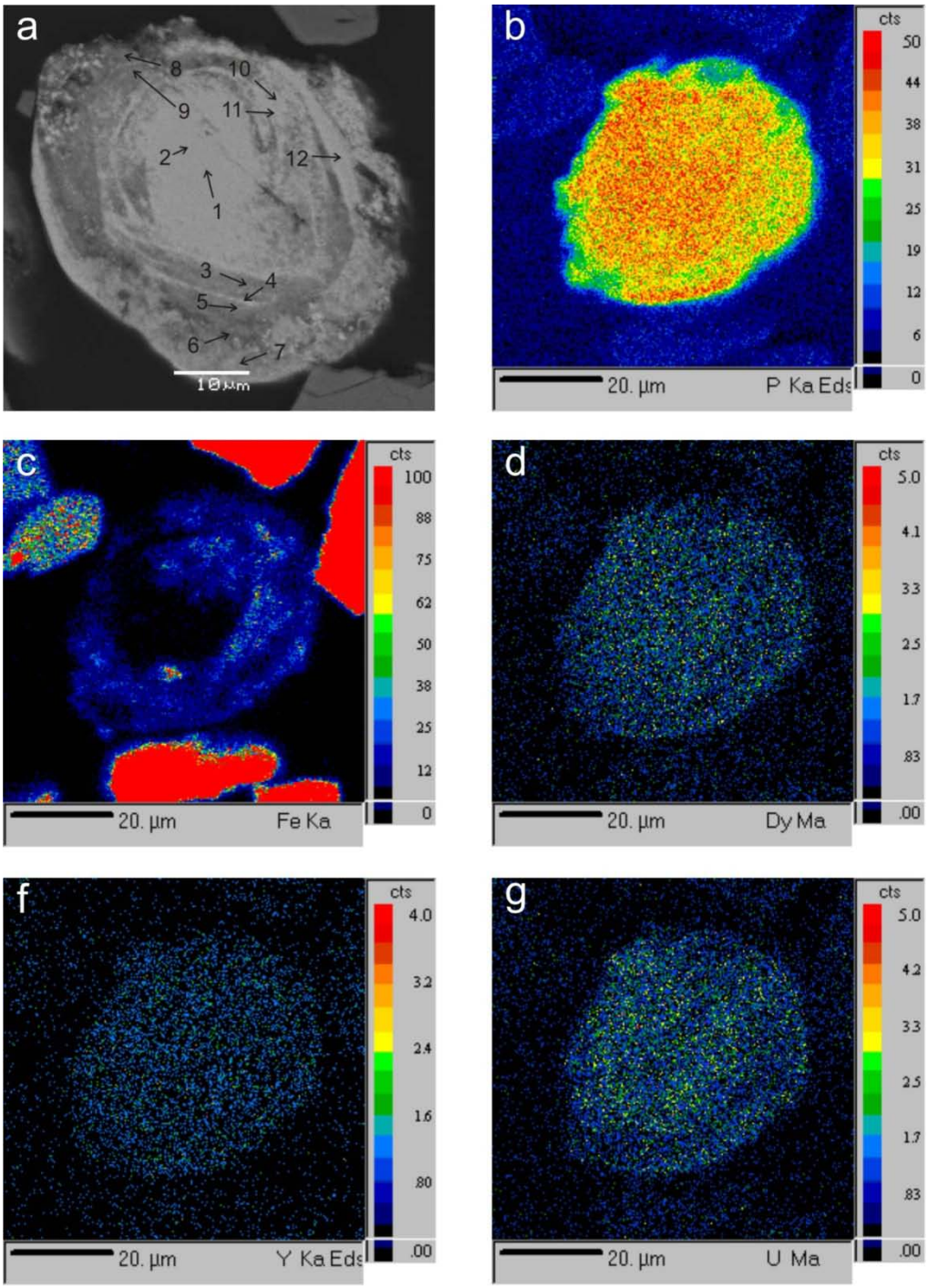

Figure 4-27: Onion structured, zoned xenotime grain with iron rich layers < 0.063 mm of sample Ask-1. a: BSE image of the grain and the analysing points; b: X-ray map of P Kα analysed by energy dispersive spectrometer (EDS); c: X-ray map of Fe Kα analysed by wavelength dispersive spectrometer (WDS); d: X-ray map of Dy Mα analysed by WDS; e: X-ray map of Y Kα analysed by EDS; f: X-ray map of U Mα analysed by WDS. BSE image has a different orientation than X-ray maps.

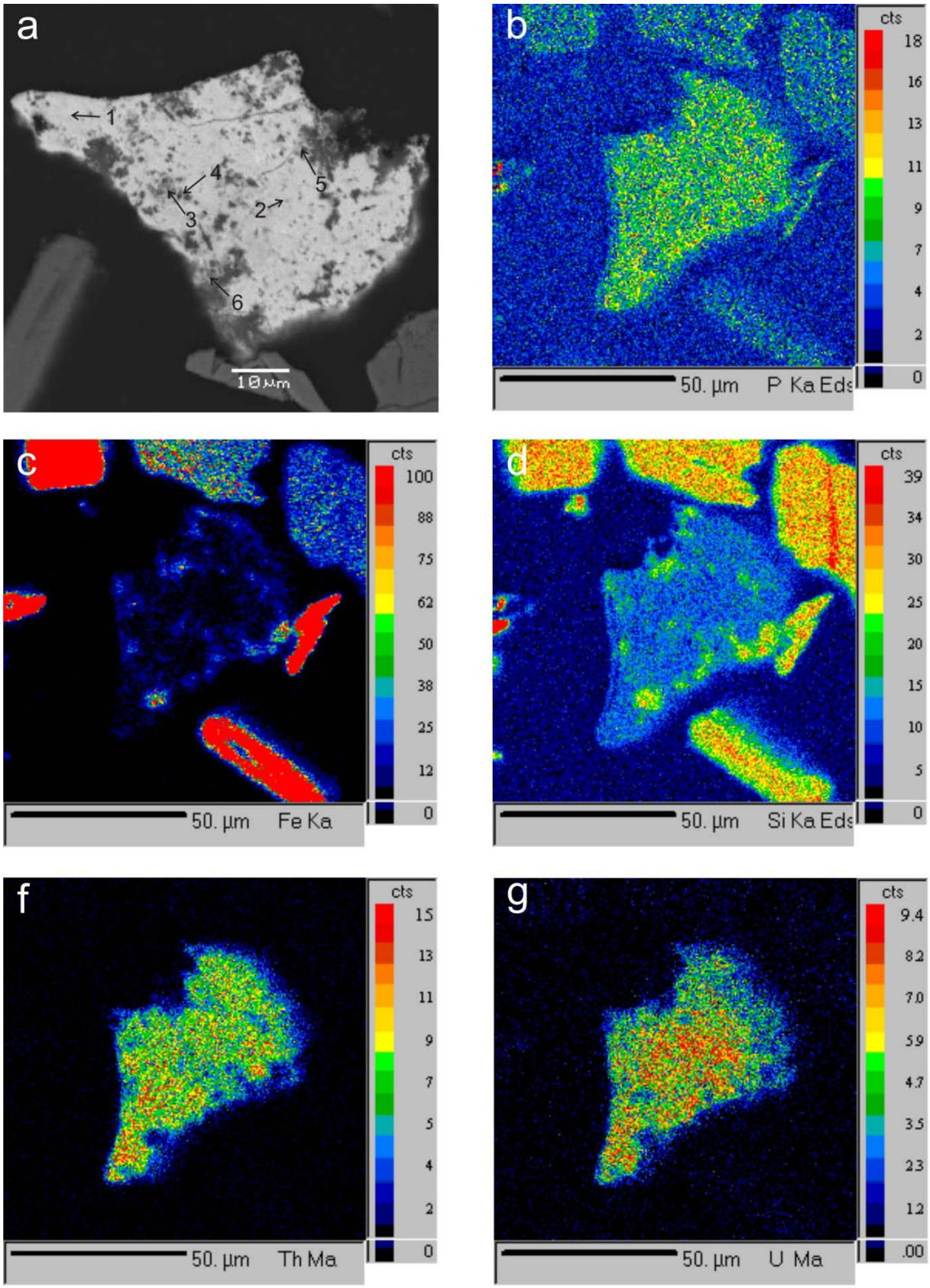

Figure 4-28: Weathered uranothorite grain from grain size fraction < 0.063 mm of sample Ask-1. a: BSE image of the grain and the analysing points; b: X-ray map of P Kα analysed by energy dispersive spectrometer (EDS); c: X-ray map of Fe Kα analysed by wavelength dispersive spectrometer (WDS); d: X-ray map of Si Kα analysed by EDS; e: X-ray map of Th Mα analysed by WDS; f: X-ray map of U Mα analysed by WDS. BSE image has a different orientation than X-ray maps.

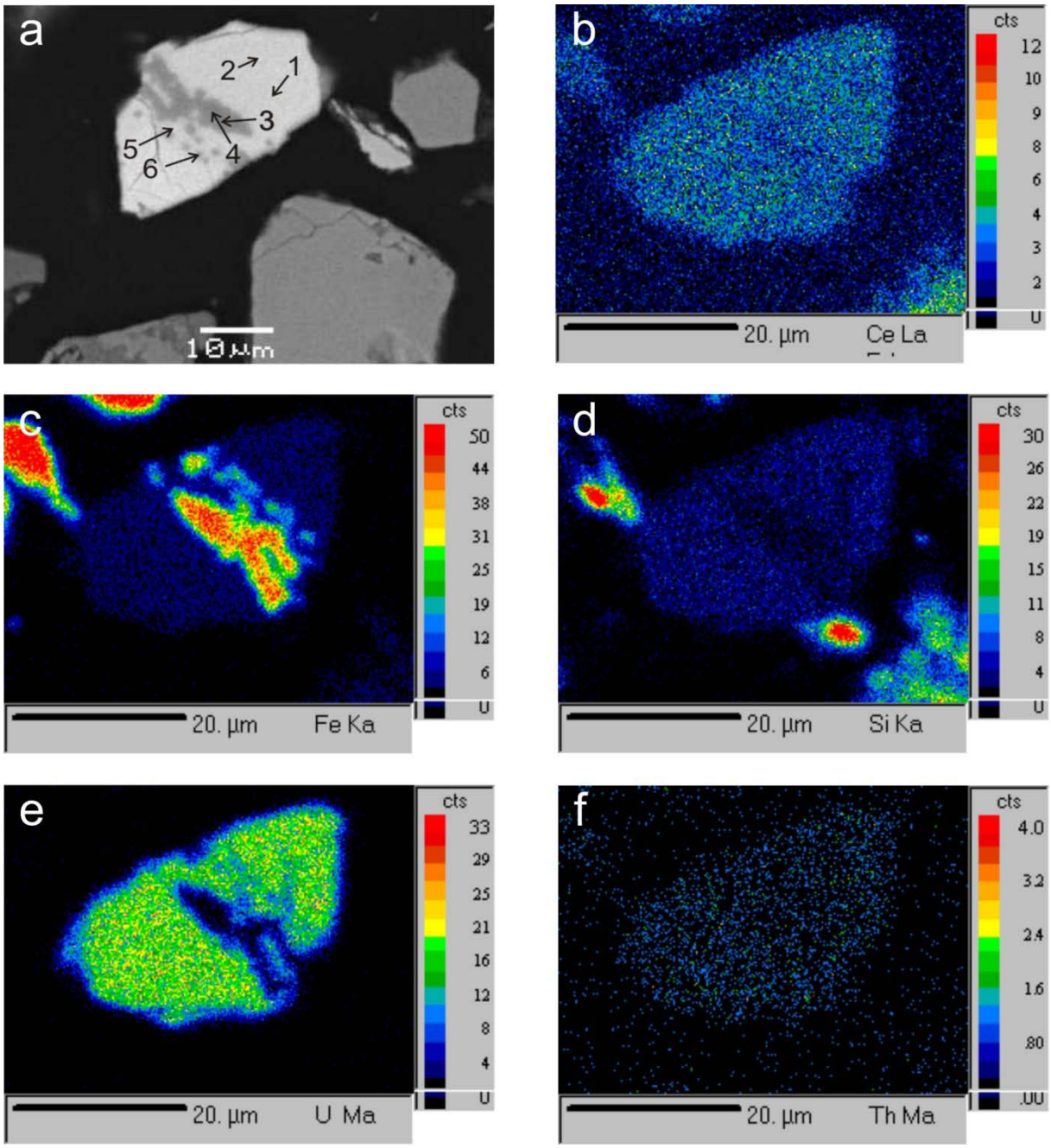

Figure 4-29: Uraninite grain with goethite filling in the middle from grain size fraction < 0.063 mm of sample Ask-3. a: BSE image of the grain and the analysing points; b: X-ray map of Ce Lα analysed by energy dispersive spectrometer (EDS); c: X-ray map of Fe Kα analysed by wavelength dispersive spectrometer (WDS); d: X-ray map of Si Kα analysed by WDS; e: X-ray map of U Mα analysed by WDS; f: X-ray map of Th Mα analysed by WDS. BSE image has a different orientation than X-ray maps.

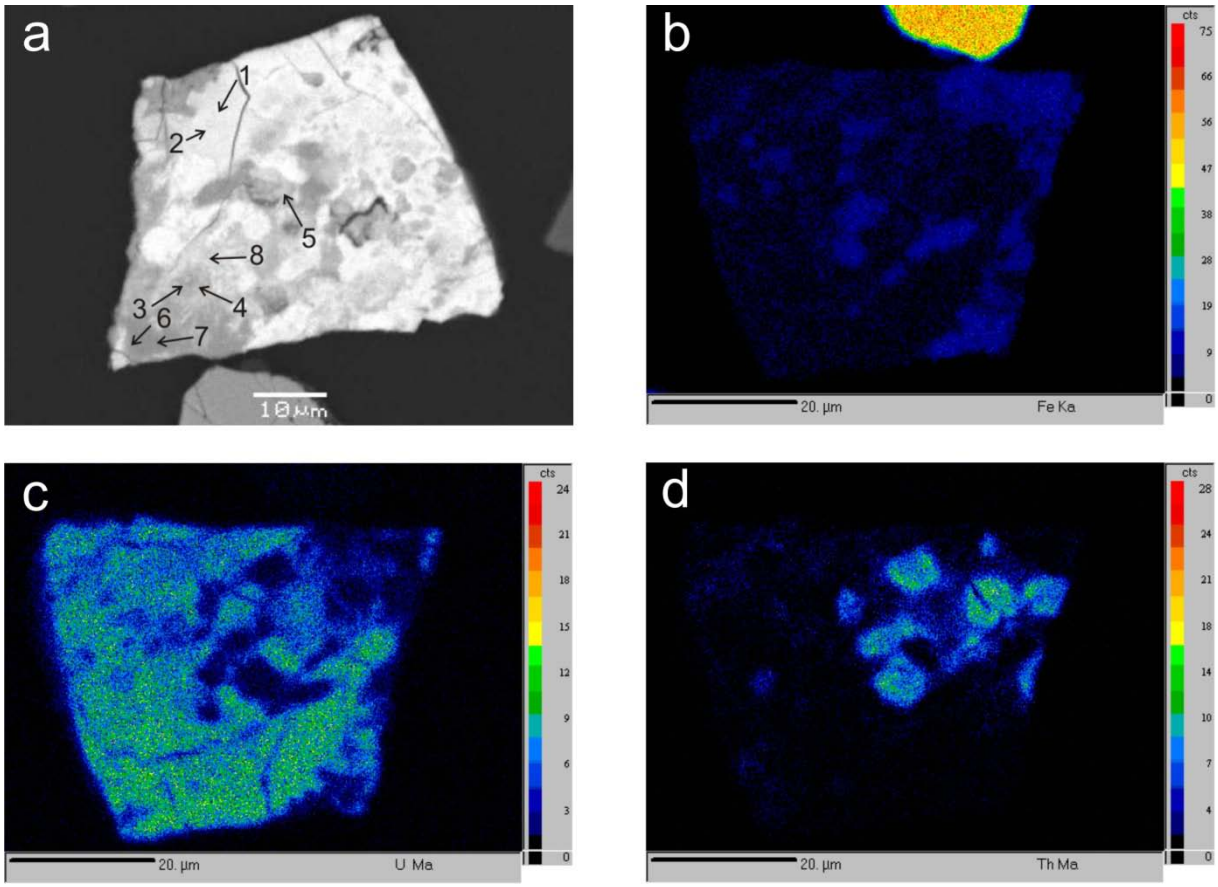

Figure 4-30: Th-bearing orthobrannerite grain from grain size fraction < 0.063 mm of sample Ask-3. a: BSE image of the grain and the analysing points; b: X-ray map of Fe Kα analysed by wavelength dispersive spectrometer (WDS); c: X-ray map of U Mα analysed by WDS; d: X-ray map of Th Kα analysed by WDS. BSE image has a different orientation than X-ray maps.

Table 4-3: Chemical composition of different areas of the weathered, zoned xenotime grain presented in Figure 4-27 from grain size fraction of < 0.063 mm of sample Ask-1. Concentrations are presented in wt.%.

	F	Na_2O	MgO	Al_2O_3	SiO_2	P_2O_5	Cl	K_2O	CaO	TiO_2	MnO	Fe_2O_3	Y_2O_3	Nd_2O_3	ThO_2	U_2O_3	La_2O_3	SmO	Ce_2O_3	PbO	Nb_2O_5	Total
1	0.06	0.00	0.00	0.00	0.45	40.05	0.00	0.00	0.31	0.00	0.00	0.00	54.48	0.06	0.23	2.48	0.00	0.67	0.05	0.86	0.30	100.00
2	0.10	0.00	0.00	0.00	0.52	40.71	0.01	0.00	0.40	0.00	0.00	0.00	54.01	0.12	0.16	2.46	0.00	0.78	0.00	0.71	0.00	100.00
3	0.69	0.00	0.00	0.80	1.71	31.82	0.15	0.00	0.85	0.33	0.01	14.20	44.64	0.10	0.32	2.68	0.00	0.45	0.38	0.87	0.00	100.00
4	0.57	0.01	0.00	0.72	1.48	32.27	0.16	0.00	0.81	0.30	0.02	14.51	43.88	0.32	0.37	2.49	0.00	0.80	0.28	0.65	0.36	100.00
5	0.61	0.01	0.00	0.89	1.60	33.19	0.20	0.00	0.92	0.24	0.06	10.23	46.46	0.48	0.45	2.34	0.02	0.73	0.46	0.80	0.30	100.00
6	1.04	0.09	0.00	1.49	2.10	28.64	0.27	0.01	1.32	1.89	0.10	18.24	40.29	0.24	0.55	1.21	0.10	0.96	0.76	0.70	0.00	100.00
7	2.71	0.10	0.07	0.51	1.95	29.58	0.07	0.00	4.36	2.95	0.06	6.70	43.20	0.69	0.40	1.49	1.04	0.88	2.81	0.36	0.07	100.00
8	0.61	0.00	0.00	0.85	1.24	33.35	0.23	0.00	0.93	0.31	0.01	12.58	44.92	0.10	0.50	2.40	0.00	0.80	0.48	0.64	0.04	100.00
9	0.79	0.00	0.01	1.07	1.31	33.43	0.28	0.00	1.10	0.41	0.00	10.12	46.44	0.17	0.53	2.38	0.04	0.70	0.62	0.35	0.23	100.00
10	0.15	0.00	0.00	0.00	0.87	38.15	0.03	0.00	0.49	0.08	0.00	2.59	51.65	0.00	0.49	3.79	0.00	0.67	0.22	0.74	0.09	100.00
11	0.24	0.00	0.00	0.05	0.90	37.52	0.08	0.00	0.52	0.11	0.04	2.41	50.84	0.50	0.57	3.85	0.00	0.85	0.25	1.17	0.09	100.00
12	0.77	0.00	1.96	3.01	4.90	32.19	0.12	0.03	1.05	0.61	0.13	7.01	44.67	0.11	0.18	1.79	0.00	0.40	0.42	0.67	0.00	100.00

Elements are normalised by hundred/total ratio in order to the easier comparison. Raw concentrations are presented in Annex 3.

Table 4-4: Chemical composition of different areas of the weathered uranothorite grain presented in Figure 4-28 from grain size fraction of < 0.063 mm of sample Ask-1. Concentrations are presented in wt.%.

	F	Na_2O	MgO	Al_2O_3	SiO_2	P_2O_5	Cl	K_2O	CaO	TiO_2	MnO	Fe_2O_3	Y_2O_3	Nd_2O_3	ThO_2	U_2O_3	La_2O_3	SmO	Ce_2O_3	PbO	Nb_2O_5	Total
1	0.28	0.00	0.10	2.80	14.01	5.38	0.03	0.00	0.46	0.30	0.01	1.03	1.89	2.62	56.59	11.40	0.00	0.84	2.28	0.00	0.00	100.00
2	0.32	0.00	0.06	2.70	13.84	5.49	0.02	0.00	0.39	0.19	0.00	0.85	1.94	2.76	57.14	10.96	0.02	0.95	2.38	0.00	0.00	100.00
3	0.18	0.00	0.12	2.81	12.64	4.08	0.13	0.00	0.32	0.19	0.08	0.78	1.53	2.20	58.33	13.20	0.09	0.95	2.38	0.00	0.00	100.00
4	0.26	0.00	0.07	2.73	14.71	5.22	0.06	0.00	0.40	0.20	0.00	1.03	2.27	3.48	51.33	14.11	0.00	1.25	2.86	0.00	0.00	100.00
5	0.10	0.06	7.58	25.78	34.15	1.63	0.07	0.16	0.22	0.08	0.34	15.31	0.34	0.23	9.65	3.53	0.00	0.18	0.56	0.00	0.00	100.00
6	0.28	0.00	1.36	9.61	16.74	4.72	0.32	0.00	0.39	0.28	0.03	4.91	1.56	1.96	37.32	16.90	0.04	0.88	2.59	0.00	0.12	100.00

Elements are normalised by hundred/total ratio in order to the easier comparison. Raw concentrations are presented in Annex 3.

Table 4-5: Chemical compositions of different areas of the Nb-bearing uraninite grain with goethite filling presented in Figure 4-29 from grain size fraction of < 0.063 mm of sample Ask-3. Concentrations are presented in wt.%.

	F	Na_2O	MgO	Al_2O_3	SiO_2	P_2O_5	Cl	K_2O	CaO	TiO_2	MnO	Fe_2O_3	Y_2O_3	Nd_2O_3	ThO_2	U_2O_3	La_2O_3	SmO	Ce_2O_3	PbO	Nb_2O_5	Total
1	0.14	0.09	0.02	0.80	1.92	1.93	0.12	0.00	2.11	11.84	0.03	3.54	0.07	0.00	0.86	65.36	0.00	0.17	2.06	1.02	7.91	100.00
2	0.13	0.09	0.00	0.85	1.75	1.68	0.11	0.00	1.93	11.49	0.02	3.27	0.06	0.00	0.86	63.27	0.00	0.17	1.90	1.01	11.42	100.00
3	0.19	0.00	0.11	0.13	1.11	0.15	0.02	0.00	0.25	6.11	3.10	81.92	0.00	0.00	0.38	2.67	0.00	0.09	0.23	0.75	2.77	100.00
4	0.15	0.00	0.20	0.16	1.23	0.19	0.03	0.00	0.28	6.07	3.12	81.70	0.00	0.00	0.49	2.51	0.00	0.05	0.18	0.87	2.77	100.00
5	0.11	0.15	0.07	0.67	1.77	1.28	0.06	0.00	1.39	10.28	0.94	27.94	0.05	0.00	0.72	43.89	0.00	0.06	1.03	1.29	8.31	100.00
6	0.07	0.07	0.10	0.59	1.72	1.28	0.15	0.00	1.36	9.93	0.85	28.48	0.08	0.00	0.68	44.84	0.00	0.10	1.07	0.96	7.68	100.00

Elements are normalised by hundred/total ratio in order to the easier comparison. Raw concentrations are presented in Annex 3.

Table 4-6: Chemical compositions of different area of the weathered Th-bearing orthobrannerite grain presented in Figure 4-30 from grain size fraction of < 0.063 mm of sample Ask-3. Concentrations are presented in wt.%.

	F	Na_2O	MgO	Al_2O_3	SiO_2	P_2O_5	Cl	K_2O	CaO	TiO_2	MnO	Fe_2O_3	Y_2O_3	Nd_2O_3	ThO_2	UO_2	La_2O_3	SmO	Ce_2O_3	PbO	Nb_2O_5	Total
1	0.09	0.12	0.00	0.68	1.63	1.64	0.02	0.00	1.42	14.06	0.04	2.65	0.08	0.00	0.36	64.00	0.05	0.21	1.41	1.18	10.36	100
2	0.11	0.05	0.00	0.96	2.01	2.39	0.00	0.00	1.40	12.11	0.03	2.31	0.12	0.00	0.77	65.15	0.00	0.03	1.17	1.32	10.05	100
3	0.35	0.00	0.01	0.18	5.78	3.09	0.07	0.00	0.79	33.64	0.10	7.79	1.21	0.11	21.12	16.23	0.04	0.23	0.69	0.13	8.44	100
4	0.24	0.01	0.00	0.08	5.22	2.99	0.04	0.00	0.84	35.75	0.12	7.90	1.06	0.07	18.79	16.65	0.03	0.27	0.75	0.46	8.73	100
5	0.35	0.00	0.08	1.67	10.51	6.45	0.09	0.00	1.36	13.43	0.04	3.45	2.00	0.21	44.62	8.27	0.07	0.56	1.10	0.35	5.41	100
6	0.00	0.00	0.02	0.00	0.00	0.00	0.05	0.01	0.32	67.37	0.34	14.03	0.00	0.00	0.62	2.64	0.00	0.00	0.15	0.00	14.45	100
7	0.10	0.00	0.03	0.00	0.01	0.00	0.05	0.00	0.35	67.61	0.39	13.94	0.00	0.00	0.63	2.45	0.00	0.08	0.24	0.17	13.96	100
8	0.13	0.06	0.01	1.23	3.98	3.43	0.06	0.00	1.31	16.77	0.00	3.24	0.16	0.00	13.97	44.08	0.08	0.23	1.28	1.26	8.71	100

Elements are normalised by hundred/total ratio in order to the easier comparison. Raw concentrations are presented in Annex 3.

5. PALMOTTU SAMPLING SITE

5.1. Location of Palmottu sampling site

Palmottu sampling site is located at Nummi-Pusula ca.100 km NW to Helsinki, Finland (Figure 5-1). The Palmottu area was selected as part of the Finnish Nuclear Waste Disposal Programme in 1987, because of the uranium mineralisation, as a natural analogue study to the behaviour of spent nuclear fuel in crystalline rock. Furthermore, between 1996 and 2000 this site was the subject of an International Atomic Energy Agency (IAEA) international research project, which resulted in a greatly improved understanding of uranium migration (Blomqvist et al., 1998; Blomqvist et al., 2000). However, the migration in overburden was less deeply studied. Therefore, for sampling, three places, close to the uranium mineralisation, were selected (Figures 5-1 and 5-2).

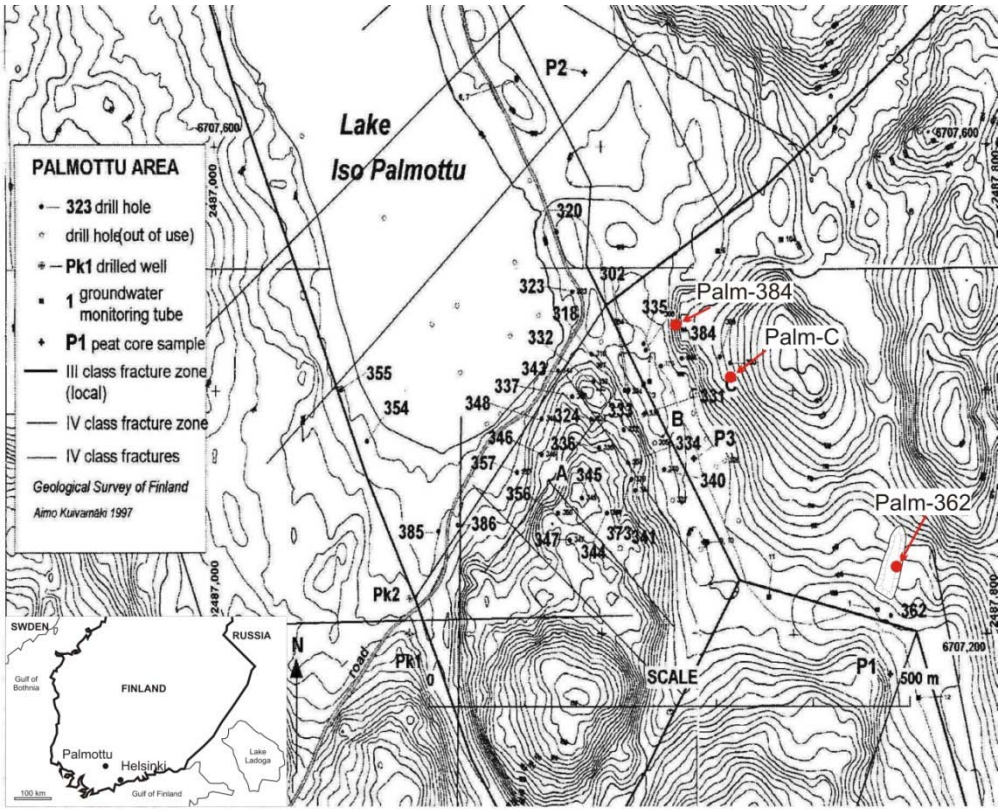

Figure 5-1: Topographical map of the sampling area in Palmottu and the location of Palmottu in Finland. The sampling points are marked by red dots on the topographical map (modified after Kaija et al. (2003)). Elevation contour data © National Land Survey of Finland

Three places were sampled along the possible surface migration path of uranium from the mineralisation (Palm-C, Figure 2a) down across the swamp (Palm-384, Figure 5-2a) along the brook (Palm-362, Figure 5-2b).The objective of the site selection was to study the

concentration changes and type of occurrences of long lived members of the ^{238}U-and ^{232}Th-decay series along the horizontal migration pathway.

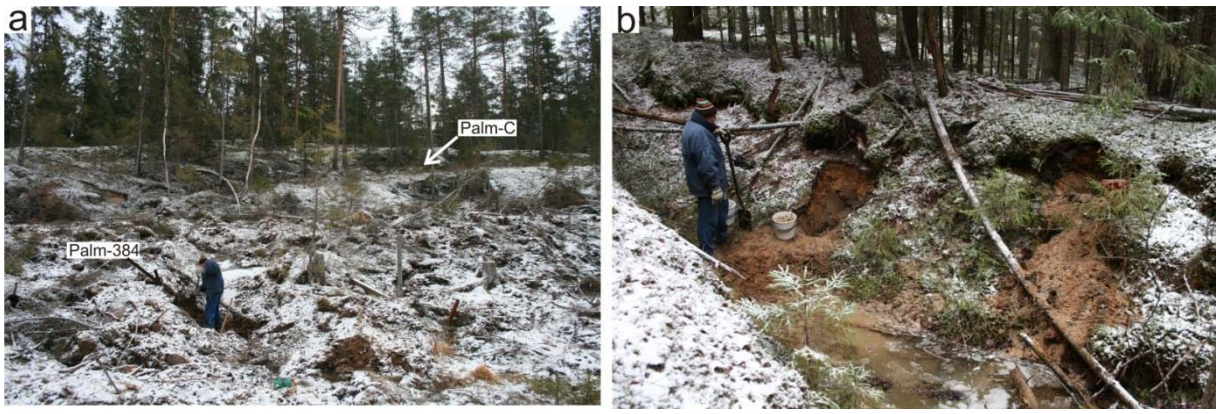

Figure 5-2: Sampling points of samples Palm-C, Palm-384 (a) and Palm-362 (b)

5.2. Geological background of Palmottu sampling site

5.2.1. Bedrock at Palmottu sampling site

Palmottu is situated within the Proterozoic Svecofennian orogenic belt, which was formed about 1.8 billion years ago in the collision of continental plates leading to the rise of Svecofennian mountain belt on the plate contact (Figure 2-1). Nowadays the highly metamorphosed gneisses are considered the roots of the ancient mountain belt (Kuivamäki et al., 1991). The Palmottu site represents a near-surface uranium occurrence located in a Precambrian metasedimentary sequence of rocks in south-western Finland. The Palmottu occurrence is situated close to the contact with the late-kinematic Perniö granite together with some other uranium indications (Figure 5-3). The major sedimentation phase took place 2400-1900 million years ago (Simonen, 1980). High-grade regional metamorphism at 600-800° C and 4-5 kb (Schreurs and Westra, 1986) provoked a thorough recrystallisation and change in the original mineralogy and destroyed largely the original sedimentary textures generating the present, variably migmatised gneissic lithologies. The present lithologies are predominantly mica gneisses frequently containing almandine garnet or pyroxene porphyroblasts as a reflection of the chemical composition of the sedimentary precursors. The culmination stage of the metamorphism was about 1.84 billion years ago (Huhma, 1986; Vaasjoki, 1996) at the same time as the late-kinematic K-granite massif of the Perniö granite intruded the surrounding sediments.

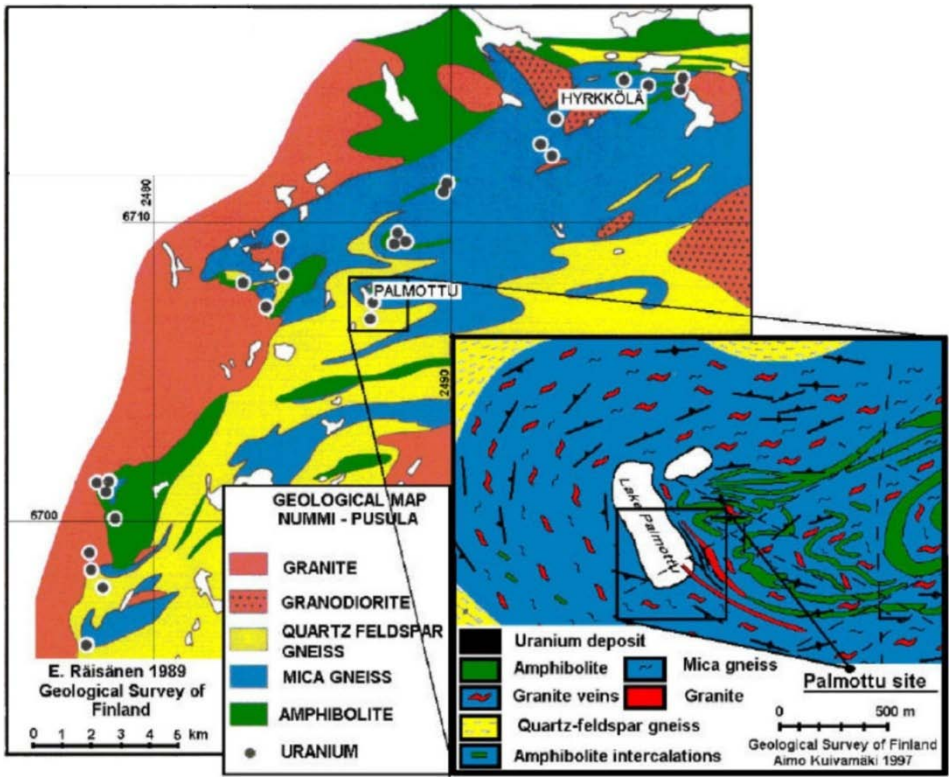

Figure 5-3: Pre Quaternary geological map of the Nummi-Pusula area, southern Finland (Räisänen, 1986; Kuivamäki, 1997)

During or soon after the peak of the metamorphism, pegmatite veins were intruded into the metasediments in the vicinity of the contact zone (Figure 5-4).

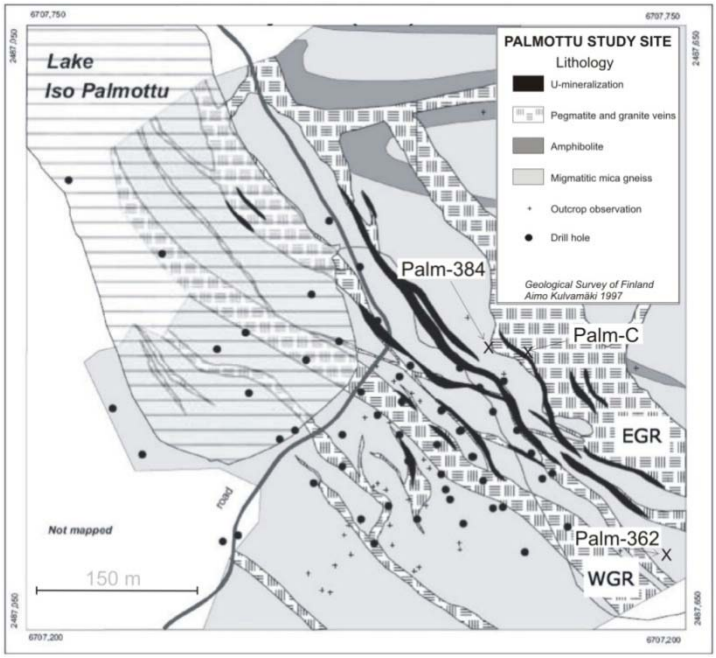

Figure 5-4: Detailed pre Quaternary geological map of the Palmottu study site (EGR: Eastern Granite, WGR: Western Granite) (modified after Kuivamäki (1997))

Three different types can be distinguished: 1) grey, even- or coarse-grained granite, referred in the text as the Western Granite (WGR), 2) coarse-grained, heterogeneous pegmatite with deep red hematite pigment, referred to as the Eastern Granite (EGR) and 3)

white or reddish coarse-grained pegmatite. The last thermal event related to the introduction of dolerite veins 1750-1400 million years ago (Aro and Laitakari, 1987).

5.2.2. Uranium mineralisation at Palmottu

The main uranium mineralisation of the site is located under substantial Quaternary deposits (up to16 m thick) and is associated with several, narrow, biotite-rich, (2-10 m) pegmatite vein types (type 3, see above in section 5.2.1.) interlayered with mica gneisses (Figure 5-5). However, only few, biotite-rich veins contain anomalous amounts of uranium. Also the eastern granite (EGR) has sporadically high uranium concentrations, while western granite (WGR) and the major part of the common pegmatite veins are essentially barren. Räisänen (1986) suggested that the pegmatites represent the late-stage residual magmatic fluids of the nearby Perniö granite massif. This is supported by a number of uranium indications observed along the contact zone of the massif (Figure 5-3). Hence, it is likely that the source of uranium at Palmottu is predominantly magmatic, but a proportion may also be derived from the surrounding metasediments by magmatic assimilation or by hydrothermal leaching. The ore estimates suspect around one million tonnes of rock grading at 0.1 % uranium down to depths of 300 m (Räisänen, 1986). Later drilling within the Palmottu Project has shown that the mineralisation partly continues to depths below 450 m (Blomqvist et al., 1998).

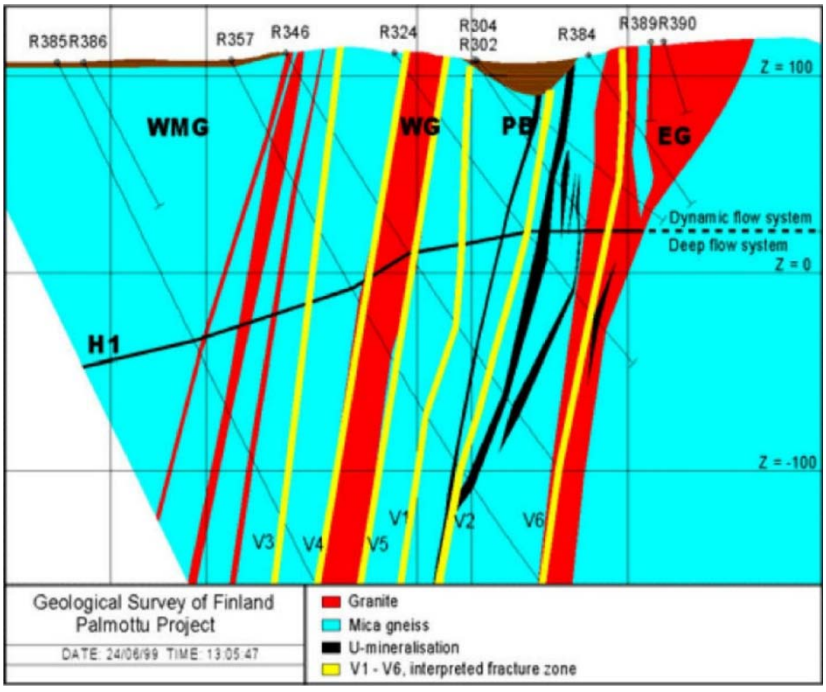

Figure 5-5: A vertical section showing the general geological setting at Palmottu. WMG = Western Mica Gneiss, WG = Western Granite, PB = Palmottu Brook Valley, EG = Eastern Granite. Yellow lines show the six subvertical fracture zones (Blomqvist et al., 1998)

Räisänen (1986) distinguished two types of uraniferous veins at Palmottu, a coarse-grained biotite-pegmatite and a sheared quartz-biotite vein. The latter type contains higher concentration, however they are usually only some tens of centimetres thick. Uranium in both vein types is mostly associated with the biotite-rich parts of the rock. Uraninite and monazite are the primary U-Th minerals of the site. Zircon and apatite contain only negligible amounts of radionuclides. Coffinite is a widespread alteration product of uraninite; it is a U(IV) mineral, which has formed soon after the precipitation of its precursor mineral. An important group of remobilised uranium phases with chemical compositions resembling that of coffinite is found in association with fracture infilling. Minor amounts of thorite and thorianite have been observed in some weathered samples. There are also some indications of U-carbonate, possibly rutherfordine, in microfractures close to altered uraninite grains (Pérez del Villar et al., 1997). Dispersion of uranium from the deposit in supragene processes is limited. Reducing conditions have prevailed in the deposit for most of its history for 1800-1700 million years. Uranium enrichments occur in soil on top of the mineralisation and in peat, naturally enriched from groundwater (Kaija et al., 2003). The most important U(VI) phase identified so far is β-uranophane. It occurs as a fracture infilling, and occasionally also in the weathered rock matrix in the uppermost part of the uraniferous Eastern Granite (Pérez del Villar et al., 1999; Ruskeeniemi et al., 2002). The scarcity of U(VI) minerals is a peculiar feature since part of the mineralised rock is exposed at ground surface. This may be due to glacial erosion that has removed most of the ancient weathered parts of the deposits, or possibly due to the tight nature of the crystalline bedrock that has prevented oxidising waters from penetrating in the mineralisation.

5.2.3. Quaternary geology

During the last million years the Palmottu area has been subjected to several glaciations (Donner, 1995), the last of which (Weichselian Ice Age) ended 10,000 years ago. The four ice-marginal formations, Salpausselkä I to III and Central Finland Ice Marginal Formation, (Figure 5-6) imply the periods of slightly cooler climatic conditions when the retreating continental ice sheet temporarily halted for some hundreds of years. The temporal standstills of the ice margin can now be observed as huge accumulations of till, gravel and sand that were deposited in front of the ice. At Palmottu, additionally a large delta formation was deposited next to the Salpausselkä III at the Yoldia Sea level. Palmottu is located in a bedrock block surrounded by prominent fracture zones; this block is topographically higher than its surroundings with a present elevation of 106-138 m (Blomqvist et al., 1995). Due to its

topographic situation, the highest points of the Palmottu area emerged from the Baltic Sea immediately after the retreat of the ice sheet during the Yoldia Sea stage, ca. 12,000 years ago, as the sea level was then at an elevation of 118 m (Figure 5-6).

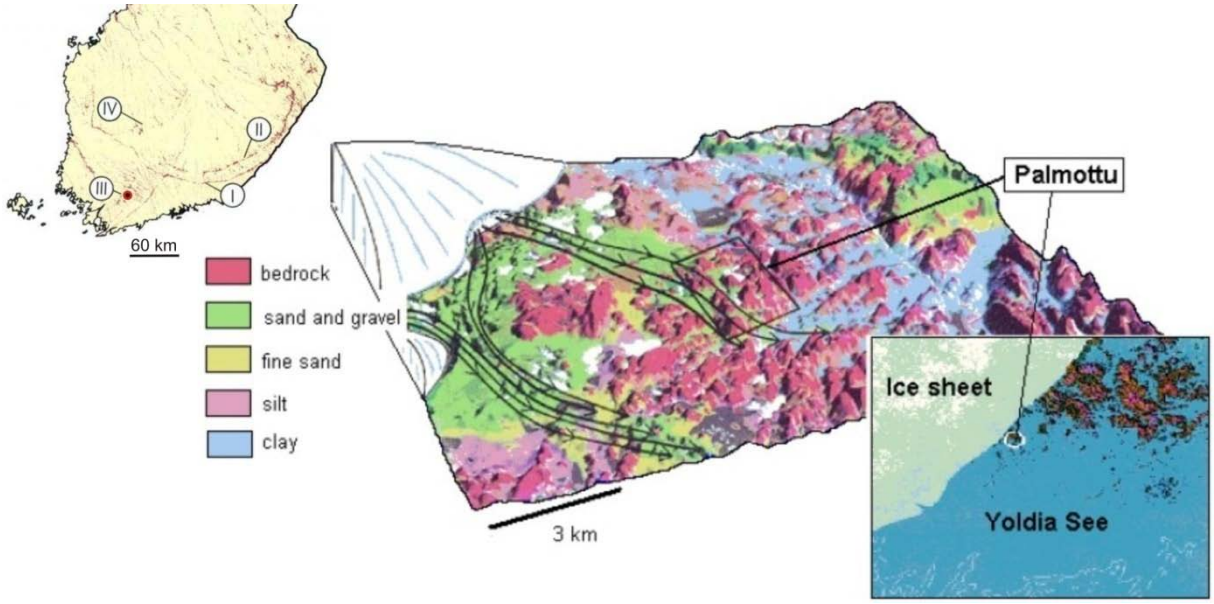

Figure 5-6: Quaternary deposits around Palmottu. Retreating ice sheet is depicted in the upper left corner. Flow lines show the main routes of melt water discharge. The insert at the lower right corner visualizes the position of the Palmottu site during retreat of the ice sheet, at the upper left corner the Palmottu site in Finland (denoted by red dot) and the four ice-marginal formations (I-III = Salpausselkä I-III and IV = Central Finland Ice Marginal Formation) (Ahonen et al., 2004)

During the Yoldia stage substantial meltwater streams flushed the Palmottu site. However, it was during the previous Salpausselkä II stage, at the time of deglaciation. That glacial melt water flowing beneath the ice sheet may have partly intruded into the bedrock, caused by the enormous hydrostatic pressures prevailing below the ice sheet. The depleted $\delta^{18}O$ values of some of the fracture groundwaters sampled at Palmottu (Blomqvist et al., 1995; Blomqvist et al., 1998; Pitkänen et al., 2002; Smellie et al., 2002) could be interpreted as glacial melt water intrusion. Presently the bedrock of Palmottu region is largely covered by glaciogen tills or glaciofluvial formations (Figure 5-7). Since the retreat of the last ice cover 12,000 years ago, mechanical and chemical weathering has eroded a negligible amount of the intact rock. Based on resistant minerals of glacially eroded and polished bedrock surfaces, the order of postglacial erosion is less than 10 mm of intact rock (Dahl, 1967). Additionally, a chemical weathering front may extend to some tens of millimetres into the rock. In the regional lows around the Palmottu block, post-glacial clays deposited during the different stages of the Baltic Sea cover the glaciogen layers (Figure 5-7). Soon after the deglaciation, peat started to form on depressions of bedrock. In about 9000 years, a peat thickness of up to 3-4 m was reached. Peat near the exposed U-mineralisation contains several hundreds ppm of uranium

(in ash), and it can be used to assess the migration of uranium in the biosphere (Kaija et al., 2003).

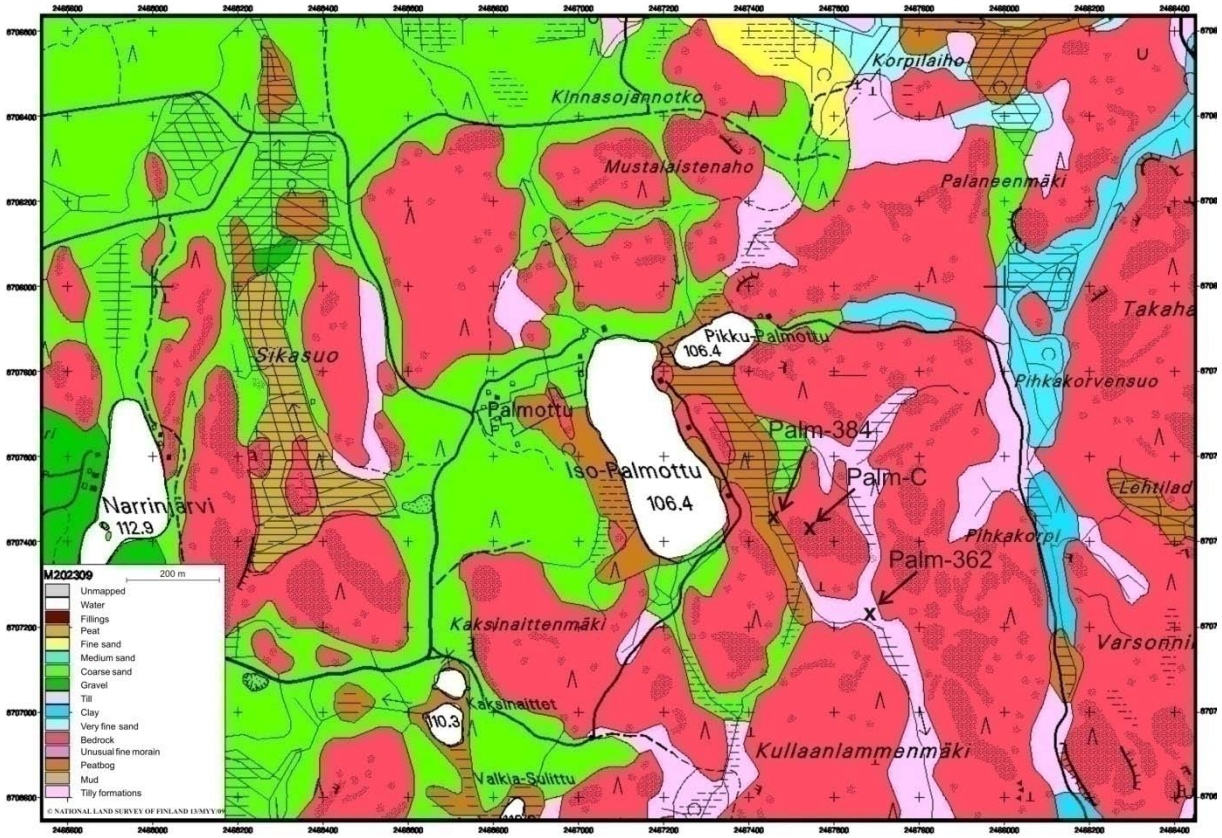

Figure 5-7: Quaternary geological map of Palmottu area (Niemelä, 1985). The arrows show the sampling points

5.2.4. Hydrogeology of the area

Based on hydraulic cross-hole tests and an integrated examination of hydraulic heads and geochemistry, bedrock groundwater flow in the bedrock at Palmottu is predominantly limited to the surface close part of the bedrock above the H1 structure (Figure 5-5), i.e. down to depths of 100-150 m. At greater depths, the bedrock is commonly more intact and hydraulically conducting fracturing is less frequent (Blomqvist et al., 1998; Blomqvist et al., 2000). Within the upper part of the bedrock, four different hydrogeological units were defined: Western Mica Gneiss, Western Granite, Palmottu Brook Valley and Eastern Granite, (Figure 5-5). Each has characteristic flow system. For example, a relatively well-characterized Eastern Flow System is related to Eastern Granite. The Eastern Granite area is a groundwater recharge area with downward groundwater flow to west towards the Palmottu Brook Valley and further either to the north or to the south (Kaija et al., 2003).

The surface water chemistry is uniform, water being of Ca-Na-Mg-HCO_3-SO_4-type and having pH levels ranging from 5.8 to 6.1. Water is very weakly mineralised; the median of the

measured total dissolved solids (TDS) was 24.4 mg/l, which is approximately 4.5 times less than that of overburden groundwater (110.5 mg/l). The median concentrations of most of the major ions (Ca, Mg, Na, K, HCO_3) were much less (1.7-7.6 times) than that of the overburden groundwater (Kaija et al., 2003).The groundwater in the overburden has more variably chemistry than surface water; the most dominant water types are Ca-Mg-HCO_3 and Ca-Na-HCO_3 ones. Mixed water types are found mainly in areas of low dissolved solids contents. Dissolved solid concentrations in groundwater from overburden range from less than 50 mg/l to over 150 mg/l; the median is 110 mg/l. Groundwater with low TDS and simultaneous low pH (5.9 to 6.5) are generally found in areas of thin soil layers (< 5 m) and in areas where the hydraulic conductivity of soil is better than in surroundings. In these areas groundwater is in active recharge and normally the groundwater table follows rapidly the changes in precipitation. Higher TDS concentrations and higher pH values (6.8 to 8.0) are primarily found in the central Palmottu area (Kaija et al., 2003), where soil layers are up to 16 m thick and consist mainly of silt and fine sand, where water conducting properties are poor. There is no clear hydrochemical trend in the composition of overburden groundwater along the general direction of local groundwater flow. The composition of groundwater correlates well with the type of soil and according to its hydraulic properties. Based on differences in hydrochemistry, it seems to be more or less isolated local groundwater bodies in the overburden along the Palmottu Brook (Kaija et al., 2003).

Uranium concentrations in the surface waters of Palmottu site (Lake Iso Palmottu, Palmottu Brook) are very low, their range is from 0.11 to 0.25 μg/l, highest values were measured from the Palmottu Brook. Uranium concentrations in Lake Iso Palmottu and Palmottu Brook are even far below the concentration in deep reducing bedrock ground waters (Kaija et al., 2003). It is interesting to note that uranium concentrations in the Palmottu Brook flowing above the uranium mineralisation seems to increase only slightly towards the lower course of the Palmottu Brook from 0.11 to 0.22 μg/l. Rainwater collected from the exposed bedrock hollows of the Eastern Granite, which is a part of the catchment area of Palmottu Brook, after few hours of rain contains 20 to 40 times higher uranium than water from Palmottu Brook. There is obviously no direct surface run-off from the uranium bearing Eastern Granite area to the Palmottu Brook. However, water must first flow through organic (peat) layers which serve as an effective natural filter enriching uranium and protecting surface water from high uranium contents (Kaija et al., 2003). The median concentrations of uranium in groundwater in the overburden are very low, over 300 times lower than in the

oxidative bedrock groundwater of Ca-HCO_3-type. In fact, the concentrations are close to uranium concentrations of the deep bedrock groundwater, which has a strongly reducing environment. Most of these groundwater observation tubes are installed in fine-grained silt layers where the hydraulic conductivity is low. This has also been demonstrated by hydraulic pumping tests in the area. Due to poor conductivities, the groundwater flow is limited and reducing conditions prevail causing low uranium concentrations. Groundwater samples taken from tubes, which have been installed in sand-till layers near the main uranium mineralisation, show also higher uranium concentrations. The hydraulic conductivities of sand-till layers are higher and, thus, more oxidative conditions are prevailed allowing higher uranium concentrations (Kaija et al., 2003).

5.3. Results of analyses made on Palmottu samples

5.3.1. Description of Palmottu samples

Palm-C (Figure 5-8)

In wet, the sample is dark brown/black (reddish) and not grainy disintegrated. In dry the sample is reddish brown, crumb structured and easy to shape and little lubricatable. The sample is rich in organic materials and some bigger pebbles are also present in it. The grains are quartz, feldspar, rock fragments and plants. It has no Ca-carbonate content (tested by 12 % HCl).

Figure 5-8: Soil sample from the top 40 cm (Palm-C) from Palmottu, Finland

Palm-384 (Figure 8-9)

In wet, the sample is reddish dark-brown and grainy disintegrated. In dry the sample is crumb structured and badly sorted. The pebbles are sub-angular; the grains are quartz, feldspar, mafic minerals and rock fragments. It contains significant amount of organic material such as root. The pebbles are mica schist, granite, mica gneiss, hieroglyphic granite,

tourmaline granite, migmatite and probably quarts sandstone. It has no Ca-carbonate content (tested by 12 % HCl).

Figure 5-9: Soil sample from depth 50-60 cm (Palm-384) from Palmottu, Finland

Palm-362 (Figure 5-10)

In wet, the sample is brown and not grainy disintegrated. In dry, the sample has pale brown colour, it is crumb structured and very well sorted. The grains are not rounded and not sub-angular. The grains are quartz, mafic minerals and micas. Roots in the sample are also observed. It has no Ca-carbonate content (tested by 12 % HCl).

Figure 5-10: Sediment sample from depth 120 to 180 cm (Palm-362) from Palmottu, Finland

Sample Palm-C and Palm-384 are sandy tills. Palm-C contains more fine and medium sand and less coarse fractions and pebbles than Palm-384. Sample Palm-362 is significantly different in grain size distribution. It is very well sorted, fine-very fine sand-silt. It contains no coarse sand fractions and pebbles (Figure 5-11). The summarised descriptions of lithology of the samples are presented on Figure 5-12.

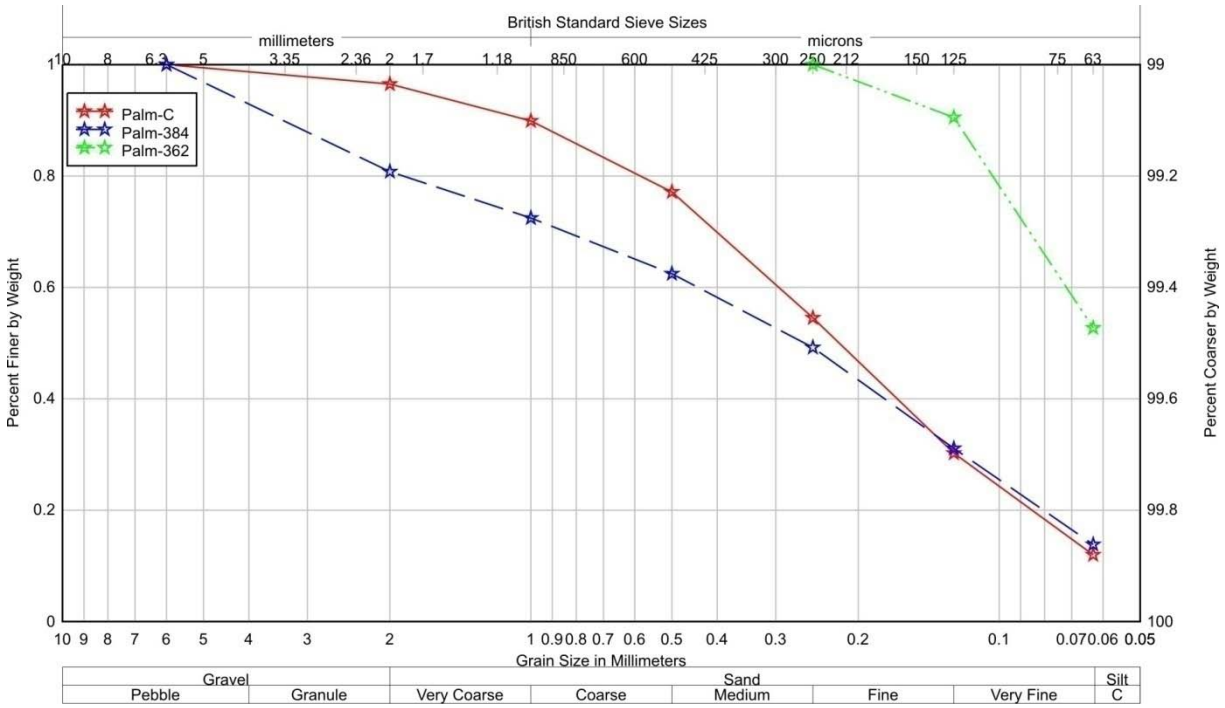

Figure 5-11: Grain size distribution of the three samples (Palm-C, Palm-384 and Palm-362) collected from Pamottu, Finland

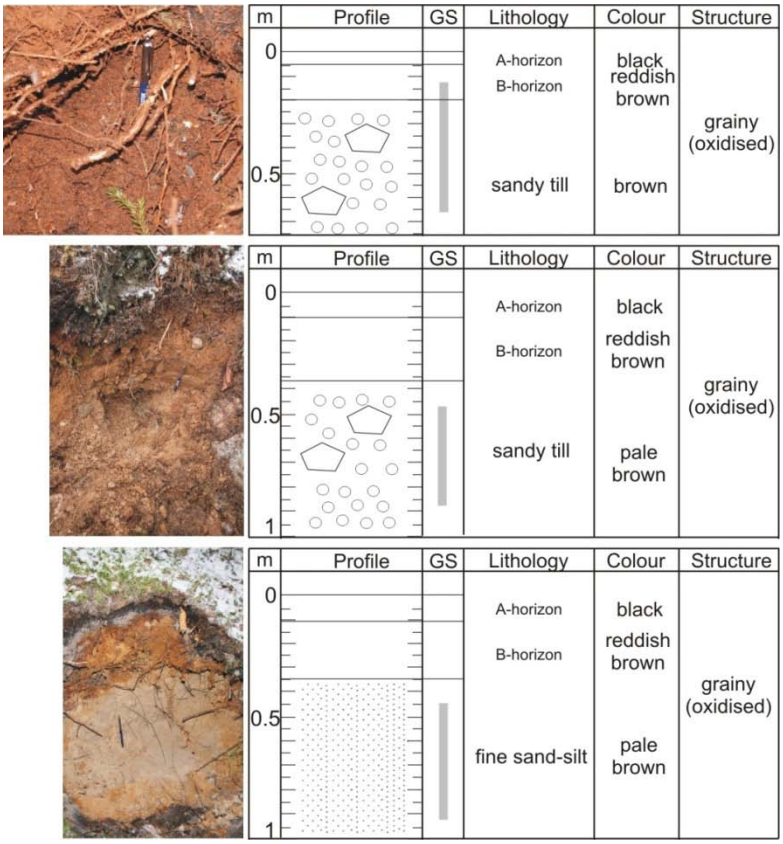

Figure 5-12: Summarised chart of lithology of the samples (Palm-C, Palm-384 and Palm-362) collected from Palmottu sampling site, Finland

5.3.2. U-, Th- and Ra-content of bulk samples from Palmottu

Naturally occurring ^{238}U-, ^{226}Ra- and ^{232}Th- (from ^{228}Ac and ^{208}Tl) activity concentrations were measured by gamma-spectrometer equipped by BEGe-detector. The results are presented in Table 5-1 and plotted on Figure 5-13.

Table 5-1: Activity concentrations (Bq/kg) of ^{238}U, ^{226}Ra and ^{228}Ra (^{228}Ac), ^{228}Th (^{208}Tl) as representing ^{232}Th-decay chain in Palmottu (Palm) samples.

Samples	Depth (cm)	^{238}U	^{226}Ra	^{226}Ra/^{238}U	^{228}Ra (^{228}Ac)	^{228}Th (^{208}Tl)	^{232}Th	^{228}Ra/^{232}Th
Palm-C	40	650±20	790±100	1.2±0.1	90±5	86±5	67±1	1.3±0.1
Palm-384	55	750±60	120±60	0.2±0.2	42±6	41±3	37±1	1.1±0.1
Palm-362	150	47±5	41±4	0.9±0.1	32±2	32±2	30±1	1.1±0.1

Activity concentration of ^{232}Th was calculated from Th concentration (ppm) measured by ICP-MS in SGS Lab, Toronto. The reported uncertainties are expanded uncertainties using a coverage factor k=1.

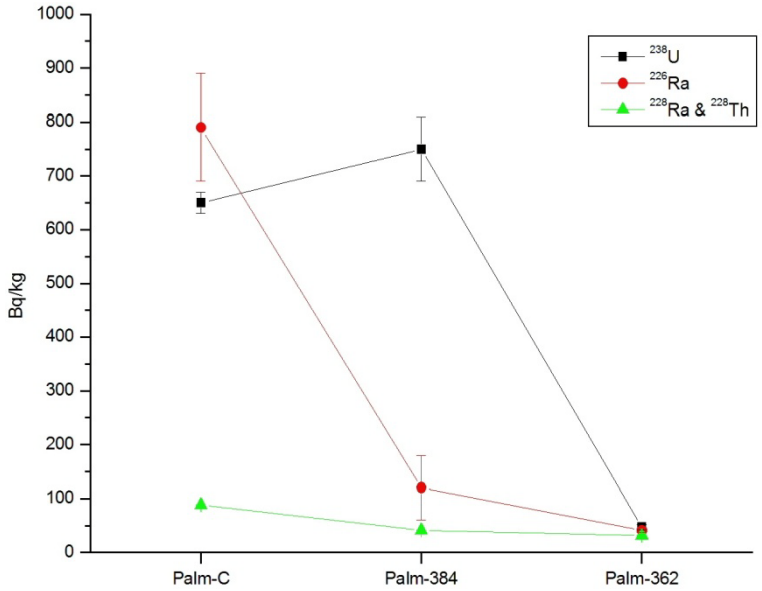

Figure 5-13: Activity concentrations of ^{226}Ra, ^{238}U and ^{228}Ra (^{228}Ac), ^{228}Th (^{208}Tl) as representing ^{232}Th-decay chain in samples from Palmottu. The reported uncertainties are expanded uncertainties using a coverage factor k=1

In sample Palm-C, where high ^{238}U- and ^{226}Ra-activity concentration 650 and 790 Bq/kg, respectively, were measured. Small disequilibrium occurred between radium and uranium (^{226}Ra/^{238}U = 1.2). Secular disequilibrium is very high in sample Palm-384 (^{226}Ra/^{238}U = 0.2), where high uranium and relatively low radium content, 750 and 120 Bq/kg, respectively, were measured. In the sample Palm-362 the secular equilibrium between ^{238}U and ^{226}Ra exists, with low, ca. 45 Bq/kg activity concentrations. In thorium decay chain disequilibrium between ^{232}Th (measured by ICP-MS) and ^{228}Ra (measured by γ-spectrometry in equilibrium with ^{228}Ac) occurred only in sample Palm-C (^{228}Ra/^{232}Th = 1.3). ^{232}Th and ^{228}Ra activity concentrations in this sample were much higher, ca. 70 and 90 Bq/kg, respectively, than in samples Palm-384 and Palm-362, ca. 40 and 30 Bq/kg, respectively.

5.3.3. Radon production and emanation rate of bulk samples from Palmottu

Palm-C has the highest radon production (ca. 6 Bq/(kg h)) and emanation factor (~ 1). In Palm-384 half of the radon formed from radium can escape into the pores, and the production is 0.5 Bq/(kg h). In Palm-362 both radon production and emanation factor are significantly lower, 0.06 Bq/(kg h) and ca. 0.2, respectively, than in the other two Palm samples (Table 5-2).

Table 5-2: Activity concentrations (Bq/kg) of ^{226}Ra, Rn production (Bq/(kg h)) and emanation factor in Palmottu (Palm) samples.

Samples	^{226}Ra	^{222}Rn production	Emanation factor
Palm-C	790±100	6.31±0.30	1.06±0.14
Palm-384	120±60	0.50±0.02	0.56±0.28
Palm-362	41±4	0.06±0.00	0.19±0.02

The reported uncertainties are expanded uncertainties using a coverage factor k=1.

5.3.4. Major and trace elements of bulk samples from Palmottu

Major and trace element concentration of the three < 250 μm bulk samples are presented in Annex 1 and plotted on Figure 5-14.

Concentrations of most of the trace elements measured in the three bulk samples from Palmottu are lower than the average chemical composition of the upper continental crust (UCC), sample/UCC ratios are varying between 0.4-0.9. Some elements such as Ra in Palm-C (> 10 sample/UCC) and U in Palm-C and Palm-384 (18 and 25 sample/UCC, respectively) have much higher ratio. Samples Palm-384 and Palm-362 contain Nb and Palm-C Sr much lower concentrations than UCC. Radium, uranium, thorium and lead are in the lowest amount in sample Palm-362. Sample Palm-C has the highest amount of Ra, Th, Nb, Fe, Pb, P and Ti, and the lowest of Ba, K, Sr and Eu of the three samples. Samples Palm-384 and Palm-362 generally have similar sample/UCC ratio (Figure 5-14a).

Rare earth elements (REE) contents of the three samples show no significant difference. Only Palm-384 has lower light rare earth element (La-Nd) content. Chondrite normalised REE contents of the three samples have granitoid pattern, they are more enriched in light rare earth elements (ratio is 100-35 from La to Nd, respectively) than in heavy ones (Dy-Lu), where the ratio is only ca 10 (Figure 5-14b).

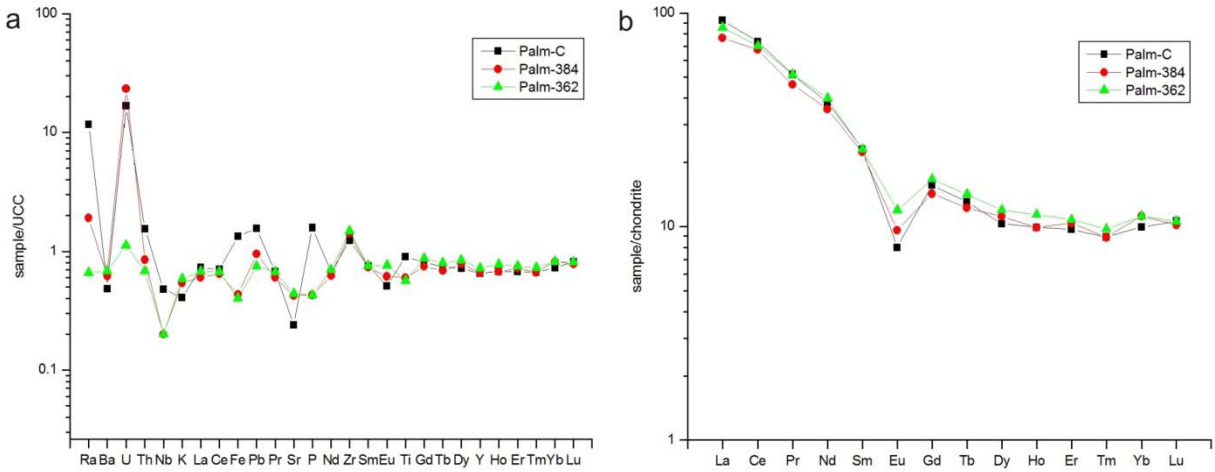

Figure 5-14: Elements of < 250 µm grain size fraction of Palmottu samples normalized to upper continental crust (UCC) (Taylor and McLennan, 1995). Activity concentration of ^{226}Ra normalized to average soil and sediment concentration of Eastern USA (Greeman and Rose, 1996) (a). Chondrite-normalised REE concentrations (McDonough and Sun, 1995) (b)

5.3.5. Major and trace elements of soil portions extracted from Palmottu samples

5.3.5.1. Exchangeable fraction

Major and trace element concentration in the leachates extracted by the first "exchangeable" sequential extraction step presented in Annex 2 and the proportion of extracted trace elements in the leachates are plotted in Figure 5-15.

By this step almost all kinds of trace element were extracted in low amount. Less than 1 % of total contents were extracted from most of the trace elements. Only Ra was extracted in high percentage: 50 % from Palm-C, 35 % from Palm-384 and 20 % from Palm-362.

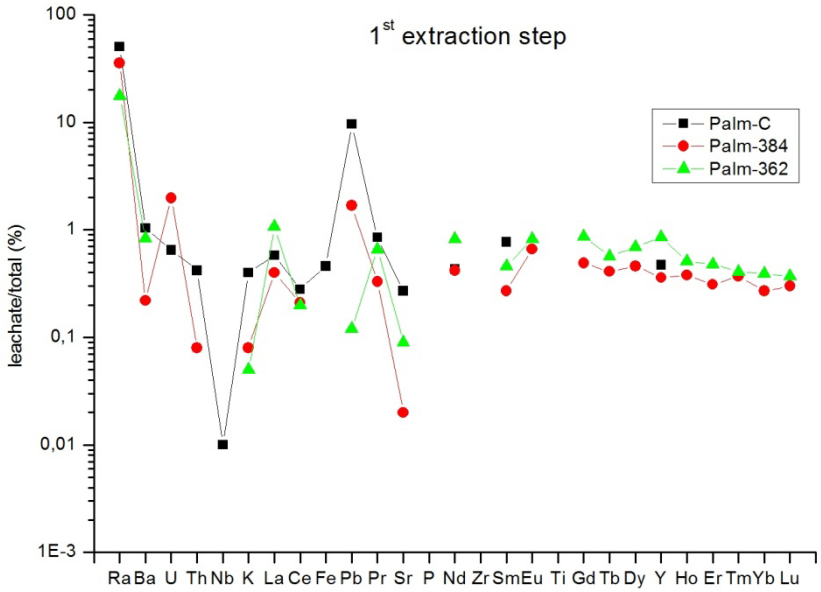

Figure 5-15: Portion (%) of elements extracted at the 1st extraction step (Figure 3-2) from the total composition of Palmottu samples

Approximately 2 % of U and Pb were leached out from Palm-384, and even higher amount (ca. 10 %) of Pb from Palm-C. Concentrations of Zr, Ti and P were under the detection limit in the leachates. From samples Palm-384 and Palm-362 neither Nb nor Fe and from Palm-362 neither U nor Th was extracted.

The leachate/chondrite ratio of REE in this first step is very low (< 1). In the extractants the ratios are higher in case of light REE (La-Sm) than in heavy REE (Dy-Yb). The patterns of ratios of samples Palm-384 and Palm-362 are similar but that of Palm-C is different. At LREE the ratios in the samples are quite similar (Figure 5-16).

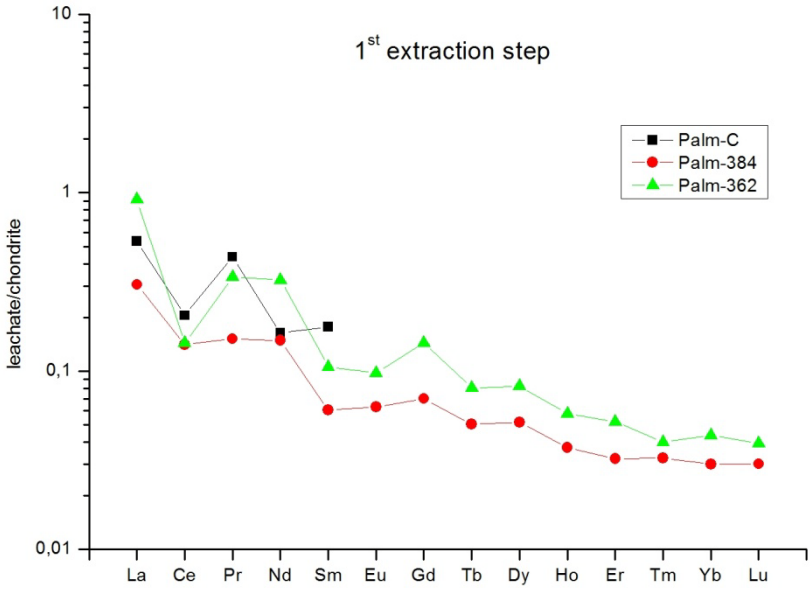

Figure 5-16: Chondrite-normalised REE concentrations (McDonough and Sun, 1995) in leachates extracted at the 1st extraction step (Figure 3-2) from Palmottu samples

5.3.5.2. Oxide fraction

Major and trace element concentration in the leachates extracted by the third "oxide" sequential extraction step presented in Annex 2 and the proportion of extracted trace elements in the leachates are plotted in Figure 5-17.

Approximately 5-10 % of the total trace element concentrations were extracted. Barium, K, Sr and Zr were in lower proportion extracted (< 1 %). In higher portion uranium (ca. 90 % from Palm-C and Palm-384 and 45 % from Palm-362), Th (40 % from Palm-C and 20 % from Palm-384), Fe (50 % from Palm-C), Pb (40 % from Palm-C and 20 % from Palm-384) and P ca. 60 % from Palm-C and Palm-362 and 20 % from Palm-384) were leached out.

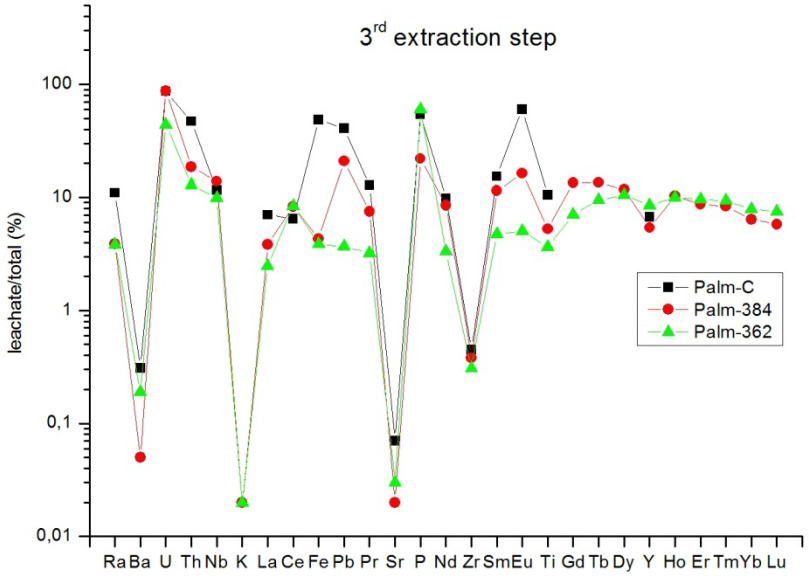

Figure 5-17: Portion (%) of elements extracted at the 3rd extraction step (Figure 3-2) from the total composition of Palmottu samples

Generally, each element was in higher proportion extracted from Palm-C. However lower portion of Nb, Ce, P and Y were leached out from Palm-C than from the others, and no K were extracted at all. In case of most of the trace elements the lowest portion were extracted from Palm-362, but Ba, Sr, P, Y and HREE were leached out in the lowest portion from Palm-384, and Ce from Palm-C.

Chondrite normalised REE patterns of the three samples are different, however, that of Palm-384-and Palm-362 are more close to each other. Lower amount of light and medium REE were extracted from Palm-362 than from samples Palm-384 and Palm-C, and higher amount of heavy REEs than from Palm-384. The highest amount of REE was leached out from Palm-C, except Ce, which was extracted in the highest amount from Palm-384 and Palm-362. Cerium in these two samples shows positive anomaly. No or only weak negative anomaly occurred in Palm-C (Figure 5-18).

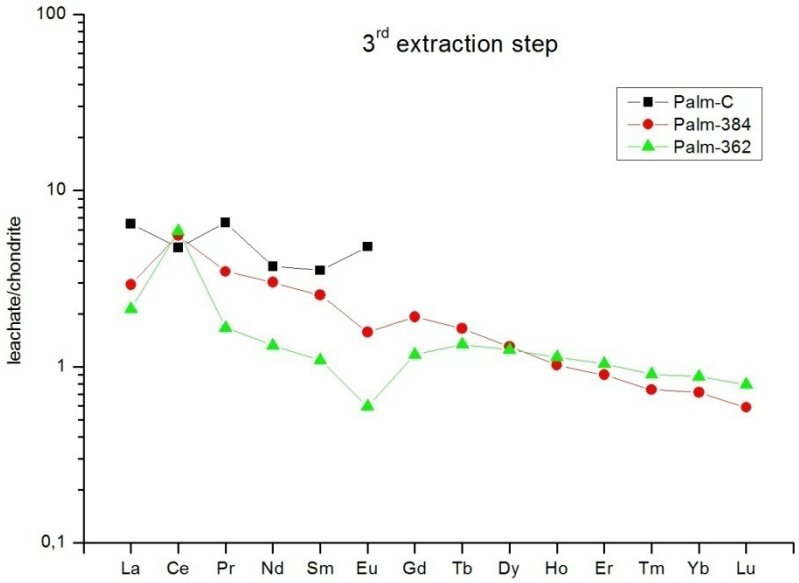

Figure 5-18: Chondrite-normalised REE concentrations (McDonough and Sun, 1995) in leachates extracted at the 3rd extraction step (Figure 3-2) from Palmottu samples

5.3.5.3. Organic fraction

Major and trace element concentration in the leachates extracted by the fourth "organic" sequential extraction step presented in Annex 2 and the proportion of extracted trace elements in the leachates are plotted on Figure 5-19. This step was performed only in case of the sample Palm-C because significant organic material was only in this sample expected.

In this step K, Zr, Eu and HREE were not extracted, and most of the others were in proportion of less than 3% in the leachate. In higher proportion Pb (~ 60 %), Ra (~ 30 %), U (15 %), P (~ 10 %), Fe (~ 6 %) and Ti (~ 5 %) were extracted.

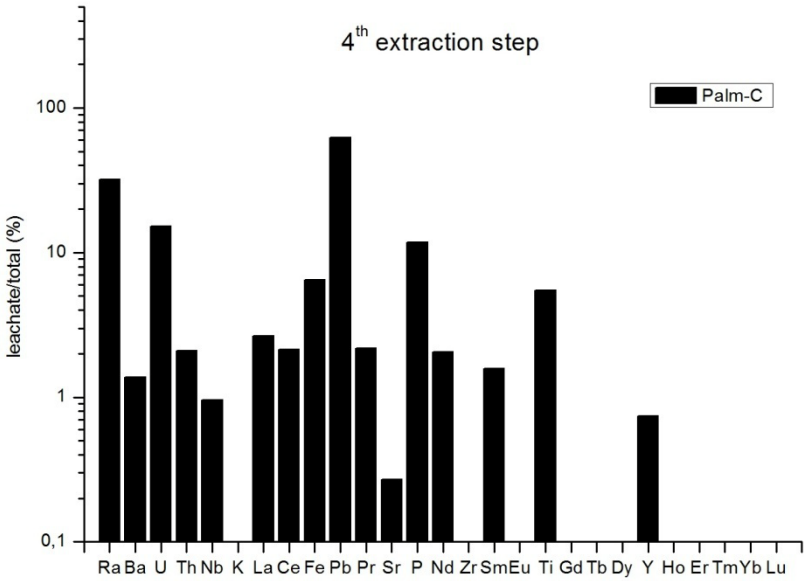

Figure 5-19: Portion (%) of elements extracted at the 4th extraction step (Figure 3-2) from the total composition of Palmottu samples

5.3.5.4. Residual fraction

Major and trace element concentration in the leachates extracted by the sixth "residual" sequential extraction step presented in Annex 2 and the proportions of extracted trace elements in the leachates are plotted in Figure 5-20.

Most of the trace elements were extracted in this step in a range of proportion of 40-80 %. In the highest amount, totally, light rare earth elements from each samples and Gd from Palm-384 were extracted. Phosphorus (88 %) was leached out from samples Palm-362 also in high percentage. Phosphorus from Palm-C and Palm-384 (41 % and 22 %, respectively), Ra from Palm-C (< 30 %), Nb from Palm-C and Palm-362 (17 % and 32 %, respectively), Pb from Palm-384 and Palm-362 (24% and 12%, respectively) and U from Palm-362 (30 %) were extracted in lower portion.

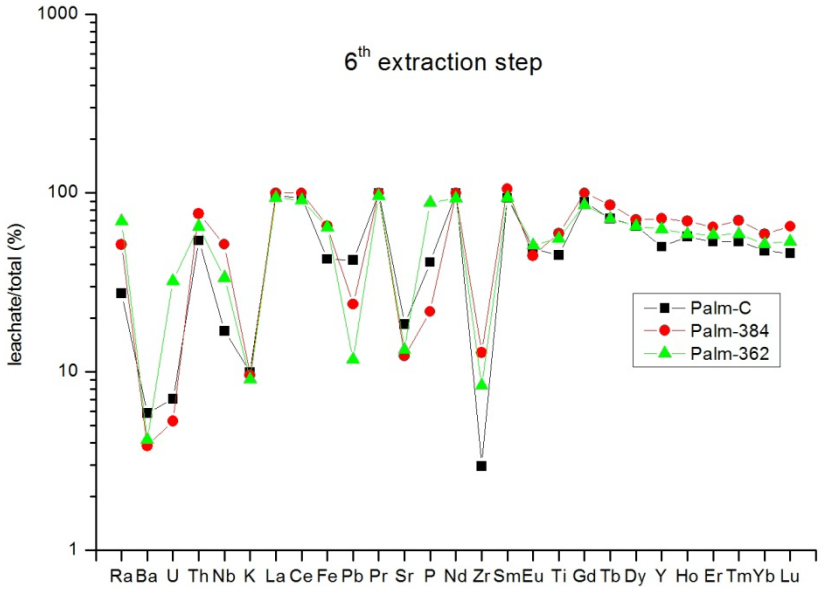

Figure 5-20: Portion (%) of elements extracted at the 6th extraction step (Figure 3-2) from the total composition of Palmottu samples

In very low percentages Sr (< 20 %), Zr (< 15 %), and in < 10 % K, Ba and U from Palm-C and Palm-384 were leached out. It can be stated that trace elements in the sample Palm-C were extracted in lower portion than from other samples. Except LREE, Gd and Pb which were leached out in higher proportion from Palm-362 and P from Palm-384. Palm-384 has the highest portion of aqua regia soluble trace elements, except phosphorus, radium and uranium, which were extracted in the highest proportion from Palm-362 and Sr and Pb from Palm-C.

Chondrite normalised rare earth elements extracted in this step show granitoid pattern. It indicates that the leachate/chondrite ratios are much higher in case of light rare earth elements

(~ 100) than heavy ones (~ 6) in the leachates. Significant europium anomaly occurred in each sample (Figure 5-21).

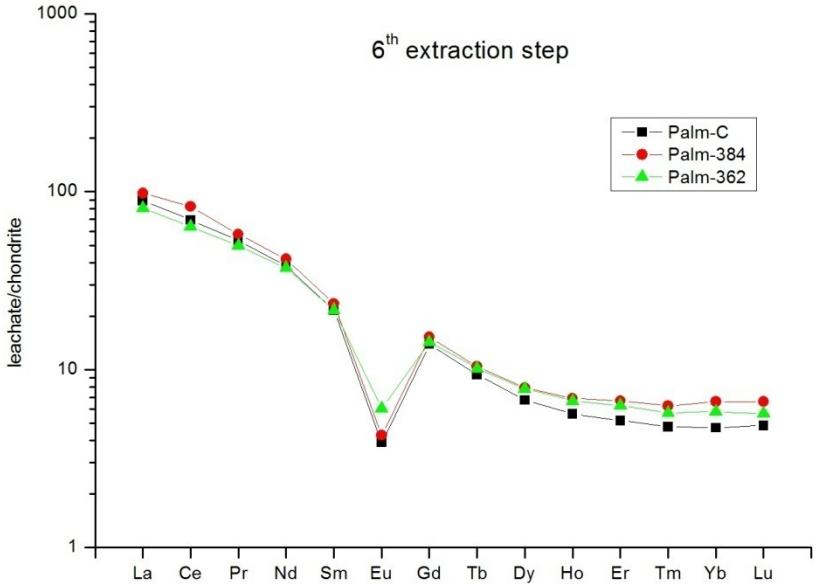

Figure 5-21: Chondrite-normalised REE concentrations (McDonough and Sun, 1995) in leachates extracted at the 6th extraction step (Figure 3-2) from Palmottu samples

The total proportions of extracted trace elements by the three (exchangeable, oxide and residual), and four (exchangeable, oxide, organic and residual, in the case of Palm-C) sequential extraction steps are plotted on Figure 5-22.

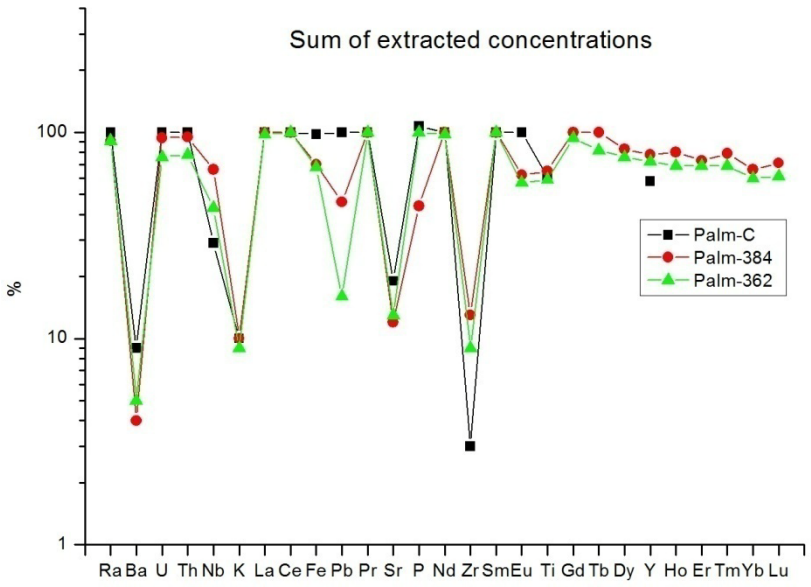

Figure 5-22: Sum of extracted concentrations (%) during the four extraction steps from Palmottu samples

Most of the trace elements were in more than 60 % extracted. Strontium (< 20 %), Zr (< 15 %), K (≤ 10 %) and Ba (< 10 %) were leached out in lower proportion. Proportion of Nb from Palm-C and Palm-384, Pb from Palm-384 and Palm-362 and P from Palm-384 were extracted

in lower than 50 %. In case of those trace elements where significant difference occurred between total extracted portions, mainly from sample Palm-362, were leached out the lowest portion. From Palm-362 by the three extraction steps only phosphorus was removed in the highest proportion.

5.3.6. Mineralogical study of Palmottu samples

5.3.6.1. Heavy mineral composition of Palmottu samples

For setting up statistical rank of heavy minerals approximately hundred randomly selected mineral grains were identified by scanning electron microscope. The proportions of heavy minerals in the < 0.063 mm grain size fraction of the three samples are plotted on Figure 5-23.

Heavy minerals ($\rho \geq 3.3$ g/cm^3) of the three samples contain garnets (mainly almandine and grossular, respectively), amphiboles (actinolite and tremolite), pyroxenes (diopside, enstatite and hypersthene), iron oxides (magnetite, hematite, goethite and Ti-magnetite), zircon, ilmenite, titanite, rutile, monazite, epidote, kyanite and spinell. Heavy mineral composition of Palm-C is significantly different than that of other two samples. Palm-C contains less Ca-garnets and much more Fe-oxides (hematite, magnetite, goethite) and ilmenite, 4 %, 31 % and 23 %, respectively, than Palm-384 and Palm-362 that contain ca 20 % Ca-garnet, ≤ 10 % FeO and ca. 10 % ilmenite.

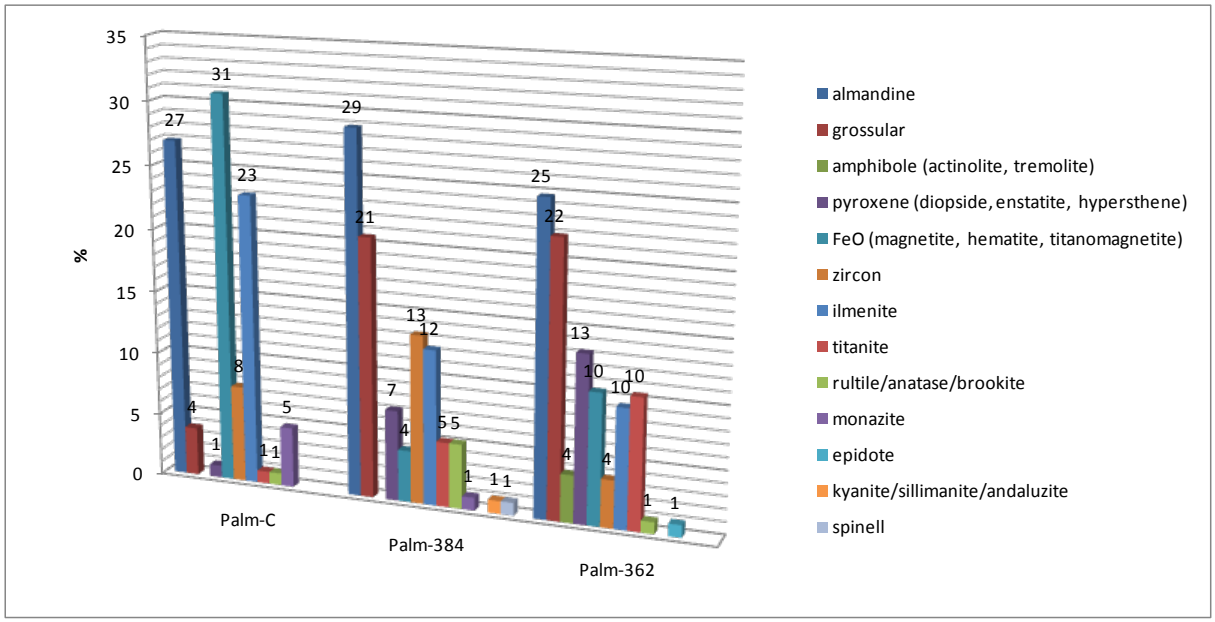

Figure 5-23: Heavy mineral ($\rho \geq 3.3$ g/cm^3) composition of < 0.063 mm grain size fractions of the three Palmottu samples

Heavy mineral assemblages of the three samples are presented on Figure 5-24. Habits of the heavy minerals in the three samples are similar. However, in Palm-C the minerals are

slightly more weathered (Figure 5-24a). Some resistant minerals such as zircon, monazite and magnetite have idiomorphic shape. Other minerals have fresh surfaces with sharp edges.

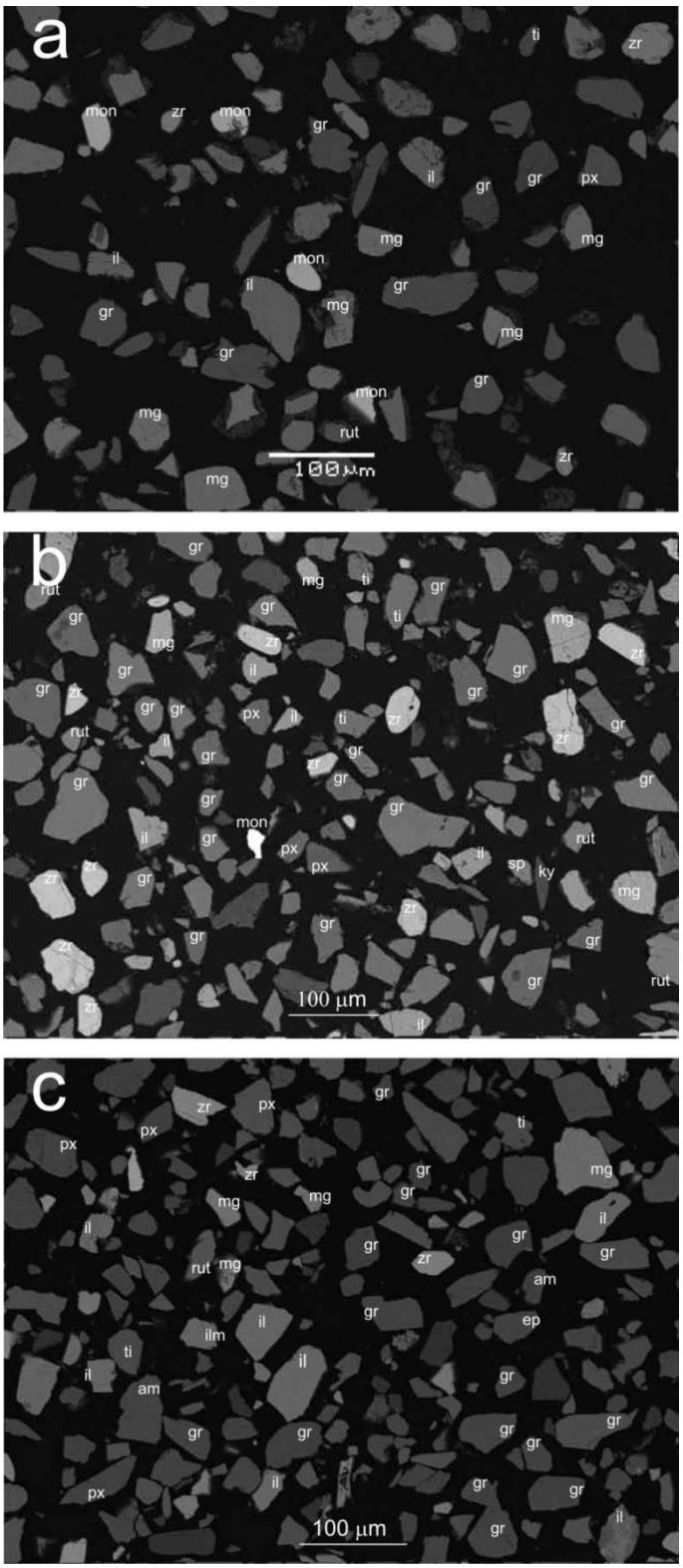

Figure 5-24: Back scattered electron images of heavy minerals ($\rho \geq 3.3$ g/cm^3) separated from the grain size fraction < 0.063 mm of the samples Palm-C (a), Palm-384 (b) and Palm-362 (c) (gr = garnet, il = ilmenite, ky = kyianite, mg = magnetite/hematite/goethite, mon = monazite, py = pyroxene, rut = rutile, ti = titanite, zr = zircon)

Major U- and Th-bearing minerals of the samples are presented on Figure 5-25. These minerals are the following: monazite, xenotime, thorite/thorianite/urano-thorite, some Th-phosphate, zirkelite and zircon. From these monazites and zircons are present in the highest amount. Monazites and xenotimes contain mainly thorium and uranium of up to 20 % and 5 %, respectively, and often contain pure U-Th-minerals as inclusion, such as urano-thorite (Figure 5-25a). These inclusions contain up to 20 % of U and more than 50 % of Th. Zircon (Figure 5-25b,c) and zirkelite are often present coexisting with monazite and xenotime (Figure 5-25d). These zirkelites frequently contain more than 30 % of Th.

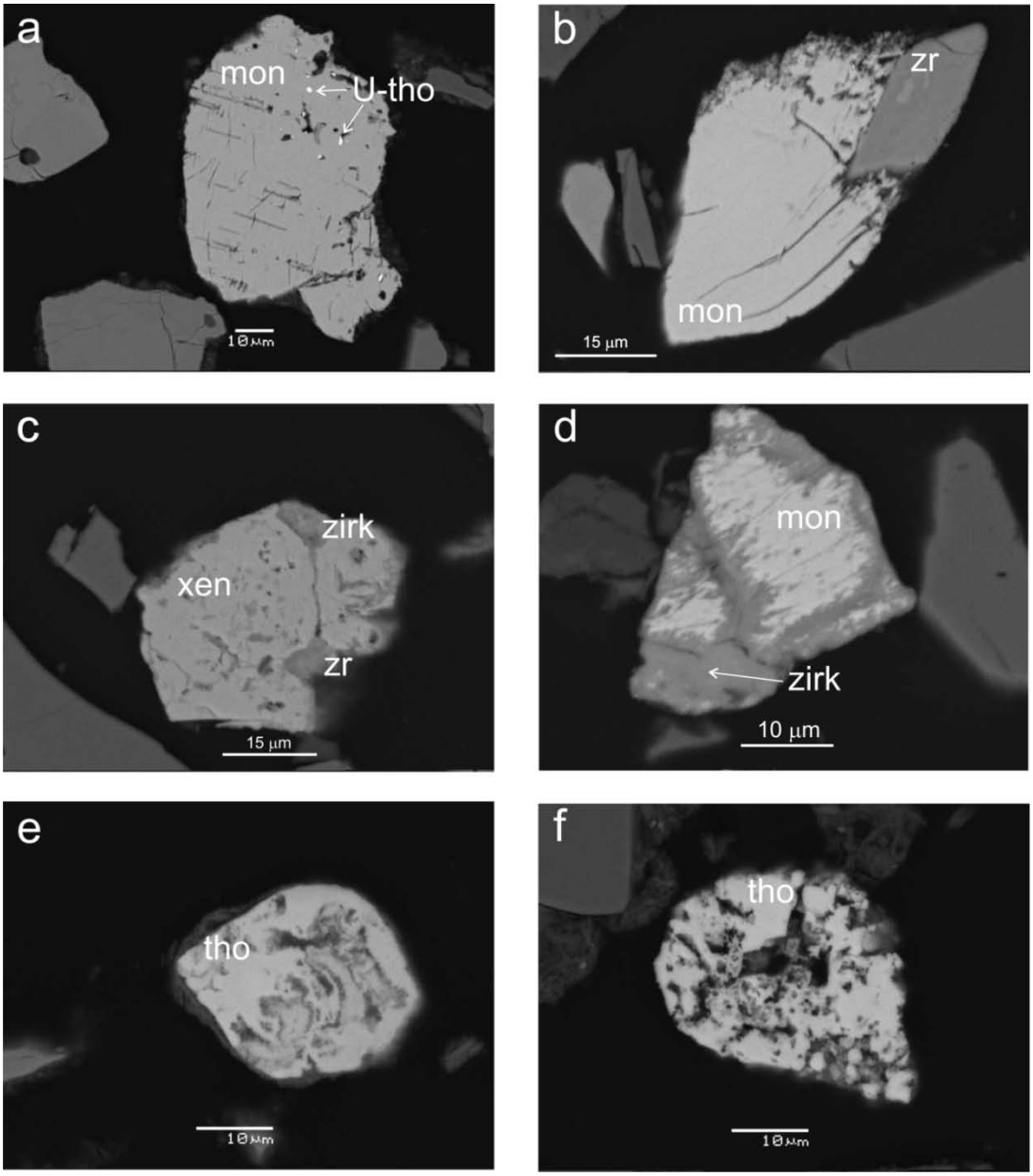

Figure 5-25: Back scattered electron images (BSE) of major U- and Th bearing minerals from grain size fraction of < 0.063 mm. a: Th containing monazite (mon) grain with U-thorite (U-tho) inclusion from sample Palm-C; b: Th-containing monazite (mon) with zircon (zr) from sample Palm-384; c: xenotime grain with Th-bearing zircon and zirkelite from the sample Palm-362; d: Th-bearing xenotime coexisting with zircelite from the sample Palm-362; e: thorite (tho) grain from the sample Palm-C; f: lenticular structured thorite (tho) from the sample Palm-C

5.3.6.2. Effect of weathering on chemical composition of U-, Th-bearing minerals in Palmottu samples

In order to study the weathering effect on U- and Th-bearing minerals, moderately and highly altered grains were selected and X-ray mapping and wavelength dispersive spectrometry at 6 – 9 distinct points were performed. The maps are presented on Figure 5-26 – 5-29 and the corresponding chemical compositions analyzed at distinct points are presented in Table 5-3 – 5-6 and Annex-3. Chemical compositions of the grains were measured by wavelength dispersive spectrometer and for the better comparison it was normalised by the ratio of 100/total concentration measured, except in case of goethite presented on Figure 5-28 because the lower total (Table 5-6) is mainly resulted in by water content of the mineral.

The partially weathered monazite grain from grain size fraction < 0.063 mm from sample Palm-C shown in Figure 5-26 has similar major components, Ce_2O_5/P_2O_5 ratio (ca. 1.1) (Table 5-3) to data published by Yang & Pattison (2006) (0.8-1), Krenn & Finger (2007) (ca 1.1) and Grew et al. (2008) (0.7-1.3). Therefore, the normalisation of the concentrations probably did not cause any significant deviation in ratios of other elements. SiO_2, Fe_2O_3, ThO_2 concentrations increase with decreasing P_2O_5, La_2O_3 and Ce_2O_3 contents. Correlation coefficients (Pierson product-moment coefficient) between Fe_2O_3 and Ce_2O_3, Fe_2O_3 and P_2O_5 and ThO_2 and P_2O_5 are high (-0.91, -0.92 and -0.81, respectively) and low between Fe_2O_3 and ThO_2 (0.57) (Annex-3). The higher the Fe_2O_3 content the lower the total of the analysis with correlation coefficient of -0.93. Thorium content varies within the grain from ca. 10 to 18 %. Uranium concentration is rather low; it was detected only at point #5 (Figure 5-26, Table 5-3).

Zoned monazite grain from grain size fraction < 0.063 mm from sample Palm-C presented on Figure 5-27 has a weathered, probably older core and a fresh rim. The Ce_2O_3/P_2O_5ratio in this grain is ~ 1. The core has higher Fe_2O_3, ThO_2 and SiO_2 and lower P_2O_5, La_2O_3 and Ce_2O_3 contents than the surrounding area (Table 5-4). Correlation coefficients (Pierson product-moment coefficient) are high between Fe_2O_3 and Ce_2O_3, Fe_2O_3 and P_2O_5, ThO_2 and P_2O_5 and Fe_2O_3 and ThO_2 (-0.95, -0.97, -0.83 and 0.80, respectively) (Annex-3). The larger the Fe_2O_3 content the lower the total of the analysis, the correlation coefficient is -0.94. Thorium content varies from 7 to 16 % in the grains. Uranium concentration of the monazite is under the detection limit (Table 5-4).

The highly weathered monazite grain from grain size fraction 0.125-0.25 mm from sample Palm-384 demonstrated in Figure 5-28 partly altered to goethite. The Ce_2O_3/P_2O_5 ratio in the unaltered part of this grain is 0.76. Two analyses of 9 were performed on a totally goethitised

grain and one on a Th-phosphate inclusion of the grain (Figure 5-28, Table 5-5). Therefore, for testing correlation between major constituent of monazite and Th, Fe and Si-content first these three points were neglected. After this the correlation coefficients (Pierson product-moment coefficient) reached a high value between Fe_2O_3 and P_2O_5, U_2O_3 and SiO_2, ThO_2 and SiO_2 (-0.83, -0.78 and 0.84, respectively) the coefficients between ThO_2 and P_2O_5, Fe_2O_3 and ThO_2 and are low (-0.43 and 0.45, respectively) and very low between Fe_2O_3 and U_2O_3 (-0.04) (Annex-3). The larger is the Fe_2O_3 content, the lower is the total value of the analysis, and the correlation coefficient is -0.83. Thorium and uranium contents vary within the grain between 5-45 % and 0-4 %, respectively (Table 5-5).

In Figure 5-28 a goethite grain surrounded by Th-silicate rim can be seen. This rim contains up to 40 % of ThO_2 compared to the goethite core, which show no Th-content. Aluminium, silica and phosphorus are also concentrated in the rim (Figure, 5-28, Table 5-6).

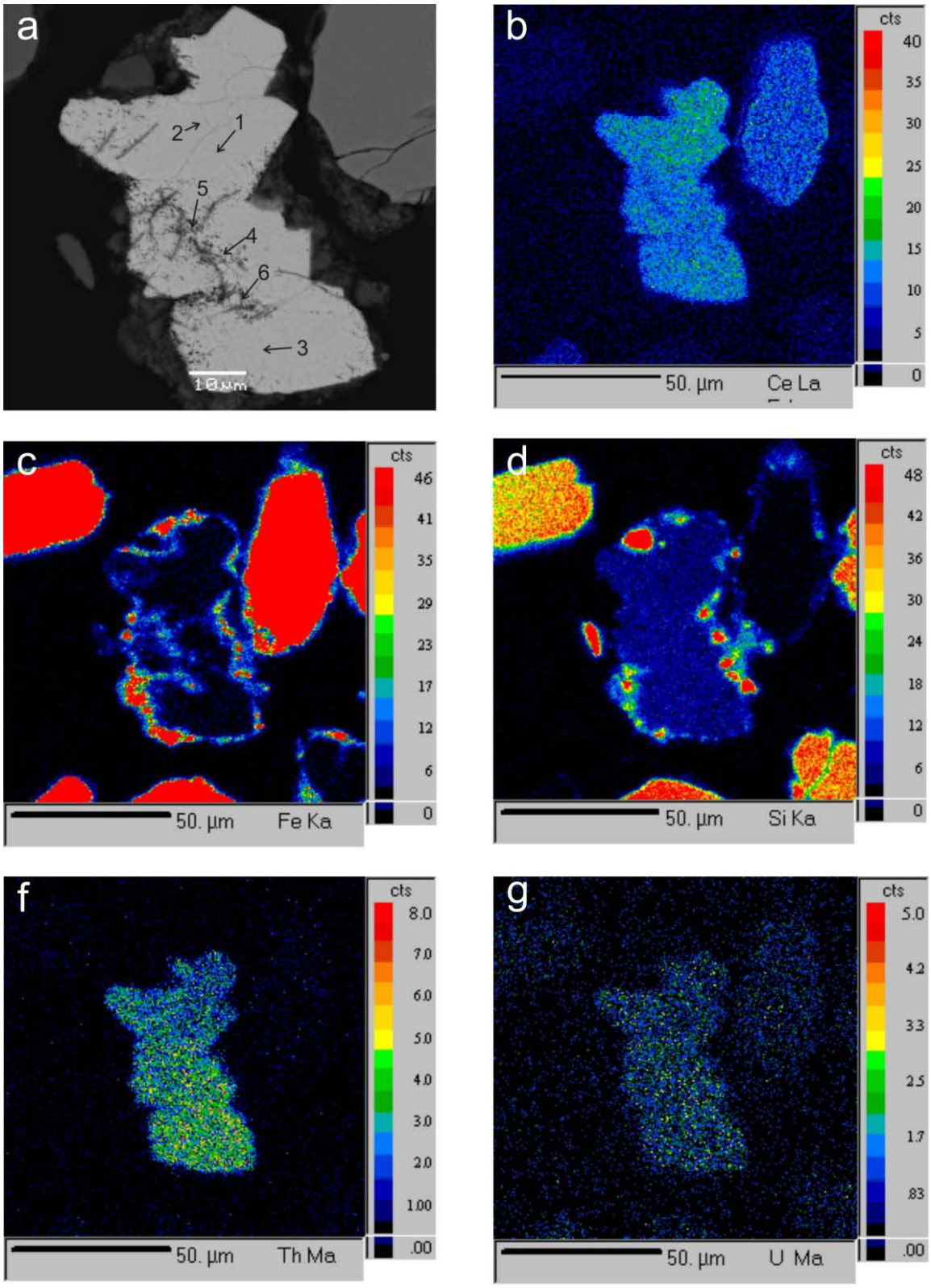

Figure 5-26: Partly weathered Th-bearing monazite grain from grain size fraction < 0.063 mm of sample Palm-C. a: BSE image of the monazite and the analysing points; b: X-ray map of Ce Lα analysed by energy dispersive spectrometer (EDS); c: X-ray map of Fe Kα analysed by wavelength dispersive spectrometer (WDS); d: X-ray map of Si Kα analysed by WDS; e: X-ray map of Th Mα analysed by WDS; g: X-ray map of U Mα analysed by WDS

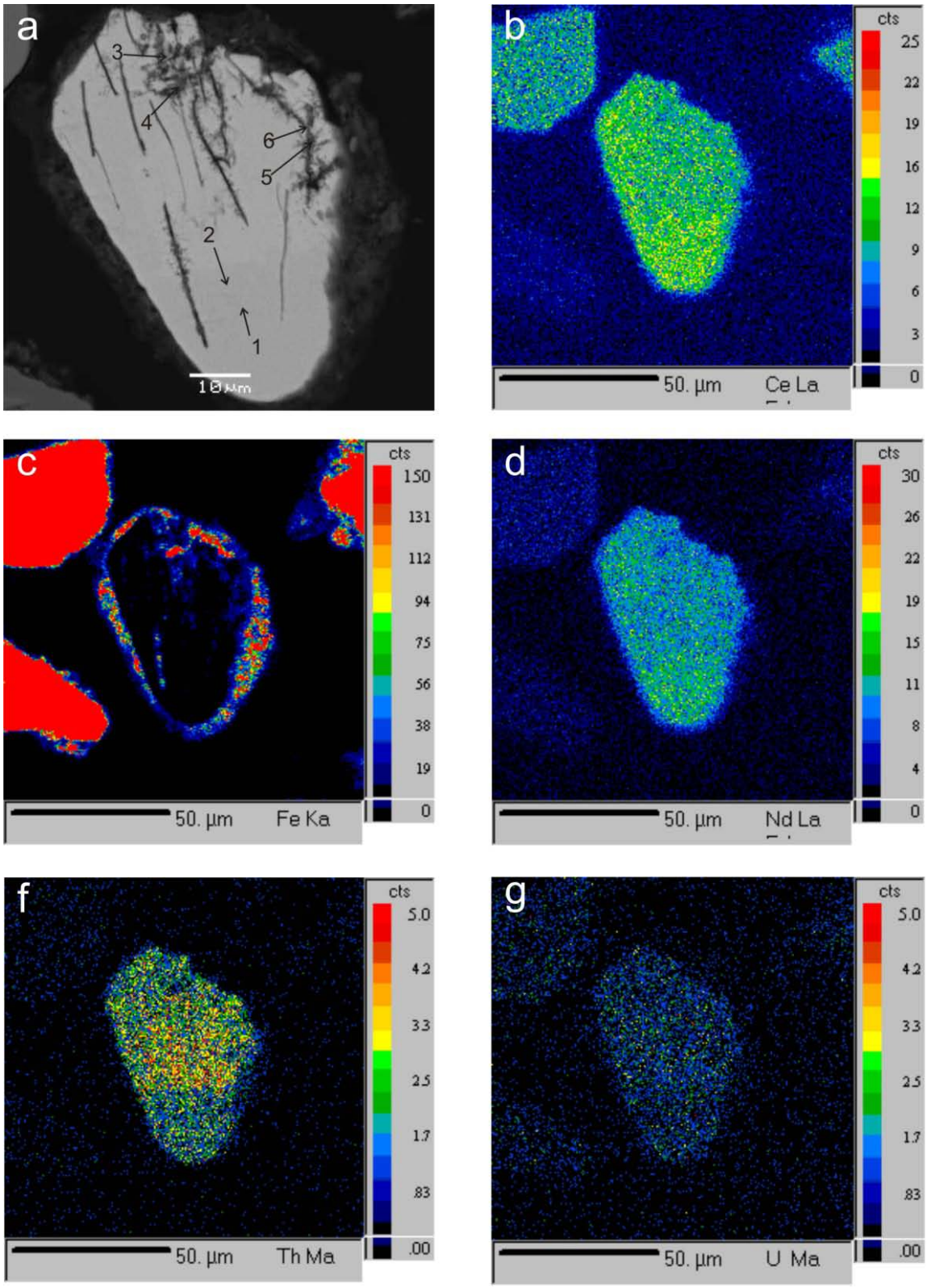

Figure 5-27: Partly weathered Th-bearing monazite grain from grain size fraction < 0.063 mm of sample Palm-C. a: BSE image of the monazite and the analysing points; b: X-ray map of Ce Lα analysed by energy dispersive spectrometer (EDS); c: X-ray map of Fe Kα analysed by wavelength dispersive spectrometer (WDS); d: X-ray map of Nd Lα analysed by EDS; e: X-ray map of Th Mα analysed by WDS; g: X-ray map of U Mα analysed by WDS

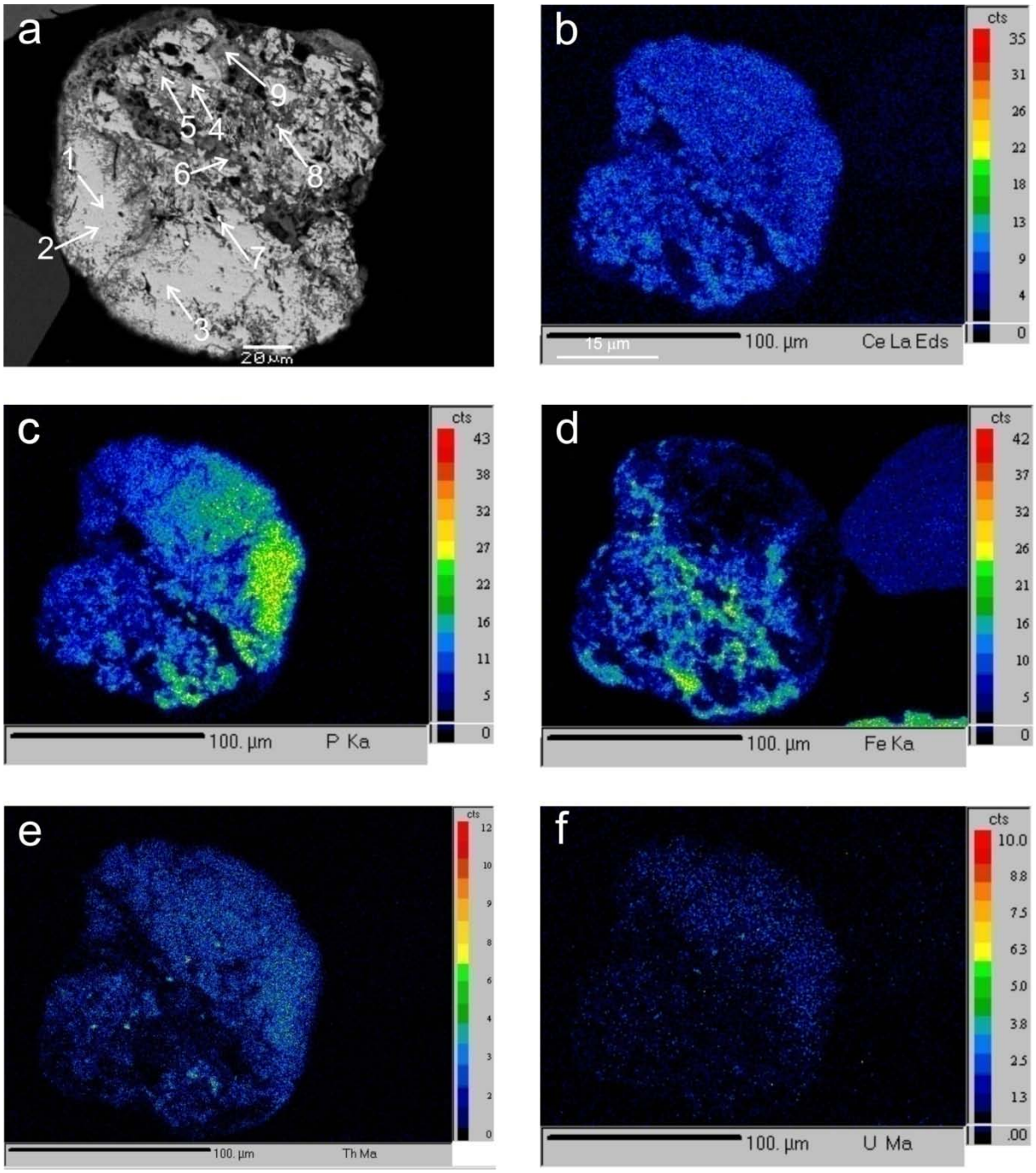

Figure 5-28: Highly weathered monazite grain from grain size fraction 0.125-0.250 mm of sample Palm-384. a: BSE image of the monazite and the analysing points; b: X-ray map of Ce Lα analysed by energy dispersive spectrometer (EDS); c: X-ray map of P Kα analysed by wavelength dispersive spectrometer (WDS); d: X-ray map of Fe Kα analysed by WDS; e: X-ray map of Th Mα analysed by WDS; f: X-ray map of U Mα analysed by WDS. BSE image has a different orientation than X-ray maps

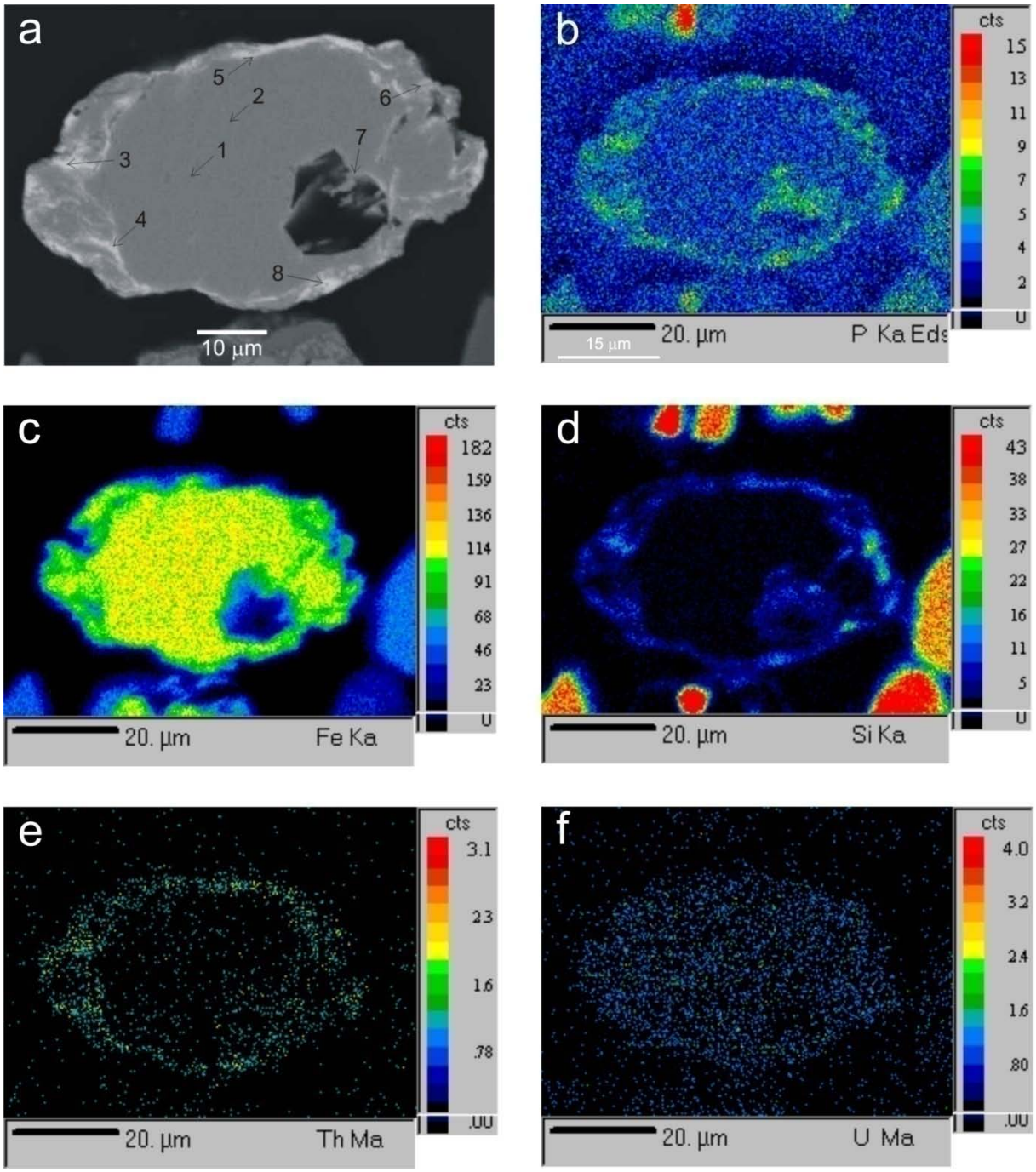

Figure 5-29: Goethite with Th-rich rim from grain size fraction <0.063 mm of sample Palm-362. a: BSE image of the goethite and the analysing points; b: X-ray map of P Kα analysed by energy dispersive spectrometer (EDS); c: X-ray map of Fe Kα analysed by wavelength dispersive spectrometer (WDS); d: X-ray map of Si Kα analysed by WDS; e: X-ray map of Th Mα analysed by WDS; g: X-ray map of U Mα analysed by WDS

Table 5-3: Chemical composition of partly weathered Th-bearing monazite grain from grain size fraction < 0.063 mm of sample Palm-C (Figure 5-26). POI = Point of interest.

POI	F	MgO	Al2O3	SiO2	P2O5	Cl	CaO	TiO2	MnO	Fe2O3	Y2O3	Nd2O3	ThO2	U2O3	La2O3	SmO	Ce2O3	PbO	Nb2O5	TOTAL
1	0.64	0.00	0.00	2.26	27.14	0.04	1.29	0.01	0.06	0.19	1.34	8.16	12.73	0.00	14.24	1.18	30.03	0.71	0.00	100
2	0.67	0.00	0.00	1.99	27.75	0.02	1.04	0.00	0.05	0.07	1.17	8.11	10.67	0.00	15.10	1.24	31.53	0.51	0.10	100
3	0.58	0.00	0.00	3.13	26.06	0.04	1.18	0.00	0.06	0.18	1.13	8.33	16.02	0.00	12.36	1.32	28.88	0.69	0.06	100
4	0.52	0.00	0.07	3.00	25.81	0.05	1.73	0.02	0.00	0.81	1.31	8.31	17.19	0.00	12.07	1.31	26.53	1.13	0.23	100
5	0.64	0.03	0.94	3.49	23.84	0.06	1.56	0.24	0.02	5.33	1.59	8.44	16.64	0.14	9.81	1.41	25.27	1.10	0.00	100
6	0.53	0.00	1.18	3.15	22.48	0.15	1.75	0.59	0.03	12.10	1.48	6.62	17.57	0.00	9.05	1.42	21.62	1.33	0.18	100

Elements are normalised by hundred/total ratio in order to the easier comparison. Raw concentrations are presented in Annex 3.

Table 5-4: Chemical composition of partly weathered Th-bearing monazite grain from grain size fraction < 0.063 mm of sample Palm-C (Figure 5-27). POI = Point of interest.

POI	F	MgO	Al2O3	SiO2	P2O5	Cl	K2O	CaO	TiO2	MnO	Fe2O3	Y2O3	Nd2O3	ThO2	La2O3	SmO	Ce2O3	PbO	Nb2O5	TOTAL
1	0.67	0.00	0.00	1.38	29.15	0.04	0.00	0.61	0.02	0.03	0.12	2.21	13.36	7.64	10.21	3.80	30.03	0.74	0.00	100
2	0.66	0.00	0.00	1.31	29.75	0.05	0.00	0.56	0.05	0.10	0.08	2.33	13.55	7.01	10.04	3.94	30.16	0.43	0.00	100
3	0.65	0.11	2.39	4.89	21.49	0.34	0.09	0.79	0.75	0.02	10.37	2.07	10.15	12.54	7.49	2.72	23.39	0.63	0.16	100
4	0.57	0.00	0.55	2.82	24.92	0.25	0.00	1.00	0.62	0.07	6.77	2.28	10.30	14.35	7.91	3.27	24.10	0.70	0.21	100
5	0.34	0.00	1.36	2.99	21.75	0.30	0.01	0.66	0.81	0.01	13.33	2.35	9.79	14.66	7.03	2.80	21.75	1.02	0.39	100
6	0.68	0.00	0.32	3.08	24.43	0.14	0.00	0.84	0.45	0.00	6.08	2.60	10.91	15.51	7.56	3.45	23.73	0.85	0.00	100

Elements are normalised by hundred/total ratio in order to the easier comparison. Raw concentrations are presented in Annex 3.

Table 5-5: Chemical composition of highly weathered Th- and U-bearing monazite grain from grain size fraction 0.063-0.125 mm of sample Palm-384 (Figure 5-28). POI = Point of interest.

POI	F	Na2O	MgO	Al2O3	SiO2	P2O5	Cl	K2O	CaO	TiO2	MnO	Fe2O3	Y2O3	Nd2O3	ThO2	U2O3	La2O3	SmO	Ce2O3	PbO	Nb2O5	TOTAL
1	0.58	0.00	0.00	0.00	0.65	30.44	0.05	0.00	4.19	0.00	0.00	0.06	2.37	8.22	18.22	0.68	8.10	2.22	23.07	1.17	0.00	100.00
2	0.56	0.00	0.03	0.00	0.63	30.26	0.03	0.00	4.06	0.04	0.02	0.23	2.56	8.13	18.30	0.67	8.06	2.46	22.91	1.07	0.00	100.00
3	0.60	0.00	0.00	0.00	0.87	29.61	0.02	0.00	2.99	0.01	0.00	0.00	2.47	9.26	15.93	0.28	8.71	2.44	25.56	1.13	0.11	100.00
4	0.51	0.00	0.49	3.33	9.45	7.71	0.01	0.00	1.27	0.23	0.09	42.01	4.31	0.42	30.04	0.00	0.76	0.55	3.01	0.00	0.06	100.00
5	0.48	0.28	0.53	4.83	10.23	5.07	0.01	0.00	0.52	0.34	0.24	41.08	4.17	0.61	30.98	0.00	0.86	0.51	3.41	0.00	0.00	100.00
6	0.18	1.05	1.29	11.96	6.03	1.68	0.05	0.04	0.30	2.31	0.10	75.68	0.11	0.00	4.90	0.00	0.43	0.16	1.38	0.00	0.00	100.00
7	0.52	0.01	0.33	2.14	1.52	9.96	0.09	0.00	0.95	0.56	0.06	17.34	0.38	2.45	43.57	3.84	3.32	0.99	9.81	3.86	0.08	100.00
8	0.60	0.64	0.96	6.82	4.23	6.76	0.10	0.00	0.33	0.89	0.11	50.90	0.54	1.62	17.79	1.18	2.61	0.70	7.00	1.26	0.08	100.00
9	0.39	0.25	1.38	7.74	8.28	1.85	0.02	0.00	0.41	1.02	0.05	71.50	2.05	0.00	11.45	0.00	0.00	0.19	0.63	0.00	0.00	100.00

Elements are normalised by hundred/total ratio in order to the easier comparison. Raw concentrations are presented in Annex 3.

Table 5-6: Chemical composition of goethite grain with Th-rich rim from grain size fraction < 0.063 mm of sample Palm-362 (Figure 5-28). POI = Point of interest.

POI	F	MgO	Al2O3	SiO2	P2O5	SO2	Cl	K2O	CaO	TiO2	MnO	Fe2O3	YO3	ZrO2	Nd2O3	ThO2	Pr2O3	Gd2O3	SmO	Ta2O5	Nb2O5	WO3	TOTAL
1	0.22	0.00	0.00	0.28	0.02	0.01	0.00	0.00	0.05	1.92	0.07	84.56	0.00	0.00	0.00	0.09	0.00	0.00	0.15	0.05	0.00	0.08	79.09
2	0.10	0.00	0.00	0.26	0.01	0.00	0.04	0.00	0.04	2.20	0.05	85.03	0.05	0.00	0.00	0.01	0.00	0.00	0.26	0.19	0.15	0.00	79.92
3	0.35	0.33	1.95	10.76	3.94	0.05	0.06	0.35	0.61	1.38	0.11	27.34	3.60	0.14	0.07	36.16	0.49	1.17	0.75	0.05	0.24	0.03	89.36
4	0.34	0.01	0.65	8.08	3.64	0.01	0.01	0.00	0.46	1.66	0.17	35.34	4.56	0.11	0.09	33.85	0.25	1.04	0.87	0.01	0.00	0.50	90.00
5	0.18	0.30	2.24	10.80	3.35	0.28	0.12	0.22	0.60	1.34	0.14	26.11	3.75	0.13	0.34	33.39	0.33	0.99	0.79	0.16	0.00	0.62	86.05
6	0.24	0.66	5.32	15.87	2.23	0.01	0.04	1.23	0.46	1.49	0.19	47.16	1.70	0.04	0.06	15.06	0.31	0.49	0.26	0.15	0.00	0.00	89.62
7	0.19	0.15	1.20	2.47	0.49	0.04	0.12	0.11	0.12	1.62	0.06	70.09	0.38	0.00	0.00	3.48	0.00	0.22	0.13	0.00	0.00	0.00	74.33
9	0.35	0.27	2.16	14.02	4.45	0.04	0.09	0.00	0.88	1.59	0.09	21.35	6.47	0.16	0.62	40.48	0.60	1.86	1.23	0.19	0.00	0.07	98.44

6. OLKILUOTO SAMPLING SITE

6.1. Location of Olkiluoto sampling site

Olkiluoto study site is located ca. 300 km from Helsinki approximately in the middle of Olkiluoto Island. For the sampling the OL-TK14 trench was selected (Figure 6-1a), which was excavated by the Posiva Oy company in 2007 in order to study the geology and fracturing of the basement rocks. The overburden was not fully studied, there were no chemical analyses of till and no determinations of its mineral composition. The sampling site is close to the Onkalo underground laboratory at the area where the underground nuclear waste repository will be constructed. The reason why the site was selected is the possibility to collect samples from a well develped redox profile (Figure 6-1b), at an area representing average natural background radiation, and because the information obtained from the study can be important for the better understanding of migration processes of the naturally occurring radionuclides in overburden at glaciated terrain. One sample was taken from each horizon distinguished based on their optical characteristics: one is from the uppermost reddish oxidised horizon (Olk-1), one from the middle light grey layer (Olk-2) and one from the deepest, dark grey layer (Olk-3) (Figure 6-1b).

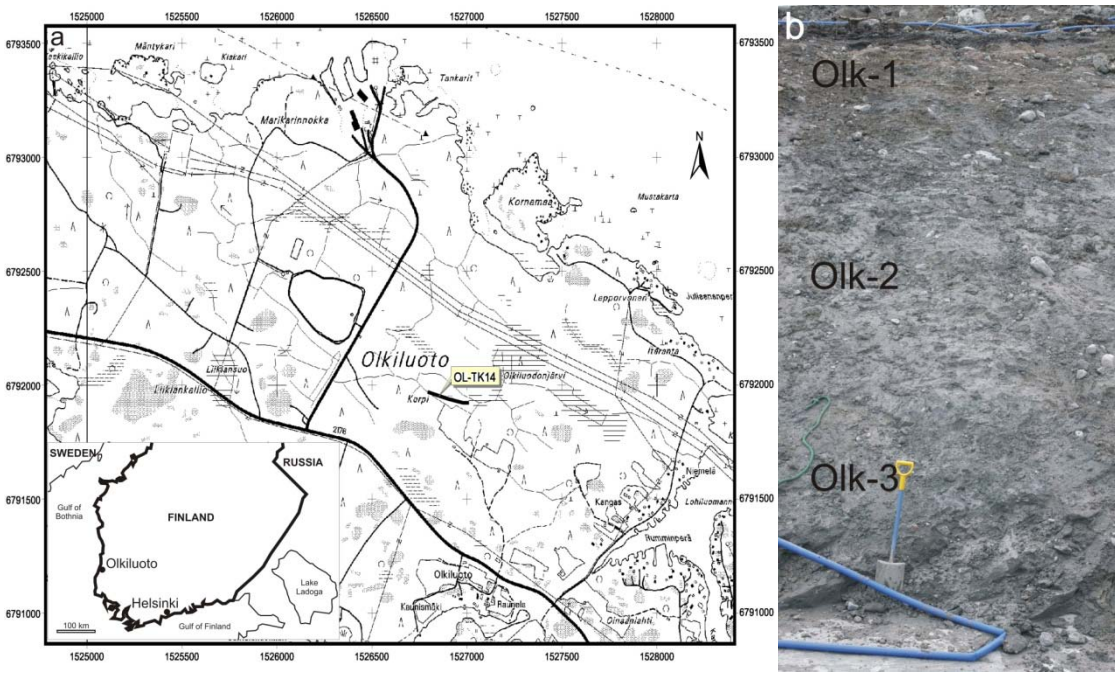

Figure 6-1: Location of the sampling area in Olkiluoto (Huhta, 2008) and Olkiluoto in Finland (a), and the position of the samples on profile 1 (b)

6.2. Geological background of Olkiluoto sampling site

The bedrock at Olkiluoto mostly comprises high-grade metamorphic supracrustal rocks, the origin of which can be traced back to epiclastic and pyroclastic material, based on geochemical characteristics and the sporadic presence of relicts of primary bedding structures, such as graded bedding in metaturbidite sequences (Kärki and Paulamäki, 2006). In terms of field relations, modal composition, texture and migmatite structure, the rocks at Olkiluoto can be divided into four major classes: 1) migmatitic gneisses with stromatic, veined and diatexitic varieties, 2) tonalitic-granodioritic-granitic (TGG) gneisses, 3) other gneisses including mica gneisses, quartz gneisses and mafic gneisses, and 4) pegmatitic granites. In addition, a few dolerite dykes cross-cut the main rock types and occur mainly in the western part of the island (POSIVA, 2009). The distribution of the various rock types at Olkiluoto is shown in Figure 6-2. The veined gneisses account for 43 % of the volume of the Olkiluoto site area, the stromatic gneisses for 0.4 % and the diatexitic gneisses for 21 %. The pegmatitic granites make up 20 % of the bedrock, the tonalitic-granodioritic-granitic gneisses 8 %, mica gneisses 7 % and the mafic gneisses 1 % (POSIVA, 2009).

On the basis of refolding and cross-cutting relationships, the supracrustal rocks have been subject to five successive phases of ductile deformation approximately 1880-1800 Ma ago. Later events reoriented the existing deformation structures and produced additional migmatite structures and shear zones (Mattila et al., 2008). The fault zones at Olkiluoto are mainly SE-dipping thrust faults formed firstly in ductile to semi-ductile regime during contraction at approximately 1800 Ma ago and later reactivated in several deformation phases as indicated by fault-slip data and isotopic age determinations. In addition to the thrust faults, NE-SW striking strike-slip faults are also common. The site-scale fault zones are also the main hydrological features of the site (Mattila et al., 2008). As major rapakivi granite plutons intruded close to the Olkiluoto Island at 1650-1540 Ma, the bedrock at the Olkiluoto site was subjected to extensive hydrothermal alteration by fluids emanating from the rapakivi pluton. The alteration took place at reasonably low temperature conditions, the estimated temperature interval being from slightly over 300 ^{o}C to less than 100 ^{o}C. Two types of hydrothermal alteration can be observed, (i.e., pervasive and fracture-controlled) and the most prominent pervasive alteration events occur as kaolinisation and sulphidisation. Sulphides are located in the surface part of the Olkiluoto bedrock, following roughly the main foliation trend (slightly dipping to the SE). Kaolinite is also located in the uppermost part, however the orientation is opposite to the main foliation trend (Mattila et al., 2008).

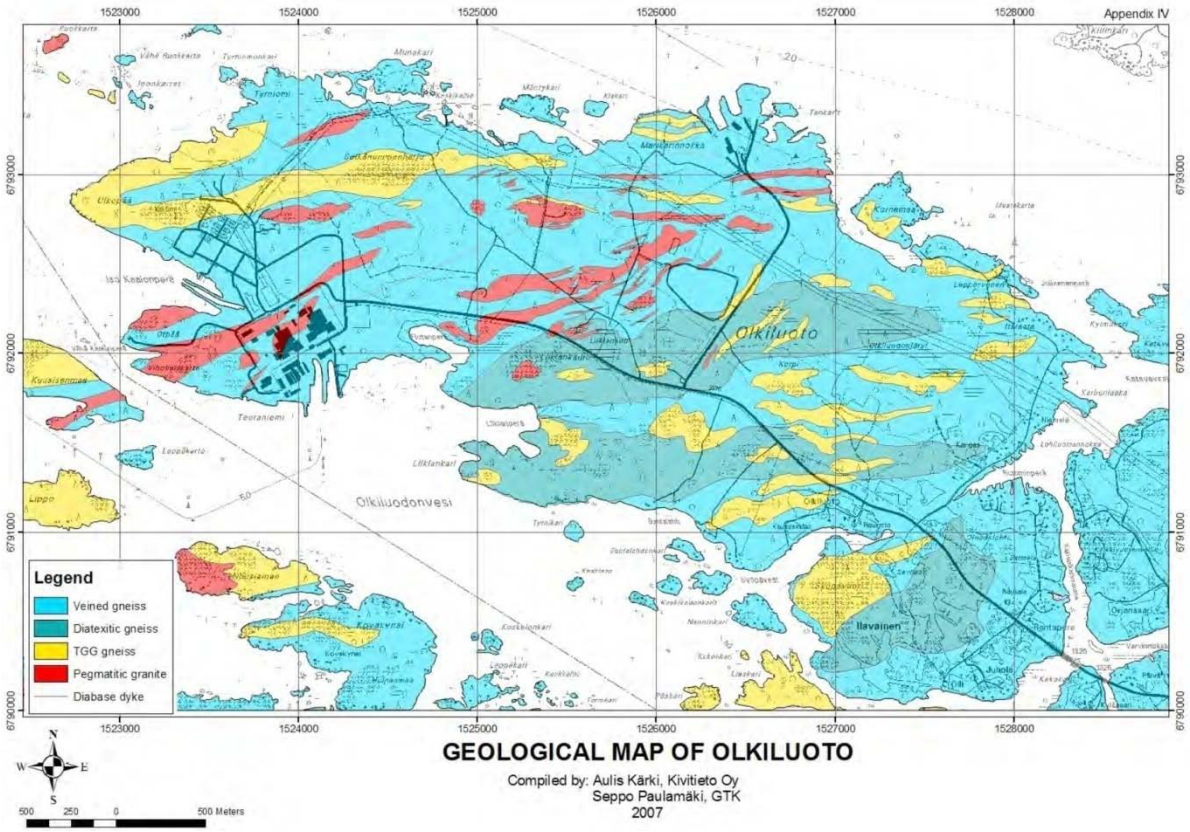

Figure 6-2: Pre-quaternary geological map of the Olkiluoto Island (W-Finland) (POSIVA, 2009)

The bedrock surface can vary locally, but the ground surface is still quite even at places where the bedrock surface abruptly changes: the depressions of rock surface are filled with thicker layer of till and the outcrops stick through the modest soil layers as expected due to the past ice sheets. The overburden is mainly fine-textured sandy till. The other terrestrial sediment types are, in order of abundance, fine sand, sand, silt and clay (Figure 6-3). The thickness of the overburden is usually 2 – 4 meters, although even up to 12 – 16 meter thick layers have been observed (Lahdenperä et al., 2005).

Podzol soils covering underlying sediments are characterised by light coloured eluvial horizon immediately below the organic layer, and a reddish illuvial horizon below it also appears. The eluvial horizon has been strongly leached by acid percolation water and is low in base cations. Iron and aluminium are removed as colloids incorporated by clay minerals or as organometallic complexes, mainly in illuvial horizon. Podzol soils are heterogeneous in chemical, mineralogical and physical properties (Kontio and Kähkönen, 1991).

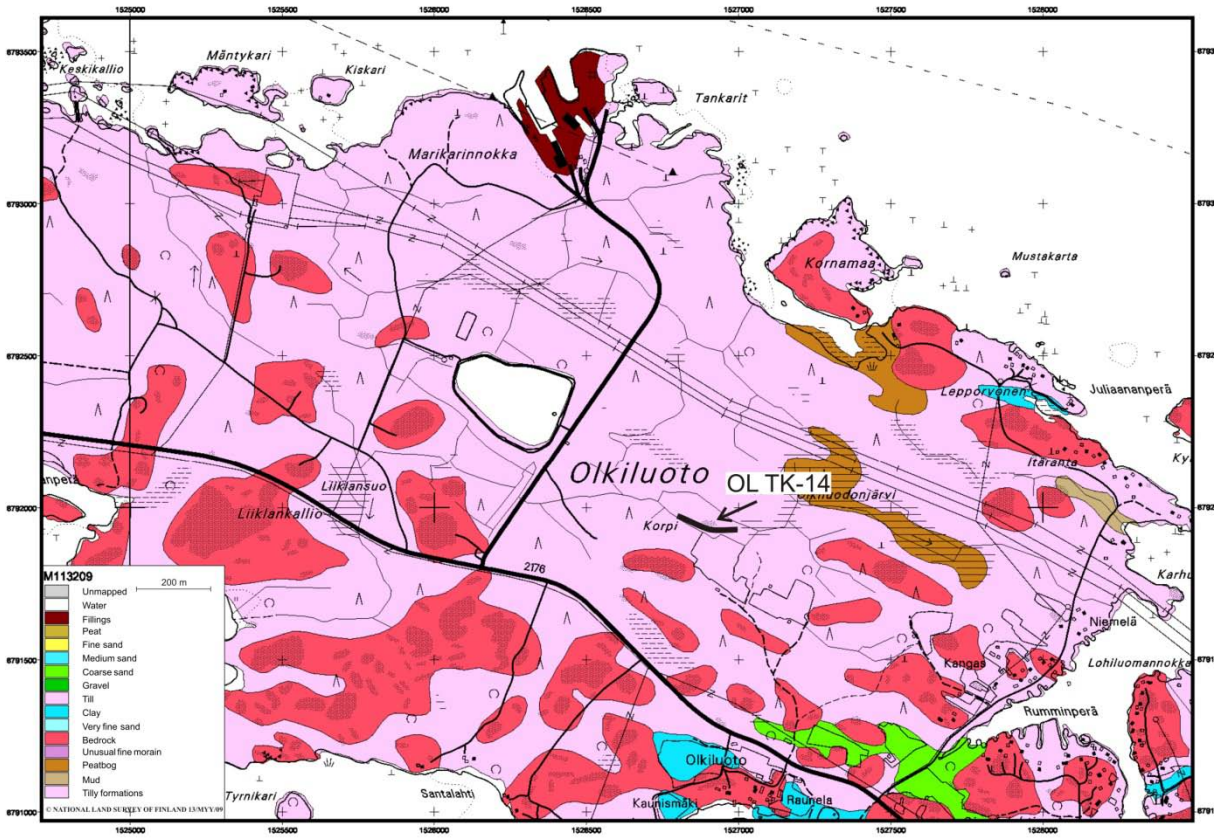

Figure 6-3: Quaternary geological map of Olkiluoto Island (W-Finland). The investigation trench OL-TK14 where from the samples were collected is marked by an arrow

This is a slow process that started on the superficial parts of mineral soil after Weichselian glaciation, about 10 000–9000 years ago in Finland (Donner, 1995). Due to the evolution of Baltic Sea, the oldest podzols are in supraaquatic areas of northern and eastern Finland. At Olkiluoto most of the podzol soil layers are not well developed, because the youngest podzol soils (4000–5000 years) are on the coast of Gulf of Bothnia, the area with the highest uplift rate in Finland. The land will rise about 40 m during the next 10 000 years (Löfman, 1999). The present rate of uplift in Olkiluoto is about 6 mm/y and thus 6 m during the next 1000 years (Eronen et al., 1995).

The length of trench OL-TK14 where the samples were taken from (Figure 6-1) is approximately 215 m long and 9 profiles were sampled from the trench. The depth of the profiles varied from 4.9 m to 1.4 m with an average of 2.9 m. Summary of the sampling profiles is presented in Figure 6-4. The figure shows, how the till cover very effectively levels out the bedrock topography. Two till beds were distinguished in the trench. The upper till bed has two layers. The upper, surface layer is oxidised, brown sandy till, whereas the lower layer is unoxidised, grey sandy till. The lower till bed has been preserved in bedrock depressions. It is compact, dark grey silty till with over 15 % of fine material (under 0.002 mm). The upper

till bed was deposited in the last flow phase of the Weichselian continental ice. Bedrock striations indicate that the ice moved in a WNW-ESE direction. The lower till bed has been deposited in an earlier flow phase (Huhta, 2008).

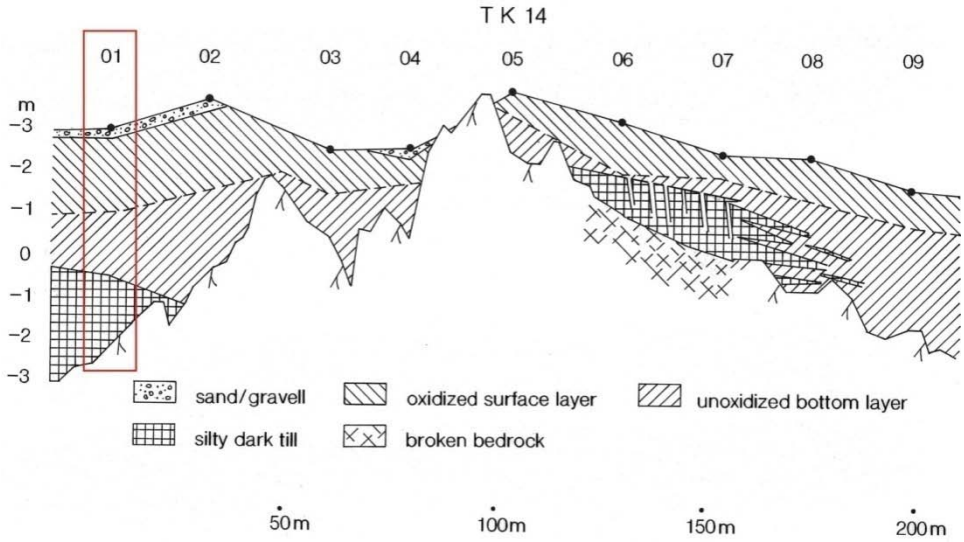

Figure 6-4: Geological section of trench OL-TK 14 (Huhta, 2008). The red frame shows section sampled

Recharge computations carried out with the surface hydrology model revealed that the Olkiluoto bedrock groundwater system is transport-limited and the overburden is supply-limited (Karvonen, 2008). The transport-limited system implies that there is more supply from the overburden to the bedrock than the bedrock system can transmit, which is due to the low hydraulic conductivity in the bedrock compared to that of the overburden soils. The supply-limited groundwater system of overburden implies that more precipitation would result in greater runoff and evapotranspiration. Average measured change in hydraulic elevation (ΔH_{MEAS}) for all tubes located in fine-textured till soil was 1.99 m and in sandy till soil was 2.12 m (Karvonen, 2008). The ground water level at the area can be as high as few cm from the surface, and varies with thickness of the overburden (Toropainen, 2009). At the Olkiluoto Island over 60 % of precipitation evaporates, directly or through transpiration. The rest forms direct surface runoff through near-surface groundwater in the overburden. Groundwater near the overburden has shorter residence time and thus contains less dissolved elements and react quicker for the percolating water and to a large extent to seasonal changes than deeper groundwater (Toropainen, 2009). We studied the groundwater level at the area close to the trench in Spring and Autumn. It was found that the level in the lower altitude was near the surface and ca. 70 cm next to the trench. The pH of the groundwater at the study site is 7.3; sulphate content is 42-59 mg/l (Pikänen, 2010, kind verbal communication).

6.3. Results of analyses made on Olkiluoto samples

6.3.1. Description of Olkiluoto samples

Olk-1 (Figure 6-5)

In wet, the sample is brown and grainy disintegrated. In dry, the sample is reddish-brown, crumb structured, badly sorted. The pebbles are rounded and sub-angular. The grains are not identifiable because of brownish film covering. The pebbles are granite, quartz pegmatite, mica schist, gneiss, sandstone and limestone. The sample has reasonable Ca-carbonate content (tested by 10 % HCl).

Figure 6-5: Photo of sample Olk-1 collected at 70 cm depth in profile 1 of trench OL-TK14, Olkiluoto, Finland

Olk-2 (Figure 6-6)

In wet, the sample is grey and grainy disintegrated. In dry, the sample is light-grey, crumb structured, little lubricatable, shapeable and badly sorted. The pebbles are rounded and sub-angular. The grains are not identifiable because of greyish film covering on grains. The pebbles are granite, quartz pegmatite, mica schist, gneiss, sandstone, limestone. The sample contains reasonable amount of Ca-carbonate (tested by 10 % HCl).

Figure 6-6: Photo of sample Olk-2 collected at 250 cm depth in profile 1 of trench OL-TK14, Olkiluoto, Finland

Olk-3 (Figure 6-7)

In wet, the sample is light grey and grainy disintegrated. In dry, it is dark-grey, crumb structured, little lubricatable, shapeable and badly sorted. The pebbles are rounded and sub-angular. The grains are not identifiable because of greyish film covering grains. The pebbles are granite, quartz pegmatite, mica schist, gneiss, sandstone, limestone. The sample has reasonable Ca-carbonate content (tested by 10 % HCl).

Figure 6-7: Photo of sample Olk-3 collected at 400 cm depth in profile 1 of trench OL-TK14, Olkiluoto, Finland

Grain size distributions of the three Olkiluoto samples (Olk-1, Olk-2 and Olk-3) are presented on Figure 6-8. Samples Olk-1 and Olk-2 among the three samples have almost the same grain size distribution. They are very slightly sorted fine sands with significant amount of fine fractions (< 0.063 mm, ca. 40 %). The deepest sample Olk-3 has more fine fractions (ca. 60 %). Therefore, Olk-1 and Olk-2 are sandy tills, whereas Olk-3 is silty till. The description of lithology of the samples is summarised in Figure 6-9.

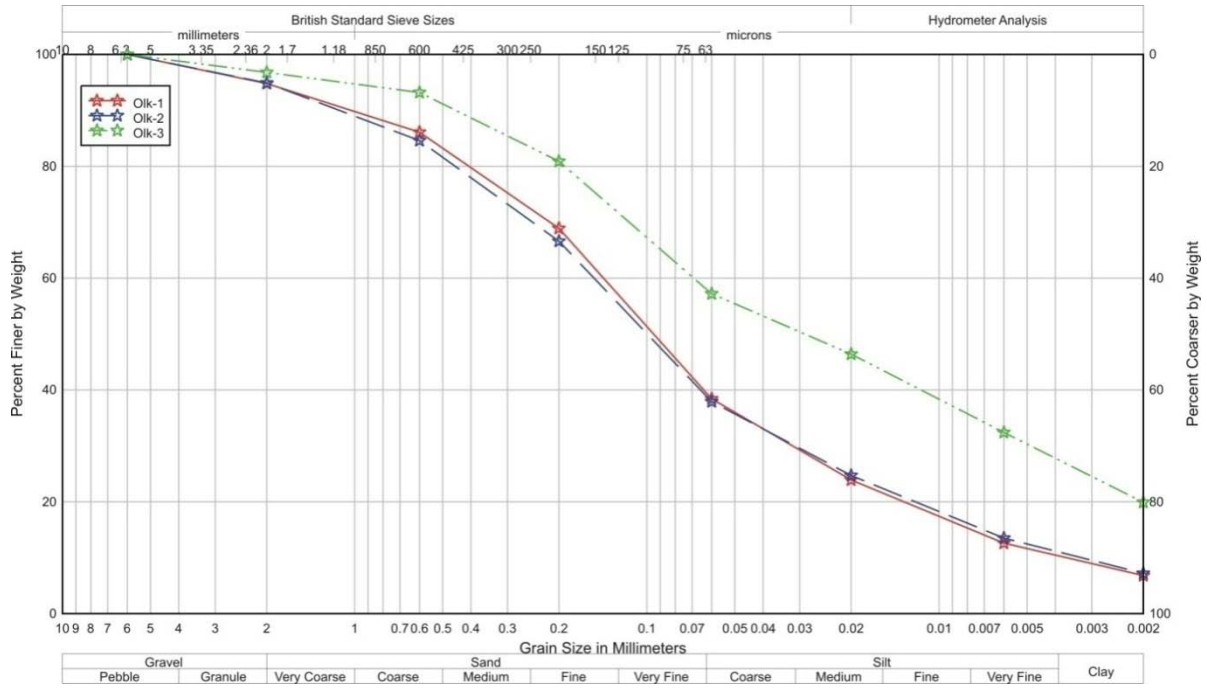

Figure 6-8: Grain size distribution of the three samples collected from the OL-TK14 trench at Olkiluoto sampling site (Huhta, 2008)

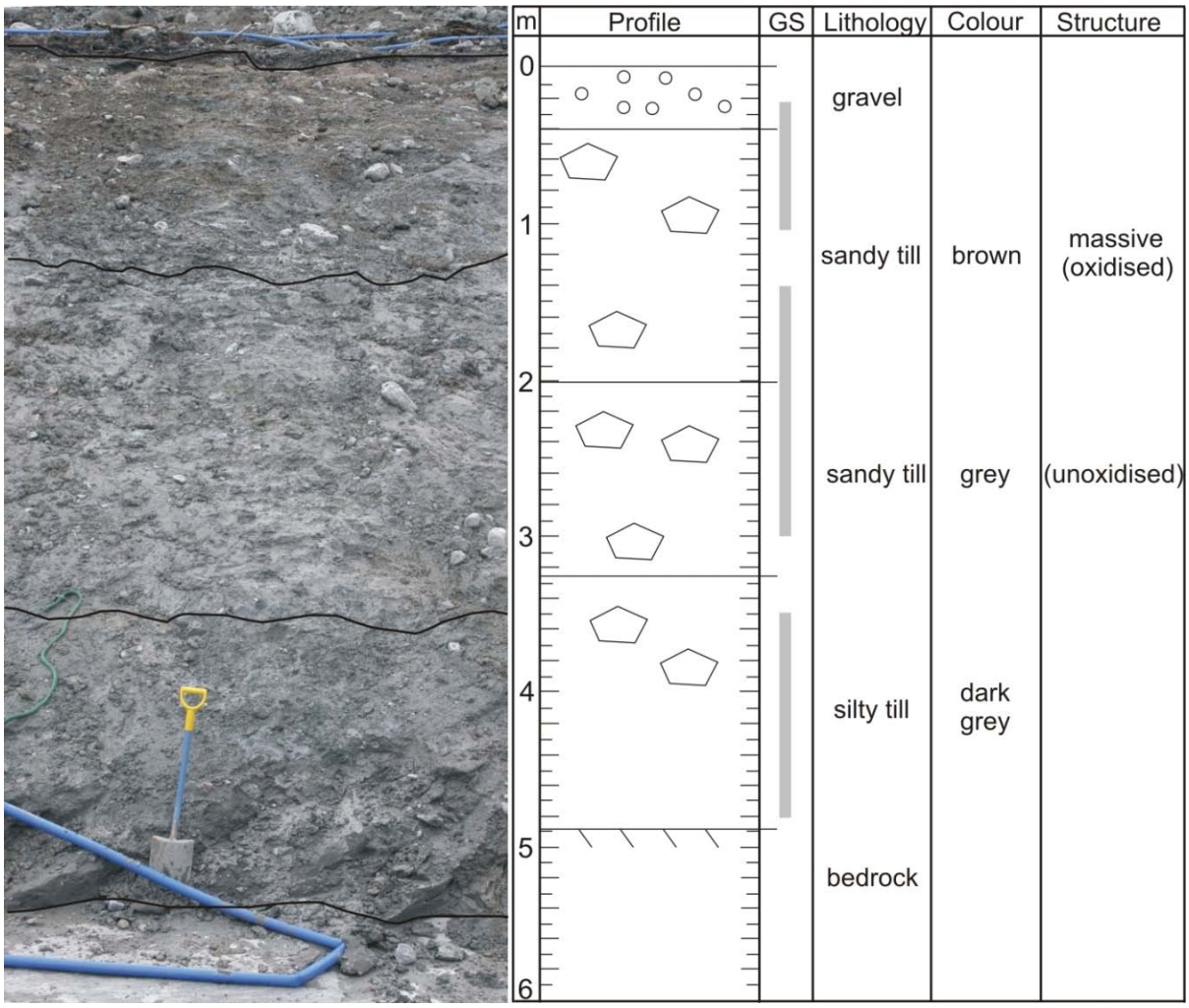

Figure 6-9: Summarised chart of lithology of the samples collected from OL-TK14 trench at Olkiluoto sampling site, Finland

6.3.2. U-, Th- and Ra-content of bulk samples from Olkiluoto

Activity concentrations of ^{238}U-, ^{226}Ra- and ^{232}Th- (from ^{228}Ac and ^{208}Tl) were measured by a gamma-spectrometer equipped by BEGe-detector (broad energy germanium). The results are presented in Table 6-1 and the variations vs. depth are plotted on Figure 6-10.

Table 6-1: Activity concentrations (Bq/kg) of ^{238}U (^{234m}Pa), ^{226}Ra and ^{228}Ra (^{228}Ac), ^{228}Th (^{208}Tl) as representing ^{232}Th-decay chain in vertical profile of trench OL-TK14, Olkiluoto, Finland.

Samples	Depth (cm)	^{238}U (^{234m}Pa)	^{226}Ra	^{226}Ra/^{238}U	^{228}Ra (^{228}Ac)	^{228}Th (^{208}Tl)	^{232}Th	^{228}Ra/^{232}Th
Olk-1	70	37±5	52±5	1.4±0.2	34±2	34±2	33±1	1.0±0.1
Olk-2	250	34±6	30±6	0.9±0.2	30±2	27±2	31±1	1.0±0.1
Olk-3	400	40±3	37±6	0.9±0.2	34±2	33±2	33±1	1.0±0.1

Activity concentration of ^{232}Th was calculated from Th concentration (ppm) analysed by ICP-MS in SGS Lab, Toronto. The reported uncertainties are expanded uncertainties using a coverage factor k=1.

In Olkiluoto bulk samples (< 20 mm) ^{238}U-concentration shows no variation within the range of error in a function of depth (ca. 40 Bq/kg). Activity concentration of ^{226}Ra in the uppermost sample (Olk-1) is higher (ca. 50 Bq/kg) than in the deeper horizons (ca. 35 Bq/kg) (Table 6-1, Figure 6-10).

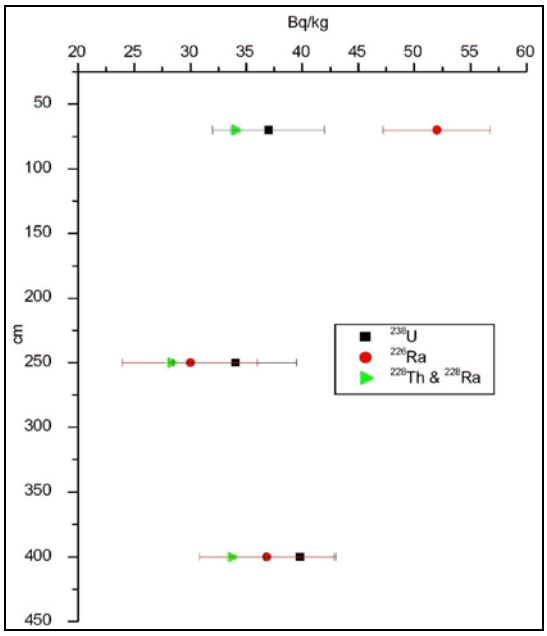

Figure 6-10: Activity concentrations of ^{226}Ra, ^{238}U and ^{228}Ra (^{228}Ac), ^{228}Th (^{208}Tl) as representing ^{232}Th-decay chain in function of depth in samples from Olkiluoto. The reported uncertainties are expanded uncertainties using a coverage factor k=1

Reductive part of the upper layer sample Olk-2 has lower ^{228}Ra activity concentration than in the oxidised part of this layer and in the deepest layer wherein similar ^{228}Ra activity concentrations were measured. In the sample Olk-1 disequilibrium occurred between ^{238}U and ^{226}Ra (^{226}Ra/^{238}U = 1.4). There are no significant differences between measured ^{228}Ra and calculated ^{232}Th (measured by ICP-MS) activity concentrations both are ca. 30 Bq/kg (Table

6-1). In ^{232}Th decay chain the secular equilibrium is existing, ^{228}Ra and ^{208}Tl have similar activity concentrations.

6.3.3. Radon production and emanation rate of bulk samples from Olkiluoto

Both radon production and emanation factors measured in the three Olkiluoto bulk samples (< 20 mm) does not differ significantly from each other. However, Olk-1 has slightly elevated radon production 0.03 Bq/(kg h) and emanation factor 0.08 (Table 6-2).

Table 6-2: Activity concentrations (Bq/kg) of ^{226}Ra, ^{222}Rn production (Bq/(kg h)) and emanation factor of Olkiluoto (Olk) samples.

Samples	^{226}Ra	^{222}Rn prod.	Emanation factor
Olk-1	52±5	0.03±0.00	0.08±0.01
Olk-2	30±6	0.01±0.00	0.04±0.01
Olk-3	37±6	0.02±0.00	0.06±0.01

The reported uncertainties are expanded uncertainties using a coverage factor k=1.

6.3.4. Major and trace elements of bulk samples from Olkiluoto

Results of the major and trace element analyses of the three < 0.250 mm size sediment samples from Olkiluoto sampling site is presented in Annex 1 and plotted on Figure 6-11.

In Olkiluoto samples were normalised to the average chemical composition of the upper continental crust (UCC) (Taylor and McLennan, 1995). The normalised value (ratio) is close to one (0.8-1.2) or below the average (< 0.8). Except zirconium, that is approximately twice as high as the UCC. Radium (0.6-0.8), Ba (0.6-0.8), Nb (ca. 0.4), K (ca. 0.7), Fe (0.4-0.7) and Sr (ca. 0.4) have lower concentration than UCC (Figure 6-11a). Major and trace element contents of the three samples are very similar. The uppermost sample Olk-1 has higher Ra and U content than the others. Sample Olk-2 has the lowest concentrations from most of the trace elements, except Zr and Pb that are in the highest concentration. The deepest sample Olk-3 has generally higher trace element contents than the others (Figure 6-11a). Chondrite normalized rare earth element (REE) compositions of the three samples show no difference (Figure 6-11b). The samples are enriched in light REEs (LREE = La-Sm) compared to heavy ones (HREE = Gd-Lu) with negative Eu anomaly that is typical for granitoid rocks. Heavy REE have similar sample/chondrite ratio (ca. 20) that decreases from LREE to HREE from 100 to 20.

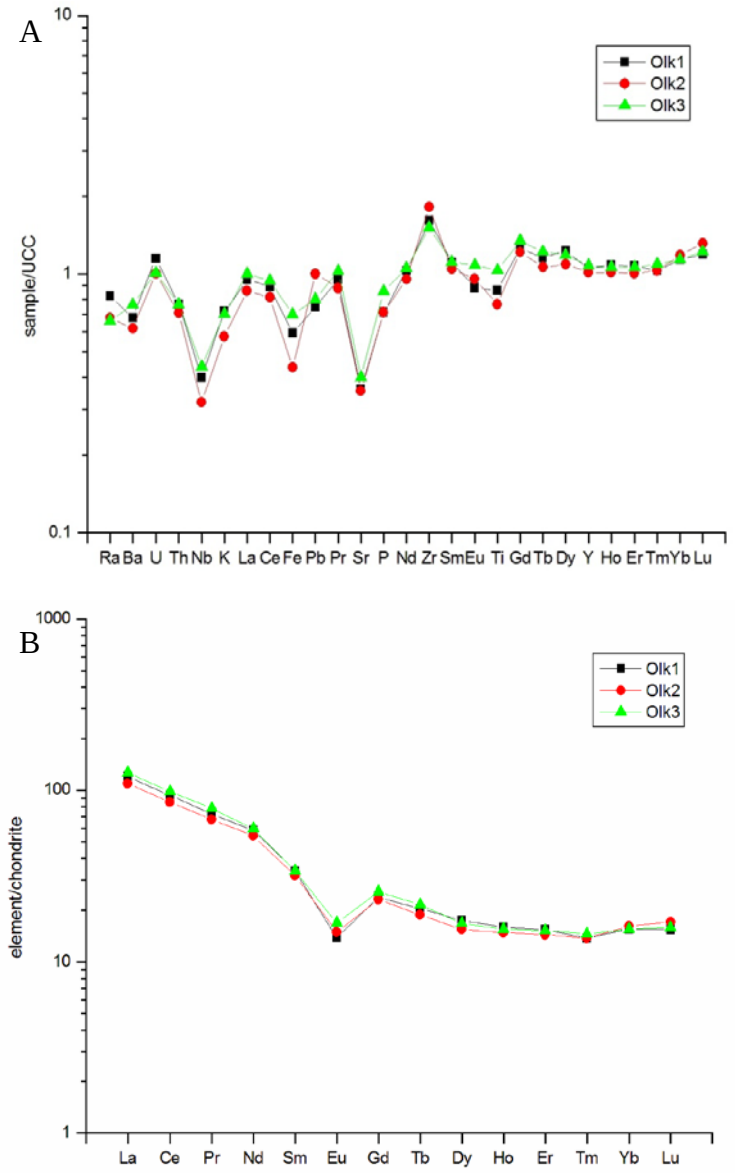

Figure 6-11: Upper continental crust- (UCC) (Taylor and McLennan, 1995) normalised trace elements of bulk samples from Olkiluoto. Activity concentration of ^{226}Ra was normalised to average soil and sediment concentration of Eastern USA (Greeman and Rose, 1996) (A). Chondrite-normalised (McDonough and Sun, 1995) REE concentrations (B)

6.3.5. Major and trace elements of soil portions extracted from Olkiluoto samples

6.3.5.1. Exchangeable fraction

Only few elements were extracted in a very low proportion by exchangeable sequential extraction step (Figure 3-2). The concentration extracted in this step is presented in Annex 2 and the proportions to bulk concentration are plotted on Figure 6-12. From trace elements radium was extracted in the highest proportion, 10-30 % of bulk Ra-concentration. Barium and Sr 1-3 %, and the others (K, La and Eu) less than 1 % were extracted. Uranium was extracted only in sample from the greatest depth (Olk-3) (2 %). It can be seen on Figure 6-12 that Ra and k were extracted in the lowest concentration from the uppermost sample Olk-1,

whereas the others elements from the sample Olk-2. Generally, elements were extracted in the highest proportion in sample Olk-3 from the greatest depth.

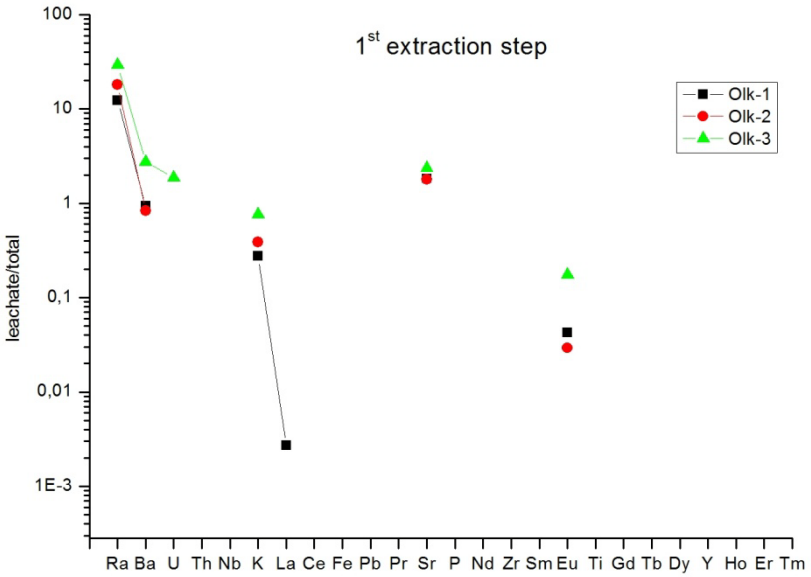

Figure 6-12: Proportion (%) of elements extracted at the 1st extraction step (Figure 3-2) from the total composition of samples from Olkiluoto

6.3.5.2. Carbonate fraction

Concentration of major and trace element extracted by "carbonate" extraction step (Figure 3-2) are presented in Annex 2, and the proportions of bulk concentration are plotted on Figure 6-13.

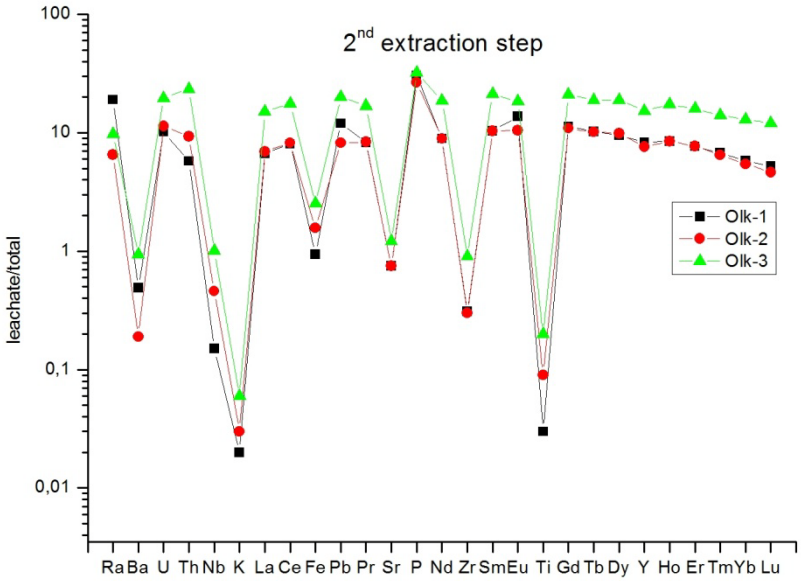

Figure 6-13: Proportion (%) of elements extracted at the 2nd extraction step (Figure 3-2) from the total composition of samples from Olkiluoto

In this step approximately 10 % of bulk concentrations were extracted. In lower amount Ba (< 1 %), Nb (< 1 %), K (< 0.1 %), Fe (ca. 1-2 %), Sr (ca. 1 %), Zr (< 1 %) and Ti (< 0.2 %) and

in higher P (ca. 30 %) were extracted. The highest concentrations were leached out from the deepest sample Olk-3. Radium is the only exception, which was extracted in the highest proportion from the uppermost sample Olk-1. Thorium, Nb, Fe and Ti were extracted in the lowest amount from the uppermost sample (Olk-1).

Chondrite normalised rare earth element (REE) contents of leachate extracted from the deepest samples (Olk-3) is approximately twice as high as it was extracted from the other two samples (Figure 6-14). REE contents of leachates extracted during this step from sample Olk-1 and Olk-2 are quite similar to each other. The REE distributions of the three extractants have granitoid pattern with slightly negative Eu anomaly.

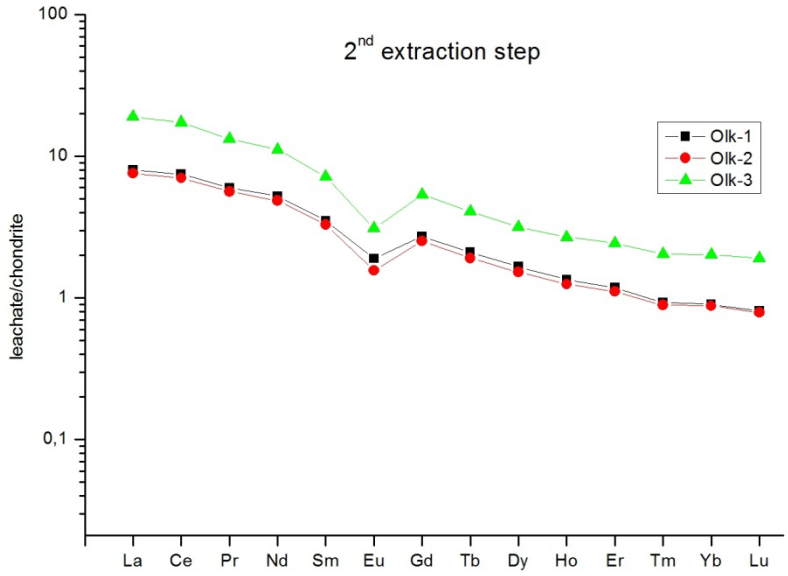

Figure 6-14: Chondrite-normalised REE concentrations (McDonough and Sun, 1995) in leachates extracted at the 2nd extraction step (Figure 3-2) from samples from Olkiluoto

6.3.5.3. Oxide fraction

Concentrations of major and trace element extracted by "oxide" extraction step (Figure 3-2) are shown in Annex 2, and the proportions of bulk concentration are plotted on Figure 6-15.

In this step ca. 5 % of bulk concentration was extracted in the majority of the elements, except for Th and Nb (~ 1 %), Ba, Sr and Zr (~ 0.5 %), K (~ 0.2 %) and Ti (~ 0.02 %). Iron (~ 10 %), U (15 %) from the deepest sample (Olk-3) and Pb (> 20 %) from the uppermost sample were extracted in higher proportion (Figure 6-15). Most of the trace elements were leached out in the highest proportion from the uppermost sample, except Ba, U, Nb, K, Zr and Ti were extracted in higher amount from the other two samples. Radium was extracted in the same proportion from the three samples.

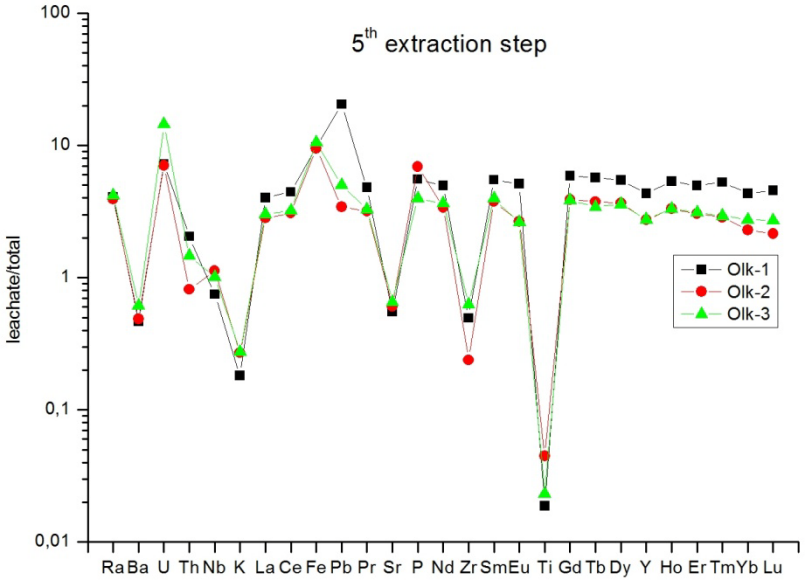

Figure 6-15: Proportion (%) of elements extracted at the 5th extraction step (Figure 3-2) from the total composition of samples from Olkiluoto

The distribution of REE in the samples is similar, only the extracted amounts are different. Especially in the case of the uppermost sample Olk-1, wherefrom the highest amount of REE was extracted. It is followed by the deepest sample Olk-3 and sample Olk-2. The chondrite normalised REE concentrations in the leachates show granitoid distribution with negative Eu anomaly (Figure 6-16).

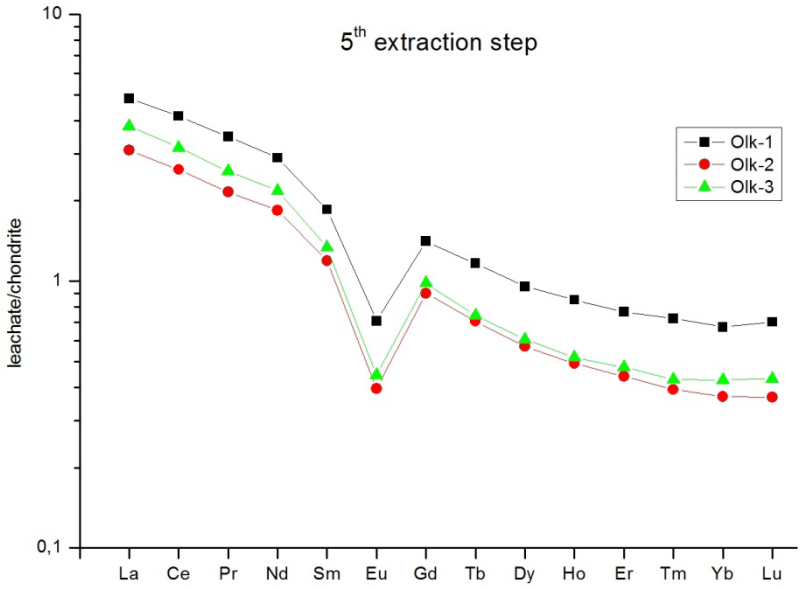

Figure 6-16: Chondrite-normalised REE concentrations in leachates extracted at the 5th extraction step (Figure 3-2) from samples from Olkiluoto (McDonough and Sun, 1995)

6.3.5.4. Residual fraction

In the last "residual" sequential extraction step aqua regia solution was used (Figure 3-2). The concentrations in the leachates are presented in Annex 2 and the proportions of bulk

concentrations are plotted on Figure 6-17. Most of the trace elements in the highest proportion were extracted from the samples by this step. More than 50 % of Ra, Th, Fe, P, Y and light and medium REE (La-Gd) were extracted. Heavy rare earth elements from Gd to Lu were extracted in lower amount (60-25 %). Uranium, K, Sr and Ti were extracted in proportion of less than 40 % Very low proportion of Ba (< 20 %), Nb (< 20 %), Pb (~ 10 %) and Zr (~ 4 %) were leached out from the samples. Significant (ca. 10 %) deviation in extracted proportion of major and trace elements by aqua regia solution was measured in the case of few elements, such as, Ra, U and Th. From these and the light rare earth elements the lowest and from Ba, K, Eu and HREE (Dy-Lu) the highest proportion were extracted in sample Olk-3 from the greatest depth.

Chondrite normalised rare earth element concentrations show differences among the three samples mainly for LREE. These elements were extracted in lower amount from sample Olk-2. The leachate/chondrite ratios decrease from ca. 100 to 5. Significant negative Eu anomaly measured in each samples (Figure 6-18).

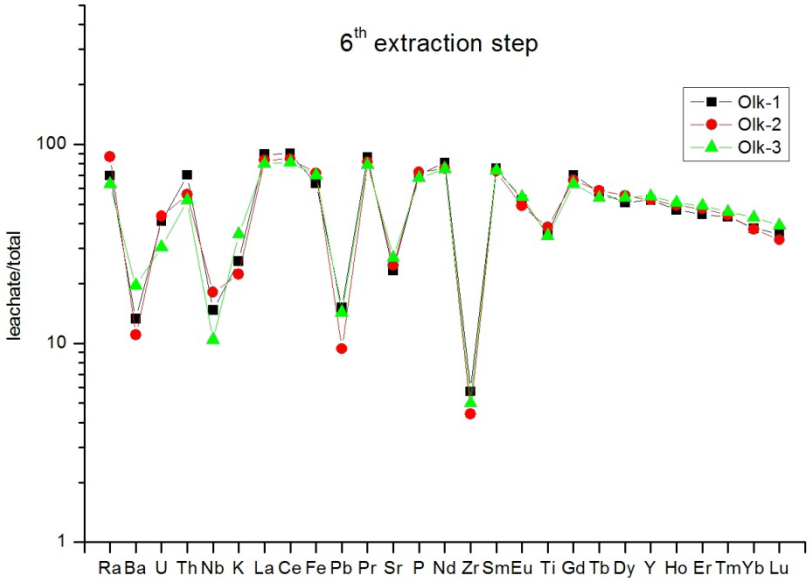

Figure 6-17: Proportion (%) of elements extracted at the 6th extraction step (Figure 3-2) from the total composition of samples collected from Olkiluoto, Finland

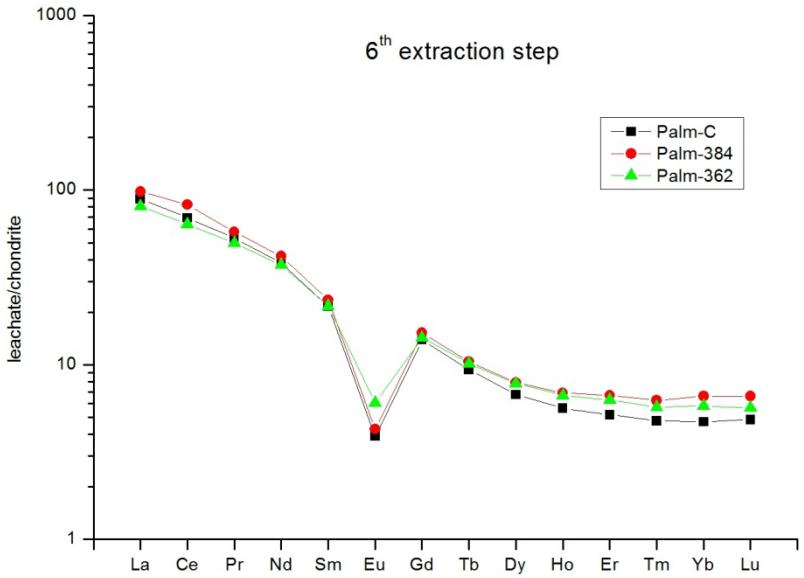

Figure 6-18: Chondrite-normalised REE concentrations (McDonough and Sun, 1995) in leachates extracted at the last extraction step (Figure 3-2) from samples collected from Olkiluoto, Finland

The total portions of trace elements extracted from bulk concentration by the four sequential extraction steps are plotted on Figure 6-19. Most of the trace elements extracted are in range of 50-100 %. Low proportion of Pb (< 50 %), K (< 40 %), Ti (30-40 %), Sr (ca. 30 %), Ba (< 25 %), Nb (≤ 20 %) and very low of Zr (ca. 5 %) were extracted in each sample. In contrast, all of the Ra, LREE and P were extracted from the samples.

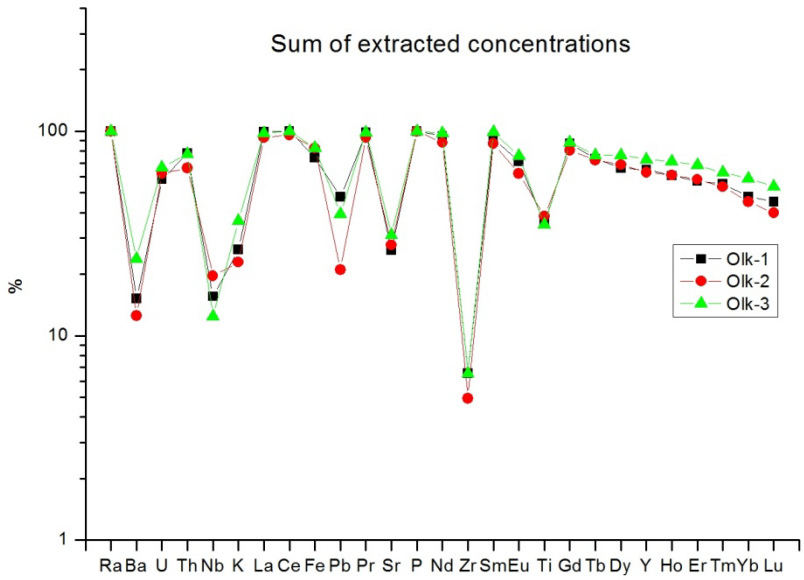

Figure 6-19: Sum of extracted concentrations (%) during the four extraction steps from samples collected from Olkiluoto

From the deepest sample Olk-3 more trace elements were extracted from the bulk concentration than from the other two samples, except Nb and Pb, which were extracted in the highest proportion from Olk-2 and Olk-1, respectively. Sample Olk-2 was the most resistant for most of the major and trace elements, with exception of Ra, U and Fe, which were

extracted in the lowest proportion from the uppermost sample Olk-1, and of Nb and Ti which were leached out in the lowest portion from the deepest sample Olk-3.

6.3.6. Mineralogical study of Olkiluoto samples

For setting up a statistical rank of heavy minerals, approximately hundred randomly selected mineral grains were analysed. The proportions of the heavy minerals are plotted on Figure 6-20. Most of the heavy minerals of Olkiluoto samples are garnets (mainly andradite and almandine) and amphiboles (hornblendes), 30-40 % and 23-27 %, respectively. The proportions of pyroxenes (augite and diopside) are between 10-15 %. Heavy minerals of the samples are suggest granitoid (apatite, titanite and idiomorphic zircon), basic-ultrabasic (augite) and metamorphic (kyanite, diopside and garnet) source rocks. Heavy mineral assemblages of the three Olkiluoto samples are similar. However, proportions of major heavy minerals of the samples show significant differences. In the uppermost two samples (Olk-1 and Olk-2), which are rather similar, have less andradite and ilmenite (16-18 % and 2-4 %, respectively) than in Olk-3 (27 % and 10 %, respectively). Furthermore, zircon also shows remarkable difference. In sample Olk-1 and Olk-2 its proportion is higher than 5 % whereas Olk-3 it is only 2 %.

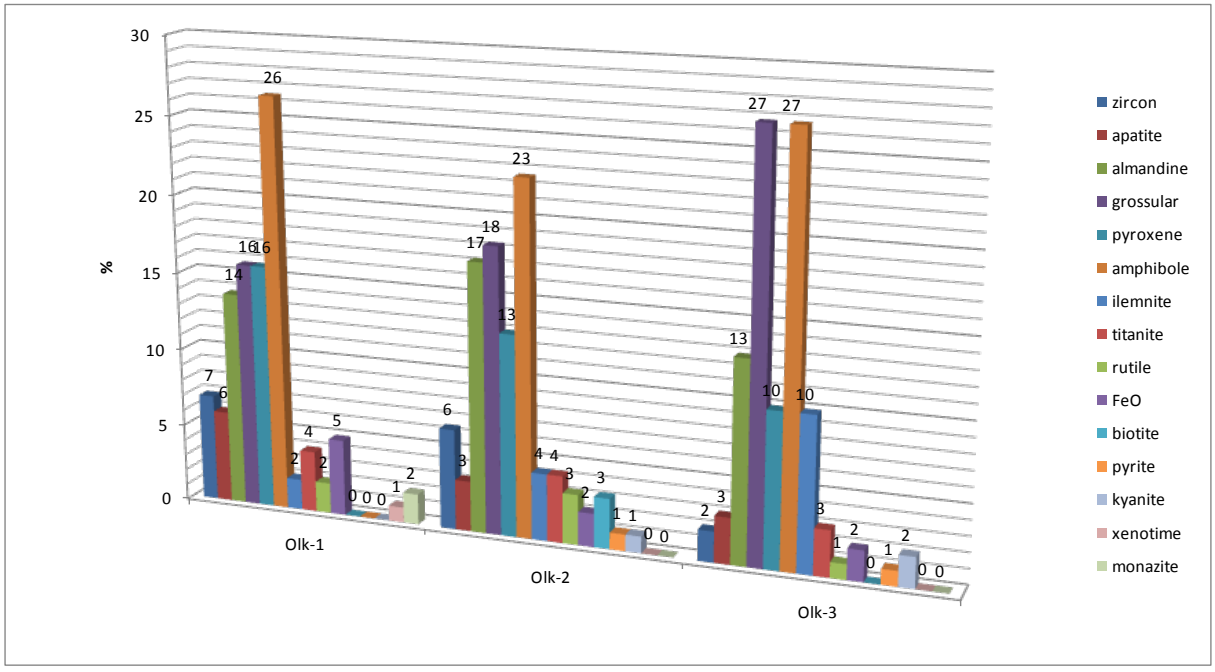

Figure 6-20: Heavy mineral ($\rho \geq 2.8$ g/cm^3) composition of < 0.063 mm grain size fractions of the three Olkiluoto samples.

Heavy minerals of the uppermost samples are more weathered than those from the deeper horizons (Figure 6-21). The minerals from the deepest samples are the least weathered ones (Figure 6-21c). The most conspicuous difference among the three horizons is the presence or absence of sulphide minerals. In the uppermost sample (Olk-1) there are no, or only a few

highly weathered pyrite grains (Figure 6-22a). In contrast, in the deeper horizons, fresh sulphide minerals (pyrite, sphalerite and arsenopyrite) were also identified (Figure 6-22).

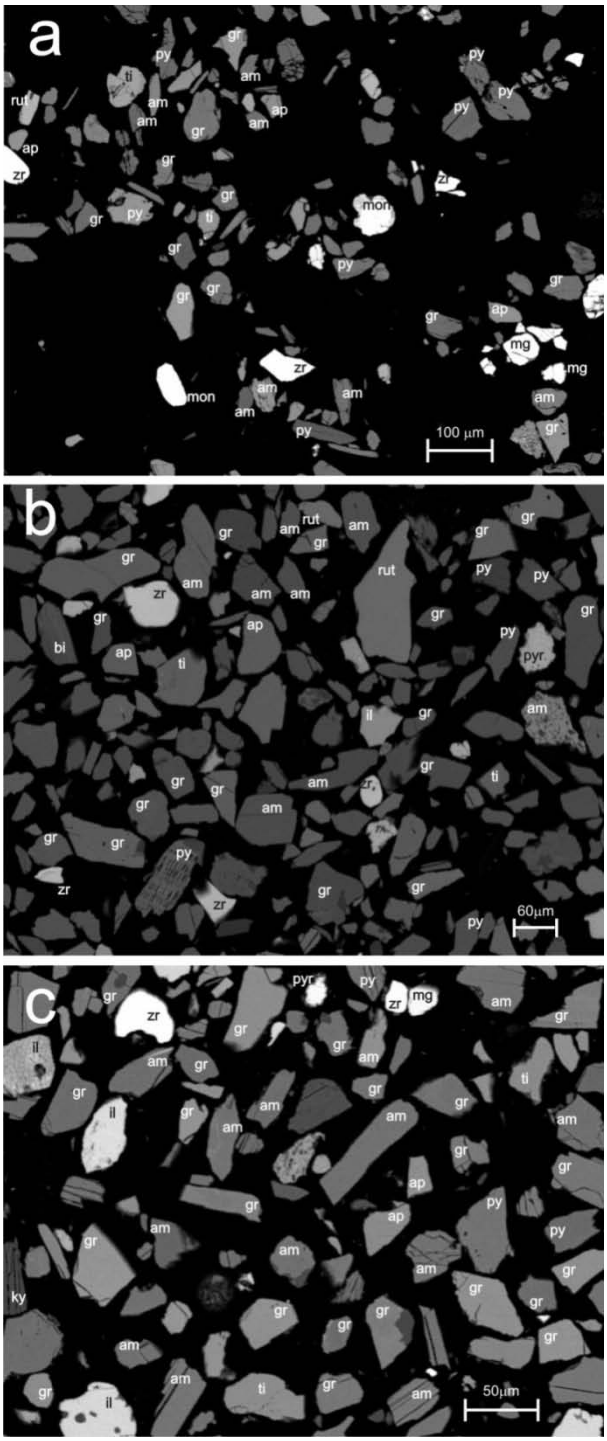

Figure 6-21: Back scattered electron images of heavy minerals ($\rho \geq 2.8$ g/cm^3) separated from the grain size fraction < 0.063 mm of the samples Olk-1 (a), Olk-2 (b) and Olk-3 (c) (am = amphibole, ap = apatite, bi = biotite, gr = garnet, il = ilmenite, ky = kyanite, mg = magnetite/hematite/goethite, mon = monazite, py = pyroxene, pyr = pyrite, rut = rutile, ti = titanite, zr = zircon)

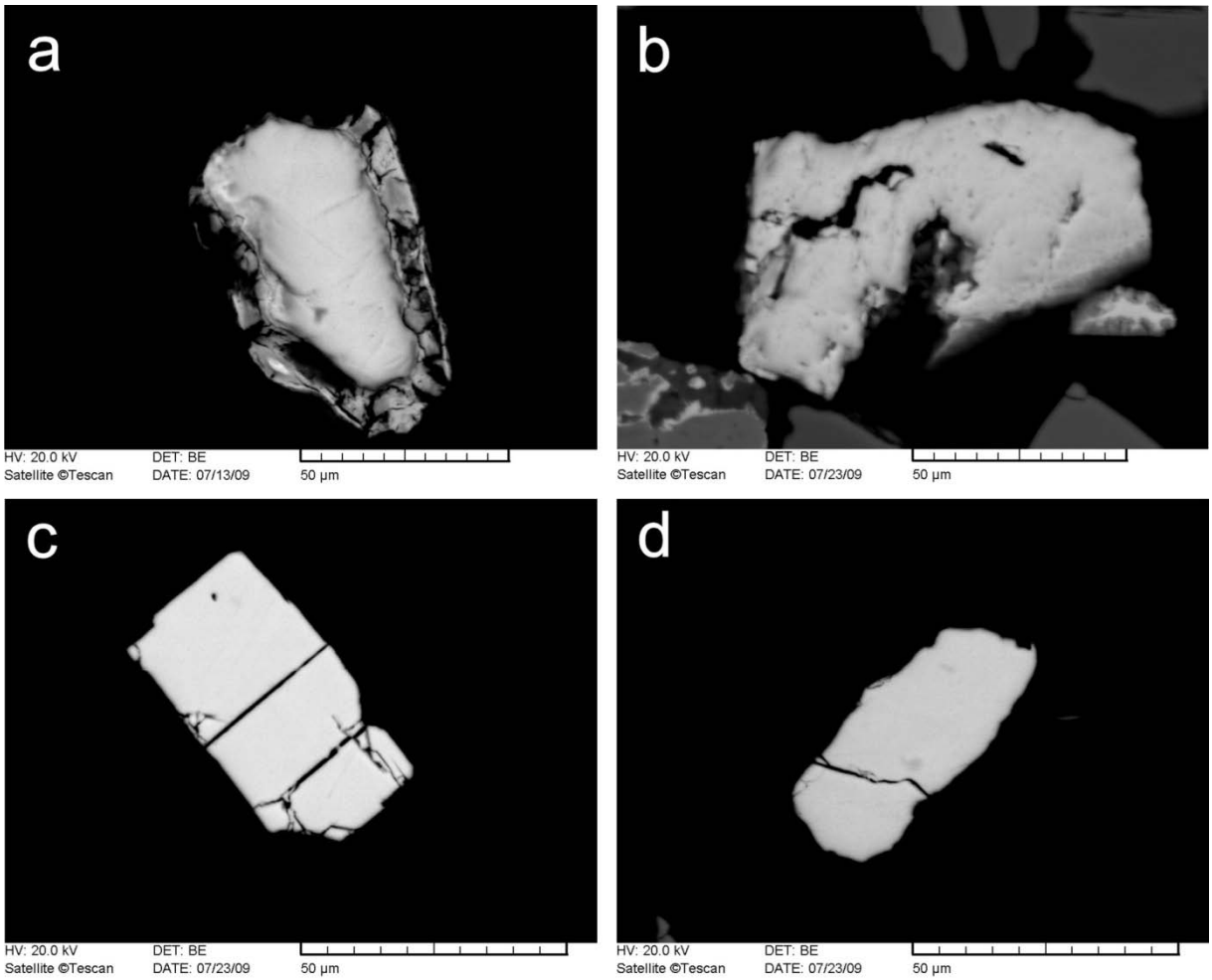

Figure 6-22: Back scattered electron images of sulphide minerals identified in the samples from Olkiluoto, Finland. a: weathered pyrite from the grain size fraction 0.063-0.125 mm of the uppermost sample Olk-1; b: moderately weathered pyrite from the grain size fraction < 0.063 mm of the sample Olk-2; c: fresh, idiomorphic sphalerite from the grain size fraction < 0.063 mm of sample Olk-2; d: fresh arsenopyrite grain from the grain size fraction < 0.063 mm of sample Olk-2

Major U- and/or Th-bearing minerals in Olkiluoto samples are monazite (idiomorphic grains or intercalating with apatite), xenotime, U-Th-oxide, U-Th-silicate or U-Th-phosphate minerals and zircon (Figure 6-23). From these minerals, monazites and zircons are present in the highest amount. Monazites as the major U-bearing minerals in the samples contain approximately 1-10 % of U and 2-10 % of Th (Figures 6-23a-c and Table 3). Xenotimes have higher U (1-5 %) than Th (0-3 %) content (Figure 6-23d-e, Table 6-3), but itself the xenotime is present in minute amount. Uranothorite and some (U)$ThPO_4$ have U and Th content of ca. 10-30 % and 30-50 %, respectively (Figures 6-23b,f and Table 6-3). Zircons have no significant U content.

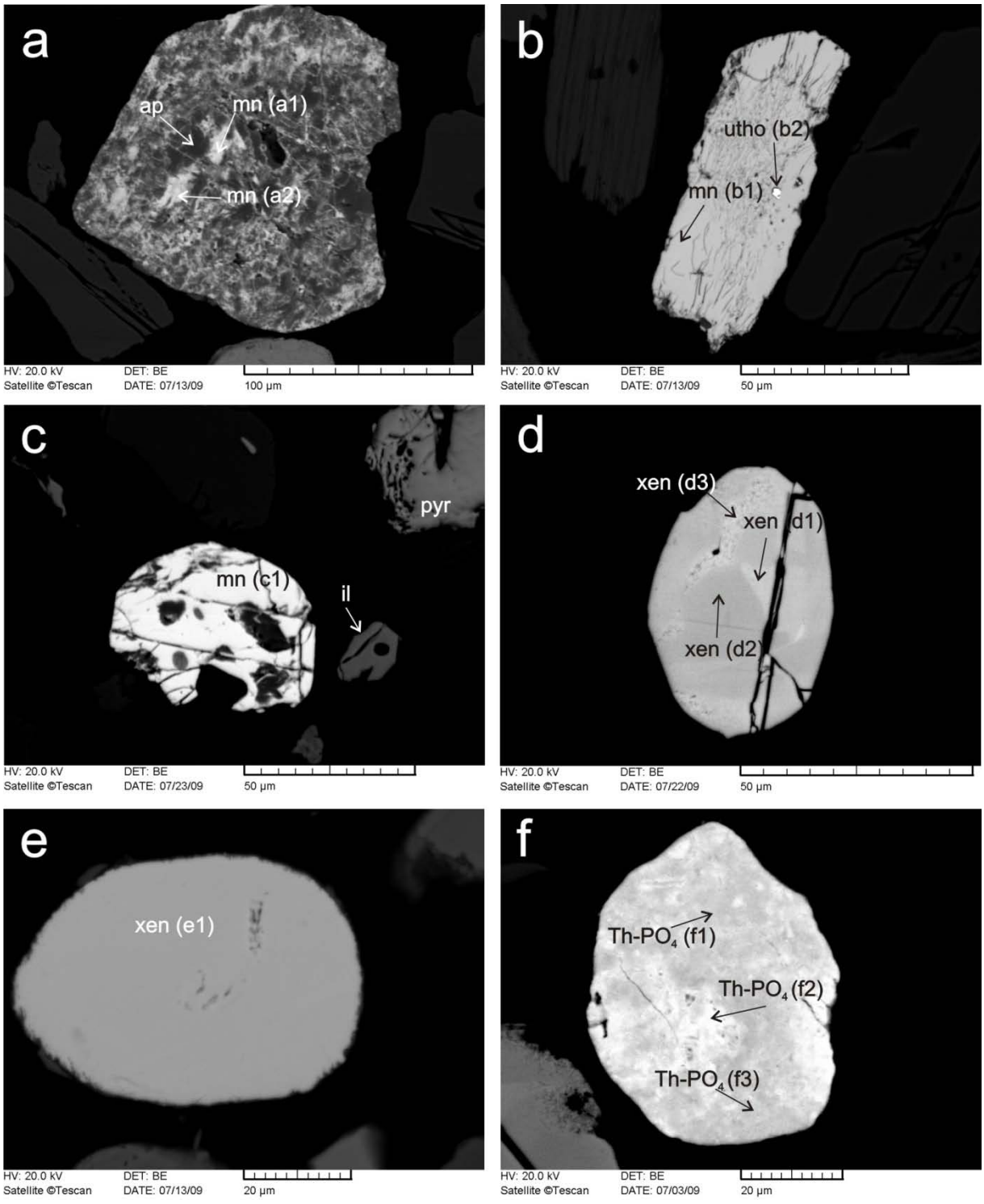

Figure 6-23: Back scattered electron images of major U- and Th-bearing minerals in Olkiluoto samples and the points of analyses marked by arrows. a: altered apatite grain with monazite intercalation from grain size fraction 0.063-0.125 mm of the sample Olk-1; b: idiomorphic monazite grain with uranothorianite inclusion from grain size fraction 0.063-0.125 mm of the sample Olk-1; c: idiomorphic monazite grain neighbouring by pyrite and ilmenite minerals from grain size fraction < 0.063 mm of the sample Olk-2; d: idiomorphic, partly weathered xenotime grain with fractures from grain size fraction < 0.063 mm of the sample Olk-3; e: idiomorphic, fresh xenotime grain from grain size fraction 0.063-0.125 mm of the sample Olk-1; f: U-$ThPO_4$ –SiO_4 mineral coexisting with iron oxide from grain size fraction 0.063-0.125 mm of the sample Olk-2

Table 6-3: Chemical composition of major uranium and thorium bearing minerals presented on Figure 6-23, The codes of analysing points are in parentheses (mn = monazite, utho = uranothorite, xen = xenotime, POI = point of interest).

Samples (POI)	SiO_2	P_2O_5	CaO	FeO	Y_2O_3	PbO_2	La_2O_3	Ce_2O_3	U_2O_3	Th_2O_3	Pr_2O_3	Nd_2O_3	Sm_2O_3	Gd_2O_3	Dy_2O_3	Er_2O_3	Yb_2O_3
mn (a1)		25.69	5.63	1.21			14.71	28.88	2.72	2.82	2.87	9.81	2.78	2.89			
mn (a2)		23.65	4.08	1.00			15.50	28.63	2.51	4.44	3.50	11.28	3.20	2.21			
mn (b1)		22.18	1.03			2.33	12.91	29.58	2.48	8.55	3.77	12.62	2.64	1.91			
utho (b2)						14.61			34.48	50.91							
mn (c1)		24.06	1.14				15.52	31.19	1.37	3.64	4.81	12.74	3.65	1.88			
xen (d1)		37.15			40.28				3.22	1.25					6.88	6.55	4.67
xen (d2)		37.35			43.33				1.03						7.07	6.05	5.17
xen (d3)		36.81			39.28				4.73	0.79					6.48	6.52	5.38
xen (e1)		38.12			39.63				4.68					2.81	10.03	4.73	
Th-PO_4 (f1)	10.28	14.04	2.01	34.45					9.31	29.91							
Th-PO_4 (f2)	9.91	11.55	1.88	15.50		1.28			15.06	44.83							
Th-PO_4 (f3)	10.95	11.73	1.69	31.57		3.55			10.59	29.93							

7. DISCUSSION

7.1. Comparison of the mineralogical and geochemical features of Askola, Olkiluoto and Palmottu sampling sites

In Askola sampling site a typical podzol soil profile was formed on esker sediment and the vertical migration of elements in it were studied. The two uppermost samples represent A (organic rich) and B (illuvial, precipitation) horizons of podzol soil (Ask-A and Ask-B). The underlying sample Ask-C, which is the C-horizon, is sandy till as well as the deepest Ask-3 sample. The two samples between these are well sorted sand layer (Ask-1) and clay layer (Ask-2) (Figure 4-12). The argillaceous layer (Ask-2) behaves as a barrier for the downward migrating fluids and retards radionuclides effectively due to low permeability and adsorbing capacity of clay minerals. The amount of trace elements analysed in < 250 μm grain size fraction are increasing with depth in the three uppermost samples (Ask-A, Ask-B and Ask-C). The elements migrated downward due to the soil formation processes. The samples (Ask-C, Ask-1, Ask-2 and Ask-3) have similar trace element content, which is close to the average chemical content of the upper continental crust (UCC) (Figure 4-14a).

In general, the highest portions of exchangeable elements were extracted from the clayey Ask-2 sample. This is because of the adsorbing capacity of clays, which represents the excellent barrier phenomenon of the clayey layer. There were no exchangeable Th and U detected in the samples, but the proportion of exchangeable Ra is high, varies between 6 and 55 % (Figure 4-15). In the third (oxide) extraction step large part of the P (30-80 %) and U (10-55 %) were extracted from deeper horizons (below the B horizon) (Figure 4-17). We used Tamm's reagent for those exchangeable cations, which were not removed by the previous step, thus amorphous or poorly crystalline Fe and Mn-oxyhydroxides were extracted. Due to the low pH of the Tamm's solution and the presence of a high concentration of complex forming agent, some U(VI)-phosphates that are common secondary-formed U-minerals (Figures 4-27 – 4-30, Tables 4-3 – 4-6), and microcrystalline apatite could also be totally or partially removed (Quejido et al., 2005). The lower proportion of Th extracted (10-24 %) revealed that resistant Th-bearing minerals such as monazite are the major source of Th. Radium extracted in this step (1-8 %) correlates with REE and Nb (Table 7-1), which means that the Ra is related to the U-Th-phosphates, U-oxides and altered monazites. As reasonable amount of organic material was expected only in the uppermost horizon, extraction of organic material was carried out only on that sample in order to reduce overlapping between the steps

as much as possible. Some of the partly dissolved minerals, like uranium dioxide, can be dissolved and therefore those elements associated with these minerals cannot be assigned to organic matter, when such minerals accompany it (Quejido et al., 2005). Low proportion of U (2 %) (Figure 4-19) extracted in this step is probably from the remaining U-oxides-phosphates. Since this step extracted the second highest proportion of Ra (15 %) (Figure 4-19), organic matter together with materials that have reactive surface with exchange capacity are the most important constituents of topsoil effecting Ra mobilisation. In the case of mineralised soils and sediments only the exchangeable Ra is significant. Hence, as it was concluded in numerous studies (Greeman et al., 1999; Girault et al., 2011) the sorption of Ra is the most important process that affects mobilisation. The most effective absorber minerals where the binding process is cation exchange are the clay minerals. However, proportion of extracted Ra shows no or very weak, mostly negative correlation with decreasing grain size fraction (Table 7-1). It indicates, that the exchangeable Ra is not related directly to the finest grain size fraction and it is also present on the surface of altered grains in the coarser grain size fractions, where the alteration product can be clay mineral, too.

In the Olkiluoto samples another vertical migration pathway was studied in glacial sediment with well-developed redox profile (Figure 6-1). In contrast to Askola sampling site this formation has no relation with uranium mineralisation. The two uppermost samples (Olk-1 and Olk-2) are same in material they differ only in redox condition (Figure 6-9). This difference results in some difference in mineral composition. Sample from reductive environment contains significant amount of sulphide minerals, while these minerals are absent or are highly weathered in sample collected from the oxidised layer (Figure 6-22). The deepest sample was deposited during an early ice age (Huhta, 2008). Its colour, grain size distribution and heavy mineral composition are different than that of the other two samples (Figure 6-20). However, the major and trace element content of the three samples studied are similar (Figure 6-11), which indicates that the major source rocks that were eroded, transported and deposited during the two different glacial events, have similar mineral composition. The measured groundwater level at the study site indicates that the uppermost 60-70 cm of the trench is vadose zone (unsaturated) all over the year, even in the wet season.

Table 7-1: Correlation (Pearson product moment) factors between total and extracted concentration of the elements (extr-total) and portion of the finest fraction and the extracted proportion of the elements analysed. Ex = “exchangeable” step, Ox = “oxide” step, Res = “residual” step.

Seq. extr. steps	Ra	Ba	U	Th	Nb	K	La	Ce	Fe	Pb	Pr	Sr	P	Nd	Zr	Sm	Eu	Ti	Gd	Tb	Dy	Y	Ho	Er	Tm	Yb	Lu
Ex (extr-total)	0.83	0.86				0.83	0.55	-0.49		-0.65	0.66	0.13		0.71		0.78	0.88		0.93	0.82	0.68	0.75	0.87	0.51	0.77	0.43	0.16
Ox (extr-total)	0.52	-0.47	0.99	0.99	0.95	0.85	0.36	0.65	0.99	-0.29	0.04	-0.96	0.58	0.00	0.75	-0.27	-0.14	0.98	-0.36	0.01	0.32	0.67	0.37	0.58	0.65	0.73	0.51
Res (extr-total)	0.94	0.82	0.92	0.98	-0.04	0.89	0.98	0.96	0.90	0.44	0.99	0.57	0.49	0.99	0.10	0.99	1.00	0.91	0.98	1.00	0.99	0.99	0.99	0.99	0.99	1.00	0.96
Ex (extr-clay)	0.02	0.76				0.74	0.94	0.84	-0.38	-0.13	0.96	0.98		0.96	-0.38	0.97	0.99		0.99	0.99	0.98	0.98	0.98	0.98	0.98	0.98	0.98
Ox (extr-clay)	-0.76	-0.43	-0.14	0.73	-0.42	0.79	-0.97	-0.57	0.07	-0.33	-0.92	-0.07	-0.16	-0.91	0.60	-0.75	-0.81	0.37	-0.81	-0.72	-0.49	0.00	-0.31	0.04	0.03	0.34	0.55
Res (extr-clay)	-0.16	0.72	0.22	0.12	-0.45	0.86	0.42	0.16	0.43	0.11	0.50	0.40	0.17	0.52	0.37	0.57	0.68	0.58	0.52	0.54	0.53	0.54	0.51	0.49	0.47	0.46	0.45

The depth of the redox front (ca. 2 m, Figure 6-9) indicates the highest position of the saturated layer. Although their trace element contents are similar, the deepest sample Olk-3 has generally higher trace element contents than others (Figure 6-11). Exchangeable Ra represents large portion of the bulk concentration (10-30 %), which is the same as in Askola samples. However, in Askola samples the proportion of exchangeable Ra is the highest one among the portions extracted (Figure 4-15), whereas in Olkiluoto samples the residual Ra shows the highest value (Figure 6-17). Among the three easily extractable soil portions exchangeable Ra was measured in the highest proportion (Figure 6-12) except from the sample Olk-1 where the highest proportion of Ra (20 %) was leached out by the "carbonate" step (Figure 6-13). The lowest proportion of Ra was extracted from the uppermost sample Olk-1 (Figure 6-19). In contrast, other elements were extracted in the lowest proportion form sample Olk-2 (Figure 6-19). Sample Olk-3 contains exchangeable and other easily removable elements in the highest proportion (Figures 6-13 – 6-16), which indicates that the redistribution of the elements was the most effective in this sample, probably due to the long time since this sediment layer has been deposited. In the carbonate step all of the trace elements, except Ra, were extracted in the highest proportion from sample Olk-3 (Figure 6-13). From the deepest sample U was in significant proportion (15 %) extracted in the oxide step (Figure 6-15), whereas Ra was extracted in the same proportion from each horizon and U from the uppermost two samples. Since proportion of U in exchangeable (Figure 6-12), carbonate (Figure 6-13), oxide (Figure 6-15) and residual (Figure 6-17) fraction in the samples Olk-1 and Olk-2 is similar, the redox condition shows no significant effect on how the U is retained in this sediment. In contrast, Ra in oxidative condition (represented by sample Olk-1) prefers the carbonate complexes (Figure 6-13), whereas in reductive condition (Olk-2 and Olk-3) it is present in exchangeable position (Figure 6-12). This is the major difference between Askola and Olkiluoto samples. In Askola, where the overburden has no carbonate content, in oxidative environment Ra is present mainly in exchangeable phase (Figure 4-15), whereas in Olkiluoto sampling site, where significant amount of carbonates are in the till the Ra is present in carbonate complexes in the oxidative zone (Figure 6-13) and in exchangeable phase in reductive environment (Figure 6-12).

In contrast to the previous two sampling sites in Palmottu the horizontal migration of the elements was studied. From the pathway three overburden sediment samples were collected. Samples Palm-C and Palm-362 are unsorted sandy tills, from the top and from the bottom of the mineralisation, respectively. Sample Palm-362 is a very well sorted (glacio-) fluviatile or

shore sediment at the outflow of the catchment area (Figure 5-1). Sample Palm-C has significantly higher concentration of Ra, Fe, Pb and P than the other two samples (Figure 5-14a). This sample contains O, E and B horizons of podzol soil. Therefore, it is rich in organic matter and oxides. The high radium content is due to the binding phenomenon of Ra on organic matters (Titaeva, 1967), the high iron concentration is typical for B-horizon in podzol soils. Lead and phosphorus also prefer to be in organic complexes in topsoils (Tyler, 2004). The high uranium concentration (ca. 25 times higher than the upper continental crust average (UCC)) was measured in the bottom of the mineralisation (Figure 5-14a). The relatively low, compared to UCC, concentration of uranium and radium measured in sample Palm-362 revealed that the uranium mineralisation has no effect on this sample, however its material is similar to the other two samples as it can be seen on REE distribution (Figure 5-14b). The proportions of exchangeable Ra in the samples are very high (> 20 %) in Palm-C or even it is higher, ca. 50 % (Figure 5-15). This feature is similar to the other two sampling sites. Exchangeable uranium and thorium are negligible, only sample Palm-384 has 2 % of exchangeable U, which indicates downward migration of uranium. The downward flow of ground water was observed on the field between the basement and the overburden. Uranium was extracted in the highest proportion in the third “oxide” step and the proportions are similar in samples Palm-C and Palm-384 (Figure 5-17). The extraction revealed that major U-bearing minerals extracted in this step are U-oxides, uranothorite and secondary formed U-minerals (Figure 5-25). Proportion of “oxide bound” Ra (< 10 %) and Th have lower significance, however, extracted Th in sample Palm-C is rather high (ca. 50 %), which indicates the high abundance of thorite and thorianite in the sample (Figure 5-25) The “organic” extraction step was performed only in case of sample Palm-C, because significant amount of organic material was expected only in this sample. Among the elements analysed, Pb, Ra and U were leached out in the highest proportion, ca. 60, 30 and 15 %, respectively (Figure 5-19). The very high proportion of extracted uranium compared to sample Ask-A from where only 2 % was extracted in this step (Figure 4-19) is probably from the remaining U-oxides and phosphates that are in higher amount in this sample than in Ask-A. From sample Ask-A this step extracted the second highest proportion of Ra, which indicates the highly effective sorption onto the organic matter. Proportion of residual Ra extracted from the sample Palm-362 and Palm-384 are ca 70 % and 50 %, respectively (Figure 5-20). In these samples the major Ra sources are accessory minerals such as monazite and xenotime compared to sample Palm-C wherein residual Ra is only from < 30 %. Proportion of residual

uranium in the samples has lower importance ca. 30 % in sample Palm-C and only a few % in samples Palm-384 and Palm-362 (Figure 5-20). Most of the U was extracted in the previous "oxide" step. Even from sample Palm-362 (ca. 40%), where no uranium-oxides and uranyl-phosphates were identified, and the major U-sources are REE-phosphates. Thorium was extracted in the highest proportion by this step. However, in sample Palm-C the proportion of "oxide bound" and "residual" Th is similar. It indicates that U-Th-oxides/phosphates and REE-phosphates are the major source of Th. Although, REE-phosphates are very resistant (Langmuir and Herman, 1980), from Palmottu samples these minerals were extracted sufficiently by aqua regia solution using microwave digestion, which is a rather aggressive method (Chen and Ma, 2001). The higher proportion of easily removable Ra and the lower proportion of mobile U in sample Palm-C compared to Palm-384 indicate a significant downward migration of U, while Ra was sorbed onto weathering products and organic matters. At the outflow of the catchment area in the well-sorted fine sand sample Palm-362 there is no sign of the effect of the nearby uranium mineralisation. Hence, the uranium migrated from the mineralisation captured in the wetland at the bottom of the hill. This is in agreement with the findings of Kaija et al. (2003).

7.2. Comparison of the radiation properties of Askola, Palmottu and Olkiluoto sampling sites

In Askola sampling site very weak ^{238}U, and significant ^{226}Ra and ^{232}Th increase against depth was measured (Pearson product-moment correlation coefficient (r) = 0.54, 0.87 and 0.78, respectively) (Figure 4-13). The secular disequilibrium in ^{238}U decay chain in samples Ask-C and Ask-1 were measured the highest value (^{226}Ra/^{238}U = 1.6). In the uppermost A and B soil horizons higher uranium than radium concentrations were observed compared to the deeper horizons wherein radium activity concentration shows higher number (Table 4-1). Secular equilibrium between ^{238}U and ^{226}Ra has been occurred only in the deepest sample (Table 4-1). In ^{232}Th decay chain significant disequilibrium measured between ^{232}Th and ^{228}Ra in all of the samples except in the deepest horizon and in the sandy till layer Ask-C. The highest discrepancy has been found in the well-sorted coarse sand sample (Ask-1) (^{228}Ra/^{232}Th = 0.4) (Table 4-1). The disequilibrium measured in decay chains of ^{238}U and ^{232}Th suggests a significant redistribution of U and Ra that is the most effective in the highly permeable sample Ask-1 caused by the continuous leaching of groundwater. Although, ^{238}U was measured by ^{234}Th in equilibrium of ^{234m}Pa, the disequilibrium between ^{238}U and ^{234}Th is unlikely due to the short half life or ^{234}Th (24.1 d) (Figure 2-3). The results indicate that Ra is more mobile than U and Th in the uppermost two organic rich samples, whereas the mobility

of the elements in the underlying sandy till (Ask-C and coarse sand (Ask-1) layers is the following: U>Ra>Th. Radium is the least mobile in the clayey layer (Ask-2). Based on these features it can be stated that Ra is more mobile than U in organic rich and therefore reductive environment, whereas in oxidative environment U is more mobile than Ra (Schott and Wiegand, 2003). Furthermore, the results suggest that the adsorbing capacity of clays is more effective for Ra than for U. This indicates that the argillaceous layer (Ask-2) behaves as barrier for the downward migrating fluids; hence the effect of the percolating water on the deeper layers is lessened. This caused the secular equilibrium in both ^{238}U and ^{232}Th decay chains measured in the deepest layer (Ask-3) (Table 4-1).

Emanation factors of Askola samples vary between 0.20-0.40 (Table 4-2). Greeman and Rose (1996) concluded that emanation fraction of 0.20 is characteristic in material without coatings like exchangeable-organic fraction, while in coatings this value can be up to 0.50. Interestingly our results revealed that emanation fraction and in some of the samples activity concentration of ^{226}Ra measured in bulk sample is higher than that in grain size fraction < 0.250 mm (Table 4-8). This is in contradiction with the findings of Megumi and Mamuro (1977), Ek and Ek (1995), Barillon et al. (2005) and Breitner et al. (2008; 2010). They found significant increase of ^{226}Ra concentration versus decreasing grain size. However, publications dealing with emanation vs. grain size behaviour have different results. For example, Sakoma et al. (2008) pointed out that emanation factor is independent of grain size, but Amin et al. (1995), Garven and Baskaran (2004), Somlai et al. (2008) and Breitner et al. (2010) have found that emanation factor increases versus decreasing grain size due to the higher specific surface area and the enrichment of Ra-bearing and Ra adsorbing minerals in the finer grain size fractions (Greeman and Rose, 1996; Breitner et al., 2008). The lower emanation factor measured in finer grain size fraction than in bulk samples indicates that grains with high emanation power generally belong to the coarse fraction. The sequential extraction revealed proportion of ^{226}Ra in different soil constituent show no correlation with emanation coefficients (Table 7-2).

Table 7-2: Summarised table of ^{226}Ra-content and emanation coefficients of bulk and < 0.250 mm grain size fraction, the proportion of the < 0.250 mm grain size fraction and proportion of ^{226}Ra in the extractants compared to the sum of Ra leached out from < 0.250 mm grain size fractions of the six studied samples from Askola, Finland.

Samples		<0.250 mm	Bulk	Ex (<0.250 mm)	Ox (<0.250 mm)	Org (<0.250 mm)	Easily rem. (<0.250 mm)	Res (<0.250 mm)
Ask-A	^{226}Ra (Bq/kg)	30±4	42±10	62%	7%	25%	94%	6%
	Emanation factor	0.34±0.13	0.35±0.08					
Ask-B	^{226}Ra (Bq/kg)	62±4	45±8	38%	25%		63%	37%
	Emanation factor	0.26±0.04	0.36±0.07					
Ask-C	^{226}Ra (Bq/kg)	138±4	96±13	81%	7%		88%	12%
	Emanation factor	0.31±0.02	0.30±0.04					
Ask-1	^{226}Ra (Bq/kg)	82±4	66±8	70%	14%		84%	16%
	Emanation factor	0.17±0.02	0.28±0.04					
Ask-2	^{226}Ra (Bq/kg)	79±4	116±11	84%	2%		86%	14%
	Emanation factor	0.20±0.02	0.41±0.04					
Ask-3	^{226}Ra (Bq/kg)	107±4	117±7	74%	7%		81%	19%
	Emanation factor	0.32±0.02	0.36±0.03					

In Palmottu sampling site an obvious trend occurred in ^{226}Ra-, ^{238}U-, ^{232}Th-concentration versus distance from the mineralisation (Figure 5-13). Radium activity concentration decreases from the top of the mineralisation (Palm-C, ca 800 Bq/kg) to the outflow of the catchment area (Palm-362, ca. 40 Bq/kg). In contrast, activity concentration of uranium is higher in the bottom of the hill (750 Bq/kg) than on the top (650 Bq/kg) (Table 5-1 and Figure 5-13). This explains the significant disequilibrium occurred between ^{238}U and ^{226}Ra in samples Palm-384 and Palm-C (ratio of ^{226}Ra/^{238}U is 0.2 and 1.2, respectively). At the outflow in Palm-362 sample secular equilibrium occurred (Table 5-1). It suggests that Ra is bound on organic matters (Titaeva, 1967) or on weathering products such as Fe-oxides, hydroxides and clay minerals (Landa et al., 1991; Greeman and Rose, 1996; Greeman et al., 1999; Breitner et al., 2008) on the top of the mineralisation. In contrast, U migrated downward causing higher concentration on the bottom of the mineralisation next to and in the peat bog (Kaija et al., 2003). The secular disequilibrium occurred in ^{232}Th decay chain (^{228}Ra/^{232}Th = 1.3) (Table 5-1) also indicates the uptake of Ra in the top of the mineralisation,

since release of ^{232}Th is unlikely due to its low mobility (Langmuir and Herman, 1980). The secular equilibrium occurred between ^{238}U and ^{226}Ra in sample Palm-362, which means no radionuclide uptake and/or release is assumed. This suggests that the peat bog is an excellent filtering media for U and Ra and/or the presence of U and Ra does not support the migration i.e. they are present in highly resistant minerals such as monazite and xenotime. In contrast to the organic rich Askola sample (Ask-A) (Table 4-1) in sample Palm-C U is the most mobile whereas Ra is the least mobile one (Table 5-1). This phenomenon was found in clayey Ask-2 sample (Table 4-1), therefore, in sample Palm-C the high amount of organic content and weathering products resulted together the highly effective immobilisation of Ra. It is indicated by the high proportion of Ra extracted in the exchangeable (42 %) and organic steps (26 %) (Table 7-3). The large disequilibrium (^{226}Ra/^{238}U ratio = 0.2) in sample Palm-384 (Table 5-1) is resulted in by the downward migrated U from the uranium mineralisation and not because the Ra removal, as it is indicated by the proportion of exchangeable Ra (39 %), which is similar to that is in the sample Palm-C (42 %) (Table 7-3).

As it was found in Askola sample, activity concentration of ^{226}Ra and emanation factor measured in <0.250 mm grain size fraction in Palmottu samples are lower than those in bulk sample (Table 7-3). In contrast to Askola samples, in Palmottu samples the activity concentration of ^{226}Ra and the proportion of easily removable Ra, for instance exchangeable Ra, show good correlation with emanation factor in the samples. The high emanation factor (> 0.40) measured in Palm-C indicates the grainsurface presence of Ra atom (Morawska and Phillips, 1993; Greeman and Rose, 1996). In contrast, the emanation factor is only 0.18 (Table 7-3) in the sample Palm-362, which is highly sorted fluvioglacial sediment, that indicates a rather homogenous distribution of Ra within the grains (Breitner et al., 2010; Sakoda et al., 2010). High proportion of residual Ra (76 %) (Table 7-3) also supports this assumption.

Table 7-3: Summarised table of ^{226}Ra-content and emanation coefficients of bulk and < 0.250 mm grain size fraction, the proportion of the < 0.250 mm grain size fraction and proportion of ^{226}Ra in the extractants compared to the sum of Ra leached out from < 0.250 mm grain size fractions of the three samples from Palmottu, Finland.

Samples		<0.250 mm	Bulk	Ex (<0.250 mm)	Ox (<0.250 mm)	Org (<0.250 mm)	Easily rem. (<0.250 mm)	Res (<0.250 mm)
Palm-C	^{226}Ra (Bq/kg)	567±7	790±100	42%	9%	26%	77%	22%
	Emanation factor	0.51±0.01	1.06±0.14					
Palm-384	^{226}Ra (Bq/kg)	92±7	120±60	39%	5%		44%	56%
	Emanation factor	0.26±0.02	0.56±0.28					
Palm-362	^{226}Ra (Bq/kg)	32±8	41±4	20%	4%		24%	76%
	Emanation factor	0.09±0.02	0.19±0.02					

Significant disequilibrium, $^{226}Ra/^{238}U = 1.4$ occurred in the oxidized till layer in Olkiluoto sampling site due to the significantly higher activity concentration of ^{226}Ra in the uppermost sample, whereas activity concentrations of ^{238}U are similar within the margins of error (Table 6-1). The higher ^{226}Ra activity concentration in the oxidative layer of the same sediment (same material) alludes to the enrichment effect of oxidised environment (Landa et al., 1991). In ^{232}Th decay chain no disequilibrium occurred, however activity concentration of ^{228}Ra and ^{228}Th in the reductive layers is lower than in the oxidized zone (Table 6-1, Figure 6-10). Dowdall and O'Dea (2002) concluded that the high disequilibrium ($^{226}Ra/^{238}U > 3$) is due to the leaching of ^{238}U and it is related to the position of the samples relative to the water level. Dowdall and O'Dea's (2002) assumption is that the disequilibrium is due to the leaching of ^{238}U is not supported by our results. In our case the highest disequilibrium occurred in sample Olk-1 (Figure 6-1) wherein the mobile U has the lowest ones (Figures 6-12, 6-13 and 6-15). In our case the uptake of ^{226}Ra by adsorption of dissolved Ra from groundwater onto exchange sites in clays, Fe-oxides is more probable than leaching of ^{238}U, however, there is no sign of ^{228}Ra enrichment. Probably the 5.75 year (half life of ^{228}Ra) is not enough for extensive separation. This is in agreement with the assumption of Greeman et al. (1999) who observed the same phenomenon in Eastern US soils, and indicated that the addition of ^{226}Ra to lower soil horizons by downward percolating soil water probably results from the net loss from the upper soil horizons. The uppermost sample (Olk-1) has the highest ^{226}Ra activity concentration and the highest emanation coefficient (Table 7-4). However, the higher Ra content does not necessarily cause higher emanation, if the Ra is present in the crystal lattice, the radon cannot escape (Morawska and Phillips, 1993; Breitner et al., 2010; Sakoda et al., 2010). This means that in this sample a significant portion of Ra atom must be close to or on the grain surface. In this sample (Olk-1) the proportion of easily removable Ra is 32 %, whereas this proportion is only 26 % in sample Olk-2, which has the lowest emanation (Table 7-4). In contrast, emanation coefficient of sample Olk-3 is only 0.06 (Table 7-4), which has the highest proportion of easily extractable Ra (39 %). Among the three easily extractable portions in sample Olk-1 the carbonate step extracted the highest proportion of Ra (18 %) (Table 7-4). Hence, the soil portion extracted in this step is responsible for the slightly higher emanation measured in Olk-1.

Table 7-4: Summarised table of ^{226}Ra-content and emanation coefficients of bulk sample, the proportion of the < 0.250 mm grain size fraction and proportion of ^{226}Ra in the extractants compared to the sum of Ra leached out from < 0.250 mm grain size fractions of the three samples from Olkiluoto, Finland

		Bulk	Ex (<0.250 mm)	Carb (<0.250 mm)	Ox (<0.250 mm)	Easily rem. (<0.250 mm)	Res (<0.250 mm)
Olk-1	^{226}Ra (Bq/kg)	52±5	10%	18%	4%	32%	68%
	Emanation factor	0.08±0.01					
Olk-2	^{226}Ra (Bq/kg)	30±6	17%	6%	3%	26%	74%
	Emanation factor	0.04±0.01					
Olk-3	^{226}Ra (Bq/kg)	37±6	25%	10%	4%	39%	61%
	Emanation factor	0.06±0.01					

7.3. Weathering effect on chemical composition of U-, Th-bearing minerals

In order to study redistribution of U and Th within major U-bearing mineral grains such as U-oxides, -phosphates and monazite and xenotime during weathering eight weathered grains with enhanced U- and/or Th-content were selected from Palmottu and Askola samples and X-ray mapping and wavelength dispersive spectrometry at distinct points were performed (Figures 4-27 – 4-30 and 5-26 – 5-29).

In the central fresh part of monazite grains similar major constituent ratios (Ce_2O_5/P_2O_5 = ca 1.1) were measured (Annex 3) to it was published by Yang & Pattison (2006) (0.8-1), Krenn & Finger (2007) (ca 1.1) and Grew et al. (2008) (0.7-1.3). In the fresh part of xenotime grains Y_2O_3/P_2O_5 measured ratio (1.3-1.4) (Annex 3) is similar to the published ratio (ca. 1.2) (Hetherington et al., 2008). Therefore, these results can be used as reference for monazites and xenotimes. For U-oxides, and phosphates there was no reference ratio, however, the feature of the central part of the grains indicates the absence of alteration effects. The presence of Si and Fe in the selected grains can be considered as weathering products since these elements are not present in the fresh central part of the mineral grain. Furthermore, the higher the Fe_2O_3 content the lower the measured total content with correlation coefficient of > -0.8 (Annex 3). The lower measured total content (Annex 3) is due to the enhanced H_2O content and structural non-homogeneity in the weathered part. SiO_2, Fe_2O_3, ThO_2 contents of the monazite grains increase with decreasing P_2O_5, La_2O_3 and Ce_2O_3 contents (Table 5-3 – 5-5). Correlation coefficients (Pierson product-moment coefficient) are generally high between Fe_2O_3 and Ce_2O_3, Fe_2O_3 and P_2O_5 and ThO_2 and P_2O_5 (> -0.8) and lower between Fe_2O_3 and ThO_2 (0.57 – 0.8) (Annex 3). Behaviour of U is different compared to Th. Correlation

coefficients between U_2O_3 and weathering products are negative and usually high (>0.7). The correlation between ThO_2 and U_2O_3 is -0.86. It can be through the lower solubility of Th (Adams et al., 1959) or by re-precipitation of Th with and sorbtion onto goethite (von Gunten et al., 1999).For xenotime, that is a resistant U-, Th-bearing mineral like monazite, correlation coefficients between Fe_2O_3 and U_2O_3, P_2O_5 and U_2O_3 and P_2O_5 and Fe_2O_3 (-0.48, 0.66 and -0.85, respectively) (Table 4-3, Annex 3) are similar to those measured in monazites (Annex 3). In less resistant U-oxide, -phosphate, -silicate minerals generally good positive correlations were calculated between Fe_2O_3 and ThO_2, Fe_2O_3 and U_2O_3 (> 0.7) (Table 4-4 – 4-6, Annex 3). This means that minerals such as monazite and xenotime which are resistant for weathering (Langmuir and Herman, 1980), Th is likely present in the weathered part of the mineral, whereas U concentration is lower in the weathered part. In contrast, in less resistant minerals U and Th behave similarly. Both remain in weathered part of the minerals.

8. SUMMARY

1. The study revealed that the developed multiple analytical methods in order to determine source of ^{222}Rn in special glacial sediment is sufficient and none of the steps can be neglected. Such a multidisciplinary study dealing with radon source identification has not been carried out before.
2. The results of the sequential chemical extraction s are pointed out that the exchangeable Ra does not relate directly to the finest grain size fraction, it is also present on the surface of altered grains in the coarser grain size fractions.
3. Based on the results of the sequential extraction carried out on carbonate rich Olkiluoto till samples, Ra is tend to present in carbonate complexes in oxidative environment and in exchangeable phase in the reductive environment. The abovementioned carbonate complex is responsible for the slightly higher emanation measured in the sample collected from the oxidative horizon.
4. The enhanced seqular disequilibrium between ^{238}U and ^{226}Ra in the sample Palm-384 revealed by γ-spectrometry is resulted by a significant downward migration of U and effective adsorption of Ra onto weathering products and organic matters. The secular equilibrium occurred at the outflow of the catchment area indicates the effectivity of the peat bog as a filtering media for U and Ra.

5. The study pointed out that in Palmottu samples the activity concentration of ^{226}Ra and the proportion of easily removable Ra, for instance exchangeable Ra show very good correlation with emanation factors. The high emanation factor (> 0.40) measured in sample Palm-C indicates the surface presence of Ra atom. In contrast, in the sample Palm-362 the emanation factor is only 0.18 that, and the high proportion of residual Ra, (76 %) indicates the rather homogenous distribution of Ra within the grains.

6. Emanation measurements of Askola samples revealed inverse emanation pattern of the Askola site, that is, the bulk sample displayed higher emanation factor than the fine (< 0.250 mm) fraction, which is explained by the assumption that grains with high emanation power belong to the coarse grain fraction.

7. Results of the correlation study prepared on weathered U- and Th-bearing minerals strongly suggests that in minerals which are resistant for weathering such as monazite and xenotime, Th prefers present in the weathered part of the mineral, whereas U concentration in the weathering part is lower. In the less resistant minerals (e.g. uraninite, uranothorite) both U and Th remain in the weathered part of the minerals.

8. Among the methods tested for ^{226}Ra determination, it is recommended to use Rad Disks method for those extractants that are highly acidic and the two phases LSC methods using water-immiscible scintillation cocktail for those that are colourful but not very aggressive ones. This study revealed that for measuring emanation coefficients the open and closed measurements using vacuum sealer is easy and fast, and can be also used for low amount of sample. However, if high amount of sample is available the LSC method can be also fruitful.

ENGLISH ABSTRACT

In this thesis the behaviour of natural radionuclides (mainly U-series) and chemical fronts in the geo-environment as a basis for assessment of radon emission were studied. Understanding the natural weathering processes in rock and overburden which cause mobilisation, migration and, eventually, subsequent immobilisation of uranium and its decay products is indispensible for the evaluation and quantification of safety risks caused by radon emission. Furtheremore, observations on primary and secondary U-bearing minerals in overburden in natural geological settings are necessary to understand and quantify the process mechanisms and the spatial and time scales involved. Therefore three sampling sites were selected in southern Finland in order to study the vertical and horizontal migration and to identify the features which effect the migration.

In the selected samples the exchangeable Ra does not relate directly to the finest grain size fraction, it is present on the surface of altered grains in the coarser grain size fractions as well. In carbonate rich Olkiluoto till samples Ra is tend to present in carbonate complexes in oxidative environment and in exchangeable phase in the reductive environment. The carbonate complexes are responsible for the slightly higher emanation measured in the sample collected from the oxidative horizon.

In Palmottu sampling site the significant downward migration of U and the effective adsorption of Ra onto weathering products and organic matters result the enhanced secular disequilibrium between ^{238}U and ^{226}Ra in the bottom of the U enrichment site. The secular equilibrium occurred at the outflow of the catchment area indicates the filtering of the peat bog. The activity concentration of ^{226}Ra and the proportion of easily removable Ra show very good correlation with emanation factors. The high emanation factor (> 0.40) measured in adjacent to the U enrichment site indicates the surface presence of Ra atom. In contrast, the low emanation factor (0.18) and the high proportion of residual Ra (76 %) at the outflow indicate the more homogenous distribution of Ra within the grains.

In Askola sampling site the higher emanation factor in bulk samples than in the fine fraction (< 0.250 mm) is explained by the assumption that grains with high emanation power generally belong to the coarse grain fraction.

The study revealed that in minerals which are resistant for weathering such as monazite and xenotime, Th prefer to be present in the weathered part of the mineral, whereas U concentration in the weathering part is lower. In less resistant minerals (e.g. uraninite, uranothorite) both U and Th remain in the weathered part of the minerals.

Doktori disszertációmban a természetes, elsősorban az U-sorba tartozó radionuklidok viselkedését és ezek radon kibocsátásra gyakorolt hatását vizsgáltam. Földtani környezetben az U és bomlástermékeinek mobilizációját, migrációját és esetenként megkötődését okozó mállási folyamatok megértése elengedhetetlen a radonemisszió okozta biztonsági kockázat mennyiségi és minőségi értékeléséhez. Továbbá, a primer és másodlagos U-tartalmú ásványok megfigyelése szükséges a folyamatok mechanizmusának térbeli és időbeli megértéséhez és számszerűsítéséhez. Ezért Dél-Finnországban három olyan mintavételi helyet választottam ki, ahol a vertikális (Askola és Olkiluoto) és horizontális (Palmottu) migráció és a migrációt befolyásoló hatások vizsgálhatóak voltak.

A vizsgált mintákban a „kicserélhető" Ra nem kapcsolódik közvetlenül a legfinomabb szemcseméret frakcióhoz, a durvább szemcsék mállott felszínén is jelen van. A karbonát gazdag olkiluotoi till mintákban, oxidatív környezetben a Ra karbonát komplexekben van jelen, míg reduktív környezetben inkább „kicserélhető" fázisban. Megállapítható, hogy az oxidatív környezetből származó mintákban a karbonát komplexekben jelenlevő Ra a felelős a mért nagyobb emanációs együtthatókért.

A Palmottu vizsgálati helyen megfigyelhető az U jelentős lefelé irányuló migrációja és a Ra kiemelkedő szorpciója a mállástermékeken és szerves anyagokon, amely nagymértékű egyenlőtlenséget eredményez a ^{238}U és ^{226}Ra között az U-ércesedés lábánál. Ezzel ellentétben a vízgyűjtő terület kivezető részénél kialakult egyenlőség a lápos terület hatékony szűrő képességére utal. A vizsgált mintákban a ^{226}Ra-aktivitás koncentrációja és a könnyen kioldható Ra teljes Ra-hoz viszonyított aránya a jól korrelál az emanációs együtthatóval. A mért nagy emanációs együttható (> 0.40) az ércesedéshez közel a Ra atom szemcse felszíni jelenlétére, míg a vízgyűjtő kifolyásánál mért kis együttható érték (< 0.18) és a „reziduális" Ra nagy aránya (76 %) a szemcsén belüli Ra atomok homogénebb eloszlására utal.

Az Askola mintavételi helyen a bulk mintákban mért, a < 0.250 mm-es frakciónál nagyobb emanációs együttható értékek arra engednek következetni, hogy a nagyobb emanációval rendelkező szemcsék a durvább frakcióhoz tartoznak.

A vizsgálatok rámutattak, hogy a mállással szemben ellenállóbb ásványokban (pl. monacit és xenotim) Th a mállott zónákban van jelen, míg a mállott területek U-tartalma kisebb. A kevésbé ellenálló ásványokban (pl. uraninit és uranotórit) az U és a Th is az ásvány mállott részén marad.

REFERENCES

Adams, J.A.S., Osmond, J.K. and Rogers, J.J.W., 1959. The geochemistry of thorium and uranium. Physics and Chemistry of the Earth, 3: 298-348.

Adams, J.A.S. and Weaver, C.E., 1958. Thorium-to-uranium ratios as indicators of sedimentary processes - an example of geochemical facies. Bulletin of the American Association of Petroleum Geologists, 42: 1898.

Ahonen, L., Kaija, J., Paananen, M., Hakkarainen, V. and Ruskeeniemi, T., 2004. Palmottu natural analogue: A summary of the studies. Final Report. YST-121, Geological Survey of Finland, Nuclear Waste Disposal Research, Espoo.

Ames, L.L., McGarrah, J.E., Walker, B.A. and Salter, P.F., 1983. Uranium and Radium Sorption on Amorphous Ferric Oxyhydroxide. Chemical Geology, 40(1-2): 135-148.

Amin, Y.M., Mahat, R.H., Doraisamy, S.J. and Subramaniam, S.Y., 1995. The Effect of Grain-Size on the Radon Emanation Rate. Pergamon-Elsevier Science Ltd, pp. 621-622.

Anderson, H.A., Berrow, M.L., Farmer, V.C., Hepburn, A., Russell, J.D. and Walker, A.D., 1982. A reassessment of podzol formation processes. Journal of Soil Science, 33(1): 125-136.

Appelquist, H. and Kinnunen, K., 1977. Raportti Geologisen Tutkimuslaitoksen Uraanitutkimuksista Askolan - Porvoon Aluella 1976-1977. M 19/3022/-77/1/10, Geological Survey of Finland, Espoo.

Appelqvist, H., 1972. Selostus Geologisen Tutkimuslaitoksen Uraanitutkimuksista Askolan Alueella Kesinä 1970-1971, Geological Survey of Finland, Espoo.

Appelqvist, H., 1982. Uranium investigation in the area of the Lakeakallio, Askola, 1978-1980, Geological Survey of Finland, Espoo.

Arey, J.S., Seaman, J.C. and Bertsch, P.M., 1999. Immobilization of uranium in contaminated sediments by hydroxyapatite addition. Environmental Science & Technology, 33(2): 337-342.

Aro, K. and Laitakari, I. (Editors), 1987. Suomen diabaasit ja muut mafiset juonikivilajit. Abstract: Diabases and other mafic dyke rocks in Finland. Report of Investigation, 76. Geological Survey of Finland, 254 pp.

Arvela, H., 1995a. Residental radon in Finland: sources variation, modelling and dose comparisons. STUK-A, 124, Helsinki, 167 pp.

Arvela, H., 1995b. Seasonal-Variation in Radon Concentration of 3000 Dwellings with Model Comparisons. Radiation Protection Dosimetry, 59(1): 33-42.

Arvela, H., 2002. Population distribution of doses from natural radiation in Finland, International Congress Series, pp. 9-14.

Arvela, H., Voutilainen, A., Honkamaa, T. and Rosenberg, A., 1994. High Indoor Radon Variations and the Thermal-Behavior of Eskers. Health Physics, 67(3): 254-260.

Aubert, D., Probst, A. and Stille, P., 2004. Distribution and origin of major and trace elements (particularly REE, U and Th) into labile and residual phases in an acid soil profile (Vosges Mountains, France). Applied Geochemistry, 19(6): 899-916.

Baranov, V.I., Morozova, N.G., Kunasheva, K.G. and Grigor'ev, G.I., 1964. Geochemistry of Some Natural Radioactive Elements in Soil. Soviet Soil Science, 8: 733.

Barillon, R., Ozgumus, A. and Chambaudet, A., 2005. Direct recoil radon emanation from crystalline phases. Influence of moisture content. Geochimica Et Cosmochimica Acta, 69(11): 2735-2744.

Bird, G.W., 1979. Geochemistry of Radioactive Waste Disposal, Canadian Geophysical Union Annual Meeting, Fredericton, New Brunswick.

Blomqvist, R., Kaija, J., Lampinen, P., Paananen, M., Ruskeeniemi, T., Korkealaakso, J., Pitkänen, P., Ludvigson, J.-E., Smellie, J., Koskinen, L., Floría, E., Turrero, M.J., Galarza, G., Jakobsson, K., Laaksoharju, M., Casanova, J., Grundfelt, B. and Hernan, P., 1998. The Palmottu Natural Analogue Project. Phase I - Hydrogeological evaluation of the site, European Commission, Nuclear Science and Technology Series, Luxembourg.

Blomqvist, R., Ruskeeniemi, T., Kaija, J., Ahonen, L., Paananen, M., Smellie, J., Grundfelt, B., Pedersen, K., Bruno, J., Pérez del Villar, L., Cera, E., Rasilainen, K., Pitkänen, P., Suksi, J., Casanova, J., Read, D. and Frape, S., 2000. The Palmottu natural analogue project. Phase II: Transport of radionuclides in a natural flow system at Palmottu. Final report. EUR 19611 EN, European Commission Nuclear Science and Technology Series.

Blomqvist, R., Suksi, J., Ruskeeniemi, T., Ahonen, L., Niini, H., Vuorinen, U. and Jakobson, K., 1995. The Palmottu natural analogue project. The behaviour of natural radionuclides in and around uranium deposits. Summary Report 1992-1994. Report YST-88, Geological Survey of Finland, Espoo.

Bossus, D.A.W., 1984. Emanating Power and Specific Surface Area. Radiation Protection Dosimetry, 7: 73-76.

Braun, J.J., Viers, J., Dupre, B., Polve, M., Ndam, J. and Muller, J.P., 1998. Solid/liquid REE fractionation in the lateritic system of Goyoum, east Cameroon: The implication for the present dynamics of the soil covers of the humid tropical regions. Geochimica Et Cosmochimica Acta, 62(2): 273-299.

Breitner, D., Arvela, H., Hellmuth, K.H. and Renvall, T., 2010. Effect of moisture content on emanation at different grain size fractions - A pilot study on granitic esker sand sample. Journal of Environmental Radioactivity, 101(11): 1002-1006.

Breitner, D., Turtiainen, T., Arvela, H., Vesterbacka, P., Johanson, B., Lehtonen, M., Hellmuth, K.H. and Szabo, C., 2008. Multidisciplinary analysis of Finnish esker sediment in radon source identification. Science of the Total Environment, 405(1-3): 129-139.

Buurman, P. and Jongmans, A.G., 2005. Podzolisation and soil organic matter dynamics. Geoderma, 125(1-2): 71-83.

Chen, M. and Ma, L.Q., 2001. Comparison of three aqua regia digestion methods for twenty Florida soils. Soil Science Society of America Journal, 65(2): 491-499.

Cortini, M., 1984. Uranium in mantle processes. In: B. De Vivo, F. Ippolito, G. Capaldi and P.R. Simpson (Editors), Uranium, geochemistry, mineralogy, geology, exploration and resources. The Institution of Mining and Mettallurgy, pp. 4-11.

Currie, L.A., 1968. Limits for qualitative detection and quantitative determination. Application to radiochemistry. Analytical Chemistry, 40(3): 586-593.

Csige, I., 1998. Radonpotenciál meghatározására eljárás kifejlesztése, MTA Atommagkutató Intézet, Debrecen.

Dahl, R., 1967. Post-glacial microweathering of bedrock surface in the Narvik district of Norway. Geografiska Annaler, 49A(2-4): 155-166.

Darby, S., Hill, D., Auvinen, A., Barros-Dios, J.M., Baysson, H., Bochicchio, F., Deo, H., Falk, R., Forastiere, F., Hakama, M., Heid, I., Kreienbrock, L., Kreuzer, M., Lagarde, F., Mäkeläinen, I., Muirhead, C., Oberaigner, W., Pershagen, G., Ruano-Ravina, A., Ruostoeenoja, E., Schaffrath Rosario, A., Tirmarche, M., Tomásek, L., Whitley, E., Wichmann, H.E. and Doll, R., 2004. Radon in homes and risk of lung cancer: collaborative analysis of individual data from 13 European case-control studies. British Medical Journal, 330(223): 1-6.

De Putter, T., Charlet, J.M. and Quinif, Y., 1999. REE, Y and U concentration at the fluid-iron oxide interface in late Cenozoic cryptodolines from Southern Belgium. Chemical Geology, 153(1-4): 139-150.

Dementyev, V.A. and Syromyatnikov, N.G., 1965. The Form of Thorium Isotopes in Ground Waters. Geokhimiya, 2: 211.

Dickson, B.L. and Herczeg, A.L., 1992. Naturally-Occurring Radionuclides in Acid Saline Groundwaters around Lake Tyrrell, Victoria, Australia, pp. 95-114.

Dongarra, G., 1984. Geochemical behaviour of uranium in the supragene environment. In: B. De Vivo, F. Ippolito, G. Capaldi and P.R. Simpson (Editors), Uranium geochemistry, mineralogy, geology, exploration and resources. The Institution of Mining and Metallurgy, London, pp. 18-22.

Donisa, C., Steinnes, E. and Sjřbakk, T.E., 2005. Nitric-acid soluble fractions of 21 elements in Norwegian podzols: Factors affecting regional differences in vertical distribution. Applied Geochemistry, 20(7): 1258-1267.

Donner, J., 1995. The Quaternary history of Scandinavia. World and Regional Geology 7. Cambridge University Press, Cambridge, 200 pp.

Dowdall, M. and O'Dea, J., 2002. Ra-226/U-238 disequilibrium in an upland organic soil exhibiting elevated natural radioactivity. Journal of Environmental Radioactivity, 59(1): 91-104.

Durecova, A., Durec, F., Auxtova, L., Adamek, P. and Lendacka, M., 1999. Determination of Ra-226 and Ra-228 in mineral and drinking waters using 3M's EMPORE (TM) Radium Rad Disks. Czechoslovak Journal of Physics, 49: 119-125.

Durrance, E.M., 1986. Radioactivity in geology: Principles and applications. Ellis Horwood Ltd, Chichester, 441 pp.

Duval, J.S., 1991. Use of aerial gamma-ray data to estimate relative amounts of radon in soil gas. In: L.C.S. Gundersen and R.B. Wnaty (Editors), Field Studies of Radon in Rocks, Soils, and Water. USGS Bulletin, pp. 155-163.

Edsfeldt, C., 2001. The Radium Distribution in Some Swedish Soils and its Effect on Radon Emanation, Royal institute of Technology, Stockholm, 52 pp.

Ek, J. and Ek, B.M., 1995. Radium and uranium concentrations in two eskers with enhanced radon emission, 6th International Symposium on The Natural Radiation Environment (NRE-VI). Pergamon-Elsevier Science Ltd, Montreal, Canada, pp. S495-S498.

Eronen, M., Glückert, G., van de Plassche, O., van der Plicht, J. and Rantala, P., 1995. Land uplift in the Olkiluoto-Pyhäjärvi area, southwestern Finland, during the last 8000 years. YJT-95-17, Voimayhtiöiden ydinjätetoimikunta, Helsinki.

Fuller, C.C., Bargar, J.R., Davis, J.A. and Piana, M.J., 2002. Mechanisms of uranium interactions with hydroxyapatite: Implications for groundwater remediation. Environmental Science & Technology, 36(2): 158-165.

Garver, E. and Baskaran, M., 2004. Effects of heating on the emanation rates of radon-222 from a suite of natural minerals. Applied Radiation and Isotopes, 61(6): 1477-1485.

Girault, F., Gajurel, A.P., Perrier, F., Upreti, B.N. and Richon, P., 2011. Radon emanation of heterogeneous basin deposits in Kathmandu Valley, Nepal. Journal of Asian Earth Sciences, 40(2): 595-610.

Grabovnikov, V.A. and Samsonova, L.M., 1968. Effect of the form of uranium occurrence in solutions on its sorption by natural mineral formations. Geokhimiya, 10: 1250-1259.

Greeman, D.J. and Rose, A.W., 1996. Factors controlling the emanation of radon and thoron in soils of the eastern USA. Chemical Geology, 129(1-2): 1-14.

Greeman, D.J., Rose, A.W., Washington, J.W., Dobos, R.R. and Ciolkosz, E.J., 1999. Geochemistry of radium in soils of the Eastern United States. Applied Geochemistry, 14(3): 365-385.

Grew, E.S., Yates, M.G. and Wilson, C.J.L., 2008. Aureoles of Pb(II)-enriched feldspar around monazite in paragneiss and anatectic pods of the Napier Complex, Enderby Land, East Antarctica:

the roles of dissolution-reprecipitation and diffusion. Contributions to Mineralogy and Petrology, 155(3): 363-378.

Grundl, T. and Cape, M., 2006. Geochemical factors controlling radium activity in a sandstone aquifer. Ground Water, 44(4): 518-527.

GTK, 2010. Quaternary Geology of Finland. GTK, Espoo.

Hamilton, E.I., 1975. Abundance and Distribution of Uranium in Some Oceanic, Continental Ultramafic Inclusions and Host Basalts. Chemical Geology, 16(3): 221-231.

Hansen, R.O. and Huntington, G.L., 1969. Thorium Movements in Morainal Soils of the High Sierra, California. Soil Science, 108(5): 257.

Harris, R.C. and Adams, J.A.S., 1966. Geochemical and mineralogical studies on the weathering of granitic rocks. American Journal of Science, 264: 146.

Hellmuth, K.H., Tarviainen, T., Backman, B., Hatakka, T., Vesterbacka, P. and Savolainen, H., 2003. Natural geochemical concentrations on the Baltic Shield of Finland for use as indicators of nuclear waste repository safety. The use of selected safety indicators (concentrations; fluxes) in the assessment of radioactive waste disposal. Report 4. Report YST-109, Geological Survey of Finland, Espoo.

Henry, M.E., Kaeding, M.E. and Monteverde, D., 1991. Radon in soil gas and gamma-ray activity of rocks and soils at the Mulligan Qarry, Clinton, New Jersey. In: L.C.S. Gundersen and R.B. Wnaty (Editors), Field Studies of Radon in Rocks, Soils, and Water. USGS Bulletin, pp. 65-75.

Herczeg, A.L., Simpson, H.J., Anderson, R.F., Trier, R.M., Mathieu, G.G. and Deck, B.L., 1988. Uranium and Radium Mobility in Groundwaters and Brines within the Delaware Basin, Southeastern New-Mexico, USA. Chemical Geology, 72(2): 181-196.

Hetherington, C.J., Jercinovic, M.J., Williams, M.L. and Mahan, K., 2008. Understanding geologic processes with xenotime: Composition, chronology, and a protocol for electron probe microanalysis. Chemical Geology, 254(3-4): 133-147.

Hirvas, H. and Nenonen, K., 1980. Malminetsintää Palvelevat Maaperätutkimukset Askolan Nietoossa ja Porvoon Maalaiskunnan Alhossa Kl. 3021 03 ja 3022 01, Geological Survey of Finland, Espoo.

Huhma, H., 1986. Sm-Nd, U-Pb and Pb-Pb isotopic evidence for the origin of the Early Proterozoic Svecokarelian crust in Finland. Bulletin of the Geological Survey of Finland, 337. Geological Survey of Finland, Espoo, 338 pp.

Huhta, P., 2008. Studies of Quaternary Deposits of Investigation Trench OL-TK14 at the Olkiluoto Study Site, Eurajoki, SW Finland. Working Report 2008-31, Geological Survey of Finland, Espoo.

IEC, 1995. International standard IEC1452:1995, nuclear instrumentation – measurement of gamma-ray emission rates of radionuclides – calibration and use of germanium spectrometers, International Electrotechnical Commission, Geneve.

Ikonen, J., Breitner, D., Koskela, P., Hellmuth, K-H., Vaaramaa, K. and Siitari-Kauppi, M., in prep. Ra-226 detection from soil samples using solid-phase extraction and liquid scintillation counting.

Itävaara, M., Vehkomäki, M.-L. and Nousiainen, A., 2008. Sulphate-Reducing Bacteria in Ground Water Samples from Olkiluoto - Analyzed by Quantitative PCR. 2008-82, Posiva Oy, Olkiluoto.

Jansen, B., Nierop, K.G.J. and Verstraten, J.M., 2005. Mechanisms controlling the mobility of dissolved organic matter, aluminium and iron in podzol B horizons. European Journal of Soil Science, 56(4): 537-550.

Jerden, J.L. and Sinha, A.K., 2003. Phosphate based immobilization of uranium in an oxidizing bedrock aquifer. Applied Geochemistry, 18(6): 823-843.

Jerden, J.L., Sinha, A.K. and Zelazny, L., 2003. Natural immobilization of uranium by phosphate mineralization in an oxidizing saprolite-soil profile: chemical weathering of the Coles Hill uranium deposit, Virginia. Chemical Geology, 199(1-2): 129-157.

Kaija, J., Rasilainen, K. and Blomqvist, R., 2003. Site-specific natural geochemical concentrations and fluxes at the Palmottu U-Th mineralisation (Finland) for use as indicators of nuclear waste repository safety. IAEA Coordinated Research Project. The Use of selected safety indicators (concentrations, fluxes) in the assessment of radioactive waste disposal. Report 6 Report YST-114, Geological Survey of Finland, Nuclear Waste Disposal Research, Espoo.

Kärki, A. and Paulamäki, S., 2006. Petrology of Olkiluoto. POSIVA 2006-02, Posiva, Olkiluoto.

Karvonen, T., 2008. Surface and Near-Surface Hydrological Model of Olkiluoto Island. Working Report 2008-17, Posiva Oy, Olkiluoto.

Keskikuru, T., Kokotti, H., Lammi, S. and Kalliokoski, P., 2001. Effect of various factors on the rate of radon entry into two different types of houses. Building and Environment, 36(10): 1091-1098.

Kirby, H.W. and Salutsky, M.L., 1964. The radiochemistry of Radium. NAS-NS 3057, USAEC.

Koczy, F.F., 1961. The Natural Radioactive Series in Organic Material. In: V. Schultz, Klement Jr., A.W. (Editor), 1st National Symposium in Radioecology, Colorado. Rheinhold, pp. 611-613.

Koistinen, T., Stephens, M.B., Bogatchev, V., Nordgulen, Ø., Wennerström, M. and Korhonen, J., 2001. Geological map of the Fennoscandian Shield 1:2 000 000.

Koljonen, T., 1992. The geochemical atlas of Finland part 2. The Geological Survey of Finland, Espoo, 218 pp.

Kontio, M. and Kähkönen, A.-M., 1991. Geochemistry and variations of the sensitivity of soils to acidification in northern Finland. In: E. Pulkkinen (Editor), Environmental Geochemistry in Northern Europe. Proceedings of the First Symposium on Environmental Geochemistry in Northern Europe held in Rovaniemi, Finland 17-19 October 1989. Special Paper 9, Geological Survey of Finland, pp. 53-60.

Koppi, A.J., Edis, R., Field, D.J., Geering, H.R., Klessa, D.A. and Cockayne, D.J.H., 1996. Rare earth element trends and cerium-uranium-manganese associations in weathered rock from Koongarra, northern territory, Australia. Geochimica Et Cosmochimica Acta, 60(10): 1695-1707.

Kovalevsky, V.V., Vorotnitskaya, I.E. and Lekarev, V.S., 1966. Bio-geochemical Food Chains of Uranium in Aquatic and Terraneous Organisms. In: B. Aberg and F.P. Hungate (Editors), International Symposium of Radioecological Concentration Processes, Stockholm. Pergamon, pp. 329-332.

Krenn, E. and Finger, F., 2007. Formation of monazite and rhabdophane at the expense of allanite during Alpine low temperature retrogression of metapelitic basement rocks from Crete, Greece: Microprobe data and geochronological implications. Lithos, 95(1-2): 130-147.

Krishnaswami, S., Graustein, W.C., Turekian, K.K. and Dowd, J.F., 1982. Radium, Thorium and Radioactive Lead Isotopes in Groundwaters - Application to the Insitu Determination of Adsorption-Desorption Rate Constants and Retardation Factors. Water Resources Research, 18(6): 1663-1675.

Kuivamäki, A., 1997. Hydrogeological classification of fracture zones of Palmottu area. The Palmottu Natural Analogue Project. Archive report. Report Y50/97/02, Geological Survey of Finland, Espoo.

Kuivamäki, A., Lindberg, A., Kurimo, M., Paananen, M., Front, K., Pitkänen, P. and Kärki, A., 1993. The geology of the Syyry area, summary report. Report YJT-93-19, Nuclear Waste Commission of Finnish Power Companies, Helsinki.

Kuivamäki, A., Paananen, M. and Kurimo, M., 1991. Structural modelling of bedrock around the Palmottu Udeposit: progress report. Report YST-72, Geological Survey of Finland, Nuclear Waste Disposal Research, Espoo.

Kuznetsov, Y.V., Simonyak, Z.N., Lisitsyn, A.p. and Frenklikh, M.S., 1968. Thorium Isotopes (Thorium-220, Thorium-232) in the Surface Layer of the Indian Ocean Sediments. Geochemistry International, 5: 169.

Lahdenperä, A.-M., Palmén, J. and Hellä, P., 2005. Summary of Overburden Studies at Olkiluoto with an Emphasis on Geosphere-Biosphere Interface. Working Report 2005-11, Posiva Oy, Olkiluoto.

Laitakari, I. and Simonen, A., 1962. Kallioperäkartta, Lapinjärvi 1:100 000. Geological Survey of Finland, Espoo.

Landa, E.R., 1984. Geochemical and Radiological Characterization of Soils from Former Radium Processing Sites. Health Physics, 46(2): 385-394.

Landa, E.R., Phillips, E.J.P. and Lovley, D.R., 1991. Release of Ra-226 from Uranium Mill Tailings by Microbial Fe(III) Reduction. Applied Geochemistry, 6(6): 647-652.

Langmuir, D., 1978. Uranium Solution-Mineral Equilibria at Low-Temperatures with Applications to Sedimentary Ore-Deposits. Geochimica Et Cosmochimica Acta, 42(6): 547-569.

Langmuir, D. and Herman, J.S., 1980. The Mobility of Thorium in Natural-Waters at Low-Temperatures. Geochimica Et Cosmochimica Acta, 44(11): 1753-1766.

Langmuir, D. and Riese, A.C., 1985. The Thermodynamic Properties of Radium. Geochimica Et Cosmochimica Acta, 49(7): 1593-1601.

Lazar, I., Toth, E., Koteles, G.J., Puho, E. and Czeizel, A.E., 2005. An inverse association between cancer mortality rate of women and residential radon in 34 Hungarian villages. Journal of Radioanalytical and Nuclear Chemistry, 266(1): 43-48.

Löfman, J., 1999. Groundwater flow modelling at the Olkiluoto site – flow under natural conditions. Report PATU-96-76e, Posiva Oy, Olkiluoto.

Mäkeläinen, I., Arvela, H. and Voutilainen, A., 2001. Correlations between radon concentration and indoor gamma dose rate, soil permeability and dwelling substructure and ventilation. The Science of the Total Environment, 272: 283-289.

Markkanen, M. and Arvela, H., 1992. Radon Emanation from Soils, pp. 269-272.

Martin, A.J., Crusius, J., McNee, J.J. and Yanful, E.K., 2003. The mobility of radium-226 and trace metals in pre-oxidized subaqueous uranium mill tailings. Applied Geochemistry, 18(7): 1095-1110.

Mattila, J., Aaltonen, I., Kemppainen, K., Wilkström, L., Paananen, M., Paulamäki, S., Front, K., Gehör, S., Kärki, A. and Ahokas, T., 2008. Geological Model of the Olkiluoto Site, Version 1.0. Working Report 2007-92, Posiva Oy, Olkiluoto.

McDonough, W.F. and Sun, S.S., 1995. The Composition of the Earth. Chemical Geology, 120(3-4): 223-253.

Megumi, K., 1979. Radioactive Disequilibrium of Uranium and Actinium Series Nuclides in Soil. Journal of Geophysical Research, 84(NB7): 3677-3682.

Megumi, K. and Mamuro, T., 1977. Concentration of Uranium Series Nuclides in Soil Particles in Relation to Their Size. Journal of Geophysical Research, 82(2): 353-356.

Morawska, L. and Phillips, C.R., 1993. Dependence of the radon emanation coefficient on radium distribution and internal structure of the material. Geochimica et Cosmochimica Acta, 57(8): 1783-1797.

Muikku, M., Arvela, H., Järvinen, H., Korpela, H., Kostiainen, E., Mäkeläinen, I., Paile, W., Vartiainen, E. and Vesterbacka, K., 2005. Annoskakku 2004 - Suomalaisten saama keskimääräinen efektiivinen annos, Radiation and Nuclear Safety Authority, Helsinki.

Murakami, T., Sato, T., Ohnuki, T. and Isobe, H., 2005. Field evidence for uranium nanocrystallization and its implications for uranium transport. Chemical Geology, 221(1-2): 117-126.

Nazaroff, W.W. and Nero, A.V., 1988. Radon and its decay products in indoor air. John Wiley & Sons, Pages: 608 pp.

Nicaise, D., DePutter, T., Andre, L., Jedwab, J. and Dupuis, C., 1996. Neoformed LREE phosphates at the nanometer scale, in acid low temperature weathering: Consequences in rare earth elements, uranium and thorium trapping. Comptes Rendus De L Academie Des Sciences Serie Ii Fascicule a-Sciences De La Terre Et Des Planetes, 323(2): 113-120.

Niemelä, J., 1985. Maaperäkartta Suomusjärvi, 1:100 000. Geological Survey of Finland, Espoo.

Payne, T.E., Edis, R., Fenton, B.R. and Waite, T.D., 2001. Comparison of laboratory uranium sorption data with 'in situ distribution coefficients' at the Koongarra uranium deposit, Northern Australia. Journal of Environmental Radioactivity, 57(1): 35-55.

Peake, R.T. and Schumann, R.R., 1991. Regional radon characterisation. In: L.C.S. Gundersen and R.B. Wnaty (Editors), Field Studies of Radon in Rocks, Soils, and Water. USGS Bulletin, pp. 163-174.

Pérez del Villar, L., Campos, R., Pelayo, M., Pardillo, J., Cózar, J.S. and Labajos, M.A., 1997. Structural, lithological and mineralogical analyses of borehole R-385 (386) from the Palmottu Site, Finland. Technical Report 97-05, Geological Survey of Finland, Espoo.

Pérez del Villar, L., Cozar, R., E., Delgado, A., Nunez, R., Crespo, M.T., Sanches de Ledesma Gimeno, M.J., Peña, J., A., Y.d.L. and Garcia, M., 1999. Activities and main results obtained by Ciemat in the Palmottu Project during 1998. Technical Report 99-06, Geological Survey of Finland, Espoo.

Pitkänen, P., Kaija, J., Blomqvist, R., Smellie, J.A.T., Frape, S., Laaksoharju, M., Negrel, P., Casanova, J. and Karhu, J., 2002. Hydrogeochemical interpretation of groundwater at Palmottu. Eight EC Natural Analogue Working Group Meeting. Proceedings of an international workshop held in Strasbourg, France on 23rd –25th March 1999, Luxembourg, 155-169 pp.

Pliler, R. and Adams, J.A.S., 1962. The distribution of thorium and uranium in Pennsylvanian weathering profile. Geochimica Et Cosmochimica Acta, 26: 1137.

POSIVA, 2009. Olkiluoto Site Description, 2008. POSIVA 2009-01, Posiva Oy, Olkiluoto.

Pouchou, J.L. and Pichoir, F., 1986. Very High Elements X-Ray-Microanalysis - Recent Models of Quantification. Journal De Microscopie Et De Spectroscopie Electroniques, 11(4): 229-250.

Purkl, S. and Eisenhauer, A., 2003. A rapid method for [alpha]-spectrometric analysis of radium isotopes in natural waters using ion-selective membrane technology. Applied Radiation and Isotopes, 59(4): 245-254.

Putnam, C.W., 1971. Geology. Oxford University Press, New york, 586 pp.

Quejido, A.J., Pérez del Villar, L., Cozar, J.S., Fernandez-Diaz, M. and Crespo, M.T., 2005. Distribution of trace elements in fracture fillings from the "Mina Fe" uranium deposit (Spain) by sequential leaching: implications for the retention processes. Applied Geochemistry, 20(3): 487-506.

Räisänen, E., 1986. Uraniferous granitic veins in the Svecofennian schist belt in Nummi-Pusula, Southern Finland. Report IAEA-TC-571.

Rama and Moore, W.S., 1984. Mechanism of Transport of U-Th Series Radioisotopes from Solids into Groundwater. Geochimica Et Cosmochimica Acta, 48(2): 395-399.

Rancon, D., 1973. The Behaviour of Underground Environments of Uranium and Thorium Discharged by the Nuclear Industry, Environmental Behaviour of Radionuclides Released in the Nuclear Industry. IAEA, Aix-en-Provence, pp. 333-346.

Rich, R.A., Holland, H.D. and Petersen, U., 1977. Hydrothermal uranium deposits. Elsevier, Amsterdam, 264 pp.

Richardson, K.A., 1964. Thorium, uranium and potassium in the Conway granite, New Hampshire, USA. In: J.A.S. Adams, Lowder, W.M. (Editor), The natural radiation environment. Chicago University Press, Chicago, pp. 51.

Roedder, E., 1972. Composition of fluid inclusions. USGS Proffesional Paper, 440-JJ: 164.

Rogers, J.J.W., 1964. Statistical tests of the homogeneity of the radioactive components of granitic rocks. In: J.A.S. Adams and W.M. Lowder (Editors), The natural radiation environment. Chicago University Press, Chicago, pp. 51.

Rosholt, J.N., 1957. Open System model for uranium-series dating of Pleistocene samples. Analytical Chemistry, 29: 1398.

Rusanova, G.V., 1962. On the Problem of Studying the Leaching Processes and Migration of Radium in Soils. Soviet Soil Science, 9: 85.

Ruskeeniemi, T., Lindberg, A., Pérez del Villar, L., Blomqvist, R., Suksi, J., Blyth, A. and Cera, E., 2002. Uranium mineralogy with implications for mobilisation of uranium at Palmottu. In: H. van Maravic and R. Alexander (Editors), Eight EC Natural Analogue Working Group Meeting. Proceedings of an international workshop held in Strasbourg, France on 23rd –25th March 1999, Luxembourg, pp. 143-154.

Sakaune, M., 1960. Geochemical Studies on the Radioactive Sediments III. Uranium, Phosphorus, and Arsenic in sedimentary Bed at Ningyo Pass. Nippon Kagaku Zasshi, 81: 898.

Sakoda, A., Hanamoto, K., Ishimori, Y., Nagamatsu, T. and Yamaoka, K., 2008. Effects of some physical conditions on leaching rate of radon from radioactive minerals originating from some hot springs. Radiation Measurements, 43(1): 106-110.

Sakoda, A., Nishiyama, Y., Hanamoto, K., Ishimori, Y., Yamamoto, Y., Kataoka, T., Kawabe, A. and Yamaoka, K., 2010. Differences of natural radioactivity and radon emanation fraction among constituent minerals of rock or soil. Applied Radiation and Isotopes, 68(6): 1180-1184.

Sasaki, T., Gunji, Y. and Okuda, T., 2005. Theoretical study of high radon emanation. Journal of Nuclear Science and Technology, 42(2): 242-249.

Sauramo, M., 1918. Geochronologische Studien über die spätglaziale Zeit in Südfinnlan. Bulletin de la Commission géologique de Finlande, 50.

Schonhofer, F., 1989. Determination of Rn-222 and Ra-226 in Mineral Water and Drinking-Water - a Survey in Austria. Analyst, 114(10): 1345-1347.

Schott, B. and Wiegand, J., 2003. Processes of radionuclide enrichment in sediments and ground waters of Mont Vully (Canton Fribourg, Switzerland). Eclogae Geologicae Helvetiae, 96(1): 99-107.

Schreurs, J. and Westra, L., 1986. The thermotectonic evolution of a Proterozoic, low pressure, granulite dome, West Uusimaa, SW Finland. Contributions to Mineralogy and Petrology, 93: 236-250.

Schumann, R.R. and Gundersen, L.C.S., 1996. Geologic and climatic controls on the radon emanation coefficient, pp. S439-S446.

Sheppard, M.I., 1980a. The Environmental Behaviour of Radium. AECL-6796, Atomic Energy of Canada Limited, Pinawa, Manitoba.

Sheppard, M.I., 1980b. The Environmental Behaviour of Uranium and Thorium. AECL-6795, Atomic Energy of Canada Limited, Pinawa, Manitoba.

Simonen, A., 1980. The Precambrian in Finland. Bulletin of the Geological Survey of Finland, 304. Geological Survey of Finland, Espoo, 58 pp.

Sinkko, K., 1981. Computer analysis for gamma-ray spectra in sample measurements, University of Helsinki, Helsinki, 56 pp.

Sinkko, K. and Aaltonen, H., 1985. Calculation of the true coincidence summing correction for different sample geometries in gamma-ray spectroscopy. STUK-B-VALO 40, STUK, Helsinki.

Smellie, J.A.T., Blomqvist, R., Frape, S.K., Pitkänen, P., Ruskeeniemi, T., Suksi, J., Casanova, J., Gimeno, M.J. and Kaija, J., 2002. Palaeohydrogeological implications for long-term hydrochemical stability at Palmottu. Eight EC Natural Analogue Working Group Meeting. Proceedings of an international workshop held in Strasbourg, France on 23rd – 25th March 1999, Luxembourg, 201-208 pp.

Somlai, J., Jobbágy, V., Somlai, K., Kovács, J., Németh, C. and Kovács, T., 2008. Connection between radon emanation and some structural properties of coal-slag as building material. Radiation Measurements, 43(1): 72-76.

Stranden, E., Kolstad, A.K. and Lind, B., 1984. The influence of moisture and temperature on radon exhalation. Radiation Protection Dosimetry, 7(1-4): 55-58.

STUK, 2007. Quality Manual of the Department of Research and Environmental Surveillance, Technical manual of the in-house method. STUK-TKO-4, Helsinki.

Szalay, S., 1964. Cation-Exchange Properties of Humic Acids to their Importance in the Geochemical Enrichment of UO_2^{++} and other Cations. Geochimica Et Cosmochimica Acta, 28: 1605.

Szalay, S. and Sámsoni, Z., 1969. Investigation of the leaching of uranium from crushed magmatic rocks. Geochemistry International, 6: 613-625.

Tachi, Y., Shibutani, T., Sato, H. and Yui, M., 2001. Experimental and modeling studies on sorption and diffusion of radium in bentonite, pp. 171-186.

Takeno, N., 2005. Atlas of Eh-pH diagrams - Intercomparison of thermodynamic databases. Open File Report No.419. Geological Survey of Japan, 287 pp.

Tanner, A.B., 1980. Radon migration in ground: A supplementary review. In: T.F. Gedsell and W.M. Lowder (Editors), The Natural Radiation Environment III. University of Chicago Press, pp. 5-56.

Taylor, S.R. and McLennan, S.M., 1995. The Geochemical Evolution of the Continental-Crust. Reviews of Geophysics, 33(2): 241-265.

Tessier, A., Campbell, P.G.C. and Bisson, M., 1979. Sequential Extraction Procedure for the Speciation of Particulate Trace-Metals. Analytical Chemistry, 51(7): 844-851.

Titaeva, N.A., 1967. On the Character of Radium and Uranium Bonding in Peat. Geokhimiya, 12: 1493.

Toropainen, V., 2009. Installation of Groundwater Observation Tubes OL-PVP30–35 at Olkiluoto in Eurajoki 2009. Working Report 2009-27, Posiva Oy, Olkiluoto.

Tripathi, V.S., 1979. Comments on Uranium Solution-Mineral Equilibria at Low Temperatures with Applications to Sedminentary Ore Deposits. Geochimica Et Cosmochimica Acta, 43: 1989.

Turtiainen, T., 2009. Measurement of radon emanation of drainage layer media by liquid scintillation counting. Journal of Radioanalytical and Nuclear Chemistry, 279(1): 325-331.

Tyler, G., 2004. Vertical distribution of major, minor, and rare elements in a Haplic Podzol. Geoderma, 119(3-4): 277-290.

Tynni, R., Hyyppä, J. and Valovirta, V., 1976. Quaternary deposits in the Lapinjärvi map-sheet area. Geological Survey of Finland, Espoo, 41 pp.

Tynni, R. and Kukkonen, E., 1968. Maaperäkartta, Lapinjärvi, 1:100 000. Geological Survey of Finland, Espoo.

Tyuryukanova, E.B. and Kalugina, V.A., 1971. Behaviour of Thorium in Soils. Soviet Journal of Ecology, 2: 467.

Vaasjoki, M., 1996. Explanation to the geochronological map of Southern Finland. Report of Investigation 135, Geological Survey of Finland, Espoo.

Vaasjoki, M., Korsman, K. and Koistinen, T., 2005. Overview. In: M. Lehtinen, Nurmi, P.A., Rämö, O.T. (Editor), The Precambrian Geology of Finland - Key to the Evolution of the Fennoscandian Shield. Elsevier B.V., Amsterdam, pp. 1-18.

Valmari, T., Mäkeläinen, I., Reisbacka, H. and Arvela, H., 2010. Radon Atlas of Finland 2010, Radiation and Nuclear Safety Authority, Helsinki.

Vareikiené, O. and Lehtonen, M., 2004. Heavy minerals in the study of soil: techniques, their limitations and advantages. Geologija, 46: 1-7.

Verkovskaja, I.N., Vavillov, P.P. and Maslov, V.I., 1966. The Migration of Natural Radioactive Elements under Natural Conditions and Their Distribution According to Biotic and Abiotic Environmental Components. In: B. Aberg and F.P. Hungate (Editors), International Symposium in Radioecological Concentration Processes, Stockholm. Pergamon.

Vesterbacka, P., Makelainen, I. and Arvela, H., 2005. Natural radioactivity in drinking water in private wells in Finland. Radiation Protection Dosimetry, 113(2): 223-232.

Vinogradov, A.P., 1959. The Geochemistry of Rare and Dispersed Chemical Elements in Soils. Chapman and Hall Ltd, London.

Vinson, D.S., Vengosh, A., Hirschfeld, D. and Dwyer, G.S., 2009. Relationships between radium and radon occurrence and hydrochemistry in fresh groundwater from fractured crystalline rocks, North Carolina (USA). Chemical Geology, 260(3-4): 159-171.

von Gunten, H.R., Roessler, E., Lowson, R.T., Reid, R.D. and Short, S.A., 1999. Distribution of uranium- and thorium series radionuclides in mineral phases of a weathered lateritic transect of a uranium ore body. Chemical Geology, 160(3): 225-240.

Voutilainen, A. and Mäkeläinen, I., 1993. Radon risk mapping using indoor monitoring data. Indoor Air, 3: 369-375.

Wagman, D.D., Evans, W.H., Parker, V.B., Schumm, R.H., Halow, I., Bailey, S.M., Churney, K.L. and Nuttall, R.L., 1982. The Nbs Tables of Chemical Thermodynamic Properties - Selected Values for Inorganic and C-1 and C-2 Organic-Substances in Si Units. Journal of Physical and Chemical Reference Data, 11: 1-&.

Washington, J.W. and Rose, A.W., 1990. Regional and Temporal Relations of Radon in Soil Gas to Soil-Temperature and Moisture. Geophysical Research Letters, 17(6): 829-832.

Weltner, A., Mäkeläinen, I. and Arvela, H., 2002. Radon mapping strategy in Finland, International Congress Series, pp. 63-69.

Wiederhold, J.G., Teutsch, N., Kraemer, S.M., Halliday, A.N. and Kretzschmar, R., 2007. Iron isotope fractionation in oxic soils by mineral weathering and podzolization. Geochimica et Cosmochimica Acta, 71(23): 5821-5833.

Wood, W.K., Kraemer, T.F. and Shapiro, A., 2004. Radon (Rn-222) in ground water of fractured rocks: A diffusion/ion exchange model. Ground Water, 42(4): 552-567.

Yamamoto, T., Yunoki, E., Yamakawa, M. and Shimizu, M., 1973. Studies on Environmental Contamination by Uranium 3. - Effects of Carbonate Ion on Uranium Adsorption to and Desorption from Soils Journal of Radiation Research, 14: 219-224.

Yang, P. and Pattison, D., 2006. Genesis of monazite and Y zoning in garnet from the Black Hills, South Dakota. Lithos, 88(1-4): 233-253.

Annex-1. Major and trace element content of bulk samples

Table Annex 1-1: Major and trace element concentrations (ppm) in bulk Askola samples measured with ICP-MS at SGS Laboratory, Toronto and ^{226}Ra-activity concentration (Bq/kg) measured by gamma spectrometer equipped by BEGe-detector at Radiation and Nuclear Safety Authority of Finland (STUK).

	ASK-A	ASK-B	ASK-C	ASK-1	ASK-2	ASK-3
^{226}Ra	32	61	141	85	82	110
^{137}Ba	314	437	426	424	564	473
^{238}U	1.74	3.33	4.74	4.41	5.63	9.85
^{232}Th	4.80	9.00	12.7	16.3	12.6	9.70
^{93}Nb	5.00	10.0	9.00	8.00	13.0	7.00
^{39}K	12 100	16 300	18 000	18 400	23 500	19 700
^{139}La	11.1	16.3	36.6	29.8	40.1	24.1
^{140}Ce	20.7	32.2	102	96.8	77.7	55.8
^{56}Fe	13 800	29 600	32 700	26 800	31 300	21 500
^{208}Pb	41.0	55.0	19.0	36.0	21.0	24.0
^{141}Pr	2.43	3.89	7.99	7.12	9.39	5.74
^{88}Sr	156	223	208	232	225	227
^{31}P	600	2 300	700	600	800	600
^{146}Nd	9.70	15.0	29.8	26.2	35.8	21.6
^{90}Zr	93.7	179	202	207	252	217
^{147}Sm	1.75	3.00	5.10	5.20	6.60	4.20
^{153}Eu	0.47	0.66	0.98	0.84	1.18	0.82
^{47}Ti	1 400	2 900	2 700	2 100	2 900	1 900
^{157}Gd	1.82	2.97	4.93	4.81	6.32	4.47
^{159}Tb	0.27	0.43	0.78	0.75	0.93	0.67
^{163}Dy	1.59	2.69	4.22	4.21	4.79	3.65
^{89}Y	8.70	14.6	23.6	22.9	26.4	21.0
^{165}Ho	0.32	0.53	0.84	0.84	1.02	0.77
^{166}Er	0.98	1.58	2.39	2.49	2.66	2.06
^{169}Tm	0.14	0.23	0.35	0.35	0.41	0.31
^{172}Yb	1.00	1.60	2.50	2.50	2.70	2.00
^{175}Lu	0.19	0.33	0.42	0.43	0.43	0.36

Table Annex 1-2: Major and trace element concentrations (ppm) in bulk Palmottu and Olkiluoto samples measured with ICP-MS at SGS Laboratory, Toronto and ^{226}Ra-activity concentration (Bq/kg) measured by gamma spectrometer equipped by BEGe-detector at Radiation and Nuclear Safety Authority of Finland (STUK).

	PALM-C	PALM-384	Palm-362	OLK-1	OLK-2	OLK-3
^{226}Ra	567	92	32	40	33	32
^{137}Ba	267	342	376	374	340	420
^{238}U	46.7	65.5	3.13	3.22	2.81	2.82
^{232}Th	16.4	9.1	7.3	8.2	7.6	8.2
^{93}Nb	12	5	5	10	8	11
^{39}K	11400	15200	16400	20200	16100	19700
^{139}La	21.9	18.1	20.3	28.5	25.9	30
^{140}Ce	45.1	41.3	43	57.2	52.2	60.2
^{56}Fe	46600	15200	14100	20800	15300	24500
^{208}Pb	31	19	15	15	20	16
^{141}Pr	4.78	4.29	4.78	6.73	6.27	7.28
^{88}Sr	84	148	154	126	124	140
^{31}P	1100	300	300	500	500	600
^{146}Nd	17	16	18	26.7	24.8	27.3
^{90}Zr	235	266	280	305	345	287
^{147}Sm	3.4	3.3	3.4	5	4.7	5
^{153}Eu	0.45	0.54	0.67	0.78	0.84	0.95
^{47}Ti	2700	1800	1700	2600	2300	3100
^{157}Gd	3.1	2.8	3.3	4.76	4.61	5.1
^{159}Tb	0.47	0.44	0.51	0.74	0.68	0.78
^{163}Dy	2.5	2.7	2.9	4.3	3.81	4.14
^{89}Y	14	15	16	23.1	22.3	23.7
^{165}Ho	0.54	0.54	0.62	0.87	0.81	0.85
^{166}Er	1.5	1.7	1.7	2.47	2.31	2.44
^{169}Tm	0.22	0.22	0.24	0.34	0.34	0.36
^{172}Yb	1.6	1.8	1.8	2.5	2.6	2.5
^{175}Lu	0.26	0.25	0.26	0.38	0.42	0.39

Annex-2. Major and trace element content of leachates extracted by sequential chemical extraction

Table Annex 2-1: Concentration (ppm) of elements extracted by 1st ("exchangeable") extraction step from Askola samples measured with ICP-MS at Geological Department of University of Helsinki and ^{226}Ra-activity concentration (Bq/kg) measured by liquid scintillation counter at Radiation and Nuclear Safety Authority of Finland (STUK).

	ASK-A/1	ASK-B/1	ASK-C/1	ASK-1/1	ASK-2/1	ASK-3/1
^{226}Ra	10	4	77	30	28	21
^{137}Ba	20	2.9	18	5.8	31	14
^{238}U	nd	nd	nd	nd	nd	nd
^{232}Th	0.002	nd	nd	nd	nd	nd
^{93}Nb	0.004	0.0007	nd	nd	nd	nd
^{39}K	95	33	37	16	59	31
^{139}La	0.05	0.04	0.73	0.54	4.34	1.51
^{140}Ce	0.03	0.04	0.79	0.77	2.3	1.3
^{56}Fe	206	85	7.5	nd	nd	nd
^{208}Pb	8.4	0.53	0.23	0.10	0.14	0.25
^{141}Pr	0.005	0.005	0.09	0.08	0.63	0.20
^{88}Sr	4.7	0.24	1.0	0.21	8.2	3.0
^{31}P	8.8	nd	nd	nd	nd	nd
^{146}Nd	0.02	0.02	0.40	0.40	2.9	0.92
^{90}Zr	0.002	0.001	0.0006	nd	nd	nd
^{147}Sm	0.002	0.002	0.04	0.04	0.28	0.09
^{153}Eu	0.006	0.003	0.02	0.01	0.08	0.03
^{47}Ti	nd	nd	nd	nd	nd	nd
^{157}Gd	0.004	0.004	0.09	0.08	0.57	0.16
^{159}Tb	0.002	0.001	0.009	0.007	0.05	0.016
^{163}Dy	0.004	0.004	0.07	0.05	0.35	0.12
^{89}Y	0.02	0.02	0.44	0.24	2.41	0.81
^{165}Ho	0.002	0.002	0.01	0.007	0.06	0.02
^{166}Er	0.003	0.002	0.03	0.02	0.16	0.05
^{169}Tm	0.002	0.001	0.004	0.002	0.02	0.006
^{172}Yb	0.003	0.003	0.03	0.02	0.15	0.05
^{175}Lu	0.002	0.002	0.004	0.002	0.02	0.007

Table Annex 2-2: Concentration (ppm) of elements extracted by 1st ("exchangeable") extraction step from Palmottu and Olkiluoto samples measured with ICP-MS at Geological Department of University of Helsinki and ^{226}Ra-activity concentration (Bq/kg) measured by liquid scintillation counter at Radiation and Nuclear Safety Authority of Finland (STUK).

	PALM-C/1	**PALM-384/1**	**Palm-362/1**	**OLK-1/1**	**OLK-2/1**	**OLK-3/1**
^{226}Ra	287	33	6	5	6	9
^{137}Ba	2.78	0.75	3.13	3.5	2.8	12
^{238}U	0.30	1.3	nd	nd	nd	0.05
^{232}Th	0.07	0.007	nd	nd	nd	nd
^{93}Nb	0.002	nd	nd	nd	nd	nd
^{39}K	46	13	7.7	56	62	150
^{139}La	0.13	0.07	0.22	0.0008	nd	nd
^{140}Ce	0.13	0.09	0.09	nd	nd	nd
^{56}Fe	216	0.72	nd	nd	nd	nd
^{208}Pb	3.0	0.32	0.02	nd	nd	nd
^{141}Pr	0.04	0.01	0.03	nd	nd	nd
^{88}Sr	0.23	0.03	0.13	2.3	2.2	3.3
^{31}P	nd	nd	nd	nd	nd	nd
^{146}Nd	0.08	0.07	0.15	nd	nd	nd
^{90}Zr	0.006	0.004	nd	nd	nd	0.0002
^{147}Sm	0.03	0.009	0.02	nd	nd	nd
^{153}Eu	0.04	0.004	0.006	0.0003	0.0002	0.002
^{47}Ti	nd	nd	nd	nd	nd	nd
^{157}Gd	0.04	0.01	0.03	nd	nd	nd
^{159}Tb	0.03	0.002	0.003	nd	nd	nd
^{163}Dy	0.04	0.01	0.02	nd	nd	nd
^{89}Y	0.07	0.05	0.14	nd	nd	nd
^{165}Ho	0.03	0.002	0.003	nd	nd	nd
^{166}Er	0.03	0.005	0.008	nd	nd	nd
^{169}Tm	0.03	0.0008	0.001	nd	nd	nd
^{172}Yb	0.04	0.005	0.007	nd	nd	nd
^{175}Lu	0.03	0.0007	0.001	nd	nd	2.77E-05

Table Annex 2-3: Concentration (ppm) of elements extracted by 2nd ("carbonate") extraction step from Olkiluoto samples measured with ICP-MS at Geological Department of University of Helsinki and ^{226}Ra-activity concentration (Bq/kg) measured by liquid scintillation counter at Radiation and Nuclear Safety Authority of Finland (STUK).

	OLK-1/2	**OLK-2/2**	**OLK-3/2**
^{226}Ra	8	2	3
^{137}Ba	1.8	0.63	4.0
^{238}U	0.33	0.32	0.55
^{232}Th	0.47	0.71	1.9
^{93}Nb	0.02	0.04	0.11
^{39}K	4.6	4.3	11
^{139}La	1.9	1.8	4.5
^{140}Ce	4.6	4.3	11
^{56}Fe	196	240	616
^{208}Pb	1.8	1.6	3.2
^{141}Pr	0.56	0.52	1.2
^{88}Sr	0.95	0.94	1.7
^{31}P	152	133	193
^{146}Nd	2.4	2.2	5.1
^{90}Zr	0.94	1.0	2.6
^{147}Sm	0.52	0.49	1.1
^{153}Eu	0.11	0.09	0.17
^{47}Ti	0.75	2.0	6.3
^{157}Gd	0.54	0.50	1.1
^{159}Tb	0.08	0.07	0.15
^{163}Dy	0.41	0.38	0.78
^{89}Y	1.9	1.7	3.6
^{165}Ho	0.07	0.07	0.15
^{166}Er	0.19	0.18	0.39
^{169}Tm	0.02	0.02	0.05
^{172}Yb	0.15	0.14	0.33
^{175}Lu	0.02	0.02	0.05

Table Annex 2-4: Concentration (ppm) of elements extracted by 3rd ("oxide") extraction step from Askola samples measured with ICP-MS at Geological Department of University of Helsinki and ^{226}Ra-activity concentration (Bq/kg) measured by liquid scintillation counter at Radiation and Nuclear Safety Authority of Finland (STUK).

	ASK-A/3	ASK-B/3	ASK-C/3	ASK-1/3	ASK-2/3	ASK-3/3
^{226}Ra	1	2	7	6	1	2
^{137}Ba	2.2	2.4	2.2	0.99	0.81	0.35
^{238}U	0.20	0.53	1.4	1.6	1.9	5.4
^{232}Th	0.54	1.79	2.9	3.5	3.0	2.3
^{93}Nb	0.42	0.70	0.68	0.69	0.94	0.48
^{39}K	5.9	nd	4.9	4.1	8.3	3.4
^{139}La	0.59	1.0	1.7	1.3	1.0	0.97
^{140}Ce	1.1	2.1	15	29	9.8	9.4
^{56}Fe	2434	7222	1858	1441	1758	1257
^{208}Pb	9.7	6.4	2.6	1.8	1.4	2.2
^{141}Pr	0.17	0.32	0.53	0.38	0.27	0.29
^{88}Sr	0.23	0.22	0.13	0.07	0.09	0.07
^{31}P	476	1598	612	244	389	178
^{146}Nd	0.48	1.1	2.0	1.4	0.95	1.0
^{90}Zr	0.50	0.85	1.9	2.2	3.1	1.4
^{147}Sm	0.13	0.27	0.49	0.32	0.20	0.24
^{153}Eu	0.07	0.12	0.12	0.07	0.03	0.04
^{47}Ti	42	136	125	70	125	60
^{157}Gd	0.15	0.22	0.64	0.52	0.29	0.30
^{159}Tb	0.07	0.10	0.11	0.07	0.06	0.05
^{163}Dy	0.14	0.27	0.63	0.42	0.42	0.33
^{89}Y	0.44	0.85	2.3	1.4	2.0	1.2
^{165}Ho	0.07	0.13	0.12	0.08	0.10	0.06
^{166}Er	0.10	0.18	0.32	0.21	0.28	0.18
^{169}Tm	0.05	0.09	0.05	0.03	0.04	0.03
^{172}Yb	0.09	0.10	0.28	0.18	0.28	0.17
^{175}Lu	0.05	0.06	0.04	0.02	0.04	0.02

Table Annex 2-5: Concentration (ppm) of elements extracted by 3rd and 5th ("oxide") extraction steps from Palmottu and Olkiluoto samples, respectively, measured with ICP-MS at Geological Department of University of Helsinki and ^{226}Ra-activity concentration (Bq/kg) measured by liquid scintillation counter at Radiation and Nuclear Safety Authority of Finland (STUK).

	PALM-C/3	PALM-384/3	Palm-362/3	OLK-1/5	OLK-2/5	OLK-3/5
^{226}Ra	62	4	1	1.6	1.3	1.4
^{137}Ba	0.84	0.16	0.72	1.8	1.7	2.6
^{238}U	40	57	1.4	0.23	0.20	0.41
^{232}Th	7.7	1.7	0.94	0.17	0.06	0.12
^{93}Nb	1.4	0.70	0.49	0.07	0.09	0.11
^{39}K	nd	2.8	3.3	37	43	54
^{139}La	1.5	0.69	0.50	1.2	0.73	0.90
^{140}Ce	2.9	3.4	3.6	2.6	1.6	1.9
^{56}Fe	22734	654	543	2025	1449	2582
^{208}Pb	13	4.0	0.55	3.1	0.69	0.80
^{141}Pr	0.61	0.32	0.15	0.32	0.20	0.24
^{88}Sr	0.06	0.03	0.05	0.70	0.75	0.92
^{31}P	601	66	179	28	35	24
^{146}Nd	1.7	1.4	0.60	1.3	0.84	1.0
^{90}Zr	1.1	1.0	0.88	1.5	0.82	1.8
^{147}Sm	0.52	0.38	0.16	0.27	0.18	0.20
^{153}Eu	0.27	0.09	0.03	0.04	0.02	0.03
^{47}Ti	283	95	62	0.49	1.0	0.72
^{157}Gd	0.39	0.38	0.23	0.28	0.18	0.20
^{159}Tb	0.25	0.06	0.05	0.04	0.03	0.03
^{163}Dy	0.48	0.32	0.31	0.23	0.14	0.15
^{89}Y	0.96	0.78	1.4	1.0	0.61	0.65
^{165}Ho	0.32	0.06	0.06	0.05	0.03	0.03
^{166}Er	0.37	0.14	0.17	0.12	0.07	0.08
^{169}Tm	0.26	0.02	0.02	0.02	0.01	0.01
^{172}Yb	0.21	0.12	0.14	0.11	0.06	0.07
^{175}Lu	0.16	0.01	0.02	0.02	0.01	0.01

Table Annex 2-6: Concentration (ppm) of elements extracted by 4th ("organic") extraction step from organic rich Palmottu and Askola samples, measured with ICP-MS at Geological Department of University of Helsinki and ^{226}Ra-activity concentration (Bq/kg) measured by liquid scintillation counter at Radiation and Nuclear Safety Authority of Finland (STUK).

	PALM-C/4	ASK-A/4
^{226}Ra	182	4.4
^{137}Ba	3.7	8.2
^{238}U	7.1	0.04
^{232}Th	0.34	nd
^{93}Nb	0.11	0.27
^{39}K	2.2	45
^{139}La	0.58	0.57
^{140}Ce	0.96	1.0
^{56}Fe	3017	1440
^{208}Pb	19	13
^{141}Pr	0.10	0.09
^{88}Sr	0.23	1.4
^{31}P	129	223
^{146}Nd	0.36	0.43
^{90}Zr	0.05	0.14
^{147}Sm	0.05	0.04
^{153}Eu	nd	nd
^{47}Ti	147	216
^{157}Gd	nd	nd
^{159}Tb	nd	nd
^{163}Dy	nd	nd
^{89}Y	0.11	0.13
^{165}Ho	nd	nd
^{166}Er	nd	nd
^{169}Tm	nd	nd
^{172}Yb	nd	nd
^{175}Lu	nd	nd

Table Annex 2-7: Concentration (ppm) of elements extracted by 6th ("residual") extraction step from Askola samples, measured with ICP-MS at Geological Department of University of Helsinki and ^{226}Ra-activity concentration (Bq/kg) measured by liquid scintillation counter at Laboratory of Radochemistry at University of Helsinky (HYRL).

	ASK-A/6	ASK-B/6	ASK-C/6	ASK-1/6	ASK-2/6	ASK-3/6
^{226}Ra	1	4	10	6	5	5
^{137}Ba	16	34	49	28	61	30
^{238}U	0.66	1.3	2.2	2.0	2.2	2.9
^{232}Th	3.4	5.3	7.0	8.5	7.0	6.5
^{93}Nb	2.6	5.5	2.1	2.7	1.3	1.9
^{39}K	1336	2186	3380	2528	5664	2576
^{139}La	6.8	14	37	25	35	21
^{140}Ce	14	29	95	66	68	45
^{56}Fe	4829	14348	25570	18118	25038	14614
^{208}Pb	3.6	7.4	4.8	2.8	4.8	3.8
^{141}Pr	1.7	3.4	8.0	6.1	8.6	5.2
^{88}Sr	30	52	38	37	47	36
^{31}P	40	502	241	438	400	405
^{146}Nd	6.2	12	29	22	31	19
^{90}Zr	26	11	33	16	29	22
^{147}Sm	1.3	2.4	4.9	4.3	5.9	3.7
^{153}Eu	0.17	0.32	0.59	0.44	0.76	0.42
^{47}Ti	633	1343	1580	1208	1800	1146
^{157}Gd	1.2	2.2	4.5	3.9	5.1	3.3
^{159}Tb	0.17	0.29	0.53	0.51	0.64	0.42
^{163}Dy	0.86	1.5	2.6	2.7	3.2	2.1
^{89}Y	4.2	7.4	13	12	16	11
^{165}Ho	0.16	0.28	0.48	0.49	0.58	0.39
^{166}Er	0.44	0.77	1.3	1.3	1.5	1.0
^{169}Tm	0.07	0.11	0.18	0.18	0.20	0.14
^{172}Yb	0.43	0.72	1.2	1.2	1.3	0.93
^{175}Lu	0.07	0.11	0.17	0.18	0.20	0.14

Table Annex 2-8: Concentration (ppm) of elements extracted by 6th ("residual") extraction step from Palmottu and Olkiluoto samples, measured with ICP-MS at Geological Department of University of Helsinki and ^{226}Ra-activity concentration (Bq/kg) measured by liquid scintillation counter at Laboratory of Radochemistry at University of Helsinky (HYRL).

	PALM-C/6	**PALM-384/6**	**Palm-362/6**	**OLK-1/6**	**OLK-2/6**	**OLK-3/6**
^{226}Ra	155	47	22	28	29	20
^{137}Ba	16	13	16	50	37	82
^{238}U	3.3	3.5	1.0	1.3	1.2	0.9
^{232}Th	8.9	7.0	4.7	5.8	4.2	4.3
^{93}Nb	2.0	2.6	1.7	1.5	1.4	1.1
^{39}K	1135	1451	1487	5226	3580	6970
^{139}La	21	23	19	25	21	24
^{140}Ce	42	51	39	51	44	49
^{56}Fe	19859	9928	9080	13229	10965	17085
^{208}Pb	13	4.5	1.8	2.3	1.9	2.3
^{141}Pr	4.9	5.4	4.6	5.8	5.1	5.7
^{88}Sr	15	18	20	29	31	38
^{31}P	452	65	264	352	361	407
^{146}Nd	17	19	17	22	19	20
^{90}Zr	7.0	34	23	17	15	14
^{147}Sm	3.2	3.5	3.2	3.8	3.4	3.7
^{153}Eu	0.22	0.24	0.34	0.41	0.41	0.52
^{47}Ti	1214	1069	947	916	880	1077
^{157}Gd	2.8	3.0	2.8	3.3	3.0	3.2
^{159}Tb	0.34	0.38	0.37	0.43	0.40	0.42
^{163}Dy	1.7	1.9	1.9	2.2	2.1	2.2
^{89}Y	7.2	10	10	12	12	13
^{165}Ho	0.31	0.38	0.36	0.41	0.40	0.43
^{166}Er	0.83	1.1	1.0	1.1	1.1	1.2
^{169}Tm	0.12	0.15	0.14	0.15	0.15	0.16
^{172}Yb	0.76	1.1	0.94	0.94	0.97	1.1
^{175}Lu	0.12	0.16	0.14	0.13	0.14	0.15

Annex 3: Raw chemical composition of minerals analysed by EPMA using WDS and the correlation coefficients between the selected elements.

Annex 3-1: Raw chemical composition of different areas of the weathered, zoned xenotime grain presented in Figure 4-27 from grain size fraction of <0.063 mm of sample Ask-1 and the Pierson product-moment correlation coeffitients. Concentrations are presented in wt.%, POI = Point of interest.

POI	F	MgO	Al2O3	SiO2	P2O5	Cl	CaO	TiO2	FeO	Y2O3	Nd2O3	ThO2	U2O3	SmO	Ce2O3	PbO	Nb2O5	Total
1	0,04	0,00	0,00	0,32	28,97	0,00	0,22	0,00	0,00	39,41	0,04	0,17	1,80	0,48	0,04	0,62	0,22	72,34
2	0,07	0,00	0,00	0,37	29,20	0,01	0,29	0,00	0,00	38,74	0,09	0,12	1,77	0,56	0,00	0,51	0,00	71,73
3	0,48	0,00	0,55	1,19	22,09	0,11	0,59	0,23	8,86	30,98	0,07	0,23	1,86	0,31	0,26	0,60	0,00	68,41
4	0,41	0,00	0,52	1,07	23,30	0,11	0,58	0,22	9,42	31,68	0,23	0,27	1,80	0,58	0,20	0,47	0,26	71,14
5	0,42	0,00	0,61	1,10	22,84	0,14	0,64	0,17	6,33	31,97	0,33	0,31	1,61	0,50	0,32	0,55	0,21	68,10
6	0,67	0,00	0,96	1,36	18,46	0,18	0,85	1,22	10,57	25,97	0,16	0,35	0,78	0,62	0,49	0,45	0,00	63,26
7	1,98	0,05	0,37	1,43	21,62	0,05	3,18	2,16	4,40	31,56	0,51	0,29	1,09	0,64	2,06	0,26	0,05	72,58
8	0,40	0,00	0,56	0,82	21,94	0,15	0,61	0,21	7,44	29,56	0,07	0,33	1,58	0,52	0,32	0,42	0,03	64,96
9	0,50	0,01	0,69	0,84	21,35	0,18	0,71	0,26	5,81	29,65	0,11	0,34	1,52	0,45	0,39	0,23	0,14	63,20
10	0,11	0,00	0,00	0,62	27,25	0,02	0,35	0,06	1,66	36,88	0,00	0,35	2,71	0,48	0,16	0,53	0,07	71,23
11	0,17	0,00	0,04	0,66	27,63	0,06	0,38	0,08	1,60	37,43	0,37	0,42	2,84	0,62	0,18	0,86	0,07	73,44
12	0,56	1,42	2,18	3,55	23,29	0,09	0,76	0,44	4,56	32,33	0,08	0,13	1,29	0,29	0,30	0,48	0,00	71,85

	Fe-U	P-U	P-Fe	Fe-Th	Th-U
Correlation	-48%	66%	-85%	39%	22%

Annex 3-2: Raw chemical composition of different areas of the weathered uranothorite grain presented in Figure 4-28 from grain size fraction of <0.063 mm of sample Ask-1 and the Pierson product-moment correlation coeffitients. Concentrations are presented in wt.%, POI = Point of interest.

POI	F	Na2O	MgO	Al2O3	SiO2	P2O5	Cl	K2O	CaO	TiO2	MnO	FeO	Y2O3	Nd2O3	ThO2	U2O3	La2O3	SmO	Ce2O3	PbO	Nb2O5	Total
1	0,27	0,00	0,09	2,71	13,55	5,20	0,03	0,00	0,44	0,29	0,01	0,89	1,82	2,53	54,73	11,03	0,00	0,81	2,21	0,00	0,00	96,61
2	0,30	0,00	0,06	2,55	13,07	5,19	0,02	0,00	0,37	0,18	0,00	0,72	1,83	2,61	53,96	10,35	0,01	0,90	2,24	0,00	0,00	94,35
3	0,14	0,00	0,10	2,28	10,25	3,30	0,10	0,00	0,26	0,15	0,06	0,57	1,24	1,78	47,29	10,70	0,07	0,77	1,93	0,00	0,00	81,01
4	0,20	0,00	0,06	2,06	11,09	3,94	0,05	0,00	0,30	0,15	0,00	0,70	1,71	2,63	38,72	10,64	0,00	0,95	2,15	0,00	0,00	75,36
5	0,10	0,06	7,04	23,97	31,75	1,52	0,06	0,15	0,20	0,08	0,31	12,80	0,32	0,22	8,97	3,29	0,00	0,17	0,52	0,00	0,00	91,52
6	0,21	0,00	0,99	7,00	12,20	3,44	0,24	0,00	0,28	0,20	0,02	3,22	1,13	1,43	27,20	12,32	0,03	0,64	1,89	0,00	0,09	72,53

	Fe-Th	Fe-U	Fe-Ce	Fe-Sm	Th-U
Correlation	-99%	-74%	-91%	-91%	63%

Annex 3-3: Raw chemical compositions of different areas of the Nb-bearing uraninite grain with goethite filling presented in Figure 4-29 from grain size fraction of <0.063 mm of sample Ask-3 and the Pierson product-moment correlation coeffitients. Concentrations are presented in wt.%, POI = Point of interest.

POI	F	Na2O	MgO	Al2O3	SiO2	P2O5	Cl	CaO	TiO2	MnO	FeO	Y2O3	ThO2	U2O3	Ce2O3	PbO	Nb2O5	Total
1	0,14	0,09	0,02	0,80	1,91	1,92	0,12	2,10	11,81	0,03	3,18	0,07	0,86	65,22	2	1	8	99
2	0,13	0,09	0,00	0,87	1,80	1,72	0,11	1,98	11,81	0,02	3,02	0,07	0,88	65,01	2	1	12	102
3	0,18	0,00	0,11	0,13	1,04	0,14	0,02	0,23	5,74	2,91	69,09	0,00	0,36	2,50	0	1	3	86
4	0,14	0,00	0,19	0,15	1,15	0,18	0,03	0,26	5,69	2,92	68,83	0,00	0,46	2,36	0	1	3	86
5	0,10	0,14	0,06	0,65	1,71	1,24	0,06	1,35	9,96	0,91	24,33	0,04	0,70	42,51	1	1	8	94
6	0,06	0,07	0,10	0,57	1,67	1,24	0,15	1,32	9,66	0,82	24,90	0,08	0,66	43,60	1	1	7	94

	Fe-U	Fe-Th	Th-U
Correlation	-100	-98	98

Annex 3-4: Raw chemical compositions of different area of the weathered Th-bearing orthobrannerite grain presented in Figure 4-30 from grain size fraction of <0.063 mm of sample Ask-3 and the Pierson product-moment correlation coeffitients. Concentrations are presented in wt.%, POI = Point of interest.

POI	F	Na2O	MgO	Al2O3	SiO2	P2O5	Cl	K2O	CaO	TiO2	MnO	FeO	Y2O3	Nd2O3	ThO2	UO2	La2O3	SmO	Ce2O3	PbO	Nb2O5	Total
1	0,09	0,12	0,00	0,67	1,61	1,62	0,02	0,00	1,40	13,90	0,04	2,36	0,08	0,00	0,36	63,30	0,05	0	1	1	10	99
2	0,11	0,05	0,00	0,89	1,88	2,23	0,00	0,00	1,31	11,32	0,03	1,94	0,12	0,00	0,72	60,87	0,00	0	1	1	9	93
3	0,32	0,00	0,01	0,17	5,28	2,82	0,06	0,00	0,73	30,74	0,09	6,40	1,11	0,10	19,29	14,82	0,04	0	1	0	8	91
4	0,22	0,01	0,00	0,07	4,79	2,75	0,03	0,00	0,77	32,84	0,11	6,52	0,97	0,07	17,26	15,29	0,03	0	1	0	8	91
5	0,28	0,00	0,06	1,34	8,48	5,20	0,07	0,00	1,10	10,83	0,03	2,50	1,62	0,17	35,98	6,67	0,06	0	1	0	4	80
6	0,00	0,00	0,02	0,00	0,00	0,00	0,04	0,01	0,30	63,01	0,32	11,80	0,00	0,00	0,58	2,47	0,00	0	0	0	14	92
7	0,09	0,00	0,03	0,00	0,01	0,00	0,05	0,00	0,32	63,46	0,36	11,76	0,00	0,00	0,59	2,30	0,00	0	0	0	13	93
8	0,13	0,06	0,01	1,20	3,88	3,35	0,06	0,00	1,28	16,36	0,00	2,85	0,16	0,00	13,63	43,01	0,07	0	1	1	8	97

	Fe-U	Fe-Th	Th-U
Correlation	-77	-31	-36

Annex 3-5: Raw chemical composition of partly weathered Th-bearing monazite grain from grain size fraction <0.063 mm of sample Palm-C (Figure 5-26), and the Pierson product-moment correlation coeffitients. Concentrations are presented in wt.%, POI = Point of interest.

POI	F	Na2O	MgO	Al2O3	SiO2	P2O5	Cl	K2O	CaO	TiO2	MnO	FeO	Y2O3	Nd2O3	ThO2	U2O3	La2O3	SmO	Ce2O3	PbO	Nb2O5	Total
1	0,63	0,00	0,00	0,00	2,22	26,72	0,04	0,00	1,27	0,01	0,05	0,17	1,32	8,03	12,54	0,00	14,02	1,16	29,57	0,70	0,00	98,45
2	0,65	0,00	0,00	0,00	1,93	26,87	0,02	0,00	1,01	0,00	0,05	0,06	1,13	7,85	10,33	0,00	14,62	1,20	30,53	0,49	0,09	96,82
3	0,56	0,00	0,00	0,00	3,03	25,22	0,03	0,00	1,14	0,00	0,06	0,15	1,10	8,07	15,50	0,00	11,96	1,28	27,96	0,67	0,06	96,79
4	0,50	0,00	0,00	0,07	2,84	24,47	0,05	0,00	1,64	0,02	0,00	0,69	1,24	7,88	16,30	0,00	11,44	1,24	25,15	1,07	0,22	94,80
5	0,55	0,00	0,03	0,80	2,99	20,44	0,05	0,00	1,34	0,20	0,02	4,11	1,37	7,23	14,26	0,12	8,41	1,21	21,66	0,95	0,00	85,72
6	0,44	0,00	0,00	0,99	2,63	18,77	0,13	0,00	1,46	0,49	0,02	9,09	1,24	5,53	14,68	0,00	7,56	1,19	18,06	1,11	0,15	83,53

	Fe-Th	Fe-Ce	Fe-P	Th-P	Ce-Si
Correlation	57%	-91%	-92%	-81%	-76%

Annex 3-6: Raw chemical composition of partly weathered Th-bearing monazite grain from grain size fraction <0.063 mm of sample Palm-C (Figure 5-27), and the Pierson product-moment correlation coeffitients. Concentrations are presented in wt.%, POI = Point of interest.

	F	Na2O	MgO	Al2O3	SiO2	P2O5	Cl	K2O	CaO	TiO2	MnO	FeO	Y2O3	Nd2O3	ThO2	U2O3	La2O3	SmO	Ce2O3	PbO	Nb2O5	Total
1	0,63	0,00	0,00	0,00	1,31	27,66	0,04	0,00	0,58	0,02	0,03	0,10	2,10	12,68	7,25	0,00	9,68	3,61	28,49	0,71	0,00	94,88
2	0,62	0,00	0,00	0,00	1,24	27,96	0,04	0,00	0,52	0,05	0,09	0,07	2,19	12,74	6,59	0,00	9,43	3,70	28,36	0,40	0,00	94,01
3	0,46	0,00	0,08	1,72	3,51	15,43	0,25	0,07	0,57	0,54	0,02	6,70	1,49	7,29	9,00	0,00	5,38	1,95	16,80	0,45	0,12	71,81
4	0,43	0,00	0,00	0,41	2,14	18,84	0,19	0,00	0,76	0,46	0,06	4,60	1,72	7,79	10,85	0,00	5,98	2,47	18,22	0,53	0,16	75,59
5	0,24	0,00	0,00	0,97	2,13	15,47	0,21	0,00	0,47	0,57	0,01	8,53	1,67	6,97	10,43	0,00	5,00	2,00	15,48	0,72	0,28	71,15
6	0,58	0,00	0,00	0,27	2,64	20,92	0,12	0,00	0,72	0,39	0,00	4,68	2,23	9,34	13,28	0,00	6,47	2,96	20,32	0,73	0,00	85,63

	Fe-Th	Fe-Ce	Fe-P	Th-P
Correlation	80%	-95%	-97%	-83%

Annex 3-7: Raw chemical composition of highly weathered Th- and U-bearing monazite grain from grain size fraction 0.063-0.125 mm of sample Palm-384 (Figure 5-28), and the Pierson product-moment correlation coeffitients. Concentrations are presented in wt.%, POI = Point of interest.

POI	F	Na2O	MgO	Al2O3	SiO2	P2O5	Cl	K2O	CaO	TiO2	MnO	FeO	Y2O3	Nd2O3	ThO2	U2O3	La2O3	SmO	Ce2O3	PbO	Nb2O5	Total
1	0,56	0,00	0,00	0,00	0,63	29,48	0,05	0,00	4,06	0,00	0,00	0,05	2,30	7,96	17,65	0,66	7,85	2,15	22,35	1,14	0,00	96,87
2	0,53	0,00	0,03	0,00	0,60	28,73	0,03	0,00	3,85	0,04	0,01	0,20	2,43	7,72	17,37	0,64	7,66	2,34	21,75	1,02	0,00	94,93
3	0,58	0,00	0,00	0,00	0,84	28,66	0,02	0,00	2,90	0,01	0,00	0,00	2,39	8,96	15,41	0,28	8,43	2,36	24,74	1,09	0,10	96,78
4	0,44	0,00	0,42	2,85	8,10	6,61	0,01	0,00	1,08	0,20	0,08	32,37	3,69	0,36	25,74	0,00	0,65	0,47	2,58	0,00	0,05	85,70
5	0,41	0,24	0,45	4,11	8,69	4,31	0,01	0,00	0,44	0,29	0,20	31,37	3,54	0,52	26,32	0,00	0,73	0,43	2,90	0,00	0,00	84,94
6	0,13	0,74	0,91	8,42	4,25	1,18	0,04	0,03	0,21	1,63	0,07	47,91	0,08	0,00	3,45	0,00	0,30	0,11	0,97	0,00	0,00	70,43
7	0,39	0,00	0,25	1,61	1,14	7,49	0,06	0,00	0,72	0,42	0,05	11,72	0,29	1,84	32,75	2,89	2,49	0,74	7,37	2,90	0,06	75,18
8	0,42	0,44	0,66	4,72	2,93	4,68	0,07	0,00	0,23	0,62	0,08	31,67	0,38	1,12	12,31	0,82	1,81	0,49	4,84	0,87	0,05	69,21
	Fe-Th	**Fe-U**	**Fe-Ce**	**Fe-P**	**Th-P**	**Th-Ce**	**Th-Si**	**U-Si**														
Correlation	-73%	61%	-5%	-99%	-72%	-80%	95%	-59%														